Cellulose Materials Doctoral Students Conference 2017

Organized by Graz University of Technology

Cellulose Materials Doctoral Students Conference 2017

Organized by Graz University of Technology

Editor: Ulrich Hirn

Conference Organized by Graz University of Technology.

Conference organisation: Wolfgang Bauer
Scientific program: Ulrich Hirn
Administration: Kerstin Schefzik

The support of Mondi for conducting the student workshop is gratefully acknowledged.

ISSN 1799-4896 (print)
ISSN 1799-490X (electronic)

EFPRO
EUROPEAN FIBRE AND PAPER
RESEARCH ORGANISATIONS

mondi

FPIRC
Forest Products Industry
Research College

PI

TU
Graz

Table of Contents

Papermaking Fibers

Paper

Lignin Valorization

New Fiber and Cellulose Based Products

CNF and MFC

Cellulosic Materials and Water

Posters

Appendix: Conference Program

Exploiting Fibre Network Formation for Efficient Length-Based Separation of Cellulose Pulp

JAKOB D. REDLINGER-POHN and
STEFAN RADL

Institute of Process and Particle
Engineering, Graz University of
Technology
redlinger-pohn@tugraz.at

1 INTRODUCTION

W.W. Sampson [1] wrote in his review on characterization of fibre networks, that "*the process of papermaking is one handling fibre networks and modifying their properties*". With the emphasis on fibre networks in paper formation: the *homogeneous* distribution of fibres, both with respect to their position and orientation, is certainly key. Therefore, the fibre suspension is diluted at the headbox to ensure such a homogeneous distribution, and to prevent the formation of fibre flocks and dense fibre networks.

In contrast, in fibre fractionation processes the ultimate goal is an *inhomogeneous* distribution of fibres in the suspension, i.e., the segregation of long and short fibres. Traditionally, fibre length-based separation is approached by pressure screening, where fibre and fibre-fines are separated according to their probability passing through narrow holes or slots [2,3]. Obviously, a sharp separation is achieved by smaller hole/slot size causing a larger pressure drop. Additionally, rotating internals, which prevent screens from blocking, add to an increased energy demand. To satisfy the need for efficient length-based fibre fractionation, several alternative methods have been studied, e.g., froth flotation [4,5] and cyclones [6]. However, those methods require the addition of chemicals, or result in a diffuse fractionation characteristic.

In the present talk we will present a novel approach towards length-based fibre fractionation: for fibre networks having an intermediate strength, larger fibres are locked within the network, while smaller fibres (and fibre-fines) are found in the extra-flockular region, i.e., in the "free suspension". With the hydrodynamic fractionation device (HDF) we aim on removing this fibre-fines containing free suspension, thus separating the fibre suspension with little effort.

The structure of our extended abstract is as follows: In section two we review and summarize key findings on fibre network formation in suspension flow, leading to section three where we introduce the fractionation theory. In section four we present the novel Hydrodynamic Fractionation Device (HDF), and summarize findings on its performance.

2 FIBRE NETWORKS IN SUSPENSIONS

Exploiting fibre network formation for fractionation, the relative mobility of fibre-fines is of importance. This leads to condition for upper and lower limits on the fibre mass concentration, and the network strength, which is typically expressed by the crowding number N_{CW} [7,8].

N_{CW} is the ratio of the actual fibre concentration in the suspension to a critical fibre concentration. This is the number of fibres for which their swap volume, that is the volume of sphere with the diameter of the fibre length, equals the total volume [9]. The derivation of the crowding number N_{CW} is well documented by Sampson [1] and is presented here in its typical mass-concentration based form, where N_{CW} is a function of the fibre coarseness cs [kg/m], the length-averaged mean fibre length L_1 [m], and the fibre mass concentration C in percent [%]:

$$N_{CW} = 5\left[\frac{kg}{m^3}\right]\frac{C\,L_1^{\,2}}{cs}\,. \qquad (1)$$

For $N_{CW} > 1$ fibres enter the regime of forced collisions, where they will not move freely anymore. For increasing N_{CW} the fibre flock / fibre network becomes increasingly rigid, undergoing several regime changes. $1 < N_{CW} < 16$: dilute fibre flow, $16 < N_{CW} < 60$: fibre interaction but no immobilization, and for $N_{CW} > 60$: formation of a strong coherent structure with immobilization of fibres. The range $1 < N_{CW} < 60$, predominantly observed in industrial applications, is also termed "range of forced collision" [10]. Martinez et al. [11] showed for fibres settling under gravity, that fibres of different length move without network restriction up to $N_{CW} = 16$. For increasing crowding number N_{CW}, first the longer fibres became restricted in a network with the shorter moving freely. At a N_{CW} of 56, all fibres formed a network. The crowding number presenting a change in system behaviour (i.e., $N_{CW} = 16 \pm 4$) was termed "gelification point".

Putting the fibre suspension into motion, fluid-induced forces act on the network. The resulting flow regime is thus a function of the fibre network strength and the fluid shear force, the latter is expressed by the Reynolds number Re [12, 13]. Specifically, Jäsberg and Kataja [14] identified five regimes for flows in straight pipes and channels. With increasing fluid shear they are: (I) plug flow in which fibre are in contact with the wall, (II) plug flow with a thin water gap, (III) plug flow with a smearing water annulus, (IV) mixed flow with a larger annulus containing fibres torn form the network, and (V) full fluidization of the network by the fluid shear. In an early paper, Steenberg et al. [15] describes the exclusion of fibre-fines (termed "crill") from networks in motion. However, the majority of later publications focuses on fibres in channel flow only, neglecting the motion of fibre-fines for different regimes.

Discussing the fractionation of fibres and fibre-fines, the presented work first studies the motion of fibre-fines, with the ultimate goal to develop a novel fractionator.

3 FRACTIONATION IN STRAIGHT CHANNELS

Fractionation in channels splits the fluid flow into two streams removing wall-bounded fluid by a side channel. The streams are termed (i) accept (that is the fluid removed by the side channel), and (ii) reject (that is the fluid remaining in the main channel). The accept and reject origin from distinct areas upstream the side-channel and are divided by the exit layer [2,16,17]. The separation principle is illustrated in Figure 1. For rectangular channels, the exit layer is found parallel to the wall. Particles suspended below the exit layer upstream the side channel are removed with the accept. Key to the separation is then to keep fibres above the exit layer: maintaining annular plug flow with fibre network compressed at the channel centre, and setting the accept flow rate such that the exit layer is below the network-fluid interface.

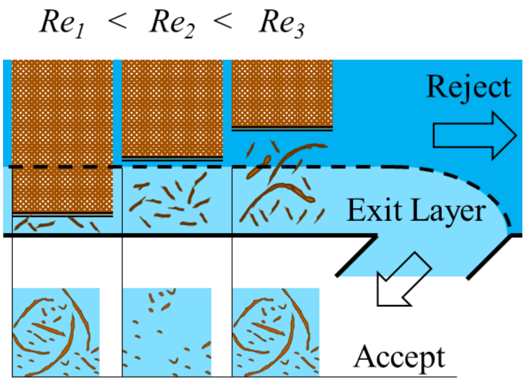

Figure 1. Illustration of the fractionation principle in straight channels. The accept stream is coloured in light blue, the reject stream is dark blue. The exit layer is indicated by the dashed line, and the network interface by a double line. Blocks above illustrate the fibre network. Particles below represent suspended fines and fibres.

Figure 1 illustrates three different cases distinct by the Reynolds number Re: Re_1 (lowest) where the exit layer is within the network, resulting to an exit layer above the network interface. Re_2 where the exit layer is just below the interface allowing best fractionation at large accept flow. Re_3 where the fluid shear is too large leading to fibres torn from the network, which are subsequently suspended in the accept and removed. For a given fibre suspension, the Reynolds numbers *Re* illustrate different flow regimes following Jäsberg and Kataja [14]. Fibres suspended below the exit layer need to turn into the accept [16,17]. A back-facing orientation of the side channels adds to the separation effect.

4 HYDRODYNAMIC FRACTIONATION DEVICE

Fractionation in straight channels is performed with the novel device named: The Hydrodynamic Fractionation Device (HDF). The HDF is sketched in Figure 2a. The channel length is 885 mm. the channel width *H* and channel width *W* can be varied between 3 mm to 15 mm and 9 mm to 9 mm, respectively. The side channel for separation is positioned downstream at 780 mm. The HDF is illustrated in Figure 2a.

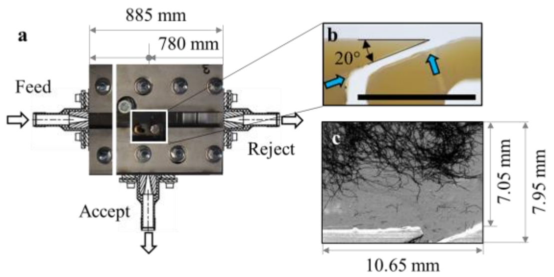

Figure 2. Hydrodynamic fractionation device (a) with magnification on the separation channel (b). Purge water channels are indicated by blue arrows. (c) is a snapshot of the suspension that has been recorded using a high-speed camera.

The side channel is 3D printed allowing a fast change and test of different designs (Figure 2b). Additionally, water purge channels are added to allow removal of stapled fibres. The separation channel is orientated backwards, with an upstream angle of 20°.

HDF fractionation behavior was evaluated based on the resulting (i) grade efficiency $T(l_{Fibre})$, and (ii) the suspension flow characteristics that was quantified from image analysis (see Figure 2c, as well as [17, 18]). Experiments were performed with unrefined chemical sulphite pulp, 100% spruce, bleached and washed, provided by Sappi Gratkorn (Austria). The length-averaged mean fibre length L_1, and the fibre coarseness *cs* were determined to 1.820 mm, and 0.174 mg/m, respectively.

4.1 HDF Fractionation Performance

The effect of geometrical parameters, within the tested range of parameters showed only a weak effect on the grade efficiency [17]. The total fractionation performance was increased with increasing channel width *W*, as larger amount of feed could be processed maintaining the Reynolds number *Re*.

The effect of operational parameters was first evaluated based on the grade efficiency [17]. Findings unveiled a dominating effect of (i) the relative accept flow rate ϕ^{+}, that is the accept relative to the feed, and (ii) the Reynolds number *Re* on the separation efficiency. These effects were studied in detail in a second study with a focus on the flow regime [18]. Figure 3 presents the condensed results from the optical investigation, i.e., the averaged grey intensity over the channel height based on 3600 recorded images per Reynolds number *Re* setting.

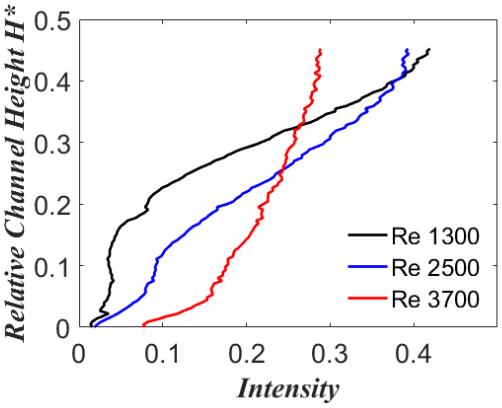

Figure 3. Grey intensity from image post-processing over the channel height normalized with the channel height H. The intensity is proportional to the local fibre concentration.

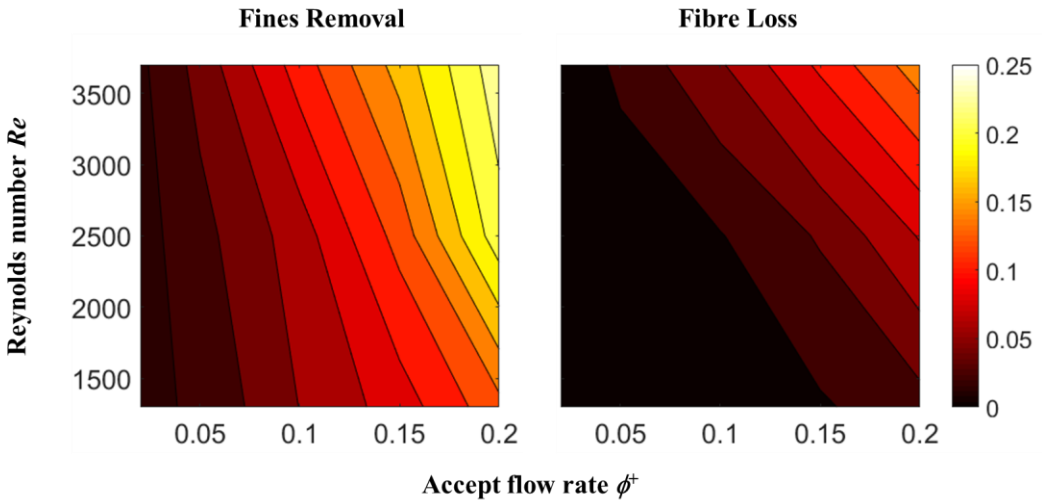

Figure 4. Fines removal and fibre loss characteristics as a function of the Reynolds number *Re* and the accept flow rate ϕ^+.

The significance of Figure 3 is, that it gives qualitative information on the density of the fibre network and the height of the network/suspension interface. For *Re* 1300 and 2500 we find that some fibres are suspended in the gap suspension, while a dense plug of fibres exists near the channel's center. For *Re* 3700 we find the fibres fluidized over the whole channel height.

The grade efficiency was determined for a large array of Reynolds numbers *Re* and relative accept flow rates ϕ^+. Integration of the grade efficiency $T(l_{Fibre})$ between 0.0 mm and 0.2 mm, and 0.2 mm and 5 mm (i.e., the longest fibre fraction considered), resulted in data for the fraction of fibre-fines removed, and the relative amount of fibres lost in the fractionation process. Figure 4 summarizes these results. It allows a direct estimation of the effect of operational parameters on the fines removal and fibre loss. The contour lines for the fines removal (see Figure 4, left panel), were nearly vertical, especially for low accept flow rate Φ^+. This indicates a weak dependency of the fines removal on the Reynolds number *Re*. In contrast the contour lines for the fibre loss were skewed at nearly 45° inclination (see Figure 4, right panel). Thus, fibre loss was found to depend significantly on the Reynolds number *Re*, a fact that originates from the dependence of the flow structure on *Re*. Best fractionation results were found for an HDF operation in the lower right corner of the panels: high accept flow rate, at low Reynolds number.

Whilst Figure 4 allows a direct comparison of fines removal and fibre loss, it needs to be mentioned that such statistical models are only valid in the range of tested parameters. Specifically, the type of pulp and the fibre concentration will affect the fractionation performance.

The effect of the fibre concentration was studied for an increase from 0.1% to 0.2%, thus doubling the crowding number N_{CW}, affecting the network strength. For constant flow rate and geometrical parameters we found a larger extend of the network plug. Thus, to maintain good fractionation, the accept flow rate Φ^+ needs to be adjusted accordingly. The impact of network strength as a such, was however yet not fully investigated. Current studies, following the experimental procedure sketched in Redlinger-Pohn, et.al. [18] include mixture of soft wood and hard wood pulp to change fibre network strength.

ACKNOWLEDGEMENTS

The authors gratefully acknowledge the industrial partners Sappi Gratkorn, Zellstoff Pöls AG, Norske Skog Bruck, and Mondi Frantschach, the Austrian Research Promotion Agency (FFG), COMET, BMVIT, BMWFJ, the Country of Styria, and Carinthia for their financial support of the K-project FLIPPR.

REFERENCES

[1] W.W. Sampson. The structural characterisation of fibre networks in papermaking processes – A review. 12th Fun. Res. Symp., Oxford, 1205-1288, (2001)

[2] R.W. Gooding. The passage of fibres through slots in pulp screening. Master thesis, The University of British Colombia (1986).

[3] S.J.S. Qazi, M. Mohamad, J.A. Olson, D.M. Martinez. Multistage fiber fractionation of softwood chemical pulp through smooth-hole screen cylinders and its effect on paper properties. *Tappi J.* **14**:216–224 (2015).

[4] M. Karjalainen. Studies on wheat straw pulp fractionation: fractionation tendency of cells in pressure screening, hydrocyclone fractionation and flotation. PhD thesis, University of Oulu (2015).

[5] J.D. Redlinger-Pohn, M. Grabner, P. Zauner, and S. Radl. Separation of cellulose fibres from pulp suspension by froth flotation fractionation. *Sep. Pur. Tech.* **169**:304-313 (2016).

[6] R. Andersson, and H. Vomhoff. Evaluation of a novel hydrocyclone design for pulp fractionation. *Nord. Pulp Pap. Res. J.* **27**:151-158 (2012).

[7] R.J. Kerekes, and C.J. Schell. Characterization of fibre flocculation regimes by a crowding number. *J. Pulp Pap. Sci.* **21**(1):J32-J38 (1992).

[8] B. Derakhshandeh, R.J. Kerekes, S.G. Hatzikiriakis, and C.P.J. Bennington. Rheology of pulp fibre suspension: A critical review. *Chem. Eng. Sci.* **66**:3460-2470 (2011).

[9] S.G. Mason. Fibre motions and flocculation. *Tappi J.* **37**(11):494-501 (1954).

[10] R.M. Soszynski. The formation and properties of coherent flocs in fibre suspension. PhD thesis, The University of British Colombia (1986).

[11] D.M. Martinez, K. Buckley, S. Jivan, A. Lindström, R. Thiruvengadaswamy, and J.A. Olson. Characterizing the mobility of papermaking fibres during sedimentation. 12th Fun. Red. Symp., Oxford, 225-254, (2001)

[12] B. Norman, K. Moller, R. Ek, and G.G. Duffy. Hydrodynamics of papermaking fibres in water suspension. 6th Fun. Res. Symp., London, 195-250, (1977).

[13] G. Hemström, K. Moller, and B. Norman. Boundary layer studies in pulp suspension flow. *Tappi J.* **59**: 115-118 (1976).

[14] A. Jäsberg, and M. Kataja. New Experimental Results on The Flow Regimes in Closed Channel Flow of Wood Fibre Suspensions. 14th Fun. Res. Symp., Oxford, 161-180, (2009).

[15] B. Steenberg, B. Sandgren, and D. Wahren. Studies on pulp crill – Part 1. Suspended fibrils in paper pulp fines. *Sven. Papperstidning* **63**: 395-397 (1960).

[16] J.A. Olson. The effect of fibre length on passage through narrow apertures. PhD thesis, The University of British Colombia (1996).

[17] J.D. Redlinger-Pohn, J. König, and S. Radl. Length-selective separation of cellulose fibres by hydrodynamic fractionation. Submitted to *Chem.Eng.Res.Des.* (2017).

[18] J.D. Redlinger-Pohn, W. Bauer, and S. Radl. Fractionation of fibre pulp in a hydrodynamic fractionation device: influence of Reynolds number and accept flow rate. 16th Fun.Res.Symp., Oxford, (2017).

Bleached pulp production from old corrugated carboards – kraft cooking of fiber mixtures modeling carboards.

LUCAS DOLLIÉ, GÉRARD MORTHA*
and NATHALIE MARLIN

Univ. Grenoble Alpes, LGP2, F-38000
Grenoble, France
CNRS, LGP2, F-38000 Grenoble, France
Agefpi, LGP2, F-38000 Grenoble, France
*Gerard.Mortha@pagora.grenoble-inp.fr

1 INTRODUCTION

Recycling of paper materials is more and more developed and gainful. Nowadays, it mainly consists in producing writing and printing papers from old magazine and newspaper, and corrugated cardboard from brown recovered paper grades.

As reported in previous studies, [1,2], old corrugated cardboard upcycling should offer the possibility to produce high quality product, i.e. bleached cellulose for paper or dissolving pulp applications from a cellulosic resource cheapest than wood. To achieve that, the raw material, i.e. brown old corrugated cardboard (OCC), must be delignified and purified. As first steps, it will be pulped and screened as usual in order to form a contaminant-free brown pulp slurry. Then, conventional Kraft and bleaching pulping processes, normally applied to wood chips, may be carry out to remove lignin and adjust the cellulose properties to the desired products.

But, the composition of OCC is versatile. In particular, the impact of the fibrous composition of the raw material, containing various fibre grades (high quality Kraft fibres and low quality highly lignified fibres and fines from mechanical pulps), on the Kraft cooking process, is unknown.

This myriad of fibre types will be submitted together to the same process. Their behaviour can influence process management and produce delignified pulp of variable quality.

In this study, brown corrugated cardboards have been simulated by mixes of virgin mechanical and Kraft pulp fibers. Then, these fibrous raw materials have been undergoing laboratory Kraft cooking in order to evaluate their cooking behaviour and to give an appreciation of the pulp quality that can be expected.

2 EXPERIMENTAL

2.1 Raw materials

To simulate the fibrous composition of OCC after pulping and screening, two virgin pulps were selected: an unbleached thermomechanical pulp (TMP) produced from a mix of spruce and Douglas pine by a French paper mill producing cardboard; and an unbleached Kraft pulp (KP) coming from Brazil and originating from eucalyptus.

Table 1. Virgin pulp composition and cellulose average DPv.

	Lignin,%	Carbohydrate, %	DPv
KP	3.2	96.3	1194
TMP	30.5	69.5	nm

nm=not measurable

The composition of the Kraft and TMP pulps are fully opposed (Table 1). TMP exhibits a high lignin content, close to wood composition whereas KP, already submitted to Kraft cooking process, has been delignified to a large extent (only 3.2% lignin). Lignin and carbohydrate nature is also very different in KP and TMP substrates since chemical reactions in Kraft process lead to slight oxidation and rather extended depolymerization due to the breakage of ether linkages, [3].

Mixes of known weight ratio of both pulps were prepared by blending in a Lhormagy mixer, at 4% fibre consistency, before drying at room temperature for storage and cooking.

2.2 Laboratory Kraft cooking

All cooking experiments were conducted on 7.8 g of dry raw material into lab sealed autoclaves (85 mL) equipped with temperature regulation, and using the same chemical conditions: liquor on solids ratio=10 L.kg^{-1}; effective alkali (Na_2O)= 20% wt. on raw material and sulfidity (Na_2S)=44% wt. on total alkali.

Cooking program temperature comprises four steps: 1st ramp up from ambient temperature to 110°C, then 1st plateau at 110°C for 10 minutes, another ramp up to 170°C (cooking temperature) and finally the last plateau at 170°C, for 180 minutes before cooling with cold water.

The resulted cooked pulp is washed with four litres of deionised water, then air dried before analyses.

2.3 Pulp and cooking analysis

Cooking yield is determined after pulp weight and moisture determination, Tappi method T 210 cm-13.

Lignin content was performed using the Klason method according to Tappi standard T 222 om-02.

Carbohydrate content was calculated by removing lignin, extractives and ashes content from the weight of cooked pulp.

Ashes and extractives are determined according to Tappi standard T 211 cm-02 and T 204 cm-97 with Acetone, respectively.

Only on cellulosic material with a lignin content inferior to 10% in weight, a cold hollocellulose treatment performed on the pulp sample as studied and described in study [4]. Limiting viscosity number (symbolized [η] in ml.g^{-1}) of a cupriethylendiamine solution was measured as indicated in NF T 12-005. Viscosity, degree of polymerization (DPv) was deduced via the empirical equation from [5]

$$DP_v = \left(0.75 \times [\eta] \right)^{0.905}$$

RESULTS AND DISCUSSION

2.4 Kraft cooking of 100% TMP and 100% KP (no mix)

TMP and KP were submitted to the laboratory Kraft cooking, alone (no mix), as described in paragraph 2.2.

Table 2. Pulp composition, pulp yield and cellulose DPv after cooking.

	KP	TMP
Lignin, %	0.6	1.2
Carbohydrate, %	78.9	38.6
Yield, %	79.5	39.8
DPv	470	910

The cooking of the Kraft pulp fibres leads to singular results. Residual lignin was almost totally removed (less than 1% after cooking) but at the expense of carbohydrates. Indeed, large amount of carbohydrates are lost as shown by the rather low yield (79.5 %) and by the strong cellulose average DPv reduction (from 1194 to 470). Usually, full delignification of Kraft pulp is not made by cooking but rather by bleaching. As expected, there is no benefit or interest to overcook an unbleached Kraft pulp.

TMP cooking results are quite different. Fibres are well delignified since at the end of the cook the amount of residual lignin is close to 1% (1.2%). Carbohydrates are partially depolymerised and dissolved, leading to 39.8% pulp yield and to a cellulose DPv of 910. Carbohydrates of TMP are less damaged than those of Kraft pulp but compared to wood chips, with same chemical composition, the yield is significantly lower (39.8 vs 45-50 % for wood chips cooking). Because delignification and carbohydrate degradation kinetics are similar in wood chips and TMP fibres (results not shown), the behaviour difference may be explained by the better accessibility of chemicals in fibres, i.e. easy mass transfer of chemicals.

To simulate OCC cooking, the cooking of various mixtures containing TMP and Kraft pulps was studied and results are presented in the following paragraph.

2.5 Kraft cooking of TMP and KP mixes

A panel of six different mixes of TMP and KP containing from 0 to 100 % TMP were prepared and cooked in the same condition. Despite the strong variation of the initial lignin content of the untreated mixes (3.2 to 30%, depending on the TMP/KP ratio), after cooking residual lignin is very low (around 1%) whatever the pulp mixture, with a maximum variation of 0.8% (Figure 1). These results confirm that TMP/KP fibre mixtures could be easily fully delignified, which augurs that OCC could replace wood for bleached pulp production.

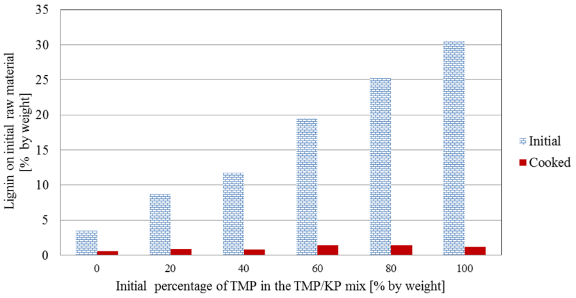

Figure 1. Lignin content before and after Kraft cooking of different TMP/KP pulp mixtures.

Unfortunately, in parallel to the delignification, the cooking yield decreases with the increasing amount of TMP in the pulp mix (Figure 2). The yield loss evolution is explained firstly by the delignification since higher the TMP fraction in the mix, higher the initial lignin content and thus higher lignin removal is; and secondly by carbohydrates degradation and dissolution, more pronounced in the mixtures containing the highest TMP fractions (results not shown).

Moreover, as shown in part 3.1, the repetition of the Kraft cooking process on the KP fraction is responsible for a strong carbohydrate depolymerisation which impacts the cellulose average DPv of the pulp mix after cooking (Figure 3). The KP fraction governs the final cellulose DPv of the pulp and huge variations are observed depending on the KP and TMP fractions (500<DPv<900). Finally, using these cooking conditions, only low cellulose DPv pulp could be obtained. Optimisation of cooking conditions (less aggressive conditions) should be tested to increase the DPv before studying bleaching and purification operations.

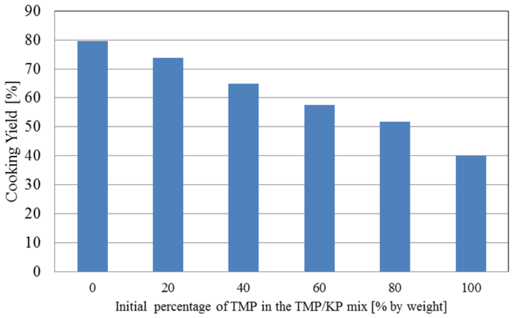

Figure 2. Kraft cooking yield of different TMP/KP pulp mixtures.

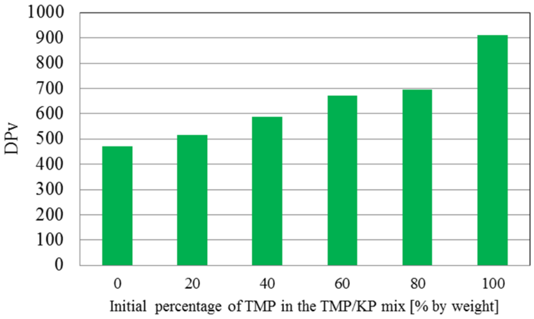

Figure 3. Cellulose average DPv after Kraft cooking of different TMP/KP pulp mixtures.

3 CONCLUSION

Kraft cooking of 100% TMP or 100% KP leads to different delignified pulps. TMP cooking is similar to wood chips standard Kraft cooking even if the global yield is lower, while KP, already partially delignified, loses huge amounts of carbohydrates leading to pulp with very low cellulose DPv.

The global behaviour of the mixes can be seen as a linear combination of the two pure TMP and KP raw materials.

These first cooking trials show that the Kraft cooking process could successfully delignify TMP/KP mixtures but attention should be paid to the resulting cellulose DPv since carbohydrates of the KP fraction are very sensitive to depolymerisation. Thus the cooking conditions should be adjusted to the pulp proportion of the mix; in particular, light cooking conditions should be preferred in the case of mixture containing high Kraft pulp fraction.

4 ACKNOWLEDGEMENT

This work has been partially supported by the LabEx Tec 21 (Investissements d'Avenir-grant agreement n°ANR-11-LABX-0030).

This research was made possible thanks to the TekLiCell platform funded by the Région Rhone-Alpes (ERDF: European regional development fund).

5 REFERENCES

[1] L. Sunyoung, W. T. McKean and R. R. Gustafson. Manufacture of Bleached Pulp from Recycled OCC Linerboard. Pulping Conference 1996, Nashville, vol. 2, 885-893 (1996).

[2] Y. Ma, M. Hummel, M. Määttänen, A. Särkilahti, A. Harlin and H. Sixta. Upcycling of waste paper and cardboard to textiles. *Green Chemistry* **18**(3):858-866 (2016).

[3] H. Sixta, J. Handbook of pulp. Wiley-VCH Verlag GmbH, (2006).

[4] G. Mortha, J. Marcon, D. Dallérac, N. Marlin, C. Vallée, N. Charon and A. Le Masle. Depolymerization of cellulose during cold acidic chlorite treatment. *Holzforschung* **69**(6): 731–736, (2015).

[5] H. Sihtola. Comparison and conversion of viscosity and DP values determined by different methods. *Paperi Ja Puu* **45** (Specialnummer 4a): 225–323, (1963).

Mineralisation of Cellulosic Structures

BIRGIT LUTSCH, MARTIN ZAHEL and TIEMO ARNDT

Papiertechnische Stiftung, Germany
birgit.lutsch@ptspaper.de

1 MOTIVATION

Mineral fillers are indispensable in many industrial branches and are used in a variety of different materials. In plastic technology they act as a classic extender to lower the costs of the production process but also as "active fillers" to improve the property profile, including mechanical and optical properties. [1,2] In the paper industry, fillers are also used to reduce raw material costs and to adjust the optical as well as surface properties. [3]

However, fillers entail the problem that their application quantity is sharply limited. Inorganic fillers show no binding properties. They reduce the product strengths during higher use and lead to complications in the further processing of the products (e. g. increased dust propensity during the packaging and printing processes). [1,2,3]

In order to expand the use of fillers and their positive effects on varying products and prevent the negative effects of the material in parallel, mineralised cellulosic structures should be created for versatile applications in different branches of industry.

1.1 Initial Situation

The compounding of carbonates with micro- or nanofibrillar cellulose, which is produced by chemical-mechanical degradation of the fibre wall into its basic constituents, has gained particular attention, since the material properties of these compounds permit various applications beyond paper production such as plastic and filter production (foam forming processes). [4,5]

Disadvantage of previously used processes for composite production (precipitation reactions by means of $Ca(OH)_2$ and CO_2 or co-grinding of carbonates with cellulose) is that there is no binding between cellulose and fillers. Rather, a mechanical accumulation of the inorganic species into fibrillar cellulosic structures is formed which compensate for the loss of strength in the paper during conventional PCC application, but no longer contribute fully to light scattering and thus to an increase in opacity. [6,7,8,9]

1.2 Objectives

To overcome this problem, we develop a process for the mineralisation of microfibrillar cellulose by the precipitation and irreversible binding of $CaCO_3$ on the nanostructure of the cellulosic fibre wall. To ensure high efficiency, we use the high consistency conditions in a twin-screw extruder. The chemical pre-treatment of the cellulose and the application of a double exchange reaction are said to favour the ionic bond to the functional groups of the cellulose.

2 MATERIALS AND METHODS

2.1 Principle of precipitation from saturated solutions

During the precipitation of calcium carbonate from saturated solutions of calcium halides and alkali metal carbonates PCC modification can be controlled by careful adjustment of the precipitation conditions:

Equation 1. Double exchange reaction for $CaCO_3$ precipitation from saturated solutions

$$CaCl_2(aq) + M_2CO_3(aq) \rightarrow CaCO_3 \downarrow +2MCl(aq)$$
$$with\ M_2 = Na_2, K_2, NH_4, NaH$$

In detail, a saturated $CaCl_2$ solution is initially provided and a solution of varying carbonates, such as Na_2CO_3, K_2CO_3, NH_4CO_3, $NaHCO_3$, is added.

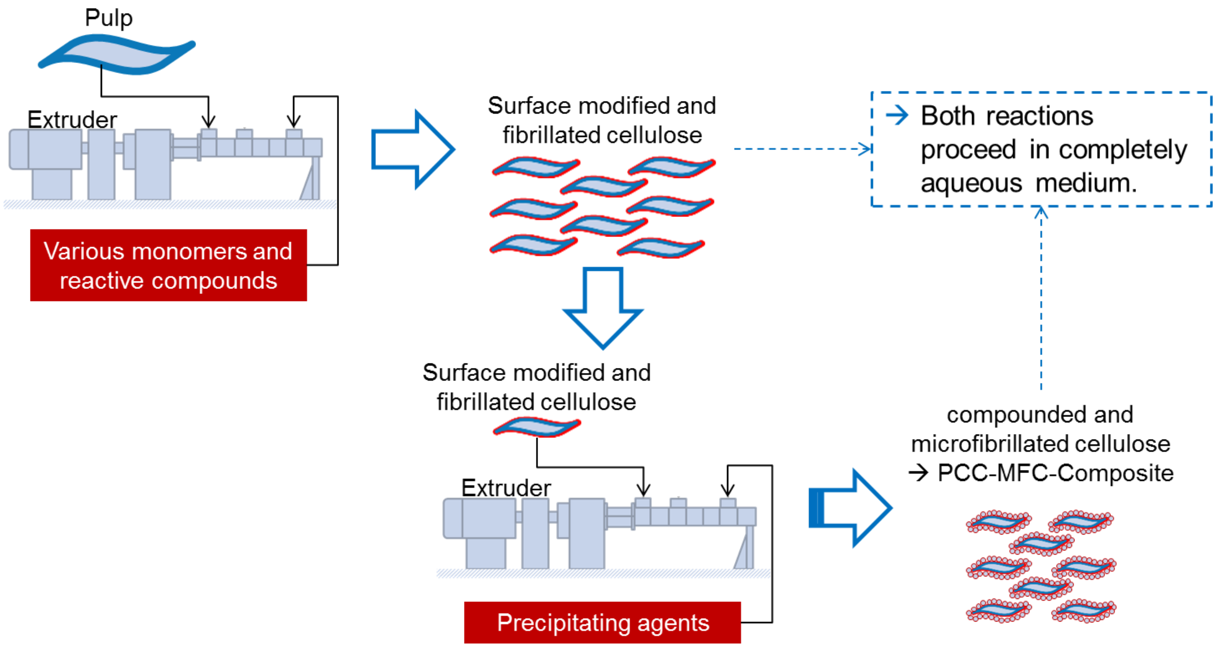

Figure 1. Schematic representation of reactive extrusion for chemical-mechanical cellulose treatment and in-situ PCC precipitation

During the mixing process of the two reagents, ACC (amorphous $CaCO_3$) is formed immediately. Due to its instability, it crystallizes rapidly into different polymorphs, all of which show different product properties, such as density and stability. It is possible to control the $CaCO_3$ modification (aragonite, calcite, vaterite) and crystal form (scalenohedral, rhombohedral, prisms, etc.) using different reaction parameters (temperature, pH, solution composition, mixing speed of the reactants and degree of supersaturation). The crystal modification can be set particularly by the adjustment of the temperature. [10]

Likewise, the fibre fractionation and the extent of the cellulose modification (for example carboxymethylation) as well as the charge of the fibre and the substrate surface roughness have an influence on the precipitation and compound formation. [11,12]

The advantage of the double exchange reaction of $CaCl_2$ with Na_2CO_3 in a fibrous material suspension is that up to 78 % of the precipitated $CaCO_3$ can be irreversibly bound in the fibre lumen and in the pores of the fibre wall even after washing. [13]

2.2 Platform technology reactive extrusion

Our concept for the mineralisation of cellulosic structures involves the mechanically (fibrilling) and chemically modification and pre-treating (e. g. carboxymethylation) of the cellulose in the extruder under varying conditions prior to the carbonate precipitation so that surface modified, fibrillated cellulose (i.e. CMC) is available for subsequent process steps. This is charged in a second extruder pass with saturated $CaCl_2$ solution and the abovementioned precipitation reagents. Thus, the fibrillated cellulose is converted to MFC and simultaneously the $CaCO_3$ is precipitated on the nanostructure of the cellulosic fibre wall and irreversibly bound. This process of PCC-MFC-Nanocomposite production in its individual steps is schematically illustrated in figure 1. An additional advantage of the process is that both steps take place in completely aqueous medium.

3 RESULTS

First attempts of PCC precipitation from $CaCl_2$ and Na_2CO_3 solution on unmodified fibres show that the precipitated PCC quantity can be controlled as expected with the reactant concentration as well as the volumetric flow in the extruder (dependency, see Figure 2). Until now, up to 45 % of PCC mass components in the composite could have been achieved.

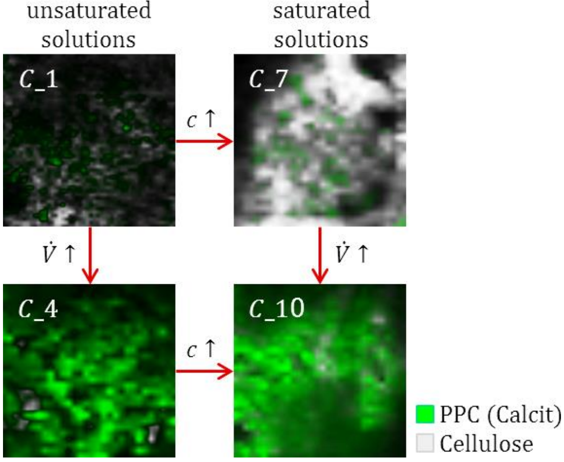

Figure 2. Filler distributions as a function of volume flow and concentration during extrusion with salt solutions (fibres in gray, PCC in green) – Raman-Imaging pictures

By the extrusion, rhombohedral calcite crystal forms with a size between 0.4 µm and 1.5 µm are formed. They adhere mainly to the fibre matrix and accumulate to agglomerates. By means of SEM images, it is shown that the fibres are fibrillated by the extrusion. They are being shortened by about 33 % of the original fibre length to a length-weighted contour fibre length of an average 0.69 mm. They are located in a defibrated state and are assembled into tissue-like structures (see Figure 3).

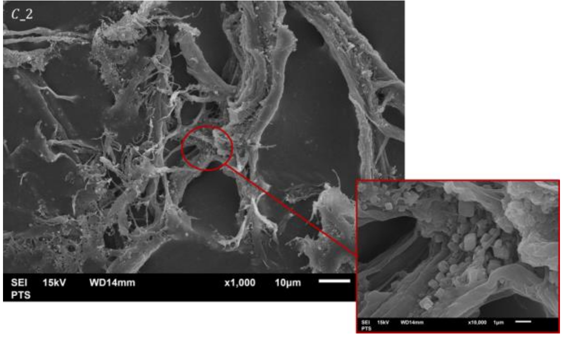

Figure 3. SEM image of a composite (C_2) after extrusion precipitation

For the assessment of the amount of the $CaCO_3$ crystals, which are irreversibly bound to the fibres, the samples are tested for the washing out behaviour in a wash cell (Figure 4). Up to now, approximately 15-30 % of the PCC has been irreversibly bound to the fibres, since the majority of it is precipitated into the aqueous phase. In order to counteract this problem in the course of the project, the fibre material is first to be chemically-mechanically modified and the PCC is to be precipitated in the second step.

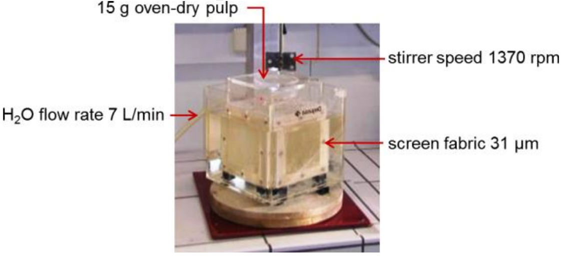

Figure 4. Washing tests for evaluation of filler bonding (10 min wash time)

First experiments on the use of composites in lab sheet formation show considerable improvements in properties. For example, through the use of 20 % composite (based on the total fibre stock) the tensile strength and the modulus can be increased by 50 % compared to a paper of long fibre pulp and commercial PCC (target sheet composition of 75 % pulp + 25 % total PCC). The breaking elongation is also increased by 30 % (see Figure 5).

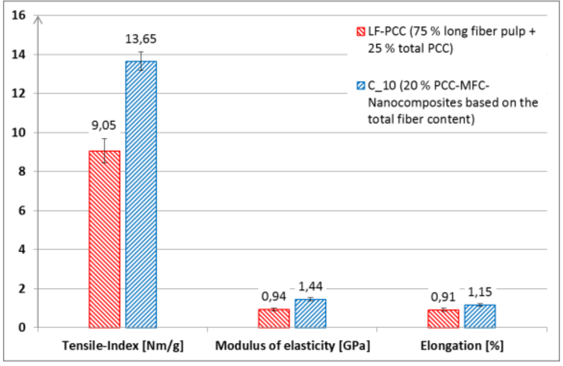

Figure 5. Strength properties of laboratory sheets of conventional formulation compared to laboratory sheets with PCC-MFC-Composite content of 20 %

Improvements are also found in the optical sheet properties (Figure 6). Through the composite insert, the light scattering coefficient is raised so that the whiteness increases as well and the opacity remains at the conventional level.

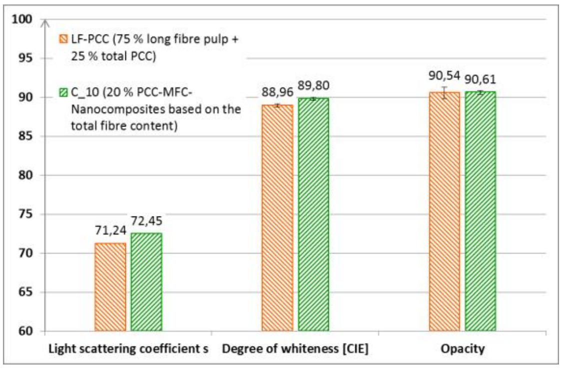

Figure 6. Optical properties of laboratory sheets of conventional formulation compared to laboratory sheets with PCC-MFC-Composite content of 20 %

4 POTENTIAL OF MINERALISED CELLULOSIC STRUCTURES

$CaCO_3$ particles as well as cellulose fibres are used in manifold fields, for example in environmental, biological and process engineering as well as other techniques. The potential offered by the novel process for the mineralisation of cellulose and the PCC-MFC-Nanocellulose thus developed is correspondingly versatile.

In the field of papermaking, it is the goal and could be demonstrated in the first experiments that various paper properties such as strength and optical properties can be improved with the aid of mineralised cellulose. The filler content in the paper can also be increased so that a reduction of the raw material use as well as the production costs is possible. [8,9,14]

The application of PCC-MFC-Cellulose is also conceivable in the field of plastics. In NFC (Natural Fibre Composites) and WPC (Wood Plastic Composites) as well as in PVC products, they can be used for strength and stiffness enhancement. Furthermore, fibres and $CaCO_3$ reduce the shrinkage of the plastic products and improve their optical properties. Accordingly, it is a cost-effective possibility to adapt and improve different plastic products both optically and mechanically. [1,2,15]

A further idea is to use PCC-MFC-Nanocellulose in plaster for lightweight plaster walls. With the help of the composites, it should be possible to increase the porosity and the volume of the material and thus to achieve a weight reduction with constant component dimensions. In addition, the fibre network can increase the strength of the plaster walls.

Foamforming offers the possibility to develop new fibre based products as well as to reduce production costs and environmental impacts. [16,17] It promises an ideal application for mineralised cellulose, as its surface properties support the voluminous formation of paper or fleece, reduces the material weight and increases air permeability. In addition, the composite increases the strength and optical properties of the products.

5 CONCLUSION

First experiments show that it is possible to modify fibres both chemically and mechanically in a twin screw extruder. Furthermore, it can be seen that an in-situ precipitation of PCC can be carried out by means of a double exchange reaction of saturated $CaCl_2$ solution and alkali metal carbonate solutions with simultaneous fibrillation of pulp to MFC in an extruder, although there are still research needs in the area to control the precipitation product properties and the composite properties.

The promising use of PCC-MFC-Composites in paper shows the positive influence the newly developed composites can have on the material properties. In the course of the project, the application and impact of the composite will be investigated in other materials, including plastics, plaster walls and foam-forming products.

REFERENCES

[1] P. Eyerer, T. Hirth and P. Elsner. Polymer Engineering - Technologien und Praxis, Springer-Verlag Berlin Heidelberg (2008)

[2] N.N. Technische Kunststoffe – Das Handbuch, Ensinger GmbH (2012)

[3] J. Blechschmidt. Taschenbuch der Papiertechnik. Fachbuchverlag Leipzig (2013)

[4] P. Silenius. Improving the combinations of critical properties and process parameters of printing and writing papers and paperboards by new paper filling methods. PhD thesis, Helsinki University of Technology (2003)

[5] R. Subramanian, H. Fordsmand and H. Paulapuro. Precipitated Calcium Carbonate (PCC) – Cellulose composite fillers; effect of PCC particle structure on the production and üproperties of uncoated fine paper. BioResources – PCC-cellulose composite fillers 2(1):91-105 (2007)

[6] N.N. FiberLean Technologies – Innovative by nature, data sheet from FiberLean Technologies Ltd, an Imerys and Omya Venture (2016)

[7] Patent: WO 2014174155 A1. A method of providing fiber web making furnish with filler, and paper or paper board. Wetend Technologies Oy, Stora Enso Oyj (2014)

[8] T. Schmid. Ermittlung von Reaktionsbedingungen zur Erzeugung von gefällten Calciumcarbonat-Cellulose-Nanocompositen in einem Extruder. Bachelor thesis, Dresden University of Applied Sciences and PTS (2015)

[9] C. Schalm. Einsatz von gefällten Calciumcarbonat-Cellulose-Nanocompositen in der Papierherstellung, Diploma thesis, Dresden University of Technology and PTS (2016)

[10] Q. Shen, H. Wei, Y. Zhou, Y. Huang, H. Yang, D. Wang and D. Xu. Properties of Amorphous $CaCO_3$ and the Template Action of Vaterite Spheres. The Journal of Physical Chemistry B. 110(7):2994-3000 (2006)

[11] C. Vilela, C. Freire, P. Marques and T. Trindade. Synthesis and characterization of new $CaCO_3$/cellulose nanocomposites prepared by controlled hydrolysis of dimethylcarbonate. Carbohydrate Polymers 79:1150-1156 (2010)

[12] A. Declet, E. Reyes and O.M. Suárez. Calcium Carbonate Precipitation: A review of the carbonate crystallization process and applications in bioinspired composites. Reviews on advanced materials science 44:87-107 (2016)

[13] M. Ciobanu, E. Bobu and F. Ciolacu. In-situ cellulose fibres loading with calcium carbonate precipitated by different methods. Cellulose Chemistry & Technology 44(9):379-387 (2010)

[14] R. Subramanian. Engineering fine paper by utilising the structural elements of the raw materials. PhD thesis, Helsinki University of Technology (2008)

[15] D. Vogt, M. Karus, S. Ortmann, C. Schmidt and C. Gahle. Wood-Plastic-Composites (WPC) Holz-Kunststoff-Verbundwerkstoffe – Märkte in Nordamerika, Japan und Europa mit Schwerpunkt auf Deutschland – Technische Eigenschaften – Anwendungsgebiete – Preise – Märkte – Akteure. Studie, nova-Institut GmbH, Hürth (2006)

[16] E. Hellén. Foam forming at VTT. VTT Technical Research Centre of Finland – Forest industry, Espoo (2013)

[17] M. Bulota, B. Maasdam and S. Tiekstra. Breakthrough technologies – More with less. Kenniscentrum Papier en Karton, Arnhem (2013)

Removal of mineral oils from newspapers and folding boxboard using supercritical CO_2

S. RUNTE, A. KERSTEN and
S. SCHABEL

TU Darmstadt, Paper Technology and
Mechanical Process Engineering (PMV)
runte@papier.tu-darmstadt.de

1 INTRODUCTION

Paper for recycling is with 64 % the most important raw material in the German paper industry [1]. In food industry, most of the used packaging products are completely or at least partially made from recycled fibers.

Mineral oils are introduced in the paper cycle from printing inks and paper converting processes. Consequently, they arise in the raw material for the production of new paper and board products [2]. Due to their toxicological properties and their potential to migrate from packaging into wrapped food they need to be removed from the recycling loop [3].

First extraction trials with supercritical carbon dioxide ($scCO_2$) have shown that it is possible to extract mineral oils from newspapers up to 100 % [4].

2 SUPERCRITICAL CO_2

The physical state of carbon dioxide (CO_2) depends on its temperature and pressure. The three states of aggregation solid, liquid or gaseous are differentiated by sublimation, melting and vapor pressure curves as shown in the phase diagram in Figure 1. At the end of the vapor pressure curve the critical point is reached at a pressure of 74 bar and a temperature of 31 °C. Above this point, CO_2 occurs in supercritical state and combines the characteristics of the gaseous and the liquid phase. Thus, the CO_2 reaches the dynamic viscosity as well as the diffusion coefficient of the gaseous state and the density level of liquid CO_2 [5]. Hence, $scCO_2$ has very good penetration and transport properties [6].

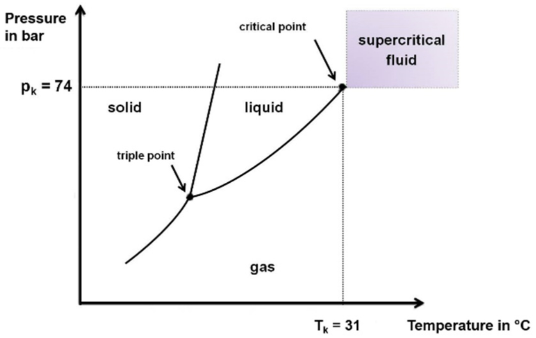

Figure 1. Phase diagram of CO_2, based on Goedecke [5].

3 MATERIAL AND METHODS

3.1 Samples

Here offset-coldset printed newspapers (NP) and uncoated folding boxboard (FBB) were investigated. Both samples were made of 100 % recycled fibers.

The initial mineral oil content (chain length C10 – C25) was around 4500 mg/kg and 1000 mg/kg in the reference newspaper and folding boxboard respectively. All products were wrapped in aluminium foil to prevent evaporation of the mineral oils.

The samples were cut into strips and subsequently shredded into 20 mm • 5 mm pieces in order to fill them into the extractor.

3.2 High Pressure Extraction Test Rig

At PMV, a high pressure extraction test rig produced by Eurotechnica GmbH is available. The extraction plant is designed with an extractor volume of 0.5 liters and a CO_2-recirculation system. The maximal adjustable extraction conditions are 500 bar and 120 °C. A simplified flow diagram of the test rig is shown in Figure 2. Forced by the piston pump the CO_2 flows in liquid state from the CO_2 cylinder in the extractor and is compressed there. The jacket of the extractor is heated to reach the desired temperature of the CO_2. Pressure sensors at the extractor inlet and outlet and a temperature sensor inside the extractor control the extraction conditions. After the extraction, the CO_2 flows in supercritical state through the back pressure valve and is expanded afterwards to the level of the CO_2 recirculation supply. Thus, a phase separation of CO_2 and the absorbed extract takes place and the CO_2 changes to the gaseous state. At the bottom of the separator the liquid extract can be collected. The regenerated CO_2 flows through a flow meter in a cooled buffer. The CO_2 changes into liquid aggregation state and can recirculate to the piston pump for further extractions.

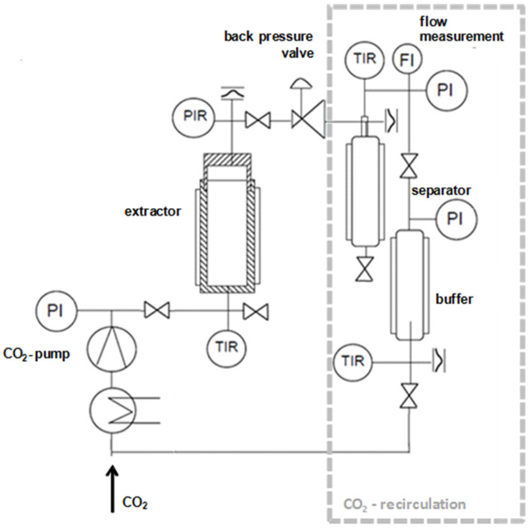

Figure 2. Flow diagram of extraction plant HPE lab500 [7].

4 RESULTS

It has already been shown [4] that the process parameters pressure, temperature and CO_2-amount as well as the moisture content of the extracted product have an essential effect on the extraction efficiency of mineral oils. This paper will show the influence of the extracted product itself by extracting newspapers (printed) and folding boxboard (unprinted).

Figure 3 shows the extraction efficiency of mineral oils regarding to the initial content in the reference samples using up to 35 $kg_{CO2}/kg_{product}$. The extraction conditions are set to 100 bar and 40 °C as well as 400 bar and 90 °C. The best-fit curve was calculated by using the Microsoft Excel Program "Solver".

Using 5 kg_{CO2}/kg_{NP}, more than 90 % of mineral oils are extracted from the newspaper sample (orange graph). By raising the CO_2 amount to 25 kg_{CO2}/kg_{NP}, more than 99 % of mineral oils are removed. Due to the very good solubility of mineral oils in $scCO_2$, a low specific volume of CO_2 is sufficient for an efficient removal of mineral oils from newspaper.

Regarding the blue graph, extraction conditions of 100 bar and 40 °C are not sufficient to extract the total amount of mineral oils from unprinted folding boxboard. In contrast to the extracted newspaper, only 50 % of the mineral oils are extracted using 2.5 kg_{CO2}/kg_{FBB}. Furthermore, after increasing the CO_2 amount to 35 kg_{CO2}/kg_{FBB}, the extraction curve approached a maximum removal of 80 %.

By raising the pressure and temperature to 400 bar and 90 °C respectively (purple graph), the extraction efficiency of mineral oils from folding boxboard increases. Using these extraction conditions and an amount of 12.5 kg_{CO2}/kg_{FBB}, a maximum removal of around 92 % is reached. Raising the CO_2 amount to 25 kg_{CO2}/kg_{FBB} shows no improved extraction efficiency.

Compared to the freshly printed newspaper, the mineral oils might be bound differently in the unprinted folding boxboard sample. The mineral oils in the newspaper sample originate primarily from the used offset-coldset printing ink and are mainly applied on the surface of the paper. However, the mineral oils in the folding boxboard sample originate completely from the mineral oil contaminated paper for recycling. These were recycled at least once and the mineral oils are bound within the produced board product.

5 CONCLUSION

This paper has shown, that it is possible to extract mineral oils from paper for recycling using supercritical CO_2. Besides the extraction conditions like pressure and temperature, the extracted recycling paper product itself has a huge impact on the extraction efficiency. Depending on the product, the extraction conditions must be optimized individually to remove the total content of mineral oils from the products.

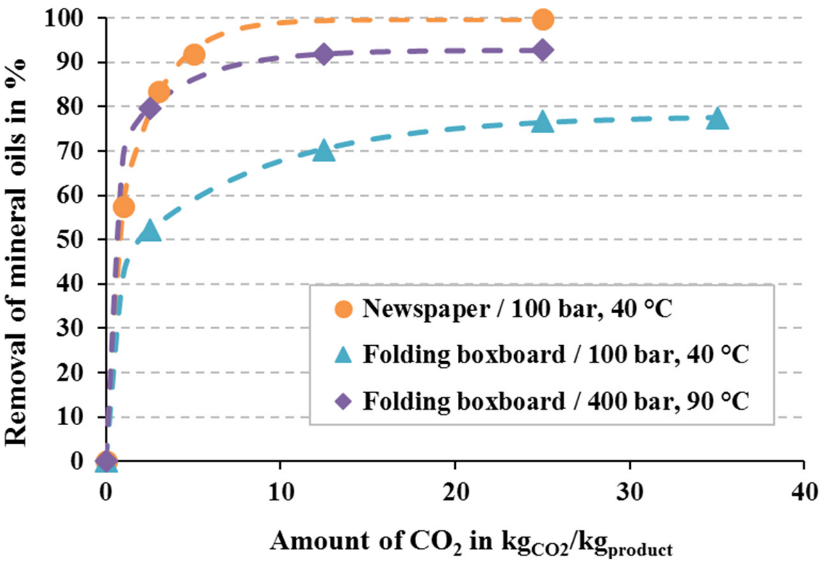

Figure 3. Extraction of mineral oil compounds (C10-C25) from newspaper and folding boxboard at different extraction parameters.

REFERENCES

[1] „Papier 2016 – ein Leistungsbericht“. Verband Deutscher Papierfabriken e.V., Bonn, (2016).

[2] H.-J. Putz, A. Kersten and S. Schabel. Anorganische und organische Inhaltsstoffe in Papier - Vorkommen, Quellen und Senken. Müll-Handbuch. Berlin, 1-36 (2012).

[3] BfR-Stellungnahme 008/2010 vom 09.12.2009: „Übergänge von Mineralöl aus Verpackungsmaterialien auf Lebensmittel“. http://www.bfr.bund.de/cm/343/uebergaenge_von_mineraloel_aus_verpackungsmaterialien_ auf_lebensmittel.pdf. downloaded on 05.05.2017

[4] S. Runte, A. Kersten and S. Schabel. Removal of mineral oils from paper for recycling. *Professional Papermaking.* **13**(1): 46-50 (2016).

[5] R. Goedecke. Fluidverfahrenstechnik - Grundlagen, Methodik, Technik, Praxis, Kapitel 11: Trennverfahren mit überkritischen Fluiden. WILEY-VCH Verlag GmbH & Co. KGaA, Weinheim, 993–1130, (2006).

[6] L.G. Randall. The Present Status of Dense (Supercritical) Gas Extraction and Dense Gas Chromatography: Impetus for DGC/MS Development. *Separation Science Technology*. **17**(1):1–118 (1982).

[7] Eurotechnica: Handbuch zur Versuchsanlage HPE Lab500 (2015).

Evaluating the Feel of Cartons

DANIEL ERIKSSON

Örebro University
School of Science and Technology
daniel.eriksson@oru.se

1 INTRODUCTION

When judging the ripeness of avocados or figs, we have learnt to rely on the sense of touch. By probing for the compliance of these fruits, we can get a feel for if they are ripe or not. A similar process goes on every time you pick up a carton from a shelf. You probe its mechanical properties to judge if there is a risk that it will fail when you lift it. The information you gain may transfer to your judgement of the product as well (cf. [1]). Hence, the mechanical properties of consumer packaging are important not only for protecting its contents, but also for the consumers' perceptions of the products. As a physical embodiment of the brand identity, the package must live up to the expectations of consumers.

From a mechanical point of view, it is important that the package is rigid enough to withstand the forces that consumers will need to use when manipulating the it. By manipulating, I mean the use of the hands to accomplish a change of the state of an object. It could be as simple as moving the package from one point to another, opening it, or extracting its contents.

The aim of this project is to devise a systematic approach to dealing with mechanical design issues related to manual handling of paperboard packages.

2 ANALYZING THE GRASP

In the literature on the haptic sense, an important concept is the exploratory procedure (EP) [2]. The EP is selected to maximize the ability to infer the sought information. In this case, the EP is generally dictated by the manipulation task that is going to be solved. It is often possible to guess the types of grasp that will be used from the task parameters and the physical characteristics of an object [3]. Another strategy could be to use ethnographic studies of consumers.

Once the number of possible grasps has been narrowed down, it is possible to approximate the forces involved by assuming quasi-static conditions.

3 MEASUREMENTS

If the aim is to study the force needed to damage a package during manipulation, I use a simple compression test with a rigid spherical probe on one side of the package and a fixed plate on the other side. This setup is meant to replicate a grasp with all four fingers engaged and thumb opposition. It is possible to measure the slope of the force-displacement curve and compare that for different materials, but if the design of the package is changed, it will be very hard to compare the two results.

While the setup is simple and straightforward to apply, the information gathered is limited, just a relation between force and displacement. Since humans predominantly use cutaneous cues to judge compliance [4], i.e. relating to the deformation of the skin, relying on just force and displacement should not be enough to understand this perception.

With this problem in mind, I have devised a similar test, where the rigid indenter is replaced with a tactile sensor (Figure 1.) with sensory capabilities and mechanical behaviour mimicking the human fingertip [5]. This means that I can now gather information on how the sensor interacts with the surface, and the interaction should be comparable to that of the human fingertip with the package.

A challenge with this method is that it generates a considerable amount of data, which needs to be interpreted. The 22 channels of the tactile sensor have a total sample rate of 4400 Hz. So far, my approach has been to analyse the relations between the applied normal force and the various outputs from the sensor.

Figure 1. Biomimetic tactile sensor.

4 RESULTS

The rigid indenter method works well for measuring the strength of the package, with little sensitivity to the test conditions. On the other hand, the measured stiffness showed a strong dependence on the test conditions [6,7]. The damage pattern produced was visually similar to damage found on packages on the shelves of retail stores.

With the tactile sensor, I have seen that higher bending stiffness translates to a higher static pressure being recorded by the sensor. This result is in line with a previous study where the higher compliance of a rubber surface in contact with the sensor led to a greater static pressure [8]. More specifically, the pressure at a given force is proportional to the logarithm of the bending stiffness.

Damage patterns are similar to the ones observed with the rigid indenter and in a retail environment.

The electrodes of the tactile sensor also give other information about the interaction with the package. It is e.g. possible to learn about the stiffness of an edge of the package in relation to the panel.

Finally, the dynamic pressure signal gives interesting information about the failure event. I have seen that otherwise identical packages that were creased in different ways showed a different amplitude at the point of failure. This event can likely be felt by the consumer, should the package be stressed to failure.

5 ACKNOWLEDGEMENTS

This work was supported by The Knowledge Foundation (KK-stiftelsen) and Stiftelsen Gunnar Sundblads Forskningsfond. Industrial partners are BillerudKorsnäs and Tetra Pak.

REFERENCES

[1] J. Peck and T.L. Childers. To have and to hold: The influence of haptic information on product judgments. *J. Mark.* **67**(2):35–48 (2003).

[2] S.J. Lederman and R.L. Klatzky. Haptic perception: a tutorial. *Atten. Percept. Psychophys.* **71**(7):1439–1459 (2009).

[3] T. Feix, J. Romero, H.B. Schmiedmayer, A.M. Dollar, and D. Kragic. The GRASP taxonomy of human grasp types. *IEEE Trans. Hum.-Mach. Syst.* **46**(1):66–77 (2016).

[4] W.M. Bergmann-Tiest and A. Kappers. Cues for haptic perception of compliance," *IEEE Trans. Haptics*. **2**(4):189–199 (2009).

[5] N. Wettels, V.J. Santos, R.S. Johansson, and G.E. Loeb. Biomimetic tactile sensor array," *Adv. Robot.* **22**(8):829–849 (2008).

[6] D. Eriksson, C. Korin, and F. Thuvander. Damage to carton board packages subjected to concentrated loads. 19th IAPRI World Conference on Packaging, Melbourne, Victoria University, 172–182, (2014).

[7] D. Eriksson and C. Korin. How small is a point load? A preliminary study of the deformation and failure of cartons subjected to non-uniform loads. *Packag. Technol. Sci.* **30**(7):309–316 (2017).

[8] Z. Su, J. A. Fishel, T. Yamamoto, and G. E. Loeb. Use of tactile feedback to control exploratory movements to characterize object compliance. *Front. Neurorobotics*, **6**(7) (2012).

INFLUENCE OF MASS DISTRIBUTION ON ELECTRIC BREAKDOWN STRENGTH OF INSULATING PRESSBOARD

MICHAEL VOGEL
Siemens Insulation Center GmbH & Co. KG
vogel.michael@siemens.com

and

HARALD GROSSMANN,
Dresden University of Technology
harald.grossmann@tu-dresden.de

1 INTRODUCTION

Paper and Pressboard made out of pure virgin unbleached kraft pulp has an outstanding importance for liquid immersed high voltage operating equipment like power transformers since the beginning of the 20th century till now [1, 2]. In a high voltage power transformer cellulosic pressboard is applied in a variety of different components, such as stripes, spacers, disks, cylinders and moulded parts. Depending on the specific function of these components in the complex assembly of a power transformer various material properties have to be provided to fulfil the design requirements for assembling, testing and decades of safe and reliable operation. Among other important properties the electric breakdown strength of pressboard barriers plays an important role for operation reliability of a power transformer.

More profound knowledge of the basic functioning and the influencing factors of material properties of high grammage insulating pressboard should offer new options for improvements in designing and manufacturing insulation components and eventually as well in the overall performance of power transformers [1, 2].

Against this background the purpose of this investigation was to evaluate the suitability of different manufacturing processes of high grammage pressboard in terms of electric insulation properties by determining the influence of fibre uniformity on electric breakdown strength.

2 EXPERIMENTS

2.1 Sample preparation

Pressboard samples with different grades of fibre uniformity were prepared using a Rapid-Köthen handsheet former. After forming, the sheets of wet board were pressed and dried using a laboratory hot press. The converting conditions chosen led to an average thickness of 1.05 mm ± 0.05 mm and an average apparent density of 0.93 g/cm³ ± 0.04 g/cm³. Pure unbleached kraft pulp with a freeness of 27 Schopper-Riegler numbers was used as raw material for all samples. These are typical characteristics of a low density pressboard. To conduct further processing square specimens of 100 mm x 100 mm were taken out of the middle of the handsheets and their basic properties were measured according to ISO 187 and ISO 534 respectively. For each board grade a set of 16 single samples was produced and examined as follows.

2.2 Evaluation of mass distribution

Mass distribution of the pressboard samples was measured using X-ray adsorption of the sample material. The measuring system consisted of an X-ray tube and a corresponding sensor to detect transmission of X-ray through the sample at discrete positions. Mass distribution data was collected and recorded over the entire surface of the sample automatically by moving the sample between the X-ray source and the transmission detector with the help of an automated XY-table. Thus the mass distribution could be examined in a quick and accurate way. After filtering, the obtained values have been converted to a resolution of 0.25 mm x 0.25 mm to get round numbers for interpretation. These values further on are named as “discrete measured values”.

2.3 Electric breakdown strength

The short-time breakdown strength (AC) according to IEC 60243-1 was measured on the vacuum dried and mineral oil (Nynas Nytro 4000x) impregnated samples to evaluate the electric strength of the produced samples. The test setup was equipped with unequal electrodes with diameters of 75 mm and 25 mm respectively. The samples were positioned centrically between the electrodes. Figure 1 show the test setup according to IEC 60243-1.

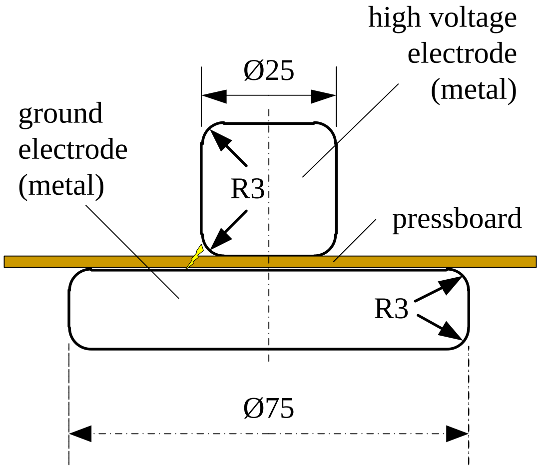

Figure 1. Used test setup for determination of electric break down strength [3]

Breakdown strength and water content of the mineral oil used were measured before and after the trials to make sure that the test conditions complied with the standard.

3 RESULTS

3.1 Mass distribution

The radiometric analysis provides a qualitative impression of the fibre uniformity of high grammage boards, similar to an optical inspection of a thin paper via light transmitting, as well as the corresponding data for a statistical evaluation.

Figure 2 shows representative examples of the 2D-charts obtained for the 5 different board grades produced. The colour code for deviation around the mean value of grammage of the individual samples in figure 2 has been chosen identical for all grades.

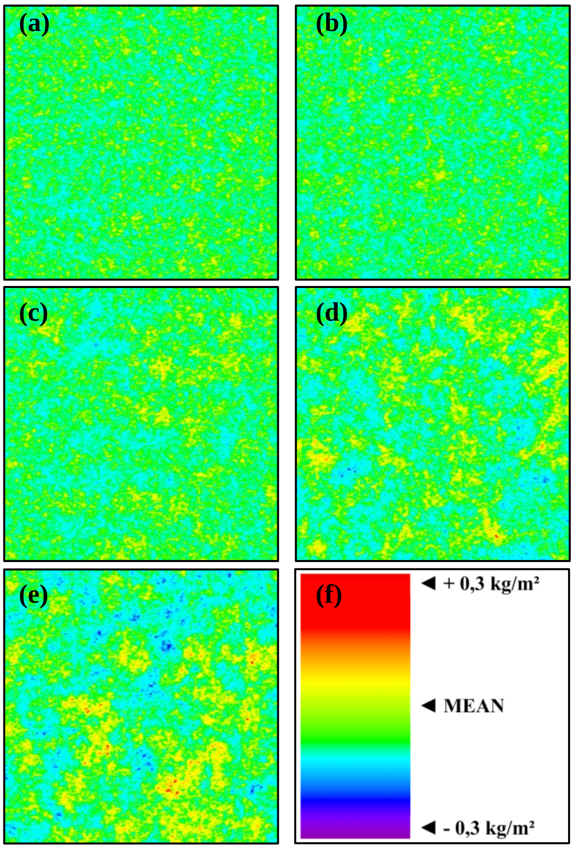

Figure 2 (a–f). 2D-Visualisation of fibre uniformity of pressboard grades (a)–(e) over the entire samples area of 100 mm x 100 mm. The used colour code for all samples is shown in chart (f).

Hence, the uniformity of the different board grades can directly be compared.

For a statistical evaluation of the different board grades the relative standard deviation (RSD) of fibre mass distribution of the samples was examined as well. Figure 3 shows the RSD of grammage distribution, in which different integration areas were chosen. The error indicators in figure 3 show the range of the RSD values determined for each test series with 16 individual samples.

As it could be expected, figure 3 shows that the RSD of mass distribution decreases with increasing integration area. What can also be observed is that the gradient of change of RSD of mass distribution over the different board grades depends on the integration area considered, if the same total area of the entire samples is examined.

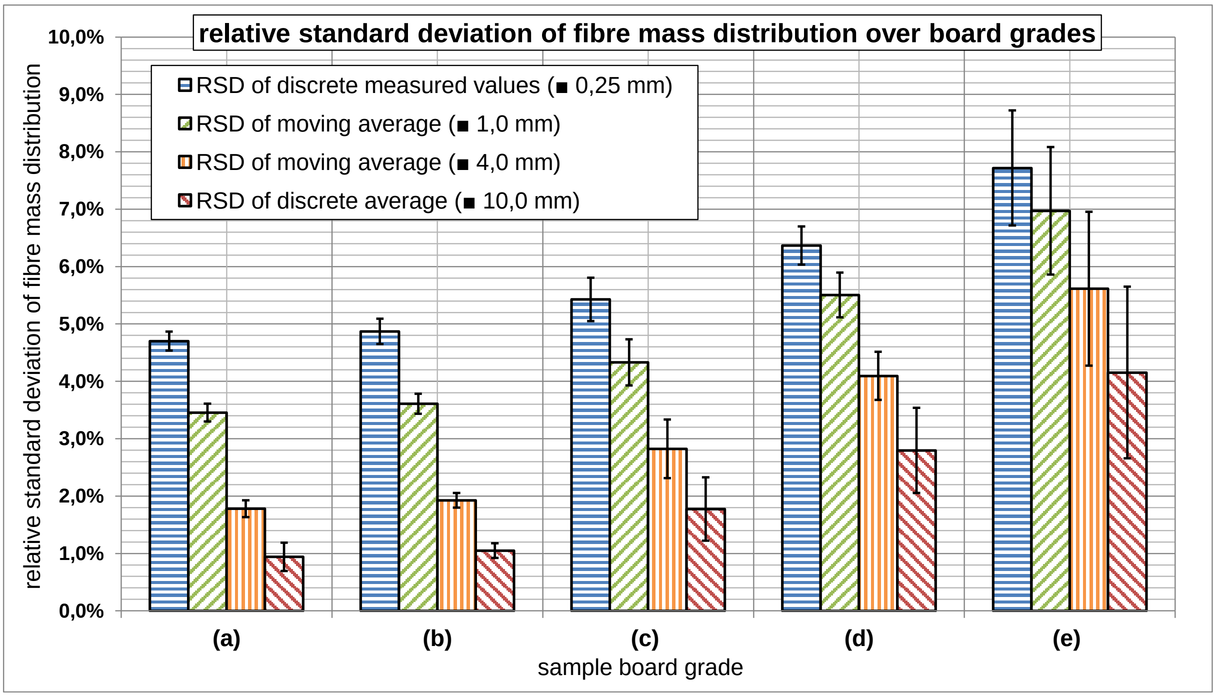

Figure 3. Relative standard deviation of fibre mass distribution (grammage) of pressboard grades (a)–(e). The ■ values in the legend give the square edge length of the considered integration area.

Whereas the relative change from grade a to grade e is about 60 % (4.7 % to 7.7 %) when considering the RSD of the discrete measured values, the same relative change can be evaluated with 340 % (0.9 % to 4.2 %) when the RSD of discrete squares of an edge length of 10.0 mm is considered. The comparison of these two evaluations has to be seen under the fact that the different values are representing the same specificity of fibre uniformity in the samples, as visualised in figure 2. The intention of the preceding approach was to figure out, which of the evaluation criteria was the most appropriate one for characterizing the influence on the properties of the pressboard, such as electric or mechanical strength.

3.2 Electric breakdown strength

The test results for the electric breakdown strength are given in figure 4. Unexpectedly no significant difference between the different pressboard grades could be observed in the tests made. Although a considerable number of individual samples had been examined for each grade, the deviation between test results gave no indication for any influence of fibre uniformity on the electric strength values measured.

4 Conclusion

It is well known from a lot of references, from deduced coherent theories and also stated in international standards derived from those, that the average apparent density and the nominal thickness are the main influencing parameters for the achievable electric strength of insulating pressboard made out of pure unbleached kraft pulp [4, 5].

Due to the fact, that the local thickness of the prepared boards varied far less than the fiber mass distribution, the specific distribution in fiber mass within the selective produced samples led to a corresponding local distribution of apparent density. Hence, a reduction in electric strength with decreasing uniformity of the local apparent density could be expected.

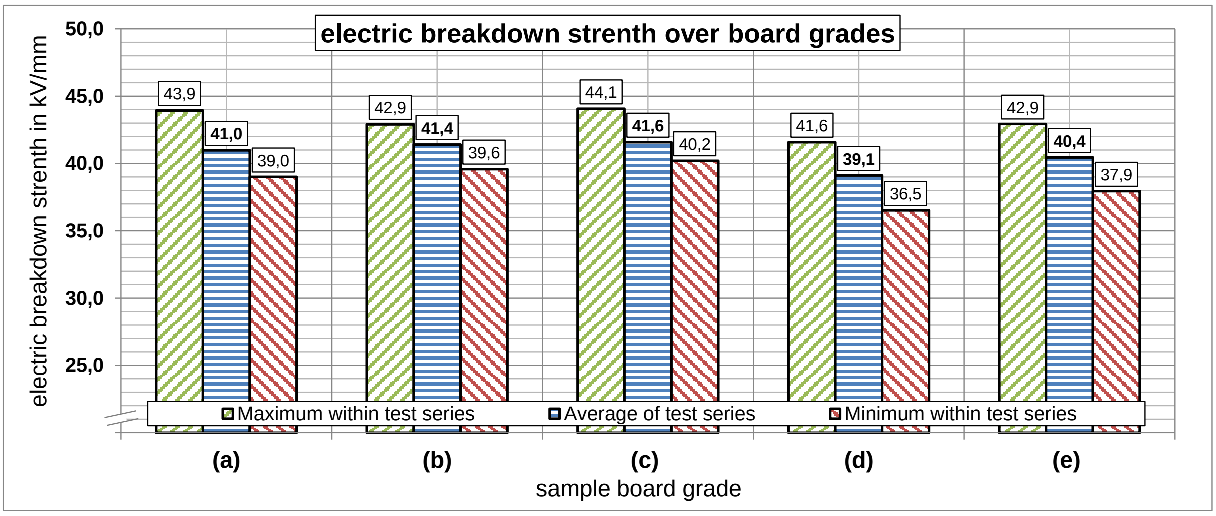

Figure 4. Average and value range of test results for electric breakdown strength (AC) of pressboard grades (a)–(e) (16 single tests for each grade)

The fact that no such influence was observed, suggests that the uniformity in local fiber mass distribution, respectively in local apparent density distribution, has no significant influence on electric breakdown strength within the examined range of material parameters of insulating pressboard. However, it should be taken into account that – at the moment – the results reported in this paper are restricted to pressboards with a thickness of about 1,0 mm and average apparent densities below 1,0 g/cm³.

5 Summary

The paper describes a non-destructive method for analyzing and evaluating the homogeneity of pressboard with grammages of 0.2 kg/m² and above, which could not be analyzed by common light transmitting methods. Examining board samples with different grades of uniformity of fiber mass distribution and their electric strength after mineral oil impregnation with the help of this method allows scientists and engineers a better understanding of the interdependencies of material properties of cellulosic pressboard and their inner structure. The results can also be used to better interpret electric breakdown phenomena in two-phase electric insulating systems, especially for liquid immersed cellulosic insulation systems.

Keywords: insulating pressboard, oil immersed solid insulation, electric breakdown strength, cellulose, formation, mass distribution

REFERENCES

[1] Thomas A. Prevost and T. V. Oommen. Cellulose Insulation in Oil-Filled Power Transformers: Part I—History and Development. IEEE Electrical Insulation Magazine January/February 2006 — Vol. 22, No. 1

[2] C. Krause. Power Transformer Insulation – History, Technology and Design. IEEE Transactions on Dielectrics and Electrical Insulation Vol. 19, No. 6; December 2012 (1941)

[3] IEC 60243-1:2013. Electric strength of insulating materials – Test methods – Part 1: Tests at power frequencies

[4] A. Küchler. Hochspannungstechnik. Springer-Verlag, 2009

[5] IEC 60641-3-1:2008. Pressboard and presspaper for electrical purposes – Part 3: Specifications for individual materials – Sheet 1: Requirements for pressboard, types B.0.1, B.0.3, B.2.1, B.2.3, B.3.1, B.3.3, B.4.1, B.4.3, B.5.1, B.5.3 and B.6.1

Sequential water absorption into linerboard

RAJESH KOPPOLU[1], MARTTI TOIVAKKA[1], PEKKA SALMINEN[2] and JANET PRESTON[3]

[1]Åbo Akademi University, [2]Trinseo Europe, [3]Imerys Minerals
rajesh.koppolu@abo.fi

1 INTRODUCTION

The increase in the cost of bleached virgin fibers has prompted the industry to consider replacing traditional white top liner with coated linerboard. The porosity and absorption characteristics of these two types of liners are very different, and the latter does not absorb liquids as readily, leading to problems in printing. During multi-color flexographic printing, the ink drying is usually based on absorption characteristics of the substrate, and the absorption becomes more challenging when multiple inks are printed on top of each other [1]. The objective of this work was to examine and better understand the water absorption characteristics of different linerboards when a pre-determined amount of water has already been applied on the substrate. The focus was to study the effect of pre-wetting amount and wetting delay between the two water applications.

2 MATERIALS AND METHODS

Three different linerboards: testliner, white top liner and a pigment coated linerboard were used for the experiments. The water absorption measurements were carried out on a custom-built hybrid printer available at the Laboratory of Paper Coating and Converting at Åbo Akademi University.

The experimental setup consisted of an initial pre-wetting step where a pre-determined amount of water was applied in an anilox nip. The pre-wetting amount could be changed by using aniloxes with different surface volumes. In the next step, the linerboard was allowed to absorb water through an applicator. The delay time (referred to as 'dwell time') between both the water application steps was varied and the water absorbed through the applicator was measured.

The hypothesis is that, when there is no external pressure in the secondary wetting unit, the absorption varies with the dwell time giving rise to three different cases. *Case 1:* At extremely short dwell times, the surface pores are still saturated with water applied by the anilox. Therefore the absorption will be lower than when there is no pre-wetting [2]. *Case 2:* As the dwell time increases, the higher capillary pressure of the smaller pores removes water from the larger pores [3,4]. This is aided by sorption into the hydrophilic fibers and evaporation. These processes empty the large pores leaving them with wetted walls, which leads to their rapid refilling during the secondary water application due to the zero effective contact angle. The end result is an increase in water absorption with increasing dwell time. *Case 3:* At longer dwell times, continuous evaporation of the water from the bulk structure can break the liquid film on the pore walls. Also as the fibers swell, the porosity of the bulk structure reduces [5]. This causes a reduction in absorption when water is reapplied. Therefore, a plot of secondary water absorption vs. dwell time after pre-wetting would show an increasing trend until a maximum absorption value is reached and then the absorption value would go down. A representation of the above cases is shown in figure 1.

Flexographic printing and wet on wet "trapping" experiments were later done using flexographic ink applied to the surface of a double coated linerboard using a Prufbau printability tester available at Imerys Minerals, Cornwall, U.K. Yellow ink was first applied to the pre-wetted linerboard and then a second layer of magenta ink was applied over the wet ink surface. The degree of ink reticulation and

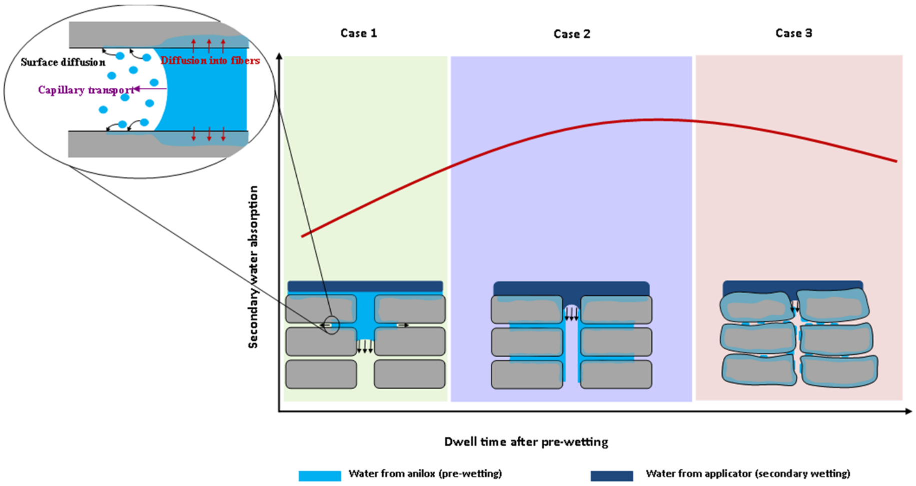

Figure 1. Representation of secondary water absorption vs. dwell time after pre-wetting.

show-through of the yellow layer is indicative of the drying speed of the first ink layer. Less show-through indicates faster drying.

3 RESULTS

It was observed that the pre-wetting volume and the delay time between the wetting units play a major role in the water absorption. A high pre-wetting volume and short delay time reduced the water absorption while a longer delay time increased the absorption. The results show that there is an optimum delay time where the absorbed amount is at its maximum. Figure 2 shows the plot of secondary water absorption vs. dwell time for the testliner pre-wetted with three different aniloxes.

Paper type plays an important role in the water absorption. When they are pre-wetted, hydrophilic papers absorb even higher amounts of water than hydrophobic papers. In some cases, the difference was three times more than in the no pre-wetting case. Pre-wetted hydrophilic coated linerboard with high porosity absorbed more water than the uncoated hydrophilic base sheet. The pinholes in the coating structure also contributed to fast water absorption. In some cases the water absorbed by the coated linerboard was observed to be 80% higher than the uncoated base sheet (testliner) under similar conditions.

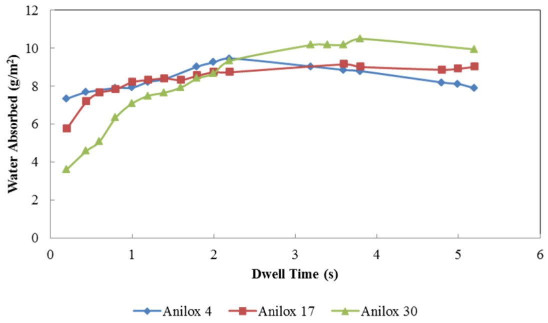

Figure 2. Water absorption vs. dwell time when testliner was pre-wetted with three different aniloxes.

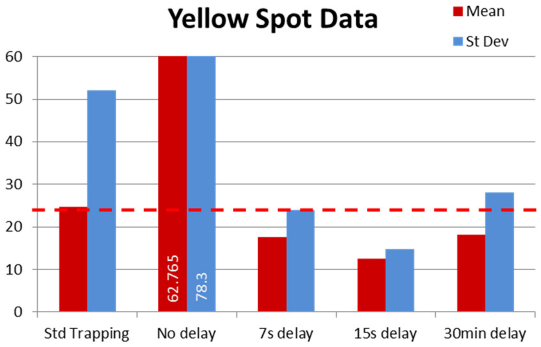

Figure 3. Yellow spot data for different delay times when double coated board was pre-wetted with a fountain solution.

The results from the Prufbau printability tester show that when the board's surface was pre-wetted with a thin layer of water and then printed with 2 layers of ink immediately (without any delay), the ink trapping became worse as the surface was filled with water from the pre-wetting step. However, as the delay time between pre-wetting and printing steps increased, the ink trapping improved compared to the no pre-wetting value. When the delay time was extended even further to around 30 minutes before printing, then the board began to dry and behaved in a similar manner to a surface without pre-wetting. Figure 3 shows the yellow spot data for different delay times when the double coated board was pre-wetted with a fountain solution. Lower value indicates faster ink drying and better trapping.

REFERENCES

[1] P. Oittinen and H. Saarelma. Print Media - Principles, Processes and Quality, Papermaking Science and Technology 13. Paper Engineers' Association/Paperi ja Puu Oy (2009)

[2] C. Tåg, M. Juuti, K. Koivunen, and P.A.C. Gane. Dynamic Water Transport in a Pigmented Porous Coating Medium: Novel Study of Droplet Absorption and Evaporation by Near-Infrared Spectroscopy. *Industrial & Engineering Chemistry Research,* vol. 49, no. 9, pp. 4181-4189 (2010).

[3] P.A.C. Gane, J. Schoelkopf, D.C. Spielmann, G.P. Matthews and C.J. Ridgway. Observing fluid transport into porous coating structures: some novel findings. *TAPPI Journal,* vol. 83, no. 5, pp. 77 (1999).

[4] H. Koivula, M. Toivakka and P. Gane. Short time spreading and wetting of offset printing liquids on model calcium carbonate coating structures. *Journal of colloid and interface science,* vol. 369, no. 1, pp. 426-434 (2012).

[5] P. Salminen. Studies of water transport in paper during short contact times. PhD thesis, Laboratory of Paper Chemistry. Department of Chemical Engineering. Åbo Akademi (1988).

Novel functional lignins as building blocks in preparation of polyurethane foams

MAREIKE ZIEGLOWSKI[1],
TAINA TRELLENKAMP[2]
and MAUNO MIETTINEN[3]

[1]Technische Universität Darmstadt,
Alarich-Weiss- Straße 8, 64287 Darmstadt,
+49-6151-16-23728,
Prof. Markus Biesalski, Technische Universität Darmstadt, Macromolecular- and Paper-Chemistry
zieglowski@cellulose.tu-darmstadt.de

[2]UPM GmbH
Georg-Haindl-Straße 5, 86153 Augsburg
taina.trellenkamp@upm.com

[3]UPM Kymmene
Paloasemantie 19, 53100 Lappeenranta,
FINLAND
mauno.miettinen@upm.com

1 Introduction

Polyurethanes (PUs) are an important class of polymers, which are synthesized by a polyaddition reaction between polyols and polyisocyanate to form a urethanic linkage. These polymers are multifunctional because they can be processed and used in various forms such as foams, elastomers, adhesives, coatings and many more. Their macromolecular properties reach from rather rigid and brittle behavior to soft and flexible properties. Due to these unique and modular properties, PUs have a wide range of applications, progressing from furniture-coatings to packaging, automotive seating and medical devices, to name only a few [1].

Currently, both the isocyanate-component and the polyols are mostly derived from petrochemical resources. Looking at all the different sustainability strategies of preparing such polymeric materials, there is a growing interest to replace petroleum based polyols by polyols from renewable feedstocks [2].

Lignin, a bio-based polymer carrying an abundant number of alcoholic functions, can be used as a substitute for petrochemical products like polyols [3]. After cellulose, lignin is the second most abundant organic material in nature. At the moment, only a small amount of lignin is used for materials applications (about 2 %). Most of the Lignin is being burned for energy production [4]. Lignin contains a large number of hydroxyl groups and it can be used as a macromonomer in polyurethane foam-formulations, as a low-cost polyol [5]. The synthesis of such lignin-based PUs often follows two major strategies: (1) the Lignin is used directly without any previous chemical modification, with/without addition of further other polyols or (2) the lignin is chemically modified prior to the reaction to make hydroxyl functions available, which could increase the efficiency of binding the lignin into the PU polymer [5].

Although, there have been some previous studies which shows demonstrators for lignin-based PU formulations, a successful transfer of this knowledge into real application is still hampered by our limited knowledge of how exactly Lignin is reacting in these formulations. This has to be examined how a distinct structure-property relation can be tailored using different Lignin materials. This is the overall task of the project that is being introduced here.

2 Material

The formulation used for the synthesis of lignin filled polyurethane foams consists of multiple educts. As polyisocyanate compound Polymethylendiphenyliso-cyanate (pMDI) was used. As polyols a trifunctional glycerol-initiated polyether, also monoethylglycol, a blowing and a growing catalysts and water were used. Crude Kraft-lignin as well as a further “Bio”- lignin, originating from a partner within an EU-Horizon2020- Project (www.valchem.eu/) were inserted into soft polyurethane foams in different percentage. The experiments were carried out by either adding lignin into the polyol component or into the polyisocyanate component under formation of a prepolymer. First, the components of the polyol were mixed together using a KPG stirrer. The lignin is then mixed well with the polyol or the isocyanate and the corresponding other component is then added and mixed for further 10 seconds.

3 Results

3.1 Foam production

Two different procedures can be used for the foam formation: (1) mixing lignin into the polyol and (2) mixing lignin into the polyisocyanate-component for establishing a pre-polymer.

Figure 1. Pure foam (top left), Kraft-lignin in the polyol component (top right), Kraft-lignin in the isocyanate component (bottom left), “bio”-lignin in the isocyanate component (bottom right).

Comparing both methods, it was evident that the lignin-isocyanate prepolymer approach results in better foams compared to mixing lignin into the polyol component first. It is assumed that lignin bound with the isocyanate and its OH-moieties were covalently reacted into the polyurethane network. In contrast, mixing lignin with polyol ensures that lignin is just incorporated as a filler. If the lignin is added to the isocyanate component, foams with a lignin content of up to 17 wt-% can be obtained (based on the total mass), which are comparable to the foam without lignin.

No differences were observed, once the “Bio”- lignin was used.

3.2 Start- and Stop-times

Important for polyurethane foams is the evaluation of the starting time as well as the time of completion of the rising of a foam. For both mixing approaches these times are shown in Figure 2(a). It is evident, that even at low lignin contents, approach (1) shows 5 times higher starting times compared to approach (2). The differences are even more significant for the stop times which rise for approach (1) up to 15 minutes whereas approach (2) takes 1.8 minutes even though this is measured for the highest amount of lignin. This means, that approach (2), the preparation of a lignin-isocyanate pre-polymer is the more suitable approach for polyurethane foams. The differences in the start and stop times of the two lignins are shown in Figure 2(b). If they are considered, there are no major deviations. The stop times for the bio-lignins are slightly below the Kraft-lignin. Here the start and stop times also increase with increasing lignin content.

3.3 Density

The polyurethane foams prepared with a lignin-isocyanate prepolymer show no changes in densities even at high lignin contents. In comparison, foams with lignin mixed into the polyol show a rapid increase of the density up to 400 g/L. For high lignin amounts above 20 % it should be noted that the foams do not rise as much as the other foams. Considering the densities of the different lignins, no significant alteration is observed. Even with the “bio”-lignin, comparable densities to crude Kraft-lignin can be achieved. Compared to the density of the pure foam, the densities with lignin are significantly lower.

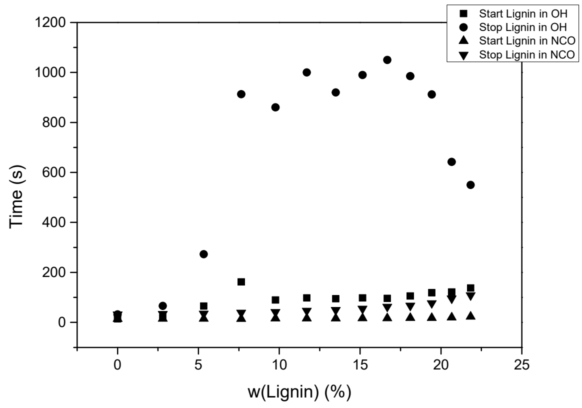

(a) Start and stop times of the different formulation methods with increasing lignin content.

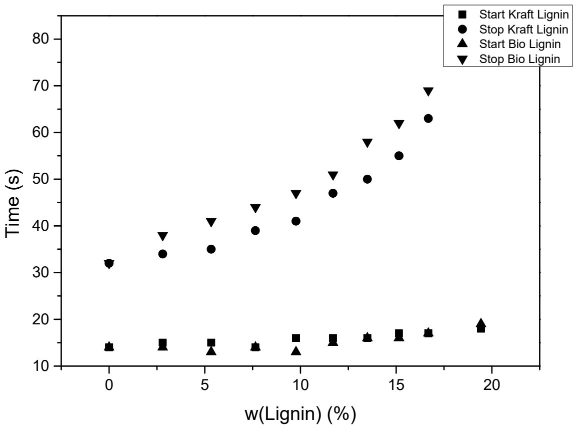

(b) Start and stop times of the different lignins with increasing lignin content.

Figure 2. Start and stop times of (a) the different formulation methods and (2) the different lignins

4 Conclusion

The most promising foams are obtained by adding the lignin into the isocyanate component and then adding the polyol. With this method, start and stop times can be well-controlled, and the lignin content can be used to tailor those parameters. Foams with decent densities in a range between 90 g/L and 100 g/L are obtained, which also accounts for foams being produced using the bio-lignin. The results presented here, can thus be taken as another important step to develop lignin-based PU materials, as well as studying possible applications in various areas.

5 Acknowledgements

This results are part of a project that has received funding from the Bio Based Industries Joint Undertaking under the European Union's Horizon 2020 research and innovation program under grant agreement No 669065.

REFERENCES

[1] J. Bernardini. Flexible polyurethane foams green production employing lignin or oxypropylated lignin. *European Polymer Journal*. **64**:147-156 (2015).

[2] N. Mahmood. Preparation of bio-based rigid polyurethane foam using hydrolytically depolymerized Kraft lignin via direct replacement or oxypropylation. *European Polymer Journal*. **68**:1-9 (2015).

[3] JH. Lora and WG. Glasser. Recent industrial applications of lignin: a sustainable alternative to nonrenewable materials. *J Polym Environ*. **10**:39–48 (2002).

[4] A.Tejado. Physico –chemical characterization of lignins from different sources for use in phenol–formaldehyde resin synthesis. *Bioresour Technol*. **98**:1655–1663 (2007).

[5] W. Xing. Functionalized lignin for halogen-free flame retardant rigid polyurethane foam: preparation, thermal stability, fire performance and mechanical properties. *Journal of Polymer Research*. **20**(9):234 (2013).

The Impact of the Fractionation Method on the Chemical Structure and Reactivity of Industrial Kraft Lignins

AYUMU TAGAMI[1,2], CLAUDIO GIOIA[3], MARIS LAUBERTS[4], GALINA DOBELE[4], TATIANA DIZHBITE[4], MIKAEL E. LINDSTRÖM[1], OLENA SEVASTYANOVA[1,3]

[1] Department of Fibre and Polymer Technology, KTH Royal Institute of Technology, Stockholm, Sweden
[2] Chemical Div. Research & Development Laboratory, Nippon Paper Industries Co., Iwakuni City, Yamaguchi 740-0003, Japan
[3] WWSC, KTH Royal Institute of Technology, Stockholm, Sweden
[4] Latvian State Inst. of Wood Chemistry, 27 Dzerbenes Str. LV 1006 Riga, Latvia
email.ayumu@kth.se

ABSTRACT

Technical lignins are main by-products from the pulp and paper industries and various biorefineries which are based on the lignocelllulosics. The main limitation regarding the use of technical lignins in value-added applications is their poor quality related to non-homogeneous molecular weight distribution and impurities coming from the biomass and process elements. In the present study, spruce and eucalyptus kraft lignin fractions with narrow molecular weight-distribution were produced by a fractionation method using a sequential solvent extraction with ethyl acetate (EtOAc), ethanol (EtOH), methanol (MeOH) and acetone. The molecular weight, number of functional groups and relative quantities of various types of polyphenolic units (PPU) available in the lignin fractions were determined by GPC, ^{31}P NMR and analytical pyrolysis (Py-GC/MS), respectively. These were correlated with the antioxidant activities of lignin, based on results from DPPH$^{\bullet}$, ABTS$^{\bullet+}$ and ORAC assays.

2 EXPERIMENTAL

Softwood (Norwegian Spruce) and Hardwood (Eucalyptus Grandis) lignin were obtained by the LignoBoost process. Four solvent fractions were obtained according to Duval *et al* [1]. Softwood lignin obtained by ceramic membrane filtration was provided by Swedish company Cleanflow (CF lignin). Molecular weight properties were determined by GPC analysis according to Guerra *et al* [2]. ^{31}P NMR analysis was used for the quantification of functional groups of lignin fractions [3]. Analytical pyrolysis (Py-GC/MS/FID) was done according to Ponomarenko *et al* [4]. The antioxidant activity of lignin fraction was evaluated according to methods published earlier [5-7].

3 RESULTS AND DISCUSSIONS

Four solvents extraction of both Spruce and Eucalyptus kraft lignins resulted in five samples with different molecular weights, including the unfractionated insoluble lignin (Fig. 1). The Mw of all Spruce lignin fractions, obtained with same solvents, are higher than Eucalyptus. However, it is possible to obtained fractions of similar molecular weights when using different solvents (see Fig. 1). The yield of the soluble fractions, content of functional groups, for selected samples are shown in Table 1.

For both types of lignin, EtOAc fractions contained highest amounts of phenolic groups. For CF sample, the content of these groups is approximatively 10% more in comparison to the original Lignoboost spruce lignin. High content of methoxylated lignin units, double bond in Cα position and units with shorten side chain ($(ArC_1+ArC_2)/ArC_3$), in lignin pyrolysis products indicate usually a high antioxidant activity [4,6,7]. Based on results shown in Table 1, the eucalyptus lignin fractions are expected to have higher antioxidant activities than corresponding spruce fractions. CF lignin has also a high content of structural descriptors with a positive antioxidant contribution. However, the high content of the oxygen-containing groups in the EtOAc eucalyptus fraction and in CF lignin may have a negative effect on the overall antioxidant activity depending on a substrate. Results from the various antioxidant tests for selected lignin samples are present in Table 2. As it was expected, eucalyptus lignin fractions demonstrated higher antioxidant activities (lower IC_{50} values in $ABTS^{\bullet +}$ and $DPPH^{\bullet}$ assays and higher TE values in ORAC test) than corresponding spruce lignin fractions of similar Mw.

4 CONCLUSIONS

Four solvents extraction produced low Mw fractions with low polydispersity for both spruce and eucalyptus LignoBoost lignins. The lower Mw fractions (EtOAc and EtOH) have a larger amount of phenolic groups than corresponding initial lignins. Eucalyptus lignin fractions, in methoxylated units and high ratio of lignin units with shortened side chain. Both spruce and eucalyptus EtOAc fractions demonstrated the high antioxidant activities in $ABTS^{\bullet +}$,).

Table 1. Yields, content of functional groups and specific structural features

Name		Yield	Aliph -OH	-COOH	Ph -OH	G+S units	Saturated side chain	Cα=Cβ bonds	O-atoms in side chains	$(ArC_1+ArC_2)/ArC_3$
		%	mmol/g	mmol/g	mmol/g	%	%	%	%	-
Spruce	Initial	-	1.91	0.46	4.28	83.8	33.5	19.0	10.9	2.9
	CF lignin	-	1.63	0.35	4.68	87.7	31.5	20.0	13.7	2.9
	EtOAc	24.5	0.84	0.71	5.04	84.6	30.3	15.4	12.5	3.4
	EtOH	32.5	1.89	0.49	4.49	84.6	35.8	18.0	9.6	3.4
	MeOH	8.2	1.94	0.32	4.15	82.2	38.8	15.9	9.8	3.7
	Acetone	14.7	1.96	0.29	4.06	82.7	35.8	18.6	11.7	2.9
	Insoluble	20.0	2.57	0.24	2.83	85.3	33.1	22.0	13.3	2.3
Eucalyptus	Initial	-	1.33	0.33	4.06	93.6	24.3	21.5	15.7	2.7
	EtOAc	35.2	0.65	0.35	5.02	94.0	24.5	16.1	20.5	4.6
	EtOH	32.8	1.52	0.40	4.45	92.6	29.9	21.7	10.0	2.8
	MeOH	15.4	1.74	0.28	3.71	92.7	27.1	22.8	9.2	2.2
	Acetone	6.1	1.74	0.21	3.58	92.3	26.9	24.1	11.5	1.9
	Insoluble	10.5	2.25	0.21	2.62	92.9	22.3	32.1	12.0	1.5

Figure. 1 Weight average molecular weights (Mw) of lignin fractions.

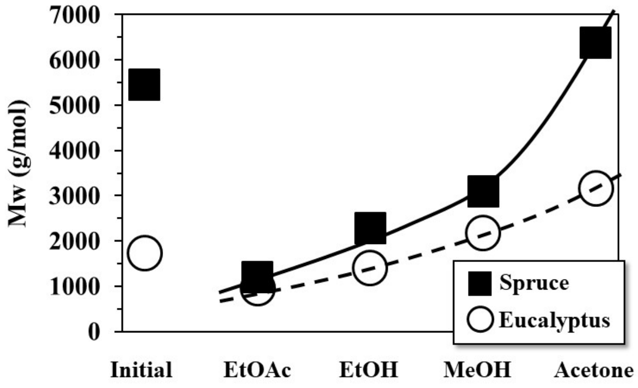

Table 2. The antioxidant properties of original lignin and associated fractions.

Name		$ABTS^{\bullet +}$	$DPPH^{\bullet}$	ORAC
		IC_{50}, mg/L	IC_{50}, mg/L	mmol/g, TE
Spruce	Initial	5.5 ± 0.1	23.7 ± 0.9	9.1 ± 0.1
	CF lignin	4.0 ± 0.1	16.8 ± 0.3	11.1 ± 0.2
	EtOAc	3.7 ± 0.1	15.0 ± 0.2	5.6 ± 0.3
	MeOH	4.2 ± 0.2	18.6 ± 0.5	8.4 ± 0.2
Eucalyptus	Initial	3.8 ± 0.1	13.0 ± 0.3	6.8 ± 0.2
	EtOAc	3.0 ± 0.2	11.2 ± 0.3	10.0 ± 0.4
	Acetone	3.7 ± 0.1	14.3 ± 0.3	3.5 ± 0.3

DPPH• tests. CF lignin, obtained by membrane filtration, demonstrated the best oxygen radical absorbance capacity (ORAC assay

5 ACKNOWLEDGEMENT

The financial support from the Knut and Alice Wallenberg foundation (WWSC) and Nippon Paper Industries Co, Ltd are gratefully acknowledged.

REFERENCES

1. Duval, A., Vilaplana, F., Crestini, C., Lawoko, M., *Holzforschung.*, **2016**, 70, 11-20.
2. Guerra, A., Filpponen, I., Lucia, L.A., Argyropolous, D.S.J., *J. Agric. Food Chem.*, **2006**, 54, 9696-9705.
3. Granata, A., Argyropolous, D.S.J., *J.Agric.Food Chem.*, **1995**, 43, 1538-1544.
4. Ponomarenko, J., Dizhbite, T., Lauberts, M., Volperts, A., Dobele, G., Telysheva, G., *J. Anal. Appl. Pyrolysis*, **2015**, 113, 360-369. Dizhbite, T., Telysheva, G.,
5. Prior, R., L., Wu, X., Schaich, K., *J. Agric. Food Chem.*, **2005**, 53, 4290-4302.
6. Dizhbite, T., Telysheva, G., Jurkjane, V., Viesturs, U., *Bioresour.Technol.*, **2004**, 95, 309-317.
7. Ponomarenko, J., Dizhbite, T., Lauberts, M., Viksna, A., Dobele, G., Bikovens, O., Telysheva, G., *Bioresources.*, **2014**, 9, 2051-2068.

Effect of autohydrolysis on lignin structure

CURMI HELENE, CHIRAT CHRISTINE
and LACHENAL DOMINIQUE

Univ. Grenoble Alpes, CNRS, Grenoble
INP, LGP2, F-38000 Grenoble, France
helene.curmi@pagora.grenoble-inp.fr

1 INTRODUCTION

Nowadays, the development around pulp mills is about their conversion into fully integrated biorefineries. The most promising way is to add an autohydrolysis step in order to extract hemicelluloses prior to degrade them during cooking. With this process, hemicelluloses can be valorised as oligomers or monomers in parallel to the production of pure cellulose for high value products [1].

Moreover, the addition of this pre-treatment increase the ability of wood to be delignified in next steps (cooking and bleaching). Several hypotheses could explain this phenomenon: during the autohydrolysis, some covalent bonds between lignin and hemicelluloses could have been destroyed or lignin structure could have been modified (lower molecular weight, increase in hydrophilicity by an increase in free phenolic hydroxyl groups) [2].

The aim of this work is to verify these hypotheses and in this paper, the focus will be put on the free phenolic hydroxyl groups.

2 EXPERIMENTAL WORK

The objective is to compare the free phenolic groups' content of lignin in wood before and after the autohydrolysis step. To measure these groups, several methods exist (UV-spectrophotometry, FTIR, ^{31}P NMR, Aminolysis…) but all these methods must be applied on lignin, which implies that lignin must be extracted from wood.

The problem with the extraction of lignin is to extract it without any modification which is not easy. The most well-known method is the milled wood lignin [3] but during the extraction, wood is heated in acidic conditions so this can lead to the same reactions that occur during autohydrolysis and it may hide the differences between the two samples.

In order to avoid this problem, we used a specific method, developed in our laboratory, which can be applied directly on wood [4].

2.1 Materials and Methods

The raw material for this study was a mixture of industrial hardwood chips.

The autohydrolysis was performed during 2h in rotating stainless steel-autoclaves placed in an oil bath at 170°C.

The two samples (wood chips before and after autohydrolysis) were then milled until obtaining particles size passing 40 mesh and extracted with acetone using a Dionex ASE 350 extractor.

The analytical method used in order to characterize free phenolic hydroxyl groups of lignin is based on the specific reaction between ClO_2 and these groups:

$$\boldsymbol{ClO_2} + \varphi OH \rightarrow H^+ + ClO_2^- + \varphi O^{\cdot}$$

$$\boldsymbol{ClO_2} + \varphi O^{\cdot} \rightarrow HClO + \varphi \mathrm{COOH}$$

To be sure that these reactions are the only ones, some precautions are necessary: pH is maintained at 6.7, temperature should stay below 0°C and DMSO is added in excess.

Concerning the experimental protocol, a certain quantity of ClO_2 is added to a mass of wood in suspension in DMSO and pH buffer. After 10 minutes reaction, remaining ClO_2 is titrated. Several trials are done with a varying quantity of ClO_2. The consumption should increase with the increase of ClO_2 applied until it reaches a plateau.

2.2 Results and discussion

Figure 1 compares the ClO_2 consumption between wood before and after autohydrolysis. The difference between the two plateaus seems to be significant, which means that there are more free phenolic hydroxyl groups in autohydrolysed wood which confirms the hypothesis according to which lignin is slightly depolymerized in autohydrolysis due to the acidic conditions.

Finally, this observation can be one explanation for the better depolymerisation of autohydrolysed wood chips in further cooking and bleaching.

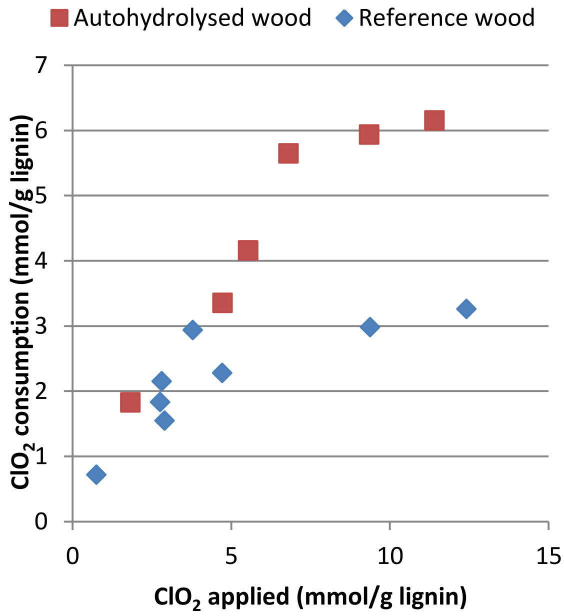

Figure 1. Comparison of ClO_2 consumption of wood before and after autohydrolysis

3 CONCLUSION AND FUTURE WORK

To conclude, thanks to a new method to estimate free phenolic groups content directly on wood, it has been shown that the autohydrolysis led to the increase of these groups. This result indicates that during prehydrolysis some ether bonds in lignin might have been cleaved due to the acidic conditions. So, lignin in autohydrolysed wood must be more hydrophilic and have a lower molecular weight which can explain the better delignification of prehydrolysed wood.

To confirm these encouraging first results, lignin was extracted from both samples with a method using “soft conditions” in order to avoid a maximum of degradation [5]. The extraction was carried out in a dioxane/water mixture at 45°C without addition of any acid. The free hydroxyl phenolic content of these extracted lignins is going to be analysed by ^{31}P NMR and with the ClO_2 method to compare these two methods.

Moreover, the molecular weight distribution of extracted lignin is going to be measured, in order to verify these results.

REFERENCES

[1] J. Liu, M. Li, X. Luo, L. Chen, and L. Huang. Effect of hot-water extraction (HWE) severity on bleached pulp based biorefinery performance of eucalyptus during the HWE–Kraft–ECF bleaching process. *Bioresour. Technol.*, vol. 181, 183‐190 (2015).

[2] M. Leschinsky, G. Zuckerstätter, H. K. Weber, R. Patt, et H. Sixta. Effect of autohydrolysis of Eucalyptus globulus wood on lignin structure. Part 1: Comparison of different lignin fractions formed during water prehydrolysis. Holzforschung, vol. 62, no 6 (2008).

[3] Bjorkman, A. Studies on finely divided wood I. Extraction of lignin with neutral solvents. SVen. Papperstidn. 59, 477- 485 (1956).

[4] D. Delmas, D. Lachenal, G. Mortha, N. Marlin, and C. Calais. Titration of free phenolic groups in pulps. 10th EWLP, Stockholm, Sweden, August 25–28, 2008. Holzforschung, vol. 63, no 6, 705–710 (2009).

[5] D. Min, S. W. Smith, H. Chang, and H. Jameel. Influence of Isolation Condition on Structure of Milled Wood Lignin Characterized by Quantitative 13C Nuclear Magnetic Resonance Spectroscopy. BioResources, vol. 8, no 2, 1790-1800 (2013).

ACKNOWLEDGEMENTS

The authors would like to thank the FUI BIO3 project for the funding of this PhD thesis work.

^{19}F NMR and ^{13}C NMR Studies on Lignin Model Compounds: Insight to Lignin New Derivatization Technique

ESAKKIAMMAL SUDHA ESAKKIMUTHU, NATHALIE MARLIN, MARIE-CHRISTINE BROCHIER-SALON, GERARD MORTHA

Univ. Grenoble Alpes, LGP2, F-38000 Grenoble, France
CNRS, LGP2, F-38000 Grenoble, France
Agefpi, LGP2, F-38000 Grenoble, France
sudha.esakkimuthu@lgp2.grenoble-inp.fr

1 INTRODUCTION

Lignin is an aromatic macromolecule, originated from biomass, with variety of functional groups. Its hydroxyl group content in particular and its molecular weight distribution are key parameters to analyze lignin reactivity, solubility and stability [1] before being used as additives in many applications [2,3]. Size exclusion chromatography (SEC) is one of the prominent techniques to determine the molecular weight distribution. However, free phenolic and aliphatic hydroxyl groups present in the lignin increase the polarity and limit the lignin solubility in chromatography solvents. To overcome these difficulties and to avoid segregation or aggregation of the macromolecule during SEC analysis, the hydroxyl groups need to be derivatized and make it into a non-polar compound, which is suitable for dissolution. Moreover, the derivatization is also a potential method to quantify hydroxyl group using NMR analyses. Quantification of free phenolic and aliphatic hydroxyl group is of primary importance to evaluate the possible lignin applications (coating, adhesives, etc.).

Direct measurement of ^{13}C NMR spectra, without any derivatization step, is not allowed, due to the **C**-OH ^{13}C chemical shifts scattering, and their overlapping with the other lignin peaks. As a result, lignin is derivatized. Classically phenolic functions are quantified after lignin acetylation followed by aminolysis (de-acetylation) [4]. However, acetylation is hardly complete, and aliphatic OH from lignin and trace sugars might interfer in the deacetylation process. Overall, aminolysis is a time consuming and two-step process. Therefore, the main aim of this work is to derivatize the lignin by new derivatization techniques such as Fluorobenzylation [5] and Fluorobenzoylation [6] - see Figure 1.

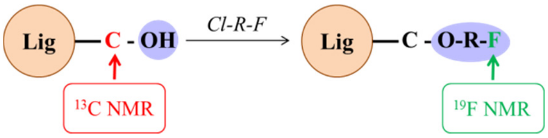

Figure 1: Fluorobenzylation derivatization.

Fluorobenzylation method converts lignin phenolic and primary aliphatic hydroxyl groups into fluorobenzyl ethers. Similarly fluorobenzoyl esters of secondary hydroxyl groups are obtained from fluorobenzolylation [6]. Fluorobenzylated and Fluorobenzoylated derivatives have already been analyzed by ^{19}F NMR technique 20 years ago but this technique was not fully described and investigated. In this paper, the ^{19}F NMR technique for lignin hydroxyl function determination is deeply studied.

In order to compare and assign phenolic and aliphatic hydroxyl group signals from ^{19}F NMR, lignin like model compounds were chosen and fluorobenzylation and ^{19}F NMR were performed. The obtained results were used to assign the signals of a commercial lignin and to give a better insight to the lignin structural analysis.

2 MATERIALS AND METHODS

Model compounds: 5 lignin model compounds, commercially available were used (Vanillin, Acetovanillone, Guaiacol, Vanillyl alcohol and Veratryl alcohol, from Sigma-Aldrich), as well as one model of cellulose (cellobiose, Sigma-Aldrich).

Commercial lignin: a commercial lignin (Protobind 1000 from Green Value Co.)

from alkaline cooking of wheat straw was studied without any purification step.

Model compound Fluorobenzylation: 100mg of model compounds were dissolved in 1 mL of 1 M tetrabutylammonium hydroxide in methanol, stirred for one hour at 50°C. After 1h, 10mL of acetonitrile and 300mg of 4-Fluorobenzyl chloride were added and the reaction mixture was stirred at 50°C for overnight [5,6]. After, H_2O (30mL) and EtOAc (30mL) were added to the reaction mixture. The aqueous layer was separated and extracted with EtOAc (2×30mL). The combined EtOAc layer was washed with H_2O (2×30mL) and saturated NaCl solution (30mL). The extracted EtOAc layer was dried (Na_2SO_4), filtered, evaporated and analyzed through ^{19}F NMR and ^{13}C NMR.

Lignin Fluorobenzylation: Lignin fluorobenzylation was performed using the same experimental conditions as for the model compounds. Then the derivatized lignin recovery is performed by precipitation in diethylether. The precipitate was filtered through 0.45µm PTFE filters, washed with diethylether several times and oven dried at 50˚C [7, 8].

NMR: Spectroscopic measurements were recorded on a Bruker AVANCE400 spectrometer equipped with a 5 mm BB/19F-1H/d Z-GRD probe operating at 100.612 MHz for ^{13}C, 376.447 MHz for ^{19}F and 400.130 MHz for ^{1}H. Acquisition and data treatment were done using the LINUX TopSpin 3.2 software. Lignin model compound derivatives were dissolved in DMSO-d6 (40-50 mg/0.7mL) using C_6F_6 as a reference (-164.90 ppm / $CFCl_3$). Lignin derivatives were dissolved in DMSO-d6 (15-20mg/0.7mL); quantification was done using 2-Fluoroacetophenone as internal standard. The measurements were performed at 298K.

^{19}F NMR the Bruker *invgate* sequence was used. The experiments were conducted with 1.25 s acquisition time, 8.76 s relaxation delay and a 30° pulse using a 65 ppm spectral width. 64k data points for model compounds were used for data acquisition. Prior to Fourier transformation, zero-filling at 64k was applied, followed by apodization with a 0.3 Hz exponential. Chemical shifts are given relative to $CFCl_3$ ($\delta = 0$ ppm). The positions of the peaks were referred for C_6F_6 as internal reference at -164.90 ppm. For lignin OH quantification, the experiments were conducted at 298K, with 4.35 s acquisition time, 8.76 s relaxation delay and a 30° pulse using a 20 ppm spectral width. 64k data points were used for data acquisition. Quantification and position of peaks were referred for 2-Fluoroacetophenone as internal reference at -112.86ppm.

^{13}C NMR the Bruker *invgate* sequence was used. The experiments were conducted with 0.648 s acquisition time, 20 s relaxation delay and a 45° pulse using a 250 ppm spectral width. Proton broad band decoupling was applied only during acquisition time. 32k data points were used for data acquisition. Prior to Fourier transformation, zero-filling at 64k was applied, followed by apodization with a 2 Hz exponential. Chemical shifts are given relative to TMS (tetramethylsilane, $\delta = 0$ ppm). The positions of the peaks were referred to DMSO signal at 39.5 ppm. **^{13}C DEPT**: the Bruker *dept* sequence was used. The experiments were conducted with 0.648 s acquisition time, 3.0 s relaxation delay, a last pulse at 135° to select CH_2 carbons reversed compared to CH and CH_3, with a 145 Hz coupling constant.

3 RESULTS AND DISCUSSION

To quantify phenolic and aliphatic hydroxyl groups through ^{19}F NMR, the exact signal range of fluorobenzylated phenolic and primary aliphatic hydroxyl groups need to be known. There have been some publications [5, 6] dealing with lignin fluorobenzylation and ^{19}F NMR analysis, but the signal assignments are not in good agreement with the current NMR technique. Therefore, in order to assign the exact signals and study the fluorobenzylation reactivity, different lignin model compounds were chosen and analyzed by ^{19}F NMR technique.

Lignin model compounds were selected based on the nature of the hydroxyl groups which could be found in lignins – see Figure 2. Vanillin (**1**) and Acetovanillone (**2**) contain phenolic hydroxyl group with a carbonyl in α position (aldehyde and ketone respectively). Guaiacol (**3**) is the basic phenol unit of lignin. Vanillyl alcohol (**4**) consists of both aliphatic and aromatic hydroxyl groups, and Veratryl alcohol (**5**) contains only aliphatic hydroxyl group. Finally a model of carbohydrate, D(+) cellobiose (**6**), was also studied because commercial lignins are usually contaminated by sugars containing hydroxyl groups which may also be derivatized. If so, lignin ^{19}F NMR spectra will also contain signals belonging to sugar carbohydrate contaminants. This potentiality will be also examined.

All these 6 compounds were fluorobenzylated, and their reaction products were analyzed by ^{19}F and ^{13}C NMR on quantitative mode, the starting reagent FBC (4-Fluorobenzyl chloride) too. Organic and aqueous layers had been treated.

First of all, the assignment of the resulting peaks with the ^{19}F NMR allows the control of the fluorobenzylation, and gives the corresponding chemical shifts. With the ^{13}C, all the non-fluoro substituted products could be detected. The chemical shifts, and the specific hyperfine structures due to the coupling ^{n}J(CF) were used for determining the F-**Φ** (aromatic ring) structure presence or not.

According to ^{19}F and ^{13}C and ^{13}C DEPT NMR experiments, it could be deduced that all the phenolic hydroxyl groups of **1**, **2**, **3** and **4** were efficiently fluorobenzylated. In the case of **4**, phenolic hydroxyl group fluorobenzylation conversion is much higher than aliphatic hydroxyl group and part of the unreacted 4-FBC reagent was recovered. Aliphatic hydroxyl group conversion is very low for **4** and **5** and most of the starting compound was recovered as unreacted, no more 4-FBC was remained after the reaction. Therefore, the derivatization reaction should be improved to get access to all hydroxyls.On the other hand, D(+) cellobiose did not show any derivatized product: lignin contamination by sugar should not interfere with the ^{19}F NMR results.

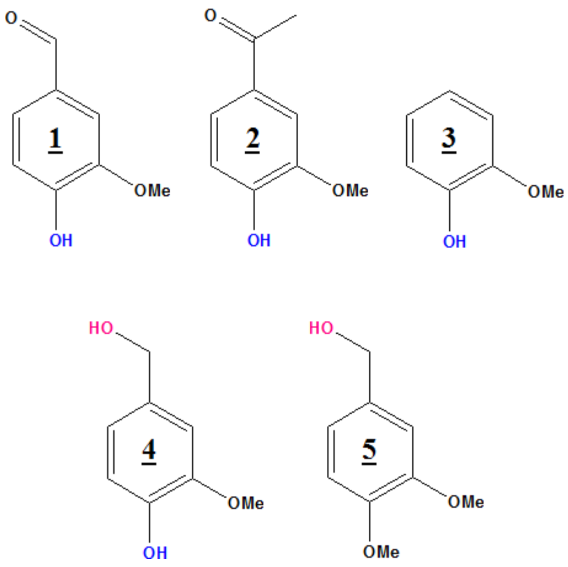

Figure 2: Model compounds studied.

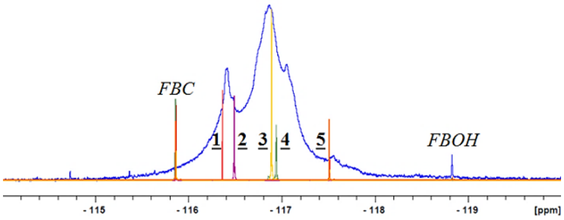

Figure 3. Comparison of ^{19}F-NMR spectra of fluorobenzylated lignin (in blue) and derivatized model compounds. (*Note: Only phenol derivatization for* ***4***).

A commercial lignin from Green Value Company was analyzed using ^{19}F NMR after Fluorobenzylation (Figure 3 and 4). Signal assignment was made with the help of the lignin model compounds spectra. Peaks ranging from -115.0 to -117.5 ppm are assigned to fluorobenzylated phenols. The sharp signal at -116.4 ppm can be assigned to conjugated α-CO phenolic structures, and peaks from -117.5 to -118.5 ppm to fluorobenzylated aliphatic primary alcohols.

The finest signal at -118.7 ppm assigned to FBOH structure corresponds to the reaction product of the starting reagent FBC with water.

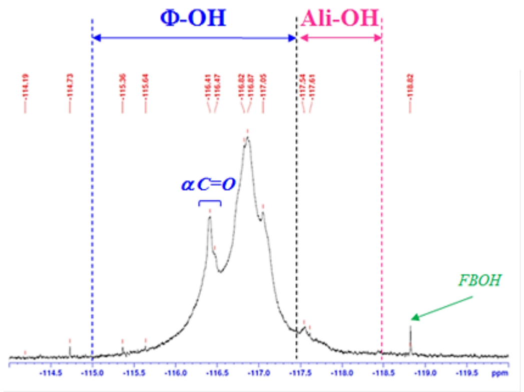

Figure 4. ^{19}F-NMR spectra of fluorobenzylated PB1000 lignin.

After ^{19}F NMR signal assignment, OH function quantification was done. According to ^{19}F NMR, PB1000 lignin contains 2.9 mmol of phenolic hydroxyl group /g lignin.

4 CONCLUSION

The results have shown that lignin fluorobenzylation is more efficient with phenolic hydroxyl groups than aliphatic hydroxyl groups. Complete derivatization is obtained with model compounds containing only phenolic hydroxyl groups. For model compounds containing also aliphatic hydroxyls, fluorobenzylation of the latter groups is partial. In the case of compounds with only primary aliphatic hydroxyl group, the derivatization is very slow and minimum. To be successfully applied on lignin for aliphatic OH characterization, the derivatization conditions still have to be improved.

No fluorobenzylation was observed with a carbohydrate model compound (cellobiose) meaning that sugar contamination should not interfere with the lignin analysis. Based on the knowledge obtained from the model compounds, ^{19}F NMR signal assignments have been made precisely and a commercial lignin was also studied in a quantitative mode. OH content results are close to those obtained with the proven aminolysis method (Publication under progress).

To conclude, further efforts are now required to improve aliphatic OH derivatization in order to make lignin fully non-polar, thus suitable for complete dissolution in SEC solvents for molecular weight distribution analysis.

REFERENCES

[1] S. Baumberger, A. Abaecherli, M. Fasching, G. Gellerstedt, R. Gosselink, B. Hortling, J. Li, B. Saake and E. de Jong. “Molar Mass Determination of Lignins by Size-Exclusion Chromatography: Towards Standardisation of the Method”, Holzforschung, **61**(4): 459-468 (2007).

[2] F.G. Calvo-Flores, J.A. Dobado, J. Isac-García and F.J. Martin-MartíNez. “Applications of Modified and Unmodified Lignins. Lignin and Lignans as Renewable Raw Materials” Chemistry, Technology and Applications, 247-288 (2007).

[3] J. Berghel, S. Frodeson, K. Granström, R. Renström, M. Ståhl, D. Nordgren and P. Tomani. “The Effects of Kraft Lignin Additives on Wood Fuel Pellet Quality, Energy Use and Shelf Life”, Fuel processing technology, 112, 64-69 (2003).

[4] S.Y. Lin, and C.W. Dence, (Eds.) “Methods in Lignin Chemistry”. Springer Science & Business Media (2012).

[5] M. Barrelle, “A New Method for the Quantitative ^{19}FNMR Spectroscopic Analysis of Hydroxyl Groups in Lignins, Holzforschung, **47**(3):261-267 (1993).

[6] R.M. Sevillano, G. Mortha, M. Barrelle, and Lachenal, D. “^{19}F NMR Spectroscopy for the Quantitative Analysis of Carbonyl Groups in Lignins”. Holzforschung, **55**(3), 286-295 (2001).

[7] M. Barrelle, J.C. Fernandes, P. Froment, D. Lachenal, "An approach to the determination of functional groups in oxidized lignins by 19F NMR”, Journal of Wood Chemistry and Technology. **12**(4): 413-424 (1992).

[8] M. Barrelle, “Improvements in the Structural Investigation of Lignins by ^{19}F NMR Spectroscopy”, Journal of Wood Chemistry and Technology, 15(2), 179-188 (1995).

Fabrication of Capacitive Sliders

TANJA PLEŠA1, MATIJA MRAOVIĆ1
and DEJA MUCK2

1 Pulp and Paper Institute, Bogišićeva 8,
1000 Ljubljana, Slovenia
2 University of Ljubljana, Faculty of
Natural Sciences and Engineering,
Snežniška 5, 1000 Ljubljana, Slovenia
tanja.plesa@icp-lj.si

1 THE RESERCH PROBLEM, THE AIM AND OBJECTIVES OF THE WORK

Printed electronics is often considered to be a new development, but the truth is that printed electronics methods have been penetrating markets that conventional electronics cannot reach for some time, e.g. packaging, posters. It brings a new dimension to electronics and its applications [1]. Printed electronics uses functional inks for printing (conductive, dielectric, semi-conducting inks) and is based on flexible materials such as plastic foils, paper and textiles, and conventional printing processes such as screen printing, flexography, gravure printing and inkjet [2]. Large print runs of low-cost electronics are products of conventional printing materials and graphic technologies of printing. Disadvantage of this kind of electronics are low level of integration, large areas of electronic components and slow switching in comparison with conventional electronics [2]. Different products such as solar cells, sensors, touch sensitive displays, RFID tags etc. can already be found in everyday life [3].

In this research, we decided to fabricate printed capacitive sliders because of two reasons. First reason is that costs of production of printed electronics are lower than in production of conventional electronics. And the second reason is that printed electronics can be made on many different materials that conventional electronics just cannot reach. In previous research, we made printed capacitive sensors based on an electrode. The sensors operate on the basis of an electrical capacitor. The printed electrode represents the first capacitor plate and the user's finger the second. The user's finger brings a charge to the electrode, which changes the capacitance. The change in capacitance is measured by a chip [4].

Touch sensors are divided into three groups (cf. Figure 1):

- zero-dimensional sensors, e.g. buttons – i.e. sensors with only one touch point;
- one-dimensional sensors, e.g. sliders, wheels – such sensors detect linear movement of a finger;
- two-dimensional sensors, e.g. touch screens – such sensors detect movement of a finger two axes [5].

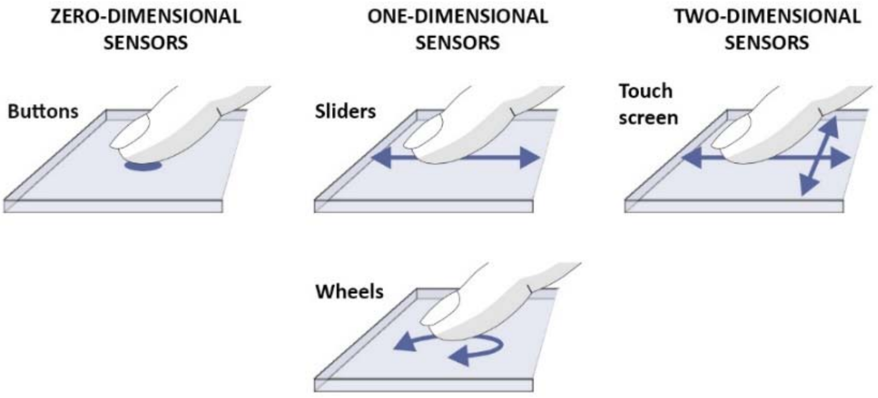

Figure 1. Three groups of touch sensors

The aim of this research is fabrication of a prototype of printed capacitive slider. Hybrid electronics combines conventional elements (chips and programing) with printed conductive layers.

The objectives of the research are:

- determination of the fabrication process for hybrid sliders
- optimization of the fabrication process
- fabrication of the slider prototype

2 WORKING HYPOTESIS

In research, we assume that:

- sliders can be made with printing using conductive inks
- sliders can be printed on different substrates
- electrical properties of printed sliders are similar to electrical properties of conventional switches
- after printing sliders need to be electrically isolated
- substrate, design and size of the sliders influenced their operation

3 METODS

Using computer **simulation,** the design of the sliders will be made. Sliders will be printed with conductive ink using screen printing technology. We will coat and laminate printed sliders to protect them from external influences and keep them electrically isolated. Different printing materials will be analysed and used as a substrate for printed sliders. Graphic, mechanic and electric measurements will be performed. The slider will be bound to the circuit in accordance with the instructions provided by manufacturer of the conventional sliders.

REFERENCES

[1] MRAOVIĆ, M., MUCK, T., PIVAR, M., TRONTELJ, J. and PLETERŠEK, A., Humidity sensors printed on recycled paper and cardboard. Sensors, 2014, no. 14, p. 14.

[2] STAREŠINIČ, M. and MUCK, T. Large-area, Organic & Printed Electronics Convention. Grafičar, 2010, no. 5, pp. 8−9.

[3] PLEŠA, T. Izdelava tiskanih stikal, diplomsko delo. Ljubljana: University of Ljubljana, Faculty of Natural Sciences and Engineering, Department of Textiles, Graphic Arts and Design, 2015

[4] PLEŠA, T., MRAOVIČ, M., PIVAR, M., KAVČIČ, U., MUCK, D. Fabrication of Printed Switches. Lancashire: PITA, Paper Technology, 2016, Volume 57, no. 2, pp. 34-37.

[5] Atmel. QTAN0079 Buttons, Sliders and Wheels Sensor Design Guide [accessible online], Atmel dokumentacija, published 2015 [cited 20 July 2015]. Accessible online: <http://www.atmel.com/products/TouchSolutions/bsw/default.aspx?tab=documents>.

Stimulus-responsive surface coatings and films from hydroxypropyl cellulose

Maximilian Nau,
Technische Universität Darmstadt,
Alarich-Weiss- Straße 8, 64287 Darmstadt,
+49-6151-16-23725,
nau@cellulose.tu-darmstadt.de

Markus Biesalski,
Technische Universität Darmstadt,
Macromolecular- and Paper-Chemistry

1 Introduction

In contrast to non-modified cellulose polymer [1,2] hydroxypropyl cellulose (HPC) exhibits excellent solubility in many organic solvents and hence, offers the possibility to carry out a large number of different homogeneous polymeranalogous reactions in order to yield a wide range of functional polymers. In this contribution, we present novel studies using hydroxypropyl cellulose polymers and its derivatives as coating materials to tailor surface-properties of materials, as well as template free preparation of cross-linked, free-standing domains.

2 Results

In a first step, we synthesized several HPC esters, ranging from lauric to stearic acid esters and degrees of substitution between 0.5 and 3. Esters prepared from single fatty acids show distinct melting points, if high DS values are established (DS 3). The latter can be attributed to side chain crystallization of the fatty acid chains. In a next step, mixed HPC-esters were prepared, which among fatty acid esters further contained reactive groups that e.g. can be used for photo-crosslinking of the macromolecules. If HPC-esters are being coated onto a solid support, water contact angle can be adjusted from 56 degree at DS 0 up to 120 degree for HPC-stearic ester at DS 3. An interesting situation occurs, if the HPC ester polymers are first (nano)precipitated to form small colloids with diameters of about 80-300 nm and such colloids are being spray-coated onto the solid substrate. In this case, water contact angles above 153° and 159° were observed, with very low CA hysteresis. This suggests a Cassie state of wetting of water on such superhydrophobic layers. Interestingly, applying a thermal stimulus with less than 1 mJ/mm² of energetic impact, the particles melt and a wetting behavior similar gto the bulk material is observed. The latter findings on the thermal response of hydroxypropyl cellulose materials, are similar to the thermal switching of cellulose-based colloids studied in previous work [3].

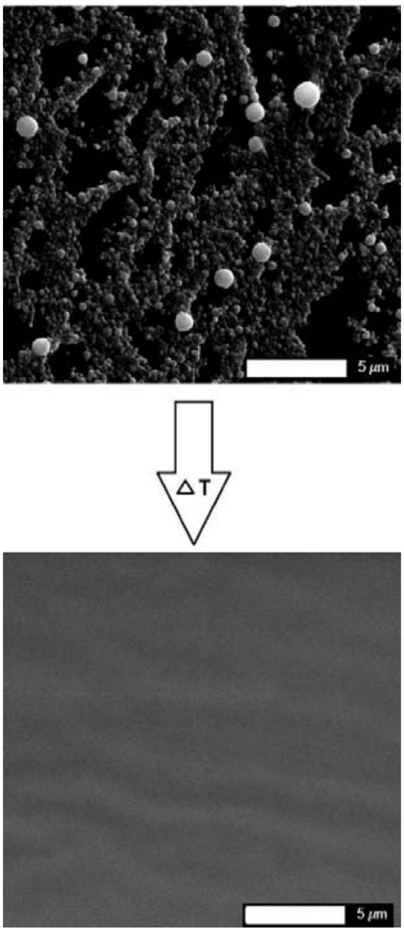

Figure 1. SEM images of hydroxypropyl cellulose ester Nanoparticles. The upper image shows nanoparticles after dropcasting from water in their native form. Another part of the sample was heated using an IR-laser, which is shown on the bottom.

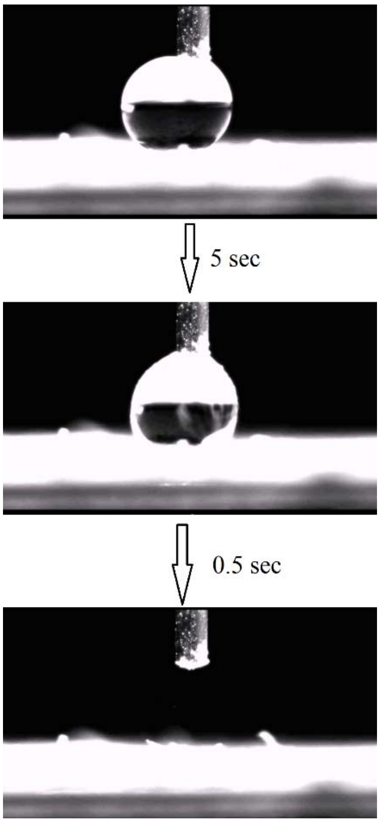

Figure 2. Switching of hydrobicity via visible light stimulus. The first image shows the then superhydrophobic surface when the illumination is started. In the second frame the drop starts to permeate into the coating due to the switched polarity. After another 0.5 seconds the droplet is completely absorbed.

Furthermore the change in wetting behavior is accompanied by a strong change on opacity.

In another part of the project we introduced Donor-Acceptor-Stenhouse-Adducts (DASA) [4] to switch hydrophobicity by visible light. The switching from CA > 150° to < 60° occurs within a few seconds of illumination, visualized in figure 2.

Currently the switching back to a superhydrophobic state is extremely slow (in the order of days), but since the system uses primarily bio-based components it is a promising introduction of green chemistry intro high-performance molecular switching. Based on this findings we are currently optimizing the chemistry of the used DASA to improve switching behavior.

3 Conclusion

Functionalized HPC materials show interesting effects, if used as surface-coating material or to produce free-standing films. In particular, they can be utilized for thermal and/or light switching of interfaces to address surface-wettability. The latter can be useful for a number of future applications in materials science, medicine or microsystem technology.

REFERENCES

[1] R. P. Wool, X. S. Sun. Bio-Based Polymers and Composites. *London, Elsevier Academic Press*. **1**:7 (2005**).**

[2] T. Heinze, et al.. Solvents applied in the field of cellulose chemistry - a mini review. *Polímero*. **15**:84-90 (2005).

[3] A. Geißler, et al.. Thermoresponsive superhydrophobic paper using nanostructured cellulose stearoyl ester. *Cellulose* **10**:283-296 (2014).

[4] S. Helmy, F. Leibfarth, S. Oh, J. Poelma, C. Hawker und J. d. Alaniz. Photoswitching Using Visible Light: A New Class of Organic Photochromic Molecules, *Journal of American Chemical Society*. **136**:8169-8172 (2014).

Efficacy of Natural plant extracts in antimicrobial packaging systems

KOFI J. BROBBEY, YANG BAORU, HANNA-LEENA ALAKOMI, JARKKO J. SAARINEN, MARTTI TOIVAKKA

Åbo Akademi University
Kofi.brobbey@abo.fi

1 PATHOGENIC BACTERIA IN THE ENVIRONMENT

The presence of pathogenic bacteria in food and personal care products can result in severe health consequences to the consumers. Excessive growth of spoilage bacteria can lead to food spoilage and render the food unsafe for human consumption while increasing food waste [1]. Proteolytic bacteria that breakdown protein in meat result in unsavory odor, while other bacteria such as *Escherichia coli (E. coli)* can cause fatal diseases such as hemolytic uremic syndrome, kidney failure and possible death [2]. The use of antimicrobials in food and packaging systems can aid in mitigating these harmful effects.

1.1 Antimicrobials in food packaging systems

Synthetic food additives are commonly used for inhibiting the growth of microbes and for maintaining the shelf life of food. The type of antimicrobial, whether natural or synthetic, sets restrictions for their use. For instance, food-packaging applications may require the use of natural antimicrobial agents since there is the tendency of migration into food. Consequently, natural antimicrobial agents have been used in several ways such as dipping and spraying onto food, and they have also been used as coatings that help to maintain freshness of food while improving shelf life. Metal and metal oxide nanoparticles have shown potential as antibacterial agents, but there are still unanswered questions about their long-term effects on the environment and human health [3].

Increasing need for natural food preservatives has been raised by food industry due to concern about the health impact of synthetic food additives. Consumer awareness and preferences have promoted the use of natural antimicrobials since they are presumed to be a healthier alternative. Food packaging material with antimicrobial properties could therefore be an important step in the overall strategy of food preservation, which aims at reducing the use of synthetic additives in food. The recent surge in the use of natural antimicrobials can also be associated with the biocompatibility and nontoxicity within the environment. Extracts from medicinal plants that have antitumor, anti-inflammatory, and antioxidant effect have also demonstrated antimicrobial properties. Thus, antimicrobials from natural extracts that are used in food packaging applications could fulfil the primary goal of maintaining food quality while delivering additional health benefits, such as nutritional supplements. There have been successful attempts at incorporating natural antimicrobials into packaging material. However, there has been limited success with incorporating natural antimicrobials directly onto paper surface for packaging applications [4].

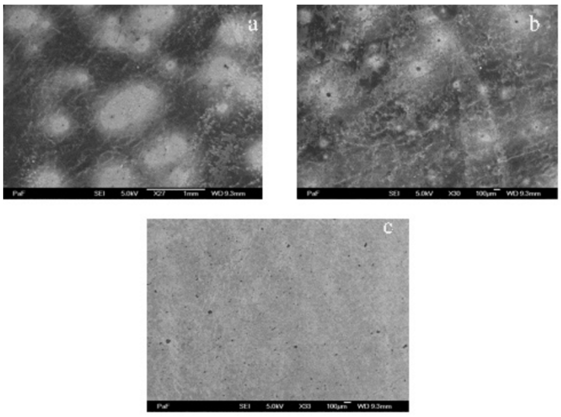

Figure 1. SEM image showing sea buckthorn (a) and pine bark (b) coatings on the surface of packaging paper. Uniform coating of antimicrobial blend is shown in (c).

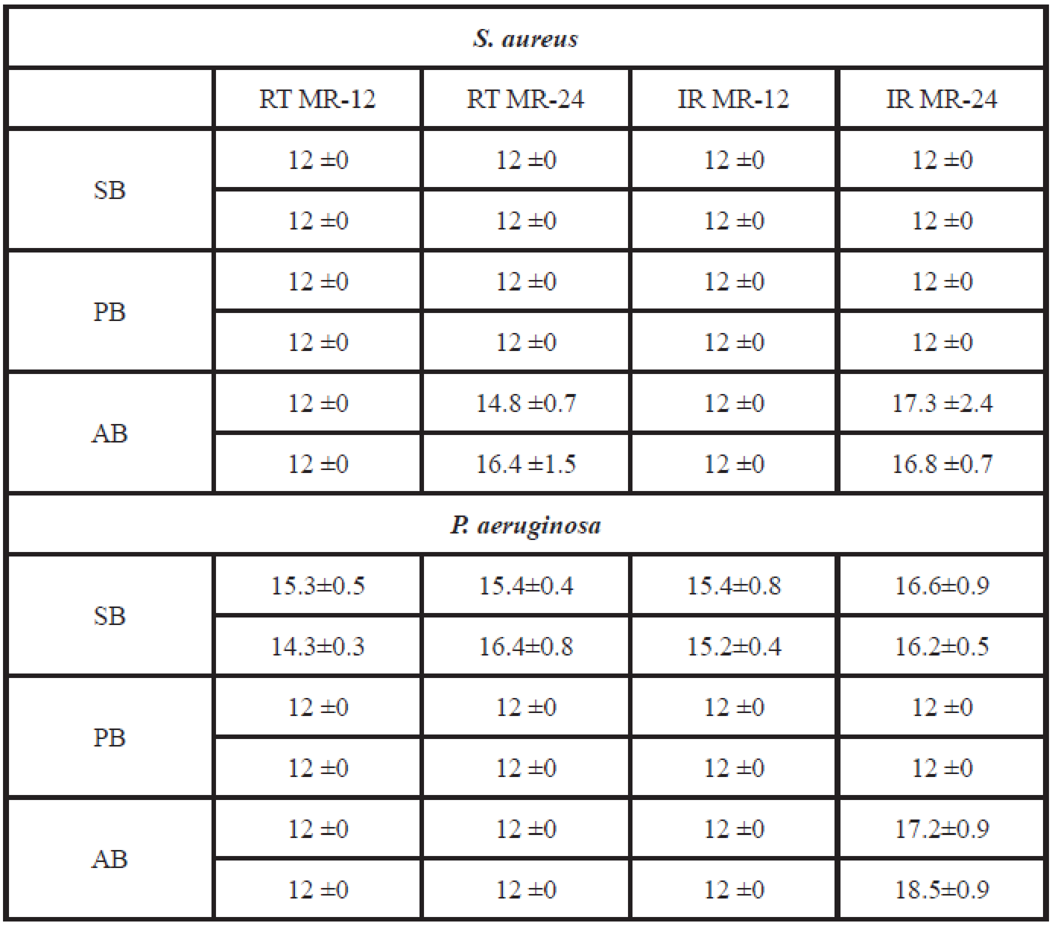

S. aureus				
	RT MR-12	RT MR-24	IR MR-12	IR MR-24
SB	12 ±0	12 ±0	12 ±0	12 ±0
	12 ±0	12 ±0	12 ±0	12 ±0
PB	12 ±0	12 ±0	12 ±0	12 ±0
	12 ±0	12 ±0	12 ±0	12 ±0
AB	12 ±0	14.8 ±0.7	12 ±0	17.3 ±2.4
	12 ±0	16.4 ±1.5	12 ±0	16.8 ±0.7
P. aeruginosa				
SB	15.3±0.5	15.4±0.4	15.4±0.8	16.6±0.9
	14.3±0.3	16.4±0.8	15.2±0.4	16.2±0.5
PB	12 ±0	12 ±0	12 ±0	12 ±0
	12 ±0	12 ±0	12 ±0	12 ±0
AB	12 ±0	12 ±0	12 ±0	17.2±0.9
	12 ±0	12 ±0	12 ±0	18.5±0.9

Table 1. Size of diffusion zone in (mm) obtained from antibacterial measurements with standard deviation (SD). 12 mm inhibition zone size indicates no antibacterial activity while diameter larger than 12 mm indicates antibacterial activity.

In this study, natural extracts from sea buckthorn *(Hippophaë rhamnoides L.)* leaves and the inner layer of pine bark *(Pinus silvestris)* are examined for their antibacterial properties, applied as coatings suitable potentially for packaging applications. Efficacy of the natural extracts is compared to an industrial antimicrobial blend.

2 MATERIALS AND METHODS

Both pine bark (PB) and sea buckthorn (SB) extracts were prepared with a similar procedure using ethanol extraction. Ethanol was then removed from the supernatant with a rotatory evaporator at 35 °C. The anti-microbial blend (AB) was a CO_2 extract of a mixture of herbs obtained from Flavex Germany. The natural extracts were coated onto a specialty paper (MLPC), which had multiple coating layers, including a barrier that prevents penetration of the extract coatings into the paper. Rod coating is used to apply the natural extracts as thin films onto paper surface, which are then dried at room temperature or using infrared. Two metering rods that correspond to coating thickness of 12 µm and 24 µm were used to deliver coatings onto paper surface. *S. aureus* (VTT E-70045) and *P. aeruginosa* (E-96728) were used as target bacteria to test antibacterial activity.

2.1 Results and Conclusions

Both SB and PB showed antibacterial activity in liquid culture medium. However only SB and industrial AB showed significant antibacterial activity after the extracts are applied as coatings onto paper. *P. aeruginosa* was more susceptible to the natural extracts compared to *S. aureus*. The results suggest that the efficacy of natural plant extracts depend on the bacteria strain. The results also demonstrate that applying natural extracts as coatings on paper for packaging application can reduce the efficacy compared to the solvent extracts. This is a result of an increase in surface area that facilitates the evaporation or inactivation of active ingredients that result in antibacterial activity. The results suggest that drying process did not impact the efficacy of natural extracts applied as coating: however, further studies would be required to confirm this.

This study demonstrates the efficacy of natural plant extracts as suitable coatings that can be used on packaging paper to obtain antibacterial activity. Antibacterial paper can be used to maintain the freshness of food, thereby extending the shelf-life of food.

3 REFERENCES

[1] K. Verghese, H. Lewis, S. Lockrey and H. Williams, "Packaging's Role in Minimizing Food Loss and Waste Across the Supply Chain," *Packaging Technology and Science*, vol. 28, pp. 603-620, 2015.

[2] T. Saxena, P. Kaushik and M. Krishna Mohan, "Prevalence of E. coli O157:H7 in water sources: an overview on associated diseases, outbreaks and detection methods," *Diagn. Microbiol. Infect. Dis.*, vol. 82, pp. 249-264, 7, 2015.

[3] S. Saini, C. Sillard, M. Naceur Belgacem and J. Bras, "Nisin anchored cellulose nanofibers for long term antimicrobial active food packaging," *RSC Adv.*, vol. 6, pp. 12422-12430, 2016.

[4] N. K. Upadhyay, M. S. Yogendra Kumar and A. Gupta, "Antioxidant, cytoprotective and antibacterial effects of Sea buckthorn (Hippophae rhamnoides L.) leaves," *Food and Chemical Toxicology*, vol. 48, pp. 3443-3448, 12, 2010.

Antibacterial Properties of CNF/PVAm modified fiber and studied by cellulose model surface

CHAO CHEN, JOSEFIN ILLERGÅRD,
LARS WÅGBERG and MONICA EK

Royal Institute of Technology (KTH)
Department of Fiber and Polymer Technology
chaoc@kth.se

Keywords: Antibacterial, CNF, Cellulose model surface

1 INTRODUCTION

Varieties of alternatives have been used so far to introduce antibacterial properties to celluloseic fibers, aiming at producing high-end value products in hygiene and environmental applications. One of alternatives, by means of the layer-by-layer (LbL) modification technique, fabricating cationic polyelectrolyte multilayers on substrates, stands out for its outstanding bacterial reduction and mild preparation conditions. Previously a 3-layer system of PVAm/PAA/PVAm was LbL assembled on cellulose fiber, which was found to be dramatically efficient for bacterial removing and high growth inhibition capabilities.[1] Later it was found that by altering the cationic polyelectrolyte i.e. replace PVAm with PDADMAC and PAH also achieved good results, and the correlation between positive charge densities and antibacterial effects had been studied, which indicatses the charge density is the dominate factor in this system.[2] On the other hand, surface structure was also been found to be a important factor that could affect the bacteria attachment.[3] However, a vision is to make a more bio-based material as the polymers used today, i.e, the PAA used as the middle layer are fossil-based. A step forwards currently was replace the anionic layer of PAA by more sustainable wood based cellulose nano fibers (CNF). The CNF is negatively charged and can be used as the component in LbL assembling[4]. It also supposed to create more structured surface than PAA did on fiber surface, which potentially increase the interaction with bacterium cells. In this study, the previous PVAm/PAA/PVAm system was relaced by PVAm/CNF/PVAm under different assembly conditions, and its antibacterial activites would be evaluated. By making cellulose model surfaces, a better visulazaion studies can be obtained and layer assembly can be also characterized.

2 EXPERIMENTAL

2.1 Fiber and model surface modification

Fiber used was bleached chemical softwood as fluff pulp. The pulp was disintegrated and washed according to the procedure, thereafter modified by adsorbing one layer of PVAm at pH 9.5 with 100 mM NaCl salt concentration. Second layer of CNF was adsorbed under different conditions i.e, pH 3.5 and pH 7.5, salt concentration ranged from 1 mM, 10 mM and 100 mM. The amount of adsorbed PVAm on fibers were determined by Antek nitrogen analysis. Same modification schemes were as well as applied on the cellulose model surfaces. The model surfaces were made on silicon wafers by spincoating the dissolved fluff pulp. The pulp was dissolved in NMMO/DMSO solution at 115 °C followed by precipitated in water and dried in oven at 105 °C. Modified model surfaces were observed under bright-field microscope.

2.2 Bacteria assays

E. coli K-12 was used as test object in both bacterial removel test and growth inhibition test. By counting the number of bacteria left in the solution after contacting with modified fibers, the bacteria removal rates can be calculated. 10% of nutrient was added to the left suspension and incubated bacteria with modified fiber for 18 hours at 37 ºC, the growth inhibition capabilities can be monitored by examine the optical density (OD) and compared with + control reference. Interactions between bacteria and modified cellulose model surfaces could be observed under microscopes, including flourscing microscopy, scanning electron microscopy, and atomic force microscopy.

3 RESULTS

3.1 Bacterial removal and growth inhibition

From Figure 1, the bacterial removal and growth inhibition shown a comparable and even better performances then previously described PAA/PVAm system. It can be found higher salt concentration and lower assembling pH in the multilayer build-ups results the highest antibacterial effects. However based on the test of nitrogen analysis, the adsorbed PVAm in CNF/PVAm samples was not as much as PAA/PVAm or even much lower. To obtain a better and clearer picture of this behaviour, more tests were done with the help of cellulose model surfaces.

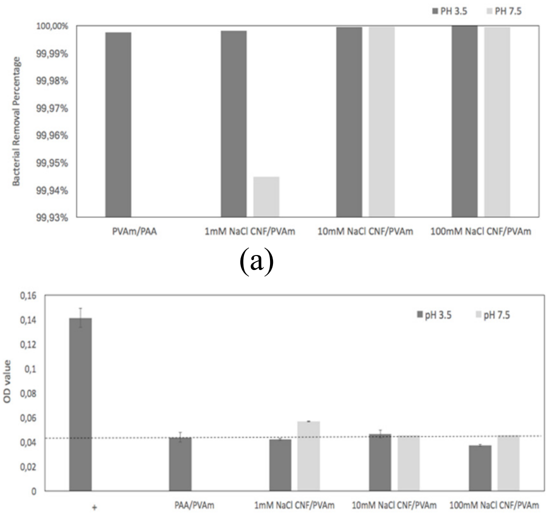

(a)

(b)

Figure 1. Bacterial assays on modified fibers (a), bacterial removal rates of PAA/PVAm and different assmebly condition of CNF/PVAm modified fibersand (b). Bacterial growth inhibition monitored by Optical Density (OD) after incubated bacteria with different modified fibers

3.2 Bacteria interaction with model surfaces

Since the surface of cellulose fiber is very heterogeneous, making it hard to characterize and visualize. While on cellulose model surfaces, it can be observed easily in Figure 2, the surface topography and bacteria adsorption can be clearly visualized and compared. The surfaces performed differently under different LbL assembly conditions. It can be observed that some of the surfaces had this island shape CNF aggregates which were appeared when assembling under pH 3.5 and higher salt concentration conditions. Interestingly, the bacteria tended to adsorbed on “island” region. Take advantages of scanning electron microscope (SEM) the adsorption amount of bacteria under island shape region and flat regeion was compared. Figure 3 shown the bacteria attachment on a same model surface (CNF assembled at pH 3.5 with 10 mM NaCl salt concentration) with different regions, left was island region, right was flat region. And it can be clearly observed that more bacteria was adsorbed on the region of CNF aggregates other than on flat areas.

This is also confirmed by AFM images. The morphologies of the bacteria on CNF modified model surfaces were similar to the surface modified by previous PAA/PVAm, which indicated that the cell damages mainly came from the cationic polyelectrolyte of PVAm, while the existence CNF could expand the primary 2D flat surface to a 3D topographical surface thus enhance the bacteria attachments. By increasing the salt concentration, the CNF tends to aggregates more and formed higher (thicker) island for a further increasing of surface areas. The roughnesses of different positions on surfaces had been determined by AFM. A positive correlation can be observed that more bacteria tend to be adsorbed on higher roughness region of CNF aggregation.

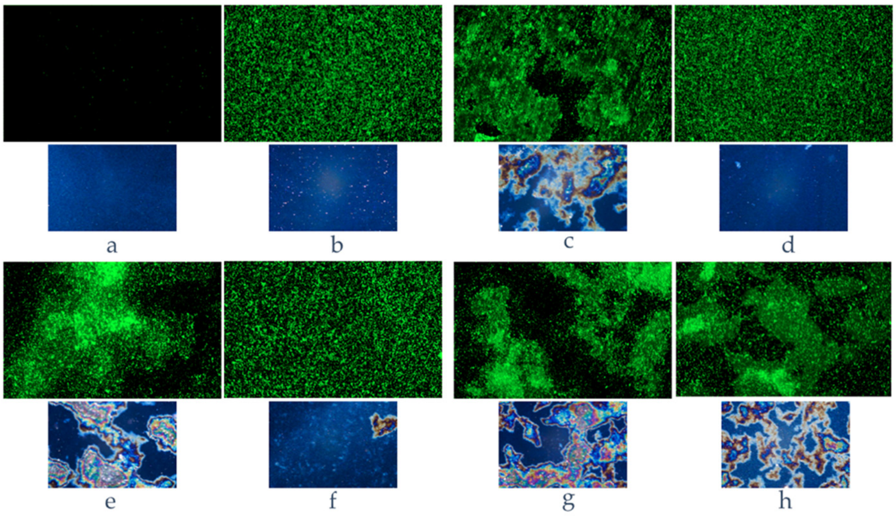

Figure 2. Flourencing microscopy images of the surfaces with bacteria adsorbed (green) and bright-field microscopy images of the surfaces without bacteria adsorbed (blue). a: Reference cellulose model surface without modification, b: PAA/PVAm modified model surface, c: CNF/PVAm modified surface, in which CNF layer assembly at pH 3.5 1 mM salt concentration, d: CNF layer assembly at pH 7.5 1 mM salt, e: CNF layer assembly at pH 3.5 10 mM salt concentration, f: CNF assembly at pH 7.5 10 mM salt concentration, g: CNF assembly at pH 3.5 100 mM salt concentration, h: CNF assembly at pH 7.5 100 mM salt concentration

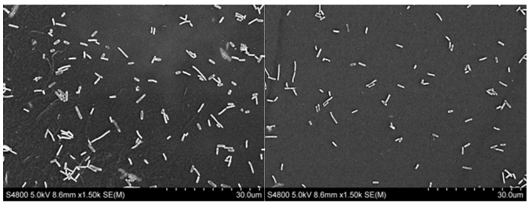

Figure 3. SEM images of Bacteria on modified model surface. Left is bacteria on island region, right is on flat region

REFERENCES

[1] J. Illergard, U. Romling, L. Wagberg, Ek. Monica. Tailoring the effect of antibacterial polyelectrolyte multilayers bu choice of cellulosic fiber substrate *Holzforschung.* **67**(5):573–578 (2003).

[2] C. Chen, J. Illergard, L. Wagberg, Ek. Monica Effect of cationic polyelectrolytes in contact-active antibacterial layer-by-layer funcrionalization *Holzforschung.*

[3] J. Henschen, PA. Larsson, J. Illergard, M. Ek, L. Wagberg. Bacterial adhesion to polyvinylamine-modified nanocellulose films. *Colloids and Surfaces B: Biointerfaces* 151 (2017): 224-231

[4] L. Wagberg, G. decher, M. Norgren, T. Lindstrom, M. Ankerfors, K. Axnas, The Build-Up of Polyelectrolyte Multilayers of Microfibrillated Cellulose and Cationic Polyelectrolytes. Langmuir (2008), 24, 784-795

Conversion of lignin-cellulose prefibres to carbon fibres

ANDREAS BENGTSSON

Department of Fibre and Polymer
Technology, Royal Institute of
Technology, Stockholm, Sweden
aben4@kth.se

1 INTRODUCTION

Lightweight composite materials, reinforced with carbon fibres (CFs) as the load bearing component are highly desired in structural applications (e.g. automotive, aerospace and sporting goods) due to their high specific strength and modulus; low specific density; high electric and thermal conductivity; as well as high creep resistance [1,2].

The remaining challenge for CF-based composites on the commercial market is the high cost associated to the high prefibre cost, including the raw material cost, which in turn has limited the use of CFs to high-end value applications [1,2,3]. Hence, in order for CF-reinforced composites to be attractive in a wider spectrum of applications, the cost must be reduced.

1.1 Manufacturing of carbon fibres

The starting route for the manufacturing of CF involves spinning of precursor fibre, usually by wet-spinning or melt-spinning methods, where the spun prefibre often is surface treated to ease handling of the prefibres in the subsequent steps [1]. The following stages during manufacturing of CFs involve the conversion of precursor fibres into CFs via heat treatments, such as oxidative stabilization, followed by subsequent carbonization, and in some cases, graphitization [1]. A schematic illustration of the conversion of precursor fibre into CF is depicted in Figure 1.

In order to obtain infusible and crosslinked fibres prior to carbonization, the oxidative stabilization is usually carried out in air by increasing temperature to 180-300˚C [1]. Much effort has been put into understanding the reaction mechanisms during stabilization, since it is the most time-consuming part of the CF manufacturing, as well as an important step to reach high carbon yields [1,4,5]. Various types of reactions can occur during stabilization, e.g. oxidation, dehydrogenation, crosslinking and cyclization, depending on what precursor material used. During the subsequent carbonization of the stabilized prefibres, temperature is increased to 1000–2000˚C in inert atmosphere, and the carbon content in the fibre is raised to >90% as the fibre lose other elements by e.g. dehydrogenation reactions [1]. Carbonization results in semi-ordered carbonaceous structures, often called a turbostratic structure of carbon [1]. In order to obtain high modulus CF, graphitization is carried out at high temperature between 2000˚C and 3000˚C [1,2].

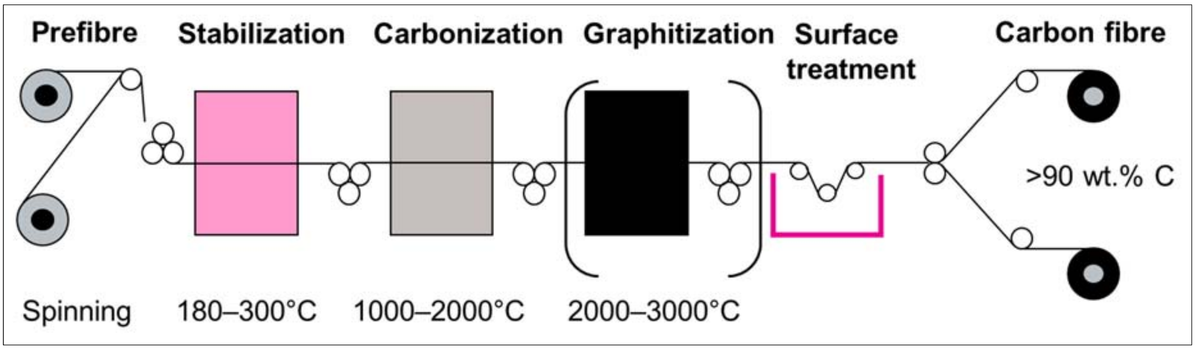

Figure 1. Schematic illustration of the commercial manufacturing route of carbon fibre. Note the non-continuity between the prefibre spinning and stabilization.

In commercial production lines, the CFs are usually surface treated after carbonization (or graphitization), in order to facilitate handling as well as increase the compatibility with the matrix in the composite [1].

1.2 Commercial precursors for carbon fibre production

Commercially, CFs are currently manufactured from three different organic precursors, namely polyacrylonitrile (PAN), pitch and regenerated cellulose (e.g. rayon) [1,2]. The vast majority of CF production (about 90%) involves the thermal conversion of wet-spun prefibres originating from the petroleum-based precursor PAN [6]. PAN is the dominating precursor mainly due to the high tensile strength (3–7 GPa) and moderately high modulus (200–300 GPa) [7], as well as high practical carbon yield (50–55%) [1]. However, for some special applications (e.g. aerospace) requiring high modulus, as well as high thermal and electrical conductivity, CFs produced from melt-spun pitch-prefibres is preferable [1,2]. Petroleum/coal-based pitch is built-up by aliphatic and aromatic hydrocarbons [1]. Yet, the lower tensile strength and higher price of high modulus CFs from pitch (compared to PAN) are limiting factors [1,2].

Wet-spun prefibres from regenerated cellulose (e.g. rayon) accounts for about 1% of total CF production worldwide [6], mainly due to the poor mechanical properties originating from defects such as voids, leading to weak and brittle CF [8]. Moreover, conversion of cellulose into CF results in low carbon yields of 10–30% (theoretical yield 44.4%) [8], which is problematic in a cost perspective. Due to the poor mechanical properties of rayon-based CF, its commercial success has been mainly focused on non-structural applications such as porous activated carbon fibres and applications where high purity is required [1,8].

1.3 Lignin and cellulose as precursor for carbon fibre production

The high cost of the PAN precursor, which accounts for 51% of the total production cost [3], implies that it is desirable to find alternative precursors in order to reduce the cost of CFs. Commercial CF made from regenerated cellulose is already present on the market. The U.S. Department of Energy (DOE) has identified lignin as a possible alternative as low-cost precursor material for the manufacturing of CFs [9]. Lignin has gained interest as raw material for the production of CFs due to its high availability; low price (compared to PAN) [3]; high theoretical carbon content (61-65%) compared to cellulose [6], as well as renewability. At present, technical lignin can be efficiently isolated at high purities (low ash content) from the black liquor in e.g. the Kraft pulping process by acidic precipitation, by using e.g. carbon dioxide [10].

While cellulose is a linear polymer consisting of D-glucose units linked by β(1→4) linkages, lignin is an racemic and amorphous macromolecule, with very complex structure built up by essentially three monolignols (*p*-coumaryl, guaiacyl and syringyl) [11]. Lignin consists of phenolic units which is partly chemically crosslinked both in its native state and after separation [11].

As cellulose fibres demonstrate a relatively ordered structure along the fibre axis [8], lignin does not, and the inhomogeneous and random-structural characteristics of lignin are a drawback for CF-production. Critical steps in order to enhance the mechanical properties of lignin-based CF are low amount of ash (minimizing defects in fibre) [7]; low polydispersity (i.e. a highly homogenous material with respect to molecular weight distribution) [12]; as well as minimizing void formation [13]. So far the mechanical properties of lignin-based CFs haven't met the requirements set by the U.S. automotive industry, who demand CFs to have a tensile strength of 1.72 GPa and a modulus of 172 GPa [3].

2 SCOPE AND OUTLINE OF THE CURRENT RESEARCH

The current research project is a part of Project LightFibre, which is a collaborative project between Research Institutes of Sweden (RISE) Bioeconomy (former Innventia AB) and Swerea IVF. The project aims to give a fundamental understanding of the conversion of dry-jet wet-spun lignin-cellulose precursor fibres into CFs. The promising results obtained by Olsson et al. [6] have shown that it is possible to make CFs from dry-jet wet-spun lignin-cellulose prefibres (70/30 w/w). The best-performing fibres in the work of Olsson et al. demonstrated a tensile strength of 780 MPa and tensile modulus of 68 GPa.

In the licentiate project the conversion steps when making CFs from lignin-cellulose prefibres is addressed and examined. The challenge lies in the lack of understanding how lignin and cellulose behaves and affect each other during thermal treatments. By building up a fundamental understanding on how lignin-cellulose precursors behave during conversion (stabilization and carbonization) into CFs, the aim is to increase efficiency (in terms of yield and conversion time), as well as mechanical properties of the final CFs.

Softwood kraft pulp and dissolving pulp will be used as cellulose raw material, and softwood kraft lignin separated by the LignoBoost process will be used as lignin source.

REFERENCES

[1] Bahl et al. Manufacture of carbon fibers. In: Carbon Fibres. Eds. J-B. Donnet, T.K. Wang, S. Rebouillat, and J.C.M. Peng. Marcel Dekker, edition 3, (1998).

[2] X. Huang. Fabrication and Properties of Carbon Fibres. *Materials* **2**(4):2369–2403 (2009).

[3] D. A. Baker and T. G. Rials. Recent Advances in Low-Cost Carbon Fiber Manufacture from Lignin. *J. Appl. Polym. Sci.* **130**(2):713–729 (2013).

[4] E. Fitzer and D.J. Müller. The influence of oxygen on the chemical reactions during stabilization of PAN as carbon fiber precursor. *Carbon* **13**(1):63–69 (1975).

[5] T. Matsumoto, I. Mochida. A structural study on oxidative stabilization of mesophase pitch fibers derived from coaltar. *Carbon* **30**(7):1041–1046 (1992).

[6] C. Olsson, E. Sjöholm and A. Reimann. Carbon fibres from precursors produced by dry-jet wet-spinning of kraft lignin blended with kraft pulps. *Holzforschung* **71**(4):275–283 (2017).

[7] A. A. Ogale, M. Zhang, J. Jin. Recent advances in carbon fibers derived from biobased precursors. *J. Appl. Polym. Sci.* **133**(45):43794–43807 (2016).

[8] A. G. Dumanli and A. H. Windle. Carbon fibres from cellulosic precursors: A review. *J. Mater. Sci.* **47**(10):4236–4250 (2012).

[9] D. A. Baker, N. C. Gallego and F.S. Baker. On the Characterization and Spinning of an Organic Purified Lignin Toward the Manufacture of Low-Cost Carbon Fiber. *J. Appl. Polym. Sci.* **124**(1):227–234 (2012).

[10] F. Öhman, H. Theliander, P. Tomani and P. Axegård. Method for separating lignin from black liquor. WO Patent 2006031175 (2006).

[11] G. Henriksson. Wood Chemistry and Wood Biotechnology. Eds. M. Ek, G. Gellerstedt and G. Henriksson. De Gruyter, 1st edition, (2009).

[12] G. Gellerstedt, E. Sjöholm and I. Brodin. The Wood-Based Biorefinery: A Source of Carbon Fiber? *The Open Agriculture Journal* **3**:119–124 (2010).

[13] W. Qin and J.F. Kadla. Carbon Fibers Based on Pyrolytic Lignin. *J. Appl. Polym. Sci.* **126**(S1):E204–E213 (2012).

A study of sealability properties of extrusion-coated fiber-based materials

MALIN KRAFT, JOHANNA LAHTI, SANNA AUVINEN and JURKKA KUUSIPALO

Tampere University of Technology, TUT
malin.kraft@tut.fi

1 BACKGROUND

Extrusion coated fiber-based materials and plastic films are used in various packages, like flexible packages (wrappings and pouches), and rigid packages (liquid packages etc). For a package there are some important properties to be achieved.

First, the most important function is to shield the product inside. Extrusion coating a polymer layer on the fiber-based material gives a barrier against water, water vapour, aroma, grease, oxygen etc. Secondly, an important factor in extrusion coating is good adhesion between the substrate and the polymer. Finally, sealability of the material is vital, it affects the ability of the material to form hermetic seals, which is a necessity in different packages. This study has been made to show how sealability properties of packaging materials can be studied with different sealing methods.

2 HEAT SEALING

2.1 Sealing theory

In package converting sealing is vital for a package to form. The seals must provide adequate mechanical strength and leak tightness. Tight and strong seals contribute to preservation of the product and, on the other hand prevent any premature leakages. There are several different methods that can be used for heat sealing, such as hot bar sealing, hot air sealing, ultrasonic sealing, impulse sealing, hot melt sealing, induction sealing etc. The suitable method depends on the material, application, packaging process, etc.

Polymer coatings are normally sealed to itself or to the substrate, in other words, the reverse surface of the laminate. The laminate can also be sealed to some other packaging material, such as a cup or a tray. Depending on if the material is sealed against itself or the reverse side, the sealing mechanism varies. Figure 1 presents the sealing process where two similar semi-crystalline polymer surfaces are sealed. In this process, the surfaces are brought together, and with the help of applied pressure, heat and time, the surfaces melt and the polymer chains entangle. Cooling of the sealing surface enables the seal to form. [1, 2]

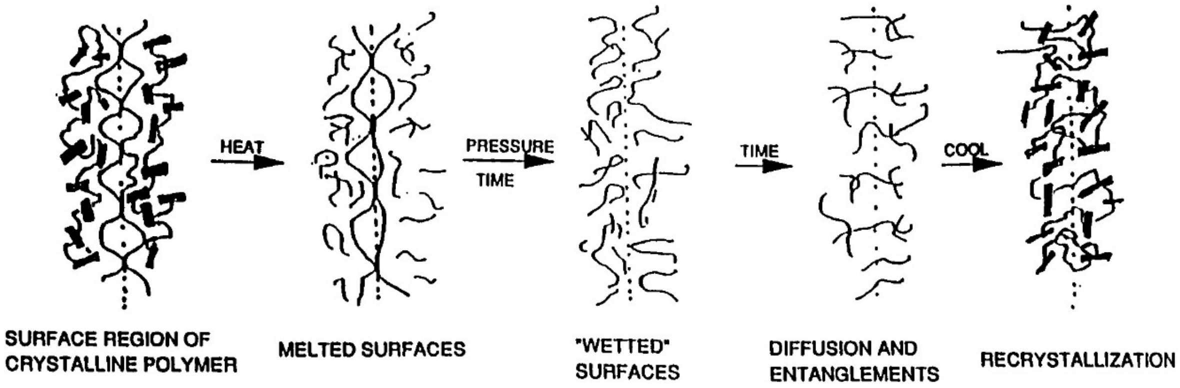

Figure 1. Sealing phenomena of semi-crystalline polymers. [1]

The sealing mechanism for sealing the polymer coating to the reverse side, differs from sealing polymer to polymer. In this case, the polymer must penetrate into the fiber substrate and hold the surfaces together by interlocking. The geometry of irregularities, the contact angle between materials and the wettability of adhesives affect this phenomenon. The surface topography of the fiber substrate also influences the rate of wetting and spreading. In order to achieve a good seal, the contact area between the substrate and the polymer must be optimal and furthermore, the polymer must have sufficient time to penetrate into the fiber network. [2]

(a) Poor adhesion between the wetting polymer and the surface.

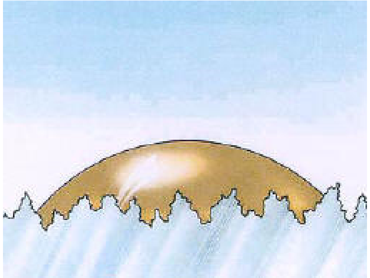

(b) Good adhesion between the liquid and the surface, good wetting.

Figure 2 the adhesion phenomena between a polymer and fiber surface.

2.2 Sealing methods

Typically sealability is studied with a hot bar sealing method. This method involves two heated bars that under a specific pressure and temperature presses together the materials to be sealed. In this method the critical factors are sealing time, temperature and pressure. When the seal is formed, it is evaluated either manually or by measuring the seal strength. [3]

Hot bar sealing is a common method for sealing, and used much in industry. However, it has been observed that this method does not correlate well with e.g. side sealing of carton cups, milk cartons and plastic bags. In industry, these types of seals are usually sealed with hot gas (typically air). Thus, there has been a clear need for a new method to simulate and study sealing process of these kind of packaging applications.

3 EXPERIMENTAL

3.1 Materials and methods

A novel hot air sealing equipment has been built at the Packaging Laboratory at Tampere University of Technology, Figure 3. The hot air sealing equipment was tested and compared to conventional hot bar sealing, the hot bar sealing equipment is presented in. For this, low-density polyethylene was extrusion coated on paper (83 gsm) and paperboard (200 gsm). Coating weights used were 10 g/m^2 and 20 g/m^2.

The samples were sealed and the seals were evaluated manually and visually according to the following scale:

0 = no seal
1 = weak adhesion
2 = adhered, but no tearing
3 = under 50% fiber tear
4 = over 50% fiber tear
4.5 = over 90% fiber tear
5 = 100% fiber tear

Typically the most interesting and valuable information is the temperature when the seal reaches a value of 5. In this case, the seal is stronger than the material and the failing is no longer due to a weak seal.

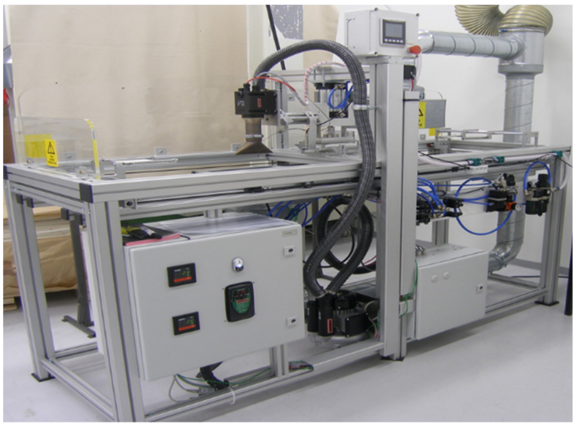

Figure 3. The hot air sealing equipment at TUT.

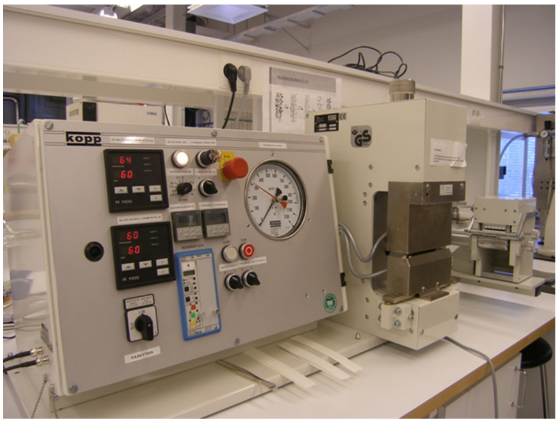

Figure 4. The hot bar sealing equipment at TUT.

3.2 Results

First the effect of heating time on the sealing temperature was evaluated with the hot air sealing equipment and the results are presented in Figure 5. For this evaluation, the PE (20 g/m^2) coated paperboard was used.

From the results two conclusions can be drawn. First, the temperature increases with decreasing heating time. Second, the sealing temperature is higher when sealing the polymer to the reverse side.

Figure 6 presents a comparison sealing test with all the included materials. From the results in Figure 6 a few conclusions can be drawn. First, the sealing temperature increases when sealing the polymer surface to the reverse side of the sample. Second, the sealing temperature for the different polymer coating weights do not differ from each other. In other words, if only considering sealing results, it would be possible to reduce coating weight in the product without loss of sealability properties. Finally, and most importantly, it can be seen that the sealing temperature for the materials sealed with the hot bar method is similar for all the materials. However, when sealing the coated paper against its reverse side,

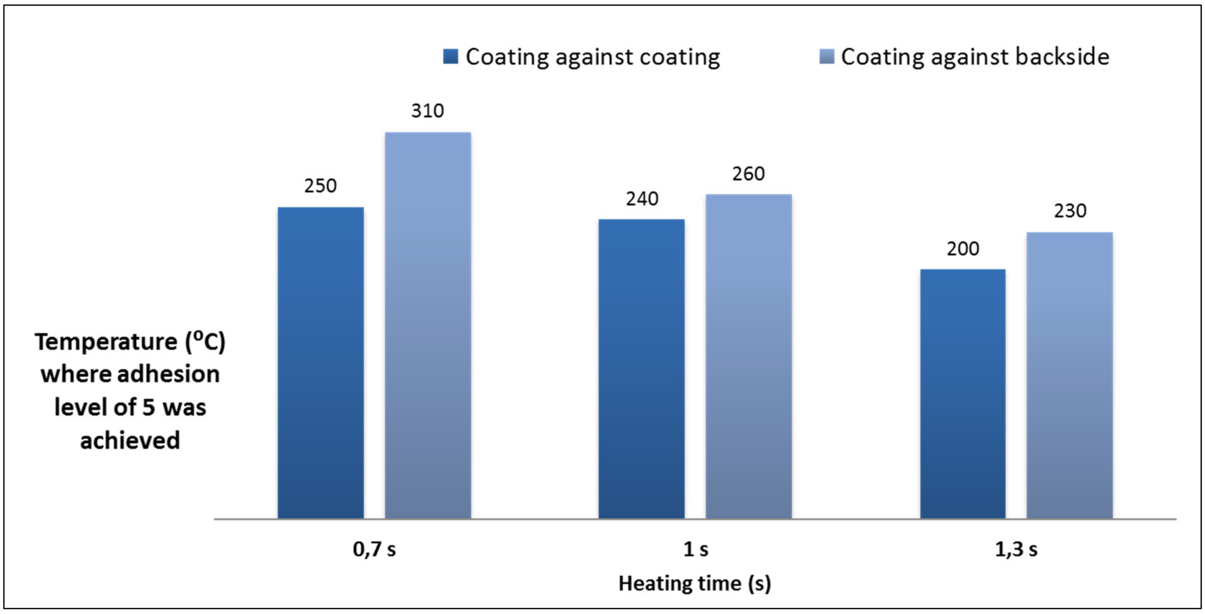

Figure 5. The effect of heating time on the sealing temperature.

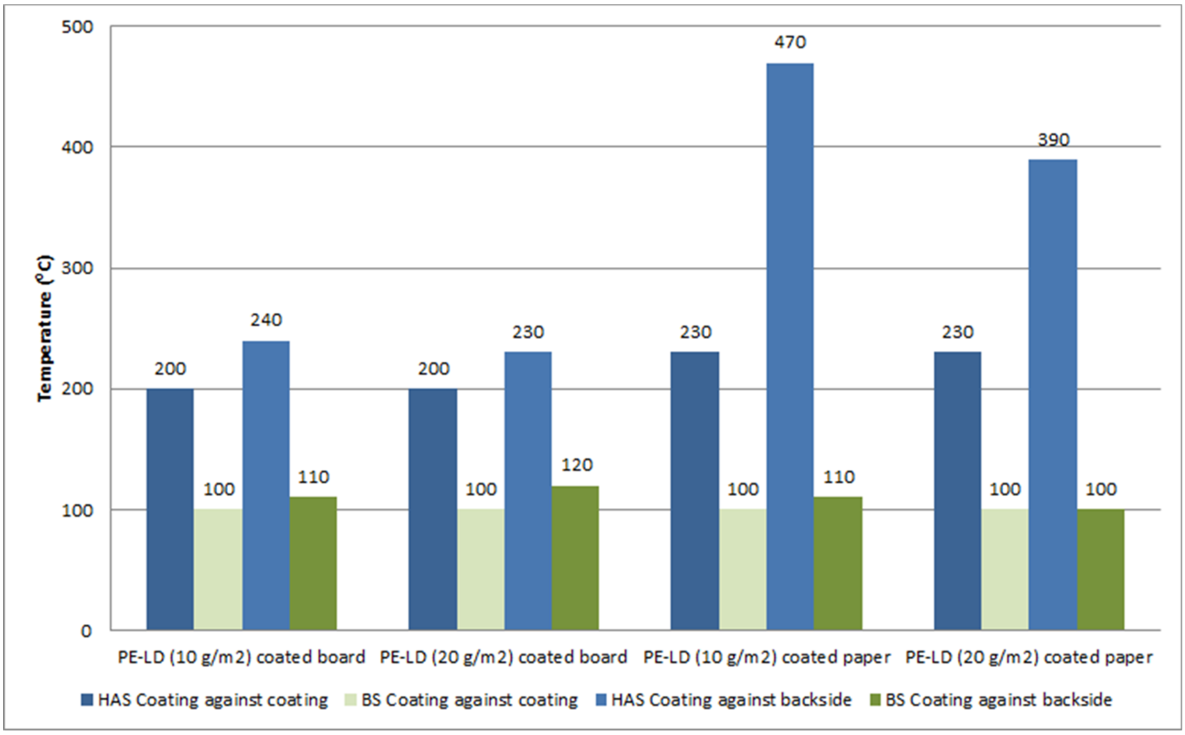

Figure 6. A comparison test between hot air sealing (HAS) and hot bar (BS) sealing.

the sealing temperature is considerably higher compared to the sealing temperature where the polymer is sealed against itself. In a production line, this information is quite important. [4]A final test was done in order to further investigate the effect of coating weight on the sealing temperature, these results are presented in Figure 7. Three different coating weights (14 g/m^2, 10 g/m^2 and 6 g/m^2) were extrusion coated on paper (83 g/m^2). Similarly, three different coating weights (17 g/m^2, 12 g/m^2

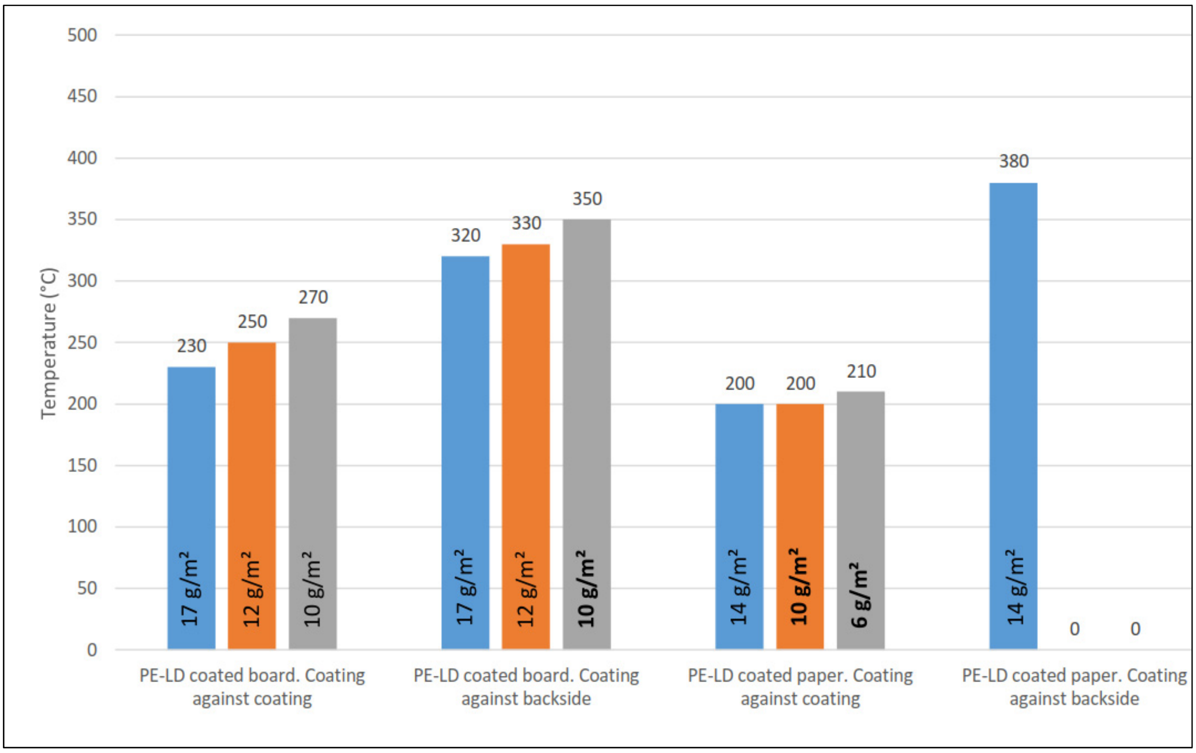

Figure 7. The effect of coating weight on the hot air sealing temperature.

and 10 g/m^2) were extrusion coated on paperboard (195 g/m^2). As there is a need for decreasing coating weights to reduce materials in production, this experiment was conducted to investigate the sealability of thin coatings.As can be expected, the sealing temperature increases with decreasing coating weight. In the case of sealing coated paper against the backside for coating weights 10 g/m^2 and 6 g/m^2, the paper started to yellow at temperatures above 430 °C. Yellowing of the paper is not acceptable in production lines, so therefore the sealing test ended at that temperature with a conclusion that these samples did not seal.

Furthermore, Figure 7 shows that for coated paperboard, thin PE coatings are possible to seal with hot air sealing, even though the sealing temperature increases. The sealing temperature is higher when sealing polymer against the backside. For paper, thin coatings are sealable, when sealing polymer against polymer, however, it is not possible to seal coatings less than 10 g/m^2.

Finally, when sealing polymer coated board against itself, the sealing temperature is considerably higher, compared to polymer coated paper sealed against itself.

CONCLUSIONS

Hot air sealing experimental data is important information when considering the sealability of different materials. This method is suitable for different materials, such as extrusion and dispersion coated paper and paperboard, even plastic films. With this method, sealing behaviour of different materials can easily be compared as well as simulate a sealing stage in the actual package forming process.

REFERENCES

[1] F.C. Stehling, P. Meka, Heat sealing of semicrystalline polymer films. II. Effect of melting distribution on heat-sealing behavior of polyolefins, Journal of Applied Polymer Science, Vol. 51, Iss. 1, 1994, pp. 105-119.

[2] J. Kuusipalo, Papermaking science and technology. Book 12, Paper and paperboard converting, 2nd ed., totally updated version ed. Finnish Paper Engineers' Association : Paperi ja puu, Helsinki, 2008, 346 p.

[3] K. Hishinuma, Heat sealing technology and engineering for packaging: principles and applications, DEStech Publications, Inc, United States of America, 2009, 251 p.

[4] Lahti, J., Auvinen, S., Kuusipalo, J., Novel equipment to simulate hot air heat sealability of packaging materials, 6-7 April, Munich, Germany.

Cellulose-fiber-based insulation materials with improved reaction-to-fire properties

CHAO ZHENG, DONGFANG LI,
MONICA EK

Department of Fiber and Polymer
Technology, KTH Royal Institute of
Technology, Teknikringen 56-58, SE-100
44 Stockholm, Sweden
chaozh@kth.se

1 INTRODUCTION

Thermal insulation made from cellulose-based fibers have advantages over other types of materials from a sustainability point of view [1]. To obtain a good thermal insulation property, cellulosic thermal insulation materials shall have a low density to ensure a low thermal conductivity [2]. However, as building components, the poor reaction-to-fire properties of cellulosic thermal insulation with low density have to be improved to ensure fire safety. Halogen and intumescent fire retardants are commercially used to improve the reaction-to-fire properties of thermal insulation. Compared with the former, the latter is more eco-friendly and safer, since no toxic gasses are produced during its combustion [3-5]. The intumescent fire retardants have been widely utilized in thermal insulation foams developed from fossil resources [6], but such applications in cellulosic foams have rarely been reported.

To obtain a CE-mark and be allowed to trade within the EU market, thermal insulation with low density needs to achieve fire class E [7], as stated by the Construction Products Directive. Different performance classes (A to F) for walls, roofing products, and floor-coverings are classified according to the standard test method [8] “The Single Flame Source Test EN ISO 11925-2: Reaction to fire tests for building products-Part 2: Ignitability when subjected to direct impingement of flame”. If the flame tip does not reach 150 mm above the flame application point during 20 s when a single flame is applied on the sample, the tested samples can be classified as E. Fire class E materials are able to resist a small flame attack without substantial flame spreading for a short period.

To evaluate the ignition behavior, the fire performance, and simulate or predict full-scale fire behavior of the cellulosic thermal insulation materials that pass class E, the cone calorimeter can be used to determine fire response parameters, such as time to ignition (TTI), heat release rate (HRR), total heat release (THR), smoke production, mass loss, and CO production. A longer time to ignition and a lower heat release rate indicate a better reaction-to-fire properties [9].

In the present study, two types of commercial intumescent fire retardants such as an expandable graphite (EG) fire retardant and a synergetic (SY) fire retardant were added at different weight ratios to the formulations to prepare cellulosic thermal insulation foams by the wet foaming technique. The fire performances of the foams were tested by the single-flame source test and cone calorimeter fire test.

2 MATERIALS AND METHODS

Sodium dodecyl sulfate surfactant and 5%, 10%, 15%, 20%, 25%, or 30% of either expandable graphite (EG) or the synergetic intumescent (SY) fire retardant were mixed with bleached mechanical pulp suspension. After mechanical stirring in a pulp disintegrator to form foams, the mats were dried in an oven. A pulp suspension without fire retardant was added to produce a reference insulation material.

Single flame source test was used to determine the ignition ability of cellulosic thermal insulation materials. Thermogravimetric analysis (TGA) and Cone Calorimeter fire test were utilized to determine the degradation and fire behaviours of the final materials respectively. The thermal insulation property of the fire-retardant insulation foams was determined by the Hot Disk TPS 2500S instrument.

3 RESULTS

3.1 Single flame source test

Cellulosic foams with more than 20% of expandable graphite in the formulations reached class E. For the foams with 15% and 20% SY in the formulations, they fulfilled the requirements of E class on one surface, but there were large burned areas on the rear surfaces, which could be attributed to a heterogeneous distribution of fire retardants and the limited retention (5–6%) of the fire retardants. The 20% EG, 25% EG, and 30% EG samples performed better than the 20% SY, 25% SY, and 30% SY samples. Based on the results of the single-flame source test, samples 20% EG and 25% SY that achieved the fire class E with the minimum amount of fire retardants (Figure 1) were subjected to testing in the cone calorimeter.

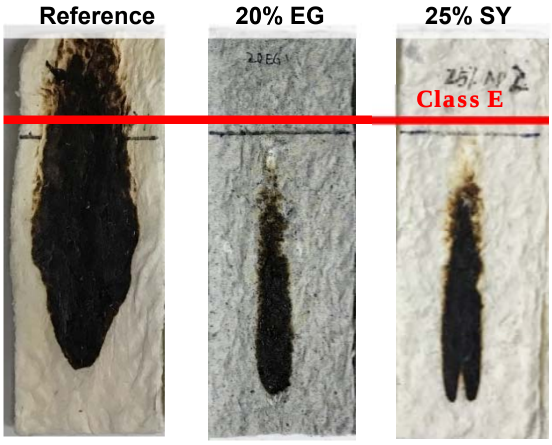

Figure 1. Single-flame source (surface) test result for reference foam without fire retardant, and foams with 20% expandable graphite (EG) fire retardant and 25% synergetic (SY) fire retardant in the formulation.

3.2 Thermogravimetric analysis(TGA)

Compared with the reference foam without fire retardant, 20% EG and 25% SY had lower decomposition temperature for 10% weight loss ($T_{onset\ 10\%}$) and a lower temperature at the maximum decomposition rate (T_{max1}), as shown in Figure 2. The lower $T_{onset\ 10\%}$ and T_{max} values indicate a lower thermal stability. A decrease in thermal stability favors early thermal decomposition of the foams and this facilitates the formation of a char layer on the foam surface at a lower temperature. The increase in residue or char (13%) can serve as a thermal barrier to protect the material from the external heat and hinder further combustion.

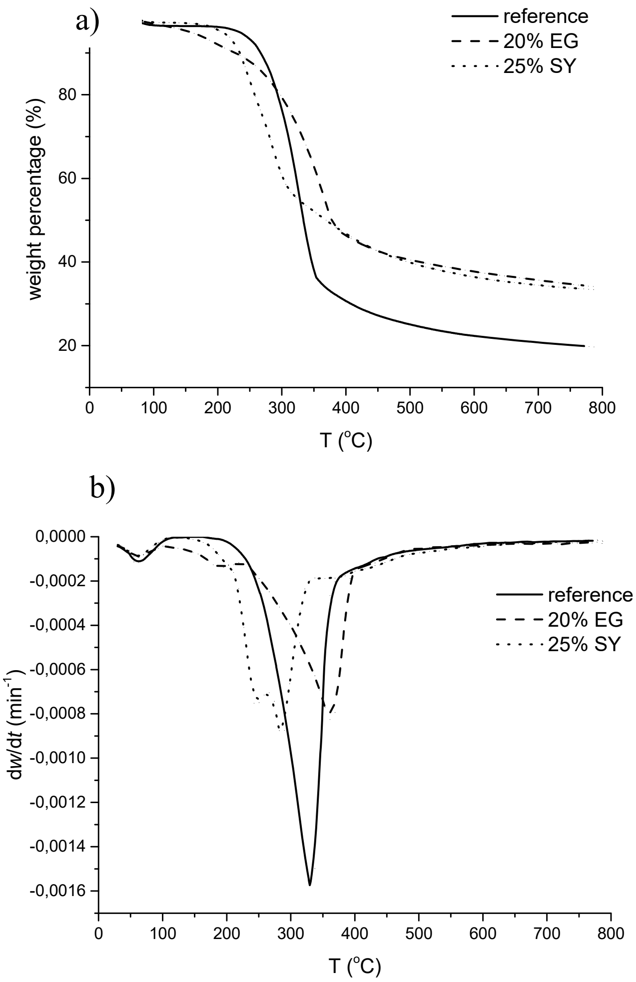

Figure 2. a) Thermogravimetric (TG) and b) Derivative curves (DTG) for the reference and fire-retardant containing insulation foams.

T_{max1} for the 20% EG sample was much lower than that for the 25% SY, but the temperature at the maximum weight loss rate (T_{max2}) for 20% EG was obviously higher than that for 25% SY. The higher T_{max2} for 20% EG may be related to the formation of a thermally stable char due to graphite expansion at T_{max1} [12]. Two peaks were observed in the DTG curve of 25% SY. The first peak could result from the onset of decomposition of aluminum hydroxide at approximately 250°C giving Al_2O_3 and water [13]. The second peak could result from the loss of APP at 300°C due to the release of NH_3 and H_2O [14].

3.3 Cone Calorimeter fire test

The peak heat release rate (Peak-HRR) and average HRR are crucial for explaining the rate of heat release during combustion. The HRR and the total heat release (THR) are also important in the evaluation of fire disaster. A lower heat release rate suggests a lower oxygen consumption and better reaction-to-fire properties.

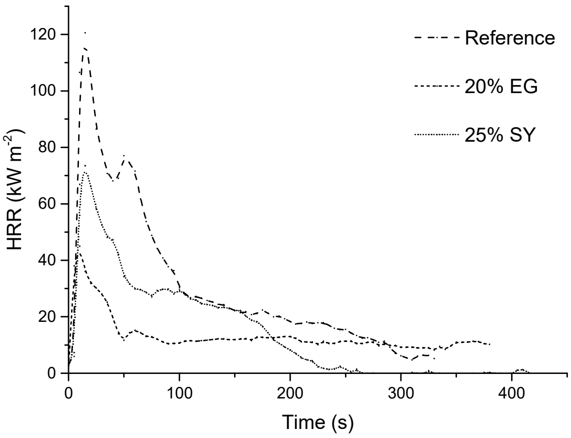

Figure 3. Heat release rate curves of the reference without fire retardant, 20% EG, and 25% SY from the cone calorimeter fire test (incident heat flux 25 kW m^{-2}).

As shown in Figure 3, compared to the reference without fire retardant, the Peak-HRR of the 20% EG and 25% SY decreased by 62% and 39% respectively, and the total heat release (THR) decreased by 56% and 38% respectively. The shorter time to ignition (TTI) of 20% EG could be related to the black color of the foams with EG as the fire retardant, which could absorb more radiant heat from the cone heater, and thus show a faster increase in the surface temperature and an earlier initiation of thermal degradation of the cellulose [15].

3.4 Thermal conductivity

The thermal conductivities of the 20% EG and 25% SY samples were similar to that of the reference (Table 1). The slightly higher thermal conductivity of 25% SY may be due to the higher density as a result of the addition of fire retardant. According to ColletandPrétot [16], higher density contributes to higher heat transfer through the solid component of the material, and this results in an increased conductivity. Furthermore, EG had no detrimental effect on the thermal conductivity of the cellulosic foams. This result is different from that the thermal conductivity of polyisocyanurate–polyurethane foams increased when EG was added [6].

Table 1. Thermal conductivity and density of the reference without fire retardant, 20% EG, and 25% SY.

Material	Thermal Conductivity (W $m^{-1}K^{-1}$)	Density (g cm^{-3})
Reference	0.050±0.001	0.047±0.003
20% EG	0.049±0.001	0.042±0.003
25% SY	0.052±0.001	0.060±0.002

4 CONCLUSIONS

The reaction-to-fire properties of cellulosic thermal insulation foams with low density were substantially improved by adding either 20% expandable graphite or 25% synergetic fire retardant into the formulation. According to the single-flame source test, the performances of these foams could meet the requirements of European fire class E. The results of the cone calorimeter fire test suggested that the peak heat release rate of these foams was significantly lower than that of the reference foam without the fire retardant. The foam with 20% expandable graphite fire retardant in its formulation had better reaction-to-fire properties than the foam with 25% synergetic fire retardant, but there is no negative effect on the thermal conductivity of the cellulosic foams.

REFERENCES

[1] I.Z. Bribián, A.V. Capilla,A.A. Usón, Life cycle assessment of building materials: Comparative analysis of energy and environmental impacts and evaluation of the eco-efficiency improvement potential. Build. Environ., 2011. 46(5):1133-1140.

[2] J. Xu, R. Sugawara, R. Widyorini, G. Han,S. Kawai, Manufacture and properties of low-density binderless particleboard from kenaf core. J. Wood. Sci., 2004. 50(1):62-67.

[3] M. ModestiA. Lorenzetti, Halogen-free flame retardants for polymeric foams. Polym. Degrad. Stabil., 2002. 78(1):167-173.

[4] O. Koklukaya, F. Carosio, J.C. Grunlan,L. Wågberg, Flame-retardant paper from wood fibers functionalized via layer-by-layer assembly. ACS Appl. Mater. Interfaces, 2015. 7(42):23750-23759.

[5] M. Ghanadpour, F. Carosio, P.T. Larsson,L. Wågberg, Phosphorylated cellulose nanofibrils: a renewable nanomaterial for the preparation of intrinsically flame-retardant materials. Biomacromolecules, 2015. 16(10):3399-3410.

[6] M. Modesti, A. Lorenzetti, F. Simioni,G. Camino, Expandable graphite as an intumescent flame retardant in polyisocyanurate–polyurethane foams. Polym. Degrad. Stabil., 2002. 77(2):195-202.

[7] B.A.-L. ÖstmanE. Mikkola, European classes for the reaction to fire performance of wood products. Holz. Roh. Werkst., 2006. 64(4):327-337.

[8] CEN ISO, Standard 11925-2: Reaction to fire tests. Ignitability of products subjected to direct impingement of flame. Single-flame source test. 2010, International Organization for Standardization: Switzerland.

[9] B. SchartelT.R. Hull, Development of fire-retarded materials—Interpretation of cone calorimeter data. Fire Mater., 2007. 31(5):327-354.

[10] CEN, Standard 13501-1: Fire classification of construction products and building elements. Classification using test data from reaction to fire tests. 2007, European Committee for Standardization: Brussels, Belgium.

[11] ISO, Standard 5660-1: Reaction-to-fire tests Heat release, smoke production and mass loss rate Part 1: Heat release rate (cone calorimeter method) and smoke production rate (dynamic measurement). 2015, International Organization for Standardization: Switzerland.

[12] X.Y. Meng, L. Ye, X.G. Zhang, P.M. Tang, J.H. Tang, X. Ji,Z.M. Li, Effects of expandable graphite and ammonium polyphosphate on the flame-retardant and mechanical properties of rigid polyurethane foams. J. Appl. Polym. Sci., 2009. 114(2):853-863.

[13] Y. Arao, S. Nakamura, Y. Tomita, K. Takakuwa, T. Umemura,T. Tanaka, Improvement on fire retardancy of wood flour/polypropylene composites using various fire retardants. Polym. Degrad. Stabil., 2014. 100:79-85.

[14] A. Riva, G. Camino, L. Fomperie,P. Amigouet, Fire retardant mechanism in intumescent ethylene vinyl acetate compositions. Polym. Degrad. Stabil., 2003. 82(2):341-346.

[15] P. Wei, S. Bocchini,G. Camino, Flame retardant and thermal behavior of polylactide/expandable graphite composites. Polimery-w., 2013. 58(5):361-364.

[16] F. ColletS. Prétot, Thermal conductivity of hemp concretes: Variation with formulation, density and water content. Constr. Build. Mater., 2014. 65:612-619.

Co-exfoliation and fabrication of graphene/microfibrillated cellulose composites and influence on functional properties

JOSPHAT PHIRI[1*]; LEENA-SISKO JOHANSSON[1]; PATRICK GANE[1, 2]; THAD MALONEY[1]
[1]School of Chemical Technology,
Department of Bioproducts and Biosystems,
Aalto University, P.O. Box 16300, 00076
Aalto, Finland
[2]Omya International AG, CH-4665
Oftringen, Switzerland

josphat.phiri@aalto.fi

1 INTRODUCTION

Polymer based nanocomposites exhibit interesting various properties that make them potentially, significant for fabrication and development of advanced materials for wide scale application [1]. Special interest is of course greater for composites based on natural polymers such as micro and nanofibrillated cellulose (MNFC). Cellulose based materials exhibit excellent properties and can, also be tailored for specific application by incorporation of nanofillers with various functional properties. Graphene is such a nanofiller with excellent properties that has shown great potential as a polymer reinforcement filler.

Graphene is a 2-dimensional material made up of a single layer of carbon atoms and has become one of the most studied materials due to its extraordinary electrical, mechanical and thermal properties. Graphene can be manufactured for example from natural graphite, which is low-cost and abundantly available [2]. However, the existing fabrication methods still offer many challenges especially for large-scale application as well as for composite fabrication. In this study, we show that graphene can be directly exfoliated in microfibrillated suspensions for direct fabrication of graphene/MFC nanocomposites. These nanocomposites showed enhanced functional properties compared to the neat MFC films.

2 METHODS

Reduced graphite oxide (RGO) was prepared by oxidation and reduction of natural graphite flakes. RGO and graphite powder were then separately mixed with MFC suspensions in various proportions. Shear exfoliation was performed using an IKA Magic Lab (1-l module micro-plant equipped with a single-walled open 1-l vessel) high shear mixing equipment with a maximum flow rate of 80 l h^{-1}. The details of the procedure can be found in our earlier publication [3]. The suspensions were then used to fabricate composites using a handsheet former. The prepared composites were stored in a controlled atmosphere for at least 48 h before performing mechanical analysis tests.

3 RESULTS AND DISCUSSION

The surface chemistry of pristine graphene and RGO differs significantly. Pristine graphene is unreactive and thus, theoretically, is not suitable as a filler for most polymer reinforcements due to lack of reactive sites suitable for interaction with the polymer matrix that can promote enhancement of the properties. For RGO however, the surface and edges of the sheets is fully decorated with oxygen functional groups. The hydroxyl (-OH) or epoxide (C-O-C) in the basal plane and carbonyl (C=O) and carboxylic (-COOH) on the edges [4]. These functional groups help RGO to disperse homogeneously and interact with the polymer matrix.

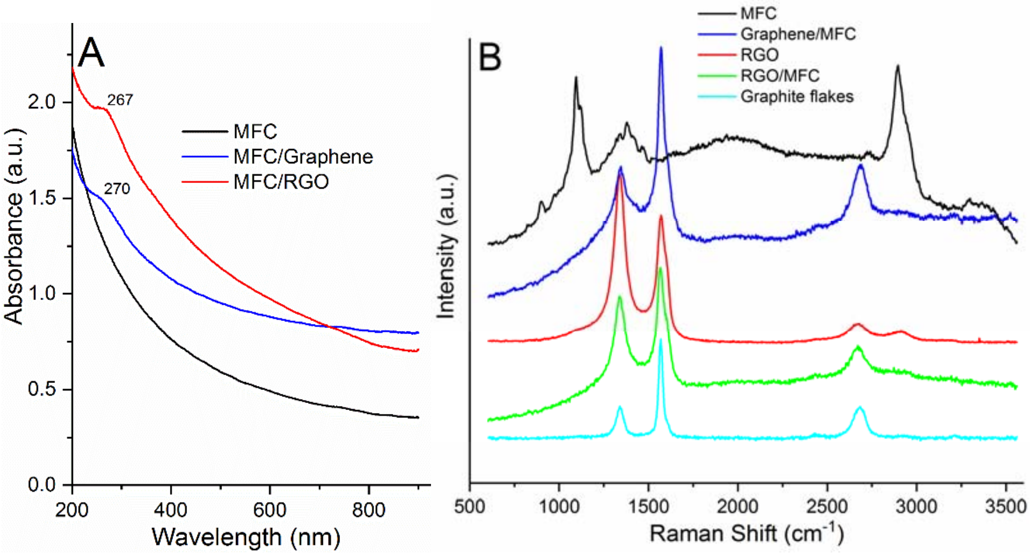

Figure 1. (A) The UV-vis spectra and (B) Raman spectra of graphene of MFC, RGO and graphene together with their respective composites at 9wt% loading

Evidence of exfoliation was investigated by UV-vis and Raman spectroscopies. The UV-vis spectrum of the neat suspension of MFC showed a featureless spectrum as shown in Figure 1A. However, with the additional of only 9 wt% of the fillers, a typical peak at around 270 nm was observed. This is a typical peak for quasi-two-dimensional material, which makes it easy to confirm the presence of 2D materials. The maximum absorption peak at around 270 nm is attributed to the π - π^* transitions of aromatic C–C bonds in graphene [5]. Graphene oxide however (not shown) has a typical peak at around 230 nm. After reduction, the peak red shifts by ~40 nm, that also confirms successful reduction of graphene as shown in Figure 1A. Therefore, the absorption peak observed and the high absorption values seen between 270 and 800 nm strongly suggest the presence of two-dimensional material in the suspensions, thus confirming the successful exfoliation of graphite in MFC suspension using high shear exfoliation.

Raman analysis (Figure 1B) of the surface of the composites showed that all they typical graphitic bands were present: the D band (~1582 cm^{-1}), G band (~1350 cm^{-1}) and 2D band (~2700 cm^{-1}). The neat MFC showed quite a different spectrum compared to that of graphite. Despite having only 9 wt% loading of the graphitic material, the spectrum was dominated by carbon based bands, which shows that the filler was homogenously dispersed in the MFC matrix.

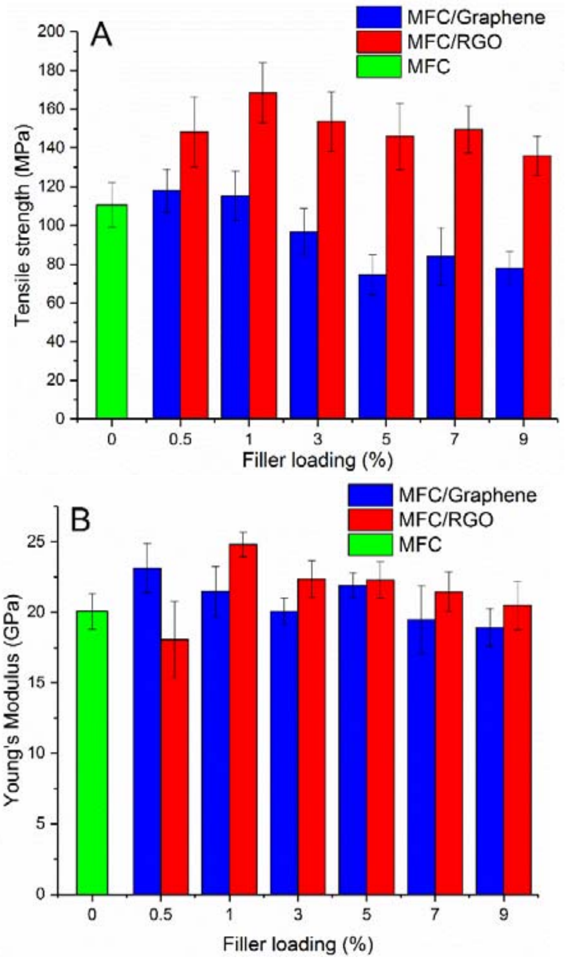

Figure 2 Mechanical properties of the composites as a function of filler loading of graphene and RGO compared to MFC (A) tensile strength (B) Young’s modulus

Analysis of the mechanical properties of the composites showed a significant increase in tensile strength for the MFC composites incorporated with RGO whilst deterioration with graphene as shown Figure 2A. Compared to the neat MFC, the Young's modulus for both filler loadings showed an increasing trend (Figure 2B).

XPS analysis (not shown) showed that the surface of RGO contains various oxygen functional groups, which are absent on the surface of graphene. The decrease in the tensile strength of the composites with graphene loading is not surprising. Although pristine graphene has excellent mechanical properties, the binding properties with other materials for example, is limited to hydrophobic and π-π interactions as well as the weak van der Waals forces. These forces however, are not strong enough to promote a strong interfacial bonding between graphene and the polymer matrix. This leads to poor stress transfer between graphene and the MFC matrix. The deterioration of the mechanical properties is also attributed to the poor distribution of graphene in the MFC matrix. Hydrophobic graphene flocculates and aggregates in the MFC matrix and disrupts the homogeneity of the fibers and leads to concentrated stress forces. However, the functional oxygen groups on RGO surface promote a homogenous distribution and a strong interaction with the MFC matrix. Strong hydrogen bonds between RGO and MFC act as efficient interfacial load transfer.

The neat MFC films showed a Young's modulus of about 20 GPa. However, with the addition of 0.5 wt% of graphene, the Young's modulus increased to ~23 GPa. The highest value of ~25 GPa for RGO was achieved at 1wt% loading. With further filler loading, a slight decrease is observed. The presence of well dispersed nanofillers in the MFC matrix provide a strong resistance pillar for the displacement or movement of the MFC chains and thus leads to an increase in Young's modulus of the composites. Slight higher values are observed for RGO reinforced composites because RGO is more evenly dispersed in the MFC matrix. However, the close nature of these values indicate that the MFC matrix is able to prevent detrimental aggregation of graphene thus the observed improvement of the mechanical properties. SEM analysis in Figure 3 showed no evidence of aggregation for both RGO and graphene based MFC composites. The cross-section structure was very similar.

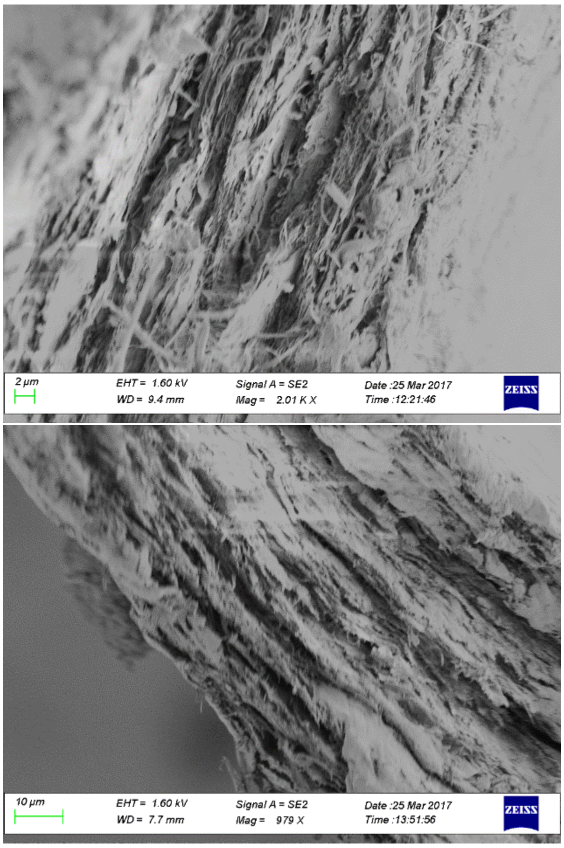

Figure 3 SEM cross-section area of (a) RGO/MFC and (b) Graphene/MFC composites at 9 wt% filler loading.

The electrical conductivity of the composites was measured by a four-point probe technique and is shown is Figure 4. At lower loading of 0.5 and 1 wt%, the graphene/MFC composites did not show any conductivity probably due to an incomplete connected network chain of graphene in the MFC matrix. However, conductivity was already detected for RGO/MFC composites even at much lower loading due to a more homogeneous dispersion of RGO in the MFC matrix, thus even at lower loading a complete connected network of RGO sheets is achieved. RGO retains many functional groups even after reduction, which have a negative effect on the electrical properties of the composites [6]. It is not surprising that, at higher loadings once the network is completely connected, higher values are observed for graphene/MFC composites once. Pristine graphene contains fewer defects which was also confirmed by Raman analysis in Figure 1B

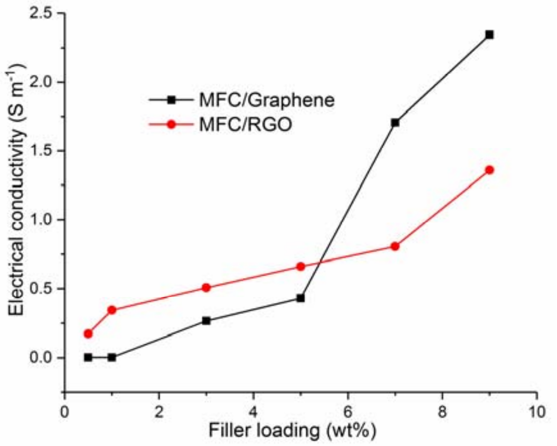

Figure 4 Electrical conductivity of MFC/graphene and MFC/RGO composite films with various concentrations of filler loading.

4 CONCLUSIONS

Graphene can be successfully exfoliated and stabilized in MNFC suspensions. At 0.5 wt% graphene loading, tensile strength and Young's modulus increased by about 4 % and 15 % respectively. At 9 wt% loading, the measured electrical conductivity was 2.4 S m^{-1}. RGO is subjected to harsh conditions during oxidation and reduction processes, which lead to irreversible defects and thus does not show the same exceptional properties observed in graphene. However, the functional groups in RGO make it more compatible with many polymer matrices and promote bonding with the polymer matrix that is essential of fabrication of high performance composites. In order to fully benefit from the exceptional properties of graphene, it is vital to develop methods for composite fabrication that can utilize graphene in its pure form.

REFERENCES

1. Phiri J, Gane P, Maloney TC (2017) General overview of graphene: Production, properties and application in polymer composites. Mater Sci Eng , B 215:9-28

2. Segal M (2009) Selling graphene by the ton. Nat Nano 4:612-614

3. Phiri J, Gane P, Maloney TC (2017) High-concentration shear-exfoliated colloidal dispersion of surfactant-polymer-stabilized few-layer graphene sheets. J Mater Sci 52:8321-8337

4. Gao W, Alemany LB, Ci L, Ajayan PM (2009) New insights into the structure and reduction of graphite oxide. Nat Chem 1:403-408

5. Wang X, Zhi L, Tsao N, Tomović Ž, Li J, Müllen K (2008) Transparent Carbon Films as Electrodes in Organic Solar Cells. Angew Chem Int Ed Engl 47:2990-2992

6. Becerril HA, Mao J, Liu Z, Stoltenberg RM, Bao Z, Chen Y (2008) Evaluation of solution-processed reduced graphene oxide films as transparent conductors. ACS Nano 2:463-470

Unique functionalization technique for tailor-made nanocelluloses

KARIN SAHLIN[1,4], MIKAELA BÖRJESSON[1], LILIAN FORSGREN[2], JOHANNES THUNBERG[2], TOBIAS MOBERG[2,4], DIANA BERNIN[3], ANTAL BOLDIZAR[2,4], MIKAEL RIGDAHL[2,4] and GUNNAR WESTMAN[1,4]

[1] Department of Chemistry and Chemical Engineering, Chalmers University of Technology, Gothenburg, Sweden
[2] Department of Industrial and Materials Science, Chalmers University of Technology, Gothenburg, Sweden
[3] Swedish NMR Centre, University of Gothenburg, Gothenburg, Sweden
[4] Wallenberg Wood Science Center, Chalmers University of Technology, Gothenburg, Sweden
karin.sahlin@chalmers.se

1 INTRODUCTION

Nanocelluloses has gained a lot of attention for their unique properties, such as large surface area, excellent mechanical properties, renewable, transparency and ease of chemical modification. One of the applications that have received most interest is nanocomposites, where nano-cellulose is added as a reinforcing element to a thermoplastic or a thermoset.

There are however issues with reaching good dispersion of the nanocellulose in the matrix, as cellulose is highly hydrophilic, while most thermoplastics and thermosets are hydrophobic. This can be addressed by chemical modification where hydrophobic groups are absorbed or grafted to the cellulosic surface. Often though, this approach does not remove the surface charge from e.g. sulphate groups and their associated counter ions, introduced on the nanocellulose surface by the sulphuric acid hydrolysis. This can have a substantial impact on compatibility and performance. Cellulose nanocrystals, CNCs, produced by sulphuric acid hydrolysis, contain small amounts of sulphate groups on the nanocrystal surface. These stabilises the particles in aqueous suspensions through electrostatic repulsion, but the drawback is lower thermal stability due to the catalytic degradation caused by the hydrogen ion associated with the sulphate ester [1,2]. For composite applications, the thermal stability can be of primary importance in order to avoid degradation since composite processing is often performed at quite high temperatures. The thermal stability can be improved either by removing the sulphate esters [2], by neutralisation [2] or by reacting the sulphate group with a suitable compound, thus removing the charge. If chosen wisely, the compound reacted with the sulphate ester could also improve the compatibility with a hydrophobic matrix.

Reagents that react with sulphate groups on polysaccharides are not very explored. However, similarly to carboxylates, amines, phenols and phosphate groups, they also have orbitals with comparable energies that are available for nucleophilic interaction with an electrophile. Studies have shown that azetidinium salts can react under mild conditions with the previously mentioned groups [3,4,5,6] through a ring-opening reaction due to the inherent four-atom ring strain.

Azetidinium salts are saturated heterocyclic four-membered rings where one of the ring atoms is a quartnized nitrogen, formed by reacting dialkylamine with epichlorohydrin in equal molar ratio. The azetidinium conjugation to the sulphate ester results in a Y-shaped grafting linked to the substrate by a short carbon chain.

In this study, CNCs produced by sulphuric acid hydrolysis were successfully reacted with azetidinium salts through a ring-opening reaction with the sulphate ester groups on the CNC surface. Furthermore, the rheological behaviour of the azetidinium grafted CNCs were studied and their reinforcing ability was evaluated by dispersing them in a polymer matrix.

2 REACTION SELECTIVTY

Azetidinium salts have previously been shown to react selectively with carboxylic acids on hemicelluloses [3]. As the sulphate half esters, such as those found on the surface of CNCs, are also soft nucleophiles and have a similar orbital arrangements as the carboxylic acids it was hypothesised that they would also be suitable for ring-opening reactions with azetidinium salts.

CNCs with different sulphate ester group contents were prepared according to procedures described in literature. [7,8,9]. Desulphated, partially desulphated, oversulphated and unmodified CNCs were reacted with azetidinium salts to study how the sulphate content affected the reaction selectivity.

One nitrogen atom is introduced at each site where an azetidinium salt is grafted. Similarly, there is one sulphur atom per sulphate ester group, i.e. grafting site.

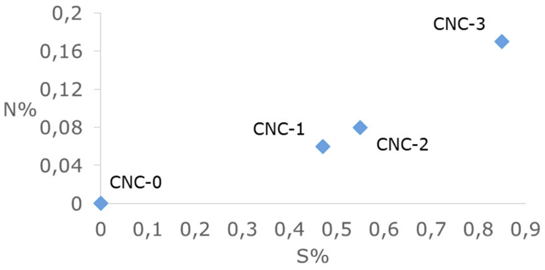

Figure 1. Elemental analysis results from CNCs with different sulphur ester content, reacted with a diethyl azetidinium salt.

Results from elemental analysis showed a clear correlation between the sulphur and nitrogen content, see figure 1, and when no sulphate groups were available for reaction, no grafting of the azetidinium salts was observed. Thus it could be concluded that the reaction is selective to sulphate groups in the presence of hydroxyl groups. [10]

3 TAILORED FUNCTIONALITIES

The functionalities introduced by the secondary amine can be varied, it could e.g. have symmetrical substituents like aliphatic hydrocarbon chains, such as dihexylamine, or oxygen containing groups like morpholine and methoxyethyl. The substituents can also be asymmetrical, such as nonylpropargyl and undecanylmethyl. Some of the obtained azetidinium salts are presented in figure 2 below.

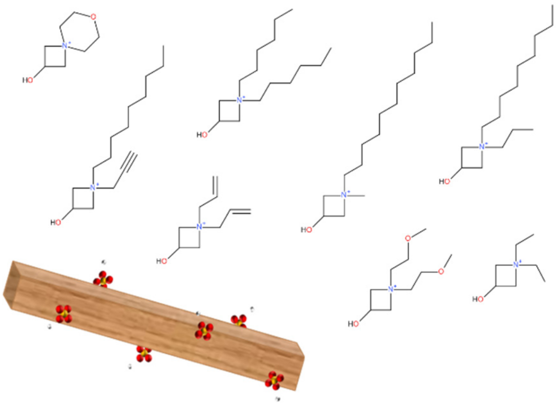

Figure 2. The amine substituents on the azetidinium salts above are from left to right: morpholine, nonylpropargyl, diallyl, dihexyl, undecanylmethyl, dimethoxyethyl, nonylpropyl and diethyl.

We have found that there are no general reaction conditions for the formation of azetidinium salts that are suitable for all secondary amines. Each reaction has to be individually optimized based on solvent, temperature and reaction time.

When grafting the azetidinium salts onto the CNC, the reaction has previously been performed in DMSO. We are now able to instead use water as a solvent, making the reaction scalable.

4 RHEOLOGICAL BEHAVIOUR

The rheological properties of suspensions of modified as well as unmodified CNC were evaluated at two solid contents; 0.65 and 1.3 wt-%. [11] From the rheological measurements it was concluded that the conjugation of azetidinium salts on the surface of CNC significantly increased the shear viscosity at a given shear rate as well as the storage and loss moduli. The azetidinium containing allyl functionality showed the greatest increase in viscosity. All samples exhibited distinct shear-thinning behaviour, with all viscosity-(shear rate)-curves approaching each other at higher shear rates.

From the dynamic-mechanical analysis, a plateau at low shear rates was observed for all samples, corresponding to the linear viscoelastic region. For all modified samples, the storage modulus was higher than the loss modulus, indicating gel-like behaviour. The opposite was observed for the unmodified CNC, displaying liquid-like characteristics. The curve for the storage modulus crossed over the loss modulus curve at 20-30 % shear strain, depending on modification. This is illustrated in the drawings in figure 3 below, depicting how the shear may affect the orientation of the nanoparticles and the disruption of the network for the modified CNCs.

The gel-point of the CNCs was estimated to be around 0.4 wt-% for the modified CNCs and 2.5 wt-% for the unmodified, based on dynamic measurements over a concentration range to find where the loss and storage moduli overlap.

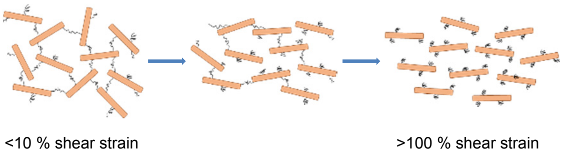

Figure 3. An illustration showing a connected network of modified CNCs at low shear rates, and the orientation and disruption of the network at higher shear rates.

The results obtained from the rheological measurements may be interpreted as that the functional groups introduced by the grafting improves the network formation of the CNCs in aqueous suspensions. The apparent increase in inter-particle interactions was attributed to stronger molecular interactions between the substituents. The allyl functional groups are prone to π-π-stacking, resulting in a stronger network compared to the other two grafted CNCs, which have different sized carbon contacting functional groups, where CNC grafted with the azetidinium salt with longer chains gave higher viscosity.

5 CNC COMPOSITES

CNC nanocomposites were prepared by wet mixing powdered LDPE with different CNCs; one unmodified and two azetidinium functionalized CNCs, containing either a diethyl or a dihexyl functionalized amine. After air-drying in room temperature, the CNC coated LDPE powder was hot-melt extruded using a twin-screw mini-compounder at 150 °C for 5 minutes. The composites where formed into films by pressing with at 150 °C and 5 tonnes pressure for 5 minutes. Tensile testing specimens were punched from the pressed films.

As expected, the stiffness of the CNC-composites were increased compared to the pure polymer matrix, where the dihexyl azetidinium displayed the highest stiffness. Severe discolouration occurred during the processing of the unmodified CNC due that the onset of thermal degradation is initiated at the required processing temperature for the LDPE. Negligible discolouration occurred for the functionalized CNCs as can be seen in figure 4.

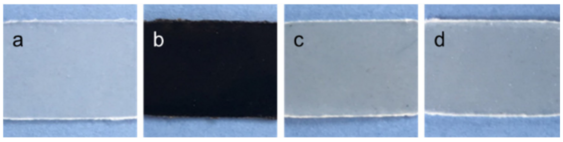

Figure 4. Tensile testing specimens from the pressed films of the LDPE composites with (a) pure LDPE, (b) 3.2 wt% non-modified CNC added, (c) 3.5 wt% diethyl functionalized azetidinium CNC added and, (d) with 2.9 wt% dihexyl functionalized azetidinium CNC added.

From the mechanical profiles of the CNC-composites and the rheological behaviour in solution, one of the azetidinium modified CNCs was scaled to half a kilo production and was used to manufacture composites with different thermoplastic matrices and at different filler content.

6 CONCLUSIONS

Azetidinium salts react selectively with sulphate esters, in the presence of hydroxyl groups. The reaction results in a significantly lower gel point in water suspensions, increased shear viscosity and a stronger interacting CNC network. When azetidinium functionalized CNCs are added to an LDPE matrix, the stiffness of the composite is increased, more or equally compared to unmodified CNC, yet without the severe discolouration observed for the composite containing unmodified CNC. This reaction, performed in water, opens up for an easy way of modifying nanocellulose to fit for specific applications, also at larger scales.

REFERENCES

[1] D.-Y. Kim, Y. Nishiyama, M. Wada and S. Kuga. High-yield carbonization of cellulose by sulfuric acid impregnation. *Cellulose* **8**(1):29-33 (2001).

[2] N. Wang, E. Ding and R. Cheng. Thermal degradation behaviors of spherical cellulose nanocrystals with sulfate groups. *Polymer* **48**(12):3486-93 (2007).

[3] M. Börjesson and G. Westman. Branching of hemicelluloses through an azetidinium salt ring-opening reaction. *Carbohydrate Research* **428**:23-30 (2016).

[4] F. Couty, O. David, F. Durrat, G. Evano, S. Lakhdar, J. Marrot and M. Vargas-Sanchezet. Nucleophilic ring-opening of azetidinium ions: insights into regioselectivity. *Eur J Org Chem* **15**:3479-90 (2006).

[5] R. H. Higgins, W. J. Faircloth, R. G. Baughman and Q. L. Eaton. Ring opening of azetidinols by phenols: regiochemistry and stereochemistry. *J Org Chem* **59**:2172-8 (1994).

[6] A. Bakalarz-Jeziorna, J. Heliński and B. Krawiecka. Synthesis of multifunctionalized phosphonic acid esters via opening of oxiranes and azetidinium salts with phosphoryl-substituted carbanions. *J Chem Soc, Perkin Trans 1* **9**:1086-90 (2001).

[7] F. Jiang, A. R. Esker and M. Roman. Acid-catalyzed and solvolytic desulfation of H_2SO_4-hydrolyzed cellulose nanocrystals. *Langmuir* **26**(23):17919-25 (2010).

[8] T. G. Kantor TG and M. Schubert. A method for the desulfation of Chondroitin sulfate. *J Am Chem Soc* **79**:152-3 (1957).

[9] A. I. Usov, K. S. Adamyants, L. I. Miroshnikova, A. A. Shaposhnikova and N. K. Kochetkov. Solvolytic desulphation of sulphated carbohydrates. *Carbohyd Res* 18:336-8 (1971).

[10] M. Börjesson, K. Sahlin, D. Bernin and G. Westman. Functionalization of the sulfate groups on nanocrystalline cellulose with azetidinium ions. *To be published.*

[11] K. Sahlin, L. Forsgren, T. Moberg, D. Bernin, M. Rigdahl and G. Westman. Surface treatment of cellulose nanocrystals (CNC) – effects on dispersion rheology. *To be published.*

Swelling and Young's modulus of nanocellulose films in liquids

RUUT KUMMALA[1], WENYANG XU[2], CHUNLIN XU[2] and MARTTI TOIVAKKA[1]

[1] Laboratory of paper coating and converting, Åbo Akademi University
[2] Laboratory of Wood and paper chemistry, Åbo Akademi University
ruut.kummala@abo.fi

Keywords: nanocellulose, swelling, AFM, force spectroscopy, Young's modulus

INTRODUCTION

Understanding mechanical properties of materials at biological interfaces is important due to stimulus they generate to the biological system. It has been stated that local extracellular matrix stiffness seemingly affects cell fate, therefore, playing a role in development, differentiation, disease and regeneration of the tissues [1]. When designing tissue scaffolds both chemistry and mechanical properties are known to be essential in success of the scaffold [2]. Depending on the target tissue, scaffold stiffness is varies, for example, human body tissue stiffness ranges from soft brain 4.25 kPa [3] to stiffer cartilage 2.6 MPa [4] to hard bone 15-20 GPa [5].

Nanocellulose is a promising material especially for biomedical applications in contact with cells due to its similar morphology with tissue collagen, low cytotoxicity and modifiability [6]. One of the most common chemical modifications of nanocellulose is 2,2,6,6-tetramethylpiperidine-1-oxyl (TEMPO) - mediated oxidation in which primary hydroxyl groups at C6 of nanocellulose is replaced by carboxyl group, increasing its charge density [9].

Cellulose is an abundant biopolymer in the nature found in the cell walls of plants. In addition, bacteria can generate it. Nanocellulose materials are commonly divided into three main groups: cellulose nanocrystals (CNC), nanofibrillated cellulose (NFC) and bacterial cellulose (BC). These differ by source, CNC and NFC originating from plants from which nanocellulose is converted from large fibres into small and BC, which is produced by bacteria from sugar units during highly controlled biosynthesis process. Both mechanical and chemical treatments are usually used in CNC and NFC production. Depending on the treatment, the produced nanocellulose may be classified as NFC with long fibres with amorphous and crystalline regions or CNC in which amorphous regions are cleaved away leaving highly crystalline rod like fibres.[7]

Here five wood-based micro- and nanofibrillated cellulose films were prepared to investigate the effects of nanocellulose charge density and fibril size on the mechanical properties of the films in liquids. Swelling behaviour of vacuum filtrated and dried films was studied in milli-Q water, in two $CaCl_2$ solutions and in cell culture media. Atomic force microscopy with a colloidal probe was used to evaluate mechanical properties of the films.

MATERIALS AND METHODS

Two processes were used to produce five nanocelluloses as detailed in Table 1. First, microfibrillated cellulose (MFC) from bleached softwood kraft pulp was produced through mechanical treatment. Part of this MFC was then further processed by TEMPO-mediated oxidation to produce three MFCs with charge densities: low (MFC_L), medium (MFC_M) and high (MFC_H). The fifth nanocellulose was nanofibrillar cellulose with medium charge density (NFC_M). This was produced from unbleached saw dust pulp with TEMPO-mediated oxidation followed by mechanical disintegration

.

Table 1. Nanocellulose characteristics.

	Laboratory	Cellulose origin	Processing steps	Charge density [mmol/g]
MFC	Maine University	Bleached softwood kraft pulp	1. Mechanical	0.14 +/- 0.02
MFC_L				1.61 +/- 0.08
MFC_M				1.82 +/- 0.07
MFC_H				2.15 +/- 0.08
NFC_M	Åbo Akademi	Unbleached sawdust pulp	1. Tempo-mediated oxidation 2. Mechanical	1.87

Table 2. Average Young's modulus of swollen films over area of 250 µm^2 in water and cell culture media.

	NFC_M	MFC	MFC_L	MFC_M	MFC_H
Milli-Q water	679 Pa ±55,5 Pa	8,23 kPa ±5,8 kPa	5,38 kPa ±1,1 kPa	823 Pa ±158 Pa	1,02 kPa ± 0,39 kPa
Compl. Media	154 kPa ±37 kPa	497 kPa ±298 kPa	57,9 kPa ±14,8 kPa	81,8 kPa ±19,1 kPa	65,1 kPa ±14,3 kPa

To produce free standing films, the nanocellulose suspensions (10 g at 0.1 % w/v) were vacuum-filtrated through polyamide membrane filter (pore size 0.2 µm) using a funnel with 35 mm inner diameter. The films were dried between two filter papers and glass plates and stored in room temperature before testing.

SWELLING RATIO

Swelling of the nanocellulose films was measured gravimetrically. The dried films were immersed in four liquids: complete cell culture media (Sigma Aldrich, Dulbecco's modified eagle's medium (DMEM)), milli-Q water, 1.8 mM $CaCl_2$ solution or 0.9 mM $CaCl_2$ solution at 37 °C for 24 hours. For each nanocellulose, three films were used to calculate average swelling ratio using equation,

$$Swelling\ ratio = \frac{m_{swollen\ film} - m_{initial}}{m_{initial}} \quad (1)$$

ATOMIC FORCE MICROSCOPY

Zeiss LSM510 JPK AFM was used to measure Young's modulus of swollen nanocellulose films in liquids at 37 °C. Prior to measurements, the films were immersed into DMEM or milli-Q water, at 37°C overnight.

Force spectroscopy measurements were recorded from randomly chosen three or more locations on a sample. From every location, inside 100 x 100 µm^2 area, a 3 x 3 matrix of measurement points was collected. On each measurement point triplicates were collected. Before collecting force curves, probes were calibrated in used liquid by pressing tip to clean glass slide. Used colloidal probes had a triangle shaped cantilever with a spring constant of approximately 0.32 N/m and 15 µm in diameter sphere tip.

In addition, quantitative imaging (QI) mode was used to collect Young’s modulus maps together with topography data. These were done for an area of 50 x 50 μm^2.

RESULTS AND DISCUSSION

Swelling of nanocellulose films clearly depends on the charge density of the film and ionic strength of the liquid. In milli-Q water swelling was largest for all the chemically treated nanocellulose films as shown in Figure 1. Only in the case of MFC, the liquid type did not affect the swelling ratio. When charge density of the MFC is increased, there is a clear step-wise increase in swelling for films in milli-Q water. NFC_M swells the most of all, possibly due to its small fibre size.

Films with high charge density, MFC_M and MFC_H, swelled in 0.9 mM $CaCl_2$ solution, whereas swelling of the films with lower charge density MFC_L and NFC_M was limited to a swelling ratio of approximately 10. This reduced swelling behaviour in liquids with calcium is consisted with the literature[10]. Maximum swelling ratio in cell culture media is 14,2 (NFC_M).

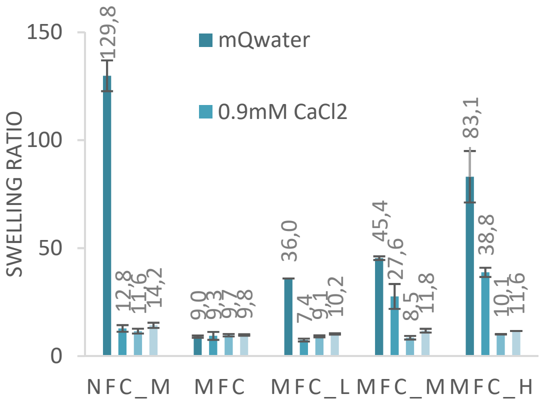

Figure 1. Nanocellulose swelling ratio after 24 h in 37 °C.

For all the films, the surface elastic modulus was higher in complete cell culture media than in milli-Q water (see Table 2 and Figure 2). In both liquids, MFC had highest average Young’s modulus but it also had largest variability in Young’s modulus values. In milli-Q water, MFC_L was stiffer than MFC_M and MFC_H but in complete cell culture media, Young’s modulus values for all three were in the same range.Height distributions (Figure 3) and Young’s modulus distributions (Figure 4) for the swollen films were extracted from the imaging maps (Figure 5). In height histograms, only MFC_M stands out and its map shows highly smooth area in comparison to others. In Young’s modulus histogram, NFC_M has a symmetric bell like distribution around its average in contrast to MFC_L, MFC_M and MFC_H more like left-skewed distribution and MFC right skewed distribution.

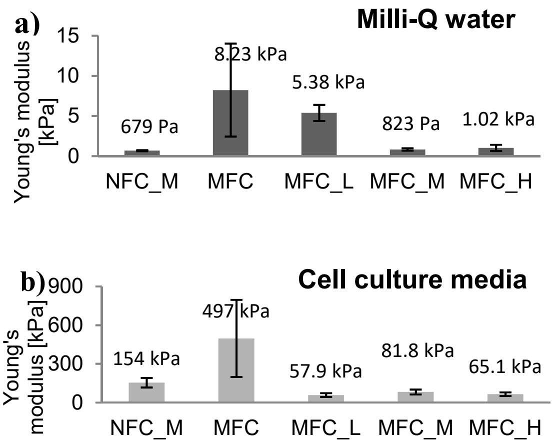

Figure 2. Average Young's modulus of swollen nanocellulose films over area of 250 μm^2 in milli-Q water (a) and cell culture media (b).

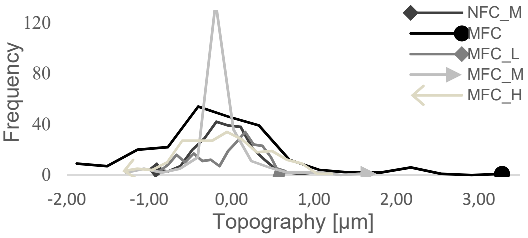

Figure 3. Histogram of height.

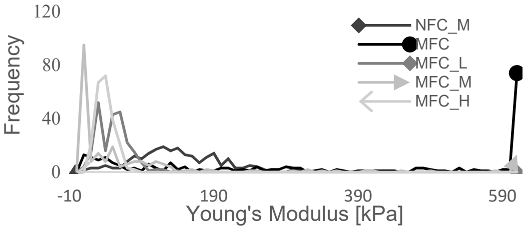

Figure 4. Histogram of Young's modulus

Figure 5 shows the 2D maps of Young’s modulus and topography. No clear correlation between height and stiffness can be detected on this length scale (see Fig. 5).

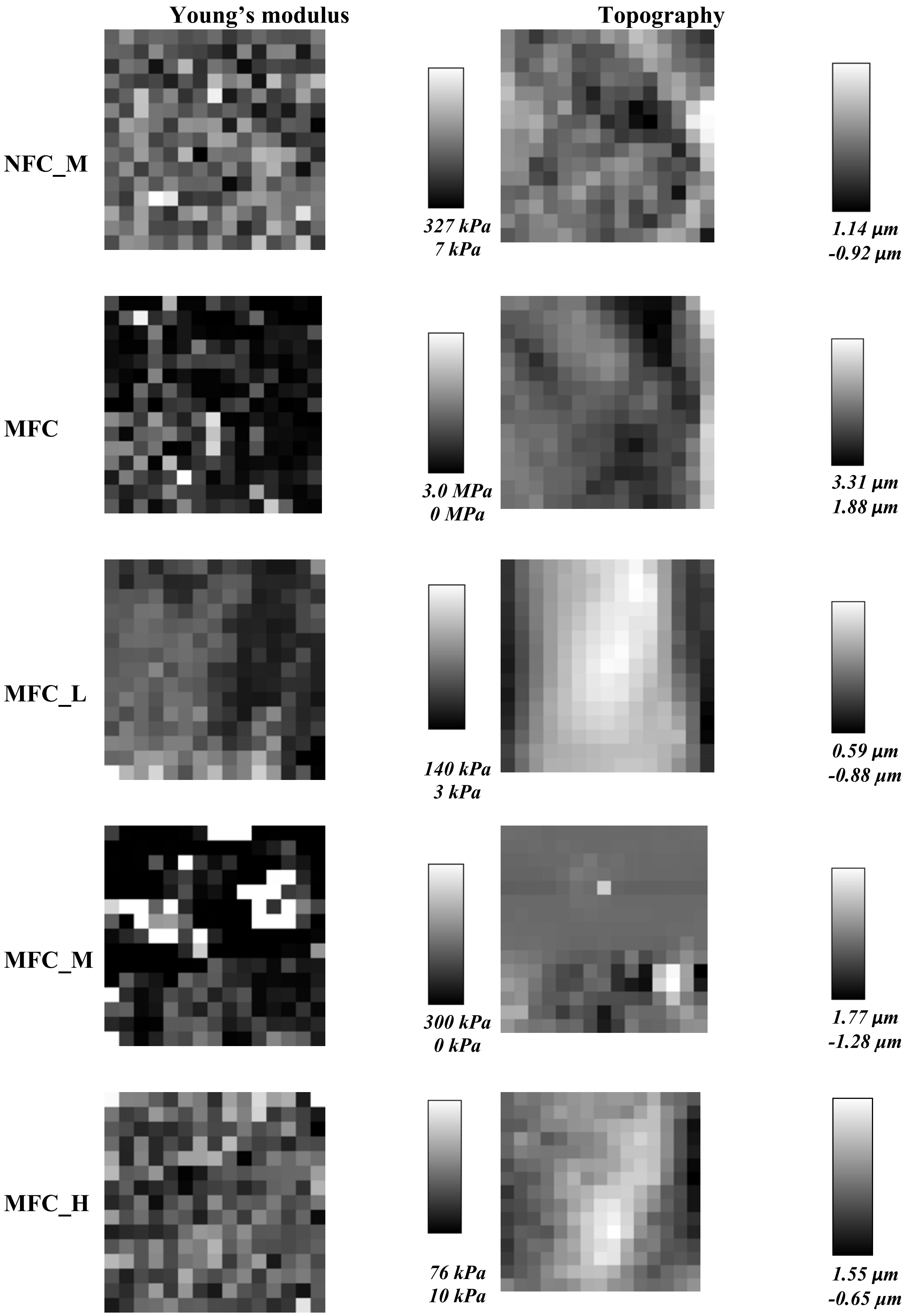

Figure 5. Nanocellulose films (50 x 50 µm2) topography and Young's modulus maps in cell culture media after 24 hours.

CONCLUSIONS

Charge density of nanocellulose greatly affects swelling of films made of it in low ionic strength liquids. In high ionic strength liquids, swelling was minimal for all the films. Stiffness is lower in milli-Q water than in cell culture media but the Young's modulus differences between the films in these liquids do not correlate with swelling degree. This may be due to Young's modulus being measured on the film surface with no contribution from the bulk of the film. The results suggest that stiffness may be related to the nanocellulose fibre size.

REFERENCES

[1] DE. Discher, P. Janmey and Y. Wang. Tissue cells feel and respond to the stiffness of their substrate. Science. 310(5751):1139-1143 (2005).

[2] O'brien FJ. Biomaterials & scaffolds for tissue engineering. Materials today. 2011;14(3):88-95.

[3] Miller K, Chinzei K, Orssengo G, Bednarz P. Mechanical properties of brain tissue in-vivo: Experiment and computer simulation. J Biomech. 2000;33(11):1369-1376.

[4] Stolz M, Raiteri R, Daniels AU, VanLandingham MR, Baschong W, Aebi U. Dynamic elastic modulus of porcine articular cartilage determined at two different levels of tissue organization by indentation-type atomic force microscopy. Biophys J. 2004;86(5):3269-3283.

[5] Agrawal CM. Reconstructing the human body using biomaterials. JOM. 1998;50(1):31-35.

[6] Lin N, Dufresne A. Nanocellulose in biomedicine: Current status and future prospect. European Polymer Journal. 2014;59:302-325.

[7] Dufresne A. (2012). Nanocellulose from nature to high performance tailored materials. De Gruyter. p. 460.

[8] Klemm D, Kramer F, Moritz S, et al. Nanocelluloses: A new family of nature-based materials. Angew Chem Int Ed. 2011;50(24):5438-5466.

[9] Saito T, Kimura S, Nishiyama Y, Isogai A. Cellulose nanofibers prepared by TEMPO-mediated oxidation of native cellulose. Biomacromolecules. 2007;8(8):2485-2491.

[10] Chinga-Carrasco G, Syverud K. Pretreatment-dependent surface chemistry of wood nanocellulose for pH-sensitive hydrogels. Journal of Biomaterials Applications. 2014;29(3):423-432.

Analysis of drying deformation of 3D printed nanocellulose structures

VILLE KLAR, PYRY KÄRKI,
HANNES ORELMA* and
PETRI KUOSMANEN

Aalto University, School of Engineering,
Department of Mechanical Engineering
ville.klar@aalto.fi

*VTT
Technical Research Centre of Finland,

1 ABSTRACT

Additive manufacturing technologies have gained much interest as a viable alternative for producing new types of products and structures. Currently additive manufacturing is predominantly based on thermoplastic polymers and metals which can be formed through melting and subsequent solidification. While these materials are well-suited for a wide variety of applications, exploration of bio-based materials is necessary as their production and use can be scaled without substantial environmental effects.

Cellulose nanofibrils (CNF) are a promising alternative as a raw material for additive manufacturing. CNF are strong, lightweight, biocompatible & biodegradable as well as chemically versatile. CNF cannot be molten and therefore lack the thermoformability necessary in most current additive manufacturing approaches. Consequently, structures must be formed relying on the high viscosity of the suspensions.

CNF suspensions exhibit high viscosities already at low solids contents. In order to enable steady extrusion through small orifices, CNF suspensions with low solids contents ranging from 1-4wt% are typically used. A drawback of the low solids content is that as water evaporates during drying the 3D-printed structures deform.

While the drying deformation can be decreased and even prevented with freeze-drying, the process has been shown to result in a reduction of the mechanical properties of the final print. [1]

In this paper we discuss an alternative approach for retaining the intended geometry in 3D printed CNF structures. By increasing the solids content of the used suspensions to 7.55 - 22.7 wt%, the structures retain geometrical fidelity without freeze-drying. Additionally, we introduce an approach for quantifying the drying deformation. By quantifying the drying deformation, software-based compensation of the deformation may be developed to improve the quality of the printed structures even further.

2 INTRODUCTION

Additive manufacturing technologies have become common-place both in industry and home use. Material extrusion based additive manufacturing, often termed three-dimensional (3D) printing is expected to bring about substantial changes across several industries. 3D printing enables efficient production of optimized structures in terms of weight, performance and cost. Additionally, 3D printing enables mass customization as the route from a digital model to a final structure is short.[2]

Thermoplastic materials such as petrochemical polymers and metals are widely used in 3D printing. Recently there has been a growing interest in shifting to the use of biomaterials. Materials such as nanocellulose have been of special interest [3]. The properties of different types of nanocellulose have been extensively reviewed by several research groups [4]–[8]. In the context of this research we focus on cellulose nanofibrils (CNF) which have a high aspect ratio and contain both amorphous and crystalline sections.

CNF can be produced from lignocellulosic biomass which is considered a nearly inexhaustible raw material.[9] The production process typically contains different chemical pre-treatments which are followed by a homogenization process [10],

[11]. CNF production remains comparatively expensive due to low production volumes and unoptimized production methods.[12] Pre-treatments with e.g. enzymes are considered as a viable means to reduce the total energy demand for nanocellulose production. [13]

Structures such as filaments and films have been produced by several research groups. The results for filaments and films have been reviewed by Lundahl et al. [14] and Dufresne [15] respectively. For example, in their review, Siró and Plackett [16] listed mechanical properties acquired for MFC films. Tensile strengths of 104–312 MPa and elastic moduli of 6.2–15.1 GPa have been acquired for wood pulp-based MFC films. While these structures can be used in a wide variety of applications, 3D printing would enable a new route for exploring more complex geometries in further applications.

Several different 3D printing technologies exist. Fused deposition modelling (FDM) is the most widely used approach. The FDM approach is based on extruding thin layers of material on top of each to produce a 3 dimensional shape. A requirement for FDM printing is that the printed material can be extruded layer by layer. Furthermore, the material needs to remain in the extruded shape and not collapse as a result of the added material, i.e. weight, on top of it. Typically, thermoplastic materials are used where the material undergoes a fast phase-change from molten to solid. Contrastively, CNF are processed as a paste. The requirements of extrudability and geometrical stability are fulfilled as CNF suspensions form a thick gel or paste already at low solids contents.

In the context of 3D printing the governing factor in the processing of nanocellulose is its flow behaviour. In FDM the material is extruded through a small orifice (typically 0.1mm to 0.6mm). The orifice diameter has a strong impact on the achievable resolution with smaller orifice diameters yielding finer detail in the printed structures.

The rheological behaviour of CNF has been reviewed by Nechyporchuk [17] et al. In terms of 3D printing the aggregation and disaggregation behaviour of fibrils results in the necessity to use low solids content pastes. A drawback of decreasing the solids content in the paste is that as the structure dries it deforms substantially. With lower solids contents 3D printed structures may collapse under their own weight. Alternative drying methods such as freeze-drying are commonly used to prevent drying deformation and collapse of the structure.

While 3D printed and subsequently freeze-dried structures retain their intended geometry as demonstrated by several research groups [1], [18]–[20], the freeze-drying process may have a negative impact on the mechanical properties of the printed structures. Håkansson et al. [1] studied the solidification of 3D printed hydrogels in more detail. Several different drying methods were researched including plain air-drying, air-drying with different pre-treatments and freeze-drying. They observed that air-drying techniques cause the printed objects to shrink approximately 70 % of their wet size, but they also form a strong structure. Freeze-drying retains the original dimensions with only negligible shrinkage but results in porous structure that is weaker than the air-dried. Additionally, surfactants were shown to decrease the distortion during drying.

Most publications on the topic of 3D printing nanocellulose have been focused in biomedical applications such as wound dressings [19], [20] and scaffold raw material for cartilage tissue engineering [18]. These studies have been focused on the biomedical properties of the utilized raw materials. Furthermore, past research has focused on utilizing printing pastes with low solids contents. We aim to extend on previous work by studying the printability and solidification at higher solids contents.

In the biomedical context, keeping the structures in a wet state may be favourable.

However, utilizing 3D printed structures in further applications requires a better understanding of the drying deformation behaviour. We introduce an alternative approach to attenuating the drying deformation of CNF pastes by increasing the total solids contents of the printing pastes. Furthermore, an imaging procedure is used in order to quantify the deformation behaviour more accurately. By quantifying the drying deformation models may be developed that apply compensation of the drying deformation in the original computer model. Software based compensations for the 3D printed structures could dramatically improve the geometrical fidelity of CNF 3D printing.

3 EXPERIMENTAL

A prototype 3D printer was developed in order to efficiently test different raw materials and printing parameters. A CNC-machine frame was used to perform XYZ-movements. Several design iterations with different extruder prototypes were performed to identify the most suitable extruder.

The syringe type extruder prototype composes an aluminium frame, a linear stepper motor, a magnetic linear encoder and a force transducer to measure the piston force. By estimating the friction between the piston gasket and the syringe body the pressure inside the syringe can be estimated without separate pressure sensors.

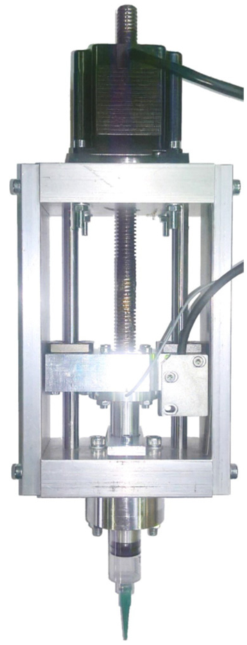

Figure 1 Extruder prototype

The measurement of the movement and piston forces enables closed-loop control of the extrusion. The extruder can be operated in either a constant speed or a constant force mode. Furthermore, the pressure can be quickly reduced to stop the extrusion.

The measurement data from the piston movement and pressure was acquired with a National Instrument data acquisition device (DAQ).

3.1 Raw materials

A total of five different printing pastes were prepared. Four pastes were produced by mixing cellulose powder and wet CNF. One paste was produced with high-consistency enzymatic fibrillation (HefCel) technology developed at VTT[21]. The pastes are listed in table 1.

Table 1 Printing pastes

Name	*Dry,wet ratio* [wt%]*	*Solids content [wt%]*
CNF1	20:80	7.55
CNF2	5:95	9.87
CNF3	10:90	13
CNF4	57:43	22.7
HefCel	100:0	22

*Powder and CNF ratio

3.2 Printing procedure and parameters

Based on initial testing, the CNF3 raw material was chosen to study the influence of printing parameters on drying deformation. A 0,84 mm tapered luer tip was used in all the test runs. Printing speeds were set to 7.5mm/s and a rectilinear infill pattern was used for each cube. A total of 10 different cubes were printed for which the varied printing parameters are shown in table 2. The parameter set A was repeated 4 times to assess the repeatability of the printing and deformation.

The scaling of the deformation was studied by using parameter set A to print both CNF3 and HefCel at 3 different scales (50%,

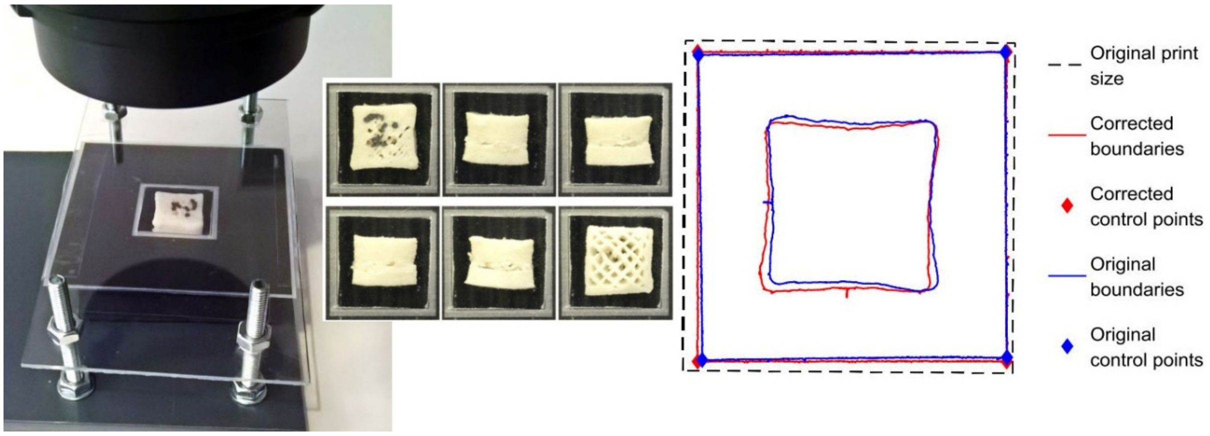

Figure 2 Image analysis process

100% and 200% of the original computer model volume). Drying was performed at room temperature and humidity. The prints allowed to dry for a minimum of 48h before handling or measurements.

Table 2 Printing parameters

Name	*Layer height [mm]*	*Infill density [%]*	*Extrusion width [mm]*
A	0.4	30	1
B	0.6	30	1
D	0.4	40	1
C	0.6	40	1
E	0.4	60	1
F	0.6	60	1
G	0,6	30	1,5
H	0,4	40	1,5
I	0,6	40	1,5
J	0,6	60	1,5

3.3 Analysis of prints

A total of 19 different cubes were analysed. Each cube was imaged from every side to measure the deformation in X, Y and Z directions as shown in figure 2. A high resolution digital single-lens reflex (DSLR) camera with a macro objective was used for imaging.

An image analysis script was developed in MATLAB for analysing the geometrical deformation of the dried samples. Concisely, the script finds the boundary edges of the imaged object, applies perspective, rotational, and translational corrections and finally compares the cube to a projection of the original computer model.

Comparisons can be made both in terms of total volumetric deformation and distortion of geometry.

The accuracy of the imaging approach was evaluated by machining a reference cube out of aluminium. The reference cube was measured with a Zeiss C400 coordinate measurement machine and the results were compared to the measurements produced with image analysis approach. Based on the measurement results the standard measurement error for the image analysis approach for height and width was calculated to be ±58µm and ±22µm respectively.

4 RESULTS AND DISCUSSION

Nanocellulose was successfully 3D printed with several different parameters. While complex geometries could be produced (Fig 3), testing was focused on rectangular shapes. Geometrical deformations can be more efficiently quantified from geometrical primitives such as cubes, blocks, tetrahedrons and cylinders.

The test pieces exhibited two distinct types of deformation which we denote as surface deformation and geometrical deformation in the context of this paper. Surface deformation refers to variations in surface roughness and quality of prints.

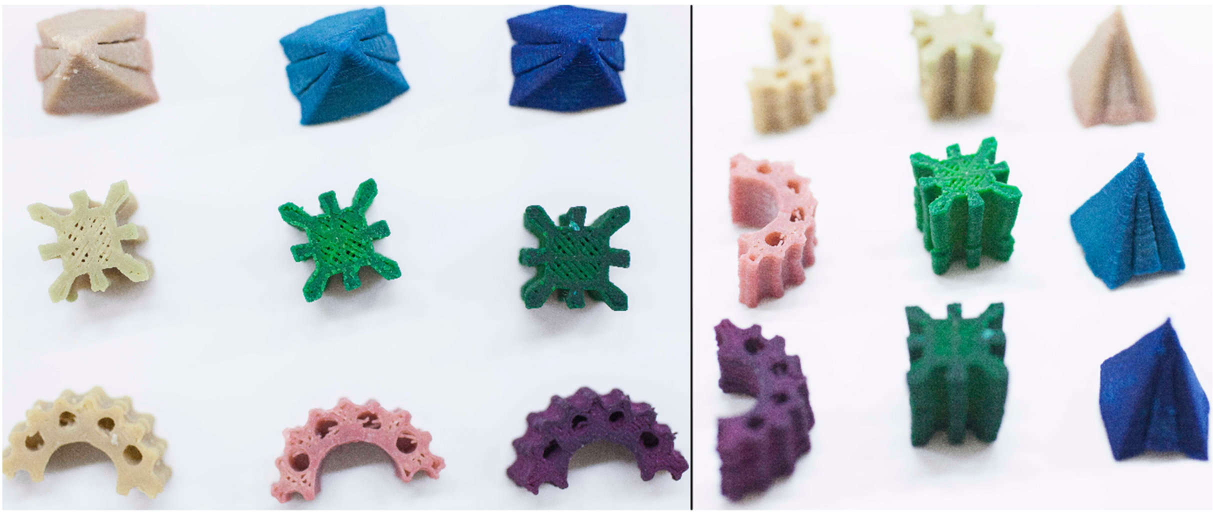

Figure 3 More complex 3D printed shapes, dyed with food colouring, Design: Anastasia Ivanova, photo: Eeva Suorlahti.

Geometrical deformation refers to a total volumetric change in the print. During testing of higher consistencies of nanocellulose frequent clogging of the extruder was experienced. This was mainly attributed to the aggregation of fibril flocs in the tapered tip of the extruder. A maximum consistency of 25 –wt% was estimated. Naturally, the maximum consistency is strongly dependent on the type of nanocellulose used. The clogging behaviour could also be reduced by using larger orifices in the syringe but this would result in a decrease in resolution.

The repeatability of the dimensions of the cube prints was found to be ±0.1 mm. This indicates that while the deformation may appear random, it can be compensated for in the print as it is repeatable.

The drying shrinkage was found not to be directly dependent on the infill density. The non-linearity of the shrinkage between the different infill densities implies that the structures with lower infill densities result in less dense dried structures. Furthermore, the lower infill density did not result in increased drying deformation or distortion. This result suggests that the weight of nanocellulose prints can be decreased to an extent by reducing the infill density while maintaining the same geometry. The reduced infill densities may have a negative effect on the mechanical properties but this was not verified in the context of this paper.

Extrusion width was found to have a minor impact on the drying deformation. The narrower 1mm extrusion width resulted in a more pronounced drying distortion compared to the 1.5mm extrusion width**.** The attenuation of shrinkage with wider extrusion width was considered to be a result of a higher wet stiffness as the printing paths were thicker.

Table 3 shows the final dry dimensions the 6 scaled prints with CNF3 and HefCel. The model dimensions of the 50%, 100% and 200% cubes were 12.7*12.7*12.7 mm, 16*16*16 mm and 20*20*20mm respectively.

Table 3 Mean dimensions of dried prints

Sample	*Height [mm]*	*Width [mm]*
CNF3, 50%	5.76	5.74
CNF3, 100%	7.92	8.00
CNF3, 200%	9.65	9.78
HefCel, 50%	5.92	8.18
HefCel, 100%	8.07	10.73
HefCel, 200%	9.55	13.46

Average volumetric ratio (dry volume / model volume) for the CNF3 prints was 0.11 and 0.21 for the HefCel prints. Both materials exhibited a higher shrinkage in height (Z-direction) compared to other dimensions. This was attributed to the flattening due to the layerwise manufacturing method. Increasing layers on the print increases the load on prior layers which compresses the structure. As the total drying time is dozens of hours the total induced compression in a wet state becomes significant. With the more complex shapes, it was observed that the available area for water evaporation plays a significant role in the drying process.

Systematic testing of mechanical properties is necessary in order to validate improved mechanical properties through air-drying. It is expected that similarly to other FDM printed structures the mechanical properties in the Z-direction are weaker due to poor layer adhesion.

Early results of CNF as a 3D printing raw materials are promising. Successful printing has been demonstrated by several research groups. Research regarding optimizing the extrudability of the printing pastes with e.g. rheological modifiers as well systematic improvement of the mechanical properties of the final prints is still needed. 3D scanning could be utilized for improving the analysis of the dried structures.

ACKNOWLEDGEMENTS

This work has been funded by Tekes (Finnish Funding Agency for Innovation) through a strategic opening titled Design Driven Value Chains in the World of Cellulose as well as Jenny and Antti Wihuri foundation. Furthermore we would like to thank Jaakko Pere (VTT) for providing the raw materials used in this study as well as Anastasia Ivanova for designing the 3D-printed models and Eeva Suorlahti for photographs.

REFERENCES

[1] K. M. O. Håkansson *et al.*, “Solidification of 3D Printed Nanofibril Hydrogels into Functional 3D Cellulose Structures,” *Adv. Mater. Technol.*, p. 1600096, 2016.

[2] I. Gibson, D. W. Rosen, and B. Stucker, *Additive manufacturing technologies: Rapid prototyping to direct digital manufacturing*. 2010.

[3] J. H. Kim *et al.*, “Review of nanocellulose for sustainable future materials,” *International Journal of Precision Engineering and Manufacturing - Green Technology*, vol. 2, no. 2. pp. 197–213, 2015.

[4] Y. Zhang, T. Nypelö, C. Salas, J. Arboleda, I. C. Hoeger, and O. J. Rojas, “Cellulose Nanofibrils: From Strong Materials to Bioactive Surfaces,” *J. Renew. Mater.*, vol. 1, no. 3, pp. 195–211, 2013.

[5] R. J. Moon, A. Martini, J. Nairn, J. Simonsen, and J. Youngblood, “Cellulose nanomaterials review: structure, properties and nanocomposites.,” *Chem. Soc. Rev.*, vol. 40, no. 7, pp. 3941–3994, Jul. 2011.

[6] D. Klemm, D. Schumann, F. Kramer, N. Hebler, D. Koth, and B. Sultanova, “Nanocellulose materials - Different cellulose, different functionality,” *Macromol. Symp.*, vol. 280, no. 1, pp. 60–71, 2009.

[7] S. J. Eichhorn *et al.*, “Review: Current international research into cellulose nanofibres and nanocomposites,” *J. Mater. Sci.*, vol. 45, pp. 1–33, 2010.

[8] N. Lavoine, I. Desloges, A. Dufresne, and J. Bras, “Microfibrillated cellulose - Its barrier properties and applications in cellulosic materials: A review,” *Carbohydr. Polym.*, vol. 90, no. 2, pp. 735–764, 2012.

[9] D. Klemm, B. Heublein, H. P. Fink, and A. Bohn, “Cellulose: Fascinating biopolymer and sustainable raw material,” *Angew. Chemie - Int. Ed.*, vol. 44, no. 22, pp. 3358–3393, 2005.

[10] M. Pääkko *et al.*, “Enzymatic hydrolysis combined with mechanical shearing and high-pressure homogenization for nanoscale cellulose fibrils and strong gels,” *Biomacromolecules*, vol. 8, no. 6, pp. 1934–1941, 2007.

[11] O. Nechyporchuk, M. N. Belgacem, and J. Bras, “Production of cellulose

nanofibrils: A review of recent advances," *Ind. Crops Prod.*, vol. 93, pp. 2–25, 2015.

[12] G. Chauve and J. Bras, *Industrial point of view of nanocellulose materials and their possible applications*. 2014.

[13] R. Wachala, T. Ramiega, A. Kaczmarek, and T. Antczak, "Nanocellulose By Enzymatic Methods," vol. 1211, no. October, pp. 4–5, 2015.

[14] M. J. Lundahl, V. Klar, L. Wang, M. Ago, and O. J. Rojas, "Spinning of cellulose nanofibrils into filaments: A review," *Ind. Eng. Chem. Res.*, vol. 56, no. 1, pp. 8–19, 2017.

[15] A. Dufresne, "Nanocellulose: A new ageless bionanomaterial," *Mater. Today*, vol. 16, no. 6, pp. 220–227, 2013.

[16] I. Siró and D. Plackett, "Microfibrillated cellulose and new nanocomposite materials: A review," *Cellulose*, vol. 17, no. 3, pp. 459–494, 2010.

[17] O. Nechyporchuk, M. N. Belgacem, and F. Pignon, "Current Progress in Rheology of Cellulose Nanofibril Suspensions," *Biomacromolecules*, vol. 17, no. 7, pp. 2311–2320, 2016.

[18] K. Markstedt, A. Mantas, I. Tournier, H. Martínez Ávila, D. Hägg, and P. Gatenholm, "3D bioprinting human chondrocytes with nanocellulose-alginate bioink for cartilage tissue engineering applications," *Biomacromolecules*, vol. 16, no. 5, pp. 1489–1496, 2015.

[19] A. Rees *et al.*, "3D bioprinting of carboxymethylated-periodate oxidized nanocellulose constructs for wound dressing applications," *Biomed Res. Int.*, vol. 2015, 2015.

[20] J. Leppiniemi *et al.*, "3D-Printable Bioactivated Nanocellulose?Alginate Hydrogels," *ACS Appl. Mater. Interfaces*, p. acsami.7b02756, 2017.

[21] J. Hiltunen, K. Kemppainen, and J. Pere, "Process for producing fibrillated cellulose material," 18-Dec-2014.

Xyloglucan adsorption for measuring specific surface area of cellulose nanofibers

CARL MOSER, HANÉLE BACKLUND, LOUISE DRENTH, GUNNAR HENRIKSSON and MIKAEL LINDSTRÖM

KTH Royal Institute of Technology
cmoser@kth.se

1 ABSTRACT

The hemicellulose xyloglucan adsorbs strongly to cellulose at neutral pH and without the addition of salt. Free xyloglucan in solution complexes with iodine to form colored complexes; by measuring the difference in absorbance at 660 nm for xyloglucan solutions with and without cellulose nanofibers it is possible to determine the amount of xyloglucan attached to the fibers. This can, in turn, be calculated to a specific surface area by fitting data from multiple measurements.

2 INTRODUCTION

Cellulose nanofibers (CNF) is a fast growing research topic with an exponential increase in publication during the last ten years. This and the fact that many companies have entered this field have resulted in a vast number of different qualities requiring characterization.

The optimal way of characterizing these materials would be to measure their specific surface area (SSA), and the most common way of doing to is through the BET-method [1] in which gas molecules are adsorbed to the surface at different pressure and by knowing the amount of gas and their size on the surface it is possible to determine the specific surface area. The limitation with this method is that the sample is required to be completely dry, which in the case of cellulose is an arduous task since the fibers hornifies as soon as they are dried. Some methods exist that prevent the major hornification such as liquid exchange procedure before the drying [2], this retains the structure and in some cases even cause and overestimation of the surface area [3]. The BET method provides numerous issues when working with cellulosic materials and it would be preferable if the SSA could be measured without having to dry the material.

Xyloglucan is a hemicellulose native to trees in the primary cell wall and in the kernel of tamarind seeds, this polymer adsorbs strongly to cellulose in water solution, and its concentration can be measured by complexation with iodine, like starch.

3 EXPERIMENTAL

14 different cellulose nanofiber qualities were produced from softwood and hardwood, both by the introduction of anionic charge and by enzymatic hydrolysis. And the disintegrated in a microfluidizer (Microfluidizer M-110EH, Microfluidics Corp., US) for either one or four passes in 200/100 µm chambers.

The samples were subjected to transmittance measurements at 500 nm and 0.1% dry content.

All CNF samples were mixed at 0.5 g/L and 0.55 g/L xyloglucan. All samples had a final volume of 2ml and incubated for 18h. 200 ul sample was added to an iodine sulfuric acid solution and centrifuged at 15k RPM (Eppendorf minispin plus). The samples were then left in the dark for 30 min before being pipetted into cuvettes to measure absorbance at 660 nm.

4 RESULTS AND DISCUSSION

SW0 corresponds to an unbleached softwood pulp with 7% lignin a DP of 2900 and a charge density of 125 µeq/g.

SW1 is a chlorite delignified SW0 with 0.2% lignin a DP of 1900 and a charge density of 100 µeq/g.

SW2 is an alkali extracted SW1 with 1% lignin, a DP of 700 and a charge density of 70 µeq/g.

HW0 corresponds to an unbleached hardwood pulp with 1.6% lignin a DP of 1700 and a charge density of 120 µeq/g.

HW1 is a chlorite delignified HW0 with 1.5% lignin a DP of 1300 and a charge density of 80 µeq/g.

HW2 is an alkali extracted HW1 with 1.1% lignin, a DP of 600 and a charge density of 70 µeq/g.

TEMPO is a tempo oxidized softwood pulp with a charge density of 800 µeq/g.

CMNC is a carboxymethylated softwood pulp with a charge density of 600 µeq/g.

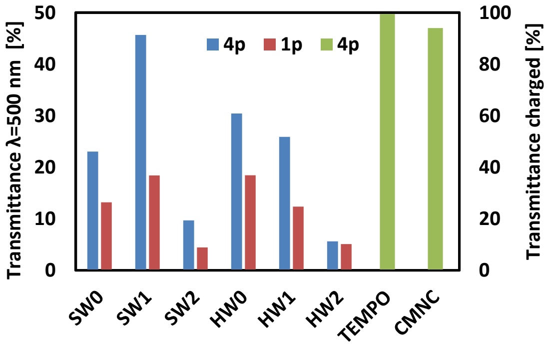

Figure 1. Transmittance values for all CNF samples. Enzymatically treated samples left and tempo oxidized and carboxymethylated samples to the right.

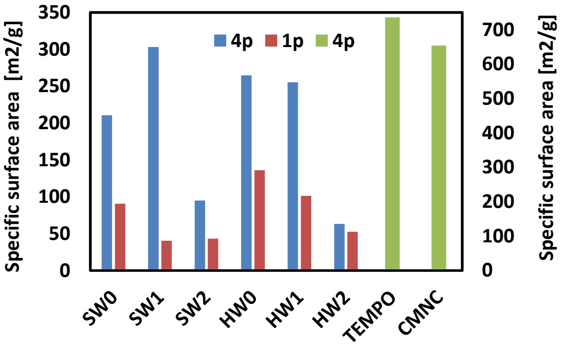

Figure 2. specific surface area calibrated against the TEMPO cnf sample which closely resembles elementary fibrils.

Transmittance is an efficient way of determining the disintegration degree of the various CNF qualities (**Figure 2**), and it is obvious from this figure that we have achieved 14 materials that differ a lot from each other.

It was possible to adsorb xyloglucan to the CNF samples and obtaining reasonable specific surface areas by doing so (**Figure 2**).

Additionally, the adsorbed amount of xyloglucan showed a close correlation with the transmittance values giving more credibility to the method.

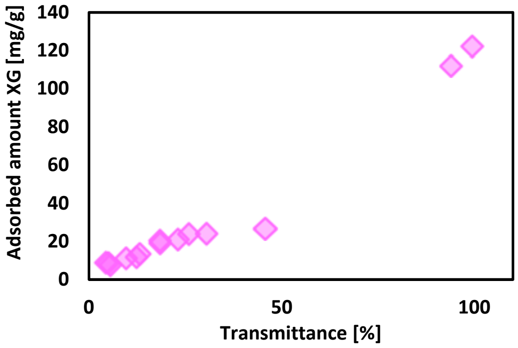

Figure 3. correlation between transmittance and the adsorbed amount of XG to CNF. Data points correspond to all 14 CNF samples. R^2=0.97 for all samples and 0.99 for the enzymatically treated samples (to the left).

REFERENCES

[1] Langmuir I (1918) The adsorption of gases on plane surface of glass, mica and platinum. Journal of the American Chemical Society 40(9):1361–1403, DOI 10.1021/ja02242a004

[2] Svensson A, Larsson PT, Salazar-Alvarez G, Wagberg L (2013) Preparation of Dry Ultra-Porous Cellulosic Fibres: Characterization and Possible Initial Uses. Carbohyd Polym 92(1):775–783

[3] Moser C, Henriksson G, Lindstrom M (2016) Specific surface area increase during cellulose nanofiber manufacturing related to energy input. BioResources 11(3)

Cellulose as a dispersion stabilizer

CAROLINA COSTA, HÅKAN EDLUND,
MAGNUS NORGREN, BJÖRN
LINDMAN

FSCN, Mid Sweden University
SE-852 30 Sundsvall, Sweden
carolina.costa@miun.se

1 SUMMARY

Using natural products with minimal modification is a strong driving force in developing biocompatible, biodegradable and nontoxic formulations. Important stabilizers of disperse systems are amphiphilic molecules. The efficient creation of an emulsion generally requires an emulsifier, which facilitates dispersion by lowering the interfacial tension, and a stabilizer that prevents flocculation of droplets by creating repulsion between droplets. Typically, a surfactant is used as the dispersant and a polymer as stabilizer; some amphiphilic polymers, notably block copolymers, can fulfil both criteria. Cellulose derivatives, such as methyl cellulose, hydroxyethyl cellulose and ethyl hydroxyethyl cellulose are well known as efficient stabilizers of dispersions. This highlights their amphiphilic nature which is clearly not a solo effect of the different chemical modifications but a direct consequence of the native cellulose backbone. In arguing that cellulose itself should be considered as an amphiphilic polymer we would naturally expect that cellulose would locate at the oil-water interfaces in an emulsion and thus acting as a good stabilizer.

Cohen's group in Haifa introduced native cellulose as a novel and efficient eco-friendly emulsifying agent for oil-in-water and water-in-oil emulsions [1, 2]. The authors suggest that the hydrophilic hydroxyl groups interact with the water while the more hydrophobic planes of the glucopyranose rings are located towards the hydrocarbon oil; besides, the dissolution-regeneration process facilitates the formation of an encapsulating coating at the water-oil interface because of the afforded higher mobility of the cellulose molecules [3]. Two approaches to obtaining emulsions were reported; the mixing of cellulose, oil and water in an ionic liquid and a second procedure consisting firstly in formation of a hydrogel from the cellulose/ionic liquid solution by coagulation with water and applying it into the sonicated water/oil or oil/water mixtures. Both procedures are suitable to form emulsions, but the obtained particle size distribution is quite broad, ranging from 200 nm to 20 µm.

Nanocrystalline celluloses have also been used as stabilizers of emulsions. However, in comparison with cellulose derivatives, the mechanisms are very different [1, 4, 5, 6, 7]. Cellulose derivatives behave similarly to any flexible or semi-flexible amphiphilic polymer, like graft and block copolymers, and provide steric stabilization. On the other hand, nanocrystalline cellulose follows the behavior observed in "Pickering emulsions". Therefore, molecular dissolved cellulose is expected to behave as typical cellulose derivatives.

1.1 Cellulose Surface Activity and Emulsion Stabilization

Our recent dynamic surface tension studies with dissolved cellulose confirmed its activity on the surface of an oil droplet (Figure 1). Interfacial tension (IFT) is already lowered by the high concentrated acidic solution (in which cellulose pulp has been dissolved), which facilitates the creation of small droplets; although IFT further decreases in the presence of dissolved cellulose, giving a clear indication of its surface activity. In addition, interfacial rheology showed an increase in the elastic modulus when cellulose was present in solution, thus suggesting that the dissolved cellulose molecules indeed migrate to the interface and form an interfacial layer around the oil droplet.

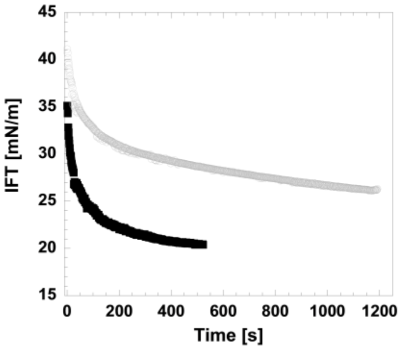

Figure 1. Interfacial tension between a paraffin oil droplet and 85 wt% phosphoric acid solutions with and without dissolved cellulose pulp.

To use cellulose as free molecules instead of particles it is crucial to select a solvent that would be able to dissolve cellulose close to a molecular level. Several solvents can be considered but it is an obvious advantage to use aqueous based systems, since the water used for dissolution can remain as either the dispersed phase or the dispersion medium in the emulsion; any other solvent would need to be removed involving a more complex process. Alkaline systems like aqueous NaO/urea, LiOH/urea and TBAH, as well as acidic solvents like aqueous phosphoric acid solutions, look like good candidates.

An emulsification procedure has been recently developed by our group starting with cellulose dissolved in an aqueous solution of 85 wt% phosphoric acid. This solution was then used as a dispersion medium for oil, which was directly introduced into the cellulose solution, being water added later, or it was introduced as a pre-dispersion of oil-in-water and added to the cellulose solution. Initial experiments suggest the formation of stable O/W emulsions with a narrower range of sizes; resultant emulsions exhibit reversible creaming by simply manual shaking (Figure 2a) and, moreover, no coalescence or oiling-off is observed. A different emulsification route have resulted in an O/W nanoemulsion with excellent stability, by slowly regenerate cellulose with a basic solution in the presence of oil (Figure 2b). Since the solution state of cellulose is expected to have a marked impact on the properties of the formed emulsions, studies using different acidic and alkaline systems are currently ongoing in order to understand how it affects the droplets size distributions and consequent stability of the emulsions.

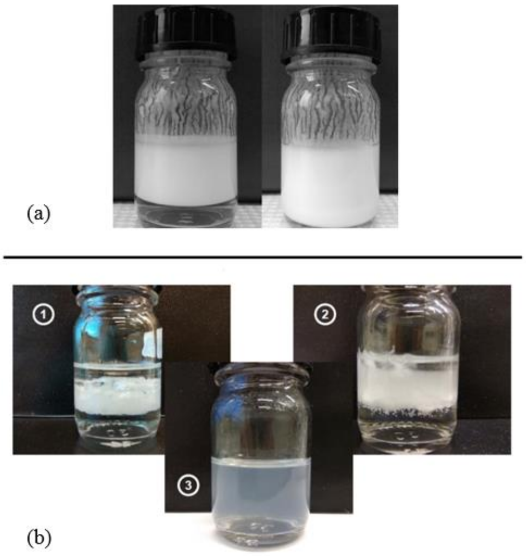

Figure 2. (a) Reversible creaming of the emulsions after shaking by hand (on the right); (b) (1) regeneration of cellulose by injection of a basic solution in the presence of oil; (2) gelation; (3) nanoemulsion.

REFERENCES

[1] D. M. Rein, R. Khalfin and Y. Cohen. Cellulose as a novel amphiphilic coating for oil-in-water and water-in-oil dispersions. *J Colloid Interf Sci.* **386**, 456-463 (2012).

[2] S. Napso, D. M. Rein, R. Khalfin, O. Kleinerman and Y. Cohen. Cellulose gel-dispersion: From pure hydrogel suspensions to encapsulated oil-in-water emulsions. *Colloid Surface B.* **137**, 70-76 (2016).

[3] H. Miyamoto, D. M. Rein, K. Ueda, C. Yamane and Y. Cohen. Molecular dynamics simulation of cellulose-coated oil-in-water emulsions. *Cellulose*. (2017)

[4] E. Melzer, J. Kreuter and R. Daniels. Ethylcellulose: a new type of emulsion stabilizer. *Eur J Pharm Biopharm*. **56**, 23-27 (2003).

[5] W. B. Sun, D. J. Sun, Y. P. Wei, S. Y. Liu and S. Y. Zhang. Oil-in-water emulsions stabilized by hydrophobicaly modified hydroxyethyl cellulose: adsorption and thickening effect. J *Colloid Interf Sci*. **311**, 228-236 (2007).

[6] I. Kalashnikova, H. Bizot, B. Cathala and I. Capron. New pickering emulsions stabilized by bacterial cellulose nanocrystals. *Langmuir*. **27**, 7471-7479 (2011).

[7] K. R. Peddireddy, T. Nicolai, L. Benyahia and I. Capron. Stabilization of water-in-water emulsions by nanorods. *Acs Macro Lett*. **5**, 283-286 (2016).

Interaction of cellulose fibres with aqueous foam

A. KETOLA, T. HJELT, H. PAJARI, T. LAPPALAINEN, T. TAMMELIN, J. A. KETOJA

VTT Technical Research Centre of Finland Ltd

annika.ketola@vtt.fi

ABSTRACT

Foam forming technology not only solves some long-standing issues related to flocculation in water forming but also enables widening of raw materials and end-use properties of fibre products. The technology can provide fibre materials with striking new features such as tailored microporous structures. Here the control of the foam properties and the interaction of air bubbles with fibres become important. We study these effects for aqueous foams using different types of surfactants and model fibre surfaces. The findings can be used to design new structures and materials that display low weight and high performance.

1 INTRODUCTION

Foam forming is a next-generation manufacturing platform for fibre-based products. It enables not only production of paper and board with high uniformity and bulk but also many other types of products extending from textiles to construction materials.

The stability and structure of the foam carrier medium provides a tool to tailor the material density and its pore size distribution [1]. Thus, affecting fibre-foam interactions by changing formulation variables would enable the manufacture of new bio-based products with properties totally different to those obtained by water forming. Other advantages of the technology are possible energy savings through improved dewatering and the possibility to introduce new raw materials ranging from nanoparticles to long fibres into the process.

The bubble size of typical fibre foams is strongly affected by the presence of micron-sized particles/fibres [2]. The rheological behaviour is affected by shear rate and nanoparticles as well. Small sized nanoparticles can easily adhere to interfaces, stabilize the liquid films and increase the viscosity.

Foam structure and rheology do not depend only on obvious physical properties, such as bubble size distribution and surface tension, but also on the characteristic adsorption time of surfactant and the interface modulus and viscosity. In addition to the size of fibres, their surface properties (surface energy and smoothness) play an important role in the foam behaviour but are still unexplored and their macroscopic effects are not clear. We have studied fundamental interactions taking place between cellulose fibres and aqueous foam in the foam forming process.

2 INTERACTION BETWEEN BUBBLES AND FIBRES

The attractive interaction between fibres and air bubbles cannot be explained by the classical theories of non-specific surface forces (DLVO). According to recent

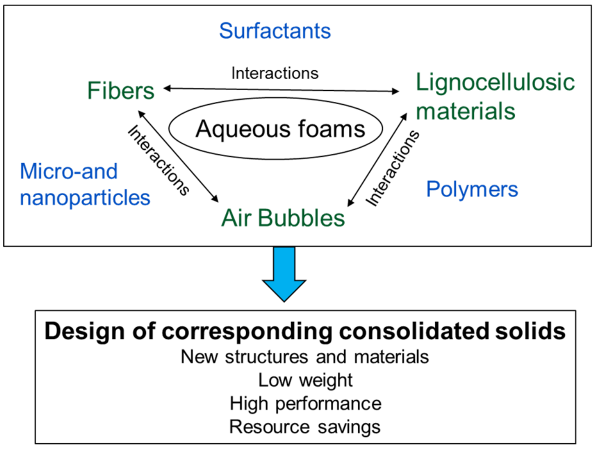

Figure 1. Understanding of physical and chemical interactions in aqueous cellulose based foams opens an avenue to design new materials.

studies, air bubbles carry a negative charge in aqueous media [3] as also does lignocellulosic fibres. Thus, non-electrostatic forces in combination with larger scale hydrophobic forces [4, 5] can cause main interactions between fibres and bubbles.

The behaviour of air bubbles on model surfaces in solutions containing surface active agents was investigated by using a contact angle measuring system. Model surfaces of different hydrophobicity and hydrophilicity were prepared and placed in a solution containing anionic or non-ionic surfactants. An air bubble was positioned on the model surface by using a hooked needle. Measured contact angles revealed the attractive force between a bubble and hydrophobic surface, whereas the interaction was repulsive for hydrophilic surfaces. This suggests that fibre surfaces have hydrophobic regions that attract air bubbles.

The complexity of the interacting system is increased gradually in the ongoing experiments. The resulting better understanding of the effects of air bubbles, fibres, surfactants and other components present in the foam forming formulations can be used to synthesize nonwovens, layered and 3D materials.

We would like to thank Academy of Finland (Project “Surface interactions and rheology of aqueous cellulose-based foams”) for financial support.

REFERENCES

[1] A. M. Al-Qararah, A. Ekman, T. Hjelt, J. A. Ketoja, H. Kiiskinen, A. Koponen, J. Timonen, A unique microstructure of the fiber networks deposited from foam-fiber suspensions. *Colloids and Surfaces A: Physicochem. Eng. Aspects* **482**, 544-553 (2015).

[2] A. M. Al-Qararah, T. Hjelt, A. Koponen, A. Harlin, J. A. Ketoja, Response of wet foam to fibre mixing. *Colloids and Surfaces A. Physicochem. Eng. Aspects* **467**, 97-106 (2015).

[3] J. Weihong, S. Ren, B. Hu. Effect of water chemistry on zeta potential of air bubbles. *Int. J. Electrochem. Sci.* **8** 5828-5837 (2013).

[4] A. V. Nguyen, H. J. Schulze, J. Ralston, Elementary steps in particle-bubble attachment. *Int. J. Miner. Process,* **51**, 183-195, (1997).

[5] D. Kosior, J. Zawala, K. Neicikowska,, K. Malysa, K. Influence of non-ionic and ionic surfactants on kinetics of the bubble attachment to hydrophilic and hydrophobic solids. *Original Colloids Surf.* **A 470** 333 (2015)

Assessing the accessibility of cellulose by dynamic vapour sorption coupled with deuterium exchange

SAIJA VÄISÄNEN, ZHEN ZENG, RAILI PÖNNI and TAPANI VUORINEN

Aalto University, Department of
Bioproducts and Biosystems, P.O. Box
16300, 00076 Aalto, Finland
saija.vaisanen@aalto.fi

1 ABSTRACT

Cellulose has a key role in the shift from fossil-based economies to renewable resource-based bioeconomies. As an abundant and renewable biopolymer, it provides an interesting choice as a raw material for many applications. The conversion of cellulose into novel products create a need for in-depth knowledge on the reactivity of cellulose. The reactivity during many of these treatments depends on the accessibility of hydroxyl groups in cellulose, i.e. cellulose accessibility. In this work, we have assessed the accessibility of cellulosic samples by employing a method based on dynamic vapor sorption coupled with deuterium exchange. This method enables the quantification of the accessible hydroxyl groups in the samples.

2 INTRODUCTION

As an abundant and renewable biopolymer, cellulose provides an interesting choice as a raw material for many novel applications. The conversion of cellulose into various products create a need for in-depth knowledge on the reactivity of cellulose. Manufacturing novel cellulosic materials, such as cellulosic nanomaterials, cellulose derivatives and textiles, often requires chemical modification of cellulose or even its dissolution [1,2,3,4,5,6]. Cellulose accessibility is one of the main factors affecting the treatments. Thus, the means to assess and control the accessibility of cellulose has gained increasing interest lately.

Cellulose accessibility has historically been of the interest mainly because of the importance of water retention properties of pulps in papermaking. Thus, it has been widely analyzed with several indirect techniques including the water retention value (WRV) and fiber saturation point (FSP) which provide information on the pore structure of the fiber wall and the fibers' ability to swell [7,8,9,10,11]. The pore structure of the fiber wall has also been studied with nuclear magnetic resonance spectroscopy (NMR), differential scanning calorimetry (DSC), inverse size exclusion chromatography (ISEC), solute exclusion and nitrogen sorption [8,12,13,14,15]. The morphology of the fibers has been visualized with atomic force microscopy (AFM), scanning electron microscopy (SEM) and transmission electron microscopy (TEM) [8,16,17]. In addition, the surface accessibility of cellulose fibrils has been analyzed with Fourier transform infrared spectroscopy (FT-IR) of deuterated samples [18,19].

Despite the numerous techniques available, to date, dynamic vapor sorption (DVS) coupled with deuterium exchange is the only method enabling the direct quantification of the amount of accessible hydroxyl (OH) groups in cellulosic samples. DVS is a gravimetric technique which is applied in determining the amount of and the rate of solvent sorped by a sample. The analysis is based on measuring the changes in the mass of the sample when the vapor concentration, i.e. the relative humidity (RH), of the measurement chamber is changed with the solvent of interest. When DVS is coupled with deuterium exchange, the hydrogens in the accessible OH groups of the sample are exchanged with deuterium by exposing the sample to deuterium oxide (D_2O) vapor. As deuterium is heavier than hydrogen, the replacement can be monitored by weight gain and the amount of accessible OH groups can be calculated from the difference in the dry mass of the sample before and after its exposure to D_2O.

Recently, DVS with deuterium exchange has been applied to determine the amount of accessible OH groups in bacterial cellulose and wood as well as pulps treated with sodium hydroxide [20,21,22]. In their study of birch kraft pulps treated with sodium hydroxide, Pönni et al. reported that DVS coupled with deuterium exchange is a powerful tool in quantifying the accessible OH groups in chemical pulps but the weakness of the experiments was their long duration [22]. In order to decrease the amount of time needed for a measurement, we have further developed the method published in [22]. In addition, we have applied the developed method to several different cellulosic samples.

3 EXPERIMENTAL

The determination of the amount of accessible OH groups with DVS coupled with deuterium exchange is based on the exchange of hydrogen to deuterium in the accessible OH groups when the sample is subjected to D_2O vapor and the subsequent change in the mass of the sample. Fig. 1 illustrates the principle of the hydrogen-deuterium exchange.

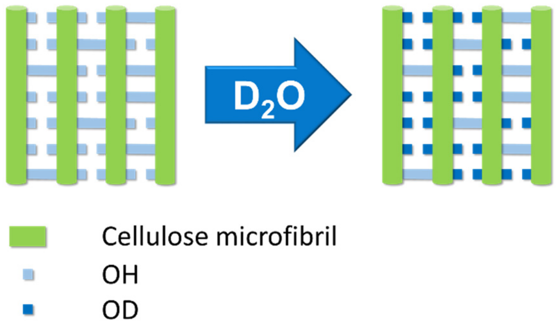

Figure 1. Principle of deuteration of the accessible OH groups when the sample is subjected to D2O vapor

The DVS measurement consists of three stages. The sample is first dried to remove excess water. Then, the RH of the measurement chamber is increased with D_2O vapor to allow the hydrogen-deuterium exchange. As the final stage, the sample is dried again to remove excess D_2O.

The amount of accessible OH groups is calculated with Eq. 1 in which the atomic mass difference between deuterium and hydrogen is 1 g/mol.

$$A = \frac{m_f - m_i}{m_i} \times 1000, \qquad (1)$$

where A is the amount of accessible OH groups in mol/kg of dry mass of sample, m_i is the dry mass of the sample in mg before exposing the sample to D_2O vapor and m_f is the dry mass of the sample in mg after the D_2O exposure.

We applied the DVS method to various cellulosic samples including pulps and commercial microcrystalline cellulose powder. For the measurements, we employed the Surface Measurement Systems Ltd DVS ET (elevated temperature) apparatus which has the measuring accuracy of 0.1 µg and the chamber volume of 100 cm^3. We studied each sample with several parallel measurements.

4 RESULTS AND DISCUSSION

We applied the developed DVS method to study the accessibility of several cellulosic samples including pulps received from Finnish pulp mills as well as commercial microcrystalline cellulose powder. Fig. 2 shows the accessibilities of the pulps and microcrystalline cellulose in % of the theoretical maximum. The theoretical maximum is calculated with the assumption that the sample is pure cellulose and all the OH groups are accessible. In the figure, the studied pulps are labeled with numbers and the microcrystalline cellulose is named as MCC.

As illustrated in Fig. 2, the accessibilities of the untreated pulps vary between 54 and 62 % of the theoretical maximum. The accessibility of the commercial microcrystalline cellulose is approximately 52 % of the theoretical maximum.

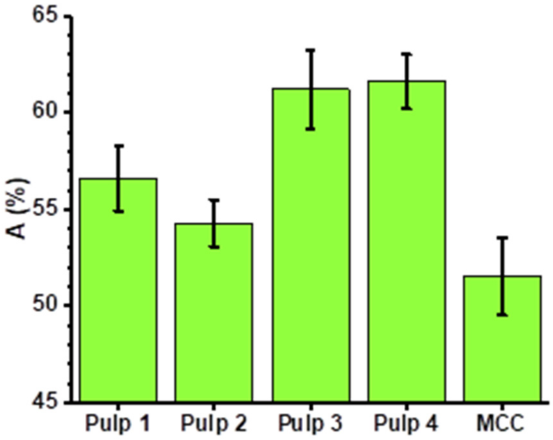

Figure 2. Accessibilities of cellulosic samples in % of the theoretical maximum

5 CONCLUSIONS

We further developed the method based on DVS coupled with deuterium exchange to quantify the accessibility of cellulosic samples in a relatively short period of time. In addition, we applied the developed method to study the accessibility of various cellulosic samples including pulps and commercial microcrystalline cellulose. The accessibilities of the pulps varied between 54 and 62 % of the theoretical maximum accessibility of cellulose, while the accessibility of the microcrystalline cellulose was approximately 52 % of the theoretical maximum.

ACKNOWLEDGMENTS

This work was a part of the ACel research program coordinated by CLIC Innovation Ltd. The funding of the Finnish Funding Agency for Technology and Innovation (TEKES) is acknowledged. In addition, the work of M.Sc. Ville Lovikka with sample preparation is acknowledged.

REFERENCES

[1] L. Brinchi, F. Cotana, E. Fortunati and J.M. Kenny. Production of nanocrystalline cellulose from lignocellulosic biomass: technology and applications. *Carbohyd. Polym.* **94**(1):154-169 (2013).

[2] Y. Habibi, L.A. Lucia and O.J. Rojas. Cellulose Nanocrystals: chemistry, self-assembly, and applications. Chem. Rev. **110**(6):3479-3500 (2010).

[3] A. Isogai, T. Saito and H. Fukuzumi. TEMPO-oxidized cellulose nanofibers. *Nanoscale* **3**(1):71-85 (2011).

[4] P.L. Nasatto, F. Pignon, J.L.M. Silveira, M.E.R Duarte, M.D. Noseda and M. Rinaudo. Methylcellulose, a cellulose derivative with original physical properties and extended applications. *Polymers* **7**(5):777-803 (2015).

[5] A. Michud, M. Tanttu, S. Asaadi, Y. Ma, E. Netti, P. Kääriäinen, A. Persson, A. Berntsson, M. Hummel and H. Sixta. Ioncell-F: ionic liquid-based cellulosic textile fibers as an alternative to viscose and Lyocell. *Text. Res. J.* **86**(5):543-552 (2015).

[6] S. Peleteiro, S. Rivas, J.L. Alonso, V. Santos and J.C. Parajó. Utilization of ionic liquids in lignocellulose biorefineries as agents for separation, derivatization, fractionation or pretreatment. *J. Agr. Food Chem.* **63**(37):8093-8102 (2015).

[7] S. Grönqvist, T.K. Hakala, T. Kamppuri, M. Vehviläinen, T. Hänninen, T. Liitiä, T. Maloney and A. Suurnäkki. Fibre porosity development of dissolving pulp during mechanical and enzymatic processing. *Cellulose* **21**(5):3667-3676 (2014).

[8] V.A. Lovikka, P. Khanjani, S. Väisänen, T. Vuorinen and T.C. Maloney. Porosity of wood pulp fibers in the wet and highly open dry state. *Micropor. Mesopor. Mat.* **234**:326-335 (2016).

[9] X.L. Luo, J.Y. Zhu, R. Gleisner and H.Y. Zhan. Effects of wet-pressing-induced fiber hornification on enzymatic saccharification of

lignocelluloses. *Cellulose* **18**(4):1055-1062 (2011).

[10] A. Roselli, M. Hummel, A. Monshizadeh, T. Maloney and H. Sixta. Ionic liquid extraction method for upgrading eucalyptus kraft pulp to high purity dissolving pulp. *Cellulose* **21**(5):3655-3666 (2014).

[11] J.E. Stone and A.M. Scallan. The effect of component removal upon the porous structure of the cell wall of wood. II. Swelling in water and the fiber saturation point. *Tappi J.* **50**(10):496-501 (1967).

[12] Å. Östlund, T. Köhnke, L. Nordstierna and M. Nydén. NMR cryoporometry to study the fiber wall structure and the effect of drying. *Cellulose* **17**(2):321–328 (2010).

[13] T.C. Maloney, H. Paulapuro and P. Stenius. Hydration and swelling of pulp fibers measured with differential scanning calorimetry. *Nord. Pulp Pap. Res. J.* **13**(1):31-36 (1998).

[14] J. Berthold and L. Salmén. Inverse size exclusion chromatography (ISEC) for determining the relative pore size distribution of wood pulps. *Holzforschung*, **51**(4):361-368 (1997).

[15] J.E. Stone and A.M. Scallan. A structural model for the cell wall of water-swollen wood pulp fibres based on their accessibility to macromolecules. *Cell. Chem. Technol.* **2**:343-358 (1968).

[16] V. Billosta, J. Brändström, A. Cochaux, J.-P. Joseleau and K. Ruel. Ultrastructural organisation of the wood cell wall can explain modifications caused in fibers during the pulping process. *Cell. Chem. Technol.* **40**(3-4):223-229 (2006).

[17] S.-Y. Ding, S. Zhao and Y. Zeng. Size, shape, and arrangement of native cellulose fibrils in maize cell walls. *Cellulose* **21**(2):863-871 (2014).

[18] R. Pönni, L. Galvis and T. Vuorinen. Changes in accessibility of cellulose during kraft pulping of wood in deuterium oxide. *Carbohyd. Polym.* **101**:792-797 (2014).

[19] E.L. Lindh and L. Salmén. Surface accessibility of cellulose fibrils studied by hydrogen-deuterium exchange with water. *Cellulose* **24**(1):21-33 (2017).

[20] J.M. Lee, J.A. Heitmann and J.J. Pawlak. Technique for the measurement of dimensional changes of natural microfibril materials under variable humidity environments. *Mat. Sci. Eng. A* **445-446**:632-640 (2007).

[21] M. Kymäläinen, L. Rautkari and C.A.S. Hill. Sorption behaviour of torrefied wood and charcoal determined by dynamic vapour sorption. *J. Mater. Sci.* **50**(23):7673-7680 (2015).

[22] R. Pönni, L. Rautkari, C.A.S. Hill and T. Vuorinen. Accessibility of hydroxyl groups in birch kraft pulps quantified by deuterium exchange in D2O vapor. *Cellulose* **21**(3):1217-1226 (2014).

Hydrophobic Coating on Cellulosic Textile Material by Betulin and a Betulin Based Copolymer

Tianxiao Huang, Dongfang Li, Monica Ek
KTH Royal Institute of Technology,
Stockholm, SE-10044, Sweden.
tiahuang@kth.se

INTRODUCTION

Cotton, a kind of cellulose fiber material, is widely used in clothes' manufacture. Cotton has attractive characteristics like cheapness, softness and sustainability. However, cotton fabric could absorb mass of water since there are lots of hydroxyl groups within the cellulose molecules. This property, in some cases, is not desired [1] Therefore, the hydrophobization of cellulose fibers has gained remarkable attention recently [1,2,3,4], because of the increased interests in various waterproof fabrics.

In this study, betulin, a naturally abundant and hydrophobic compound obtained from the outer bark of birch [5], a copolymer developed from betulin, were introduced onto the surface of cotton fabric to acquire water repellency.

EXPERIMENTAL

Solutions of betulin were used to treat cellulosic textile fibers and improve their water repellency. Cotton fabrics were impregnated in 3.75 g L^{-1} and 7.5 g L^{-1} solution of betulin in ethanol, and 7.5 g L^{-1} solution of betulin in ethyl acetate respectively. A terephthaloyl chloride-betulin copolymer was synthesized and dissolved in tetrahydrofuran to afford a solution with a concentration of 3.75 g L^{-1}. The cotton fabric was also impregnated in that solution. Changes in morphology of the cellulose fibers before and after the treatment were observed by scanning electron microscopy, hydrophobicity of treated fabrics were measured by water contact angle measurement and the water repellency was measured by a standard spray test.

RESULTS AND DISCUSSION

Figure 1 shows the change of average contact angle against time for different samples. The fluctuating range of each serial is no more than 5° or even less, which means the contact angle was stable within 170 seconds for each sample. "A2, B, A3, A1" could be identified as a descending sequence of average water contact angle within this time period.

Comparing A1 and A2, sample A2 possessed a slightly higher (6°-7°) water contact angle than A1, which proves that fabric treated by betulin solution in ethanol with higher concentration performs slightly better hydrophobicity. Comparing A2 and A3, a gap of approximately 5° could be identified, which proves that given the same concentration, the fabric treated with the betulin solution in ethanol exhibits a slightly better hydrophobicity than the one treated with the solution in ethyl acetate. The water contact angle of the sample B is almost stable, and the value is approximately 150°, which is only lower than that of A2 but higher than the other two.

A surface is considered superhydrophobic when its water contact angle is higher than 150°. It worth noting that A2 and B even reached superhydrophobic level while A3 did not reach for most of the time, and A1 did not reach for all the 170 seconds. However, the difference in average contact angle between sample A2 and A1 is only about 7°, which is so small that could be ignored for purpose of daily-use waterproof material. In other words, the hydrophobicity of all those samples are more or less the same.

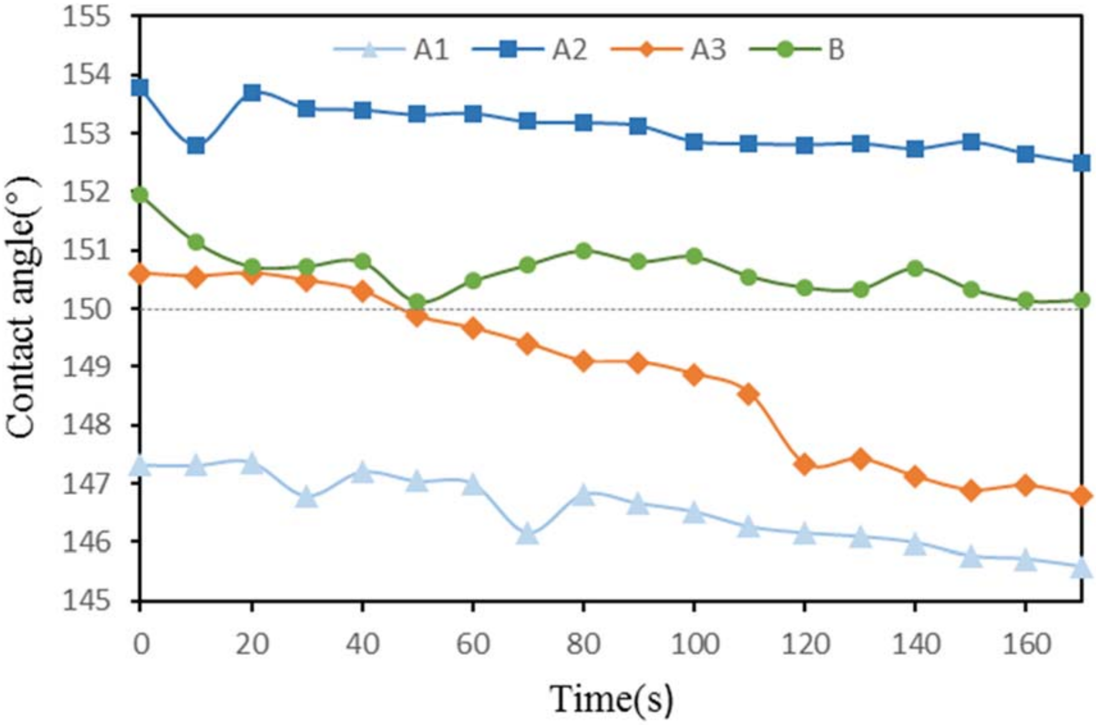

Figure 1: Water contact angles of samples treated with 3.75 g L^{-1} betulin solutions in ethanol (A1), 7.5 g L^{-1} betulin solutions in ethanol (A2) and ethyl acetate (A3), and 3.75 g L^{-1} copolymer solution in THF (B).

Water repellence was determined by a standard water spray test. As shown of sample A2 in Fig 2, thickly dotted water droplets were presented around the central part, where the pattern is just like that of untreated sample. A hypothesis for this phenomenon is that the betulin particles in the central part was rushed away by the sprayed water while those located around were not influenced. According to the rating chart, the rating for sample A2 is approximately 70 except the central parts. The rating of water repellency for the sample B is about 80 and interestingly, the difference between central part where facing the water rushing and surrounding part of B is not that obvious as sample A2. This phenomenon could be attributed to that compared with simple betulin particles, the wrapping copolymer films perform relative stronger adhesion with the textile fibers.

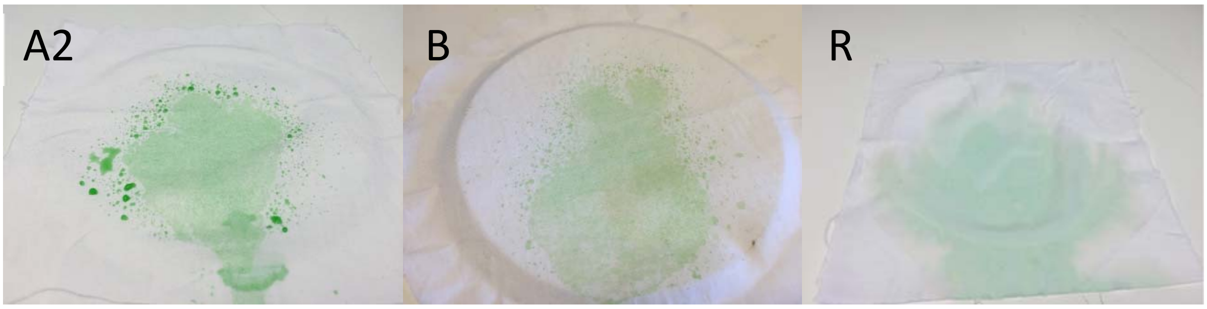

Figure 2: Result of spray test for sample A2, B, and an untreated sample.

REFERENCES

[1] Bae, G. Y., Min, B. G., Jeong, Y. G., Lee, S. C., Jang, J. H., & Koo, G. H. (2009). Superhydrophobicity of cotton fabrics treated with silica nanoparticles and water-repellent agent. Journal of colloid and interface science, 337(1), 170-175.

[2] Wi, D.-Y., Kim, I. W., & Kim, J. (2009). Water repellent cotton fabrics prepared by PTFE RF sputtering. Fibers and Polymers, 10(1), 98-101.

[3] Ivanova, N., & Zaretskaya, A. (2010). Simple treatment of cotton textile to impart high water repellent properties. Applied Surface Science, 257(5), 1800-1803.

[4] Shi, Z., Wyman, I., Liu, G., Hu, H., Zou, H., & Hu, J. (2013). Preparation of water-repellent cotton fabrics from fluorinated diblock copolymers and evaluation of their durability. Polymer, 54(23), 6406-6414.

[5] Fridén, M. E., Jumaah, F., Gustavsson, C., Enmark, M., Fornstedt, T., Turner, C., . . . Samuelsson, J. (2016). Evaluation and analysis of environmentally sustainable methodologies for extraction of betulin from birch bark with a focus on industrial feasibility. Green Chemistry, 18(2), 516-523.

Influence of mineral pigments on cell behaviour

DIOSANGELES SOTO VELIZ and
MARTTI TOIVAKKA

Laboratory of Paper Coating and
Coverting, Abo Akademi University
diosangeles.sotoveliz@abo.fi

1 INTRODUCTION

Cell fate depends strongly on the extracellular environment [1]. Cellular processes such as cell differentiation, cell growth, cell proliferation, and cell death can be potentially controlled by the cell culture platform. For that reason, there is an expanding need to develop a cell growth substrate that is capable to control cell decision making in order to improve understanding of diseases and to optimise drug development.

Recently, paper has emerged as a promising platform for cell culture purposes [2] and pharmaceutical development [3]. Some of the advantages of utilising paper as a platform include its ecological and economical sustainability its well-developed industry, and specifically, the versatility of its properties.

Additives such as minerals serve as the means to easily modify and control the physical-chemical and functional properties of paper, including those directing cell fate. For example, minerals can be used to improve functional printing, to form multilayer or multicomponent systems, and to optimise parameters such as hydrophilicity, porosity, surface potential and morphology of the desired substrate. Consequently, minerals provide a direct and inexpensive method to manipulate cell behaviour.

In contrast, minerals are currently used in biomedicine for guided drug delivery, bone engineering, wound healing and as antibacterial agents. The intention of this project is to provide insight of a novel use for minerals in cell growth substrates.

The objective of this research is to understand the influence of minerals on cell behaviour under the hypothesis that minerals will actively influence cell processes either by changes in the cell-growth substrate properties or by ion-induced signalling. In order to achieve this aim, the project has been divided into three different stages (Figure 1). This abstract includes the experimental design and results obtained from the treatment of cells with mineral pigments.

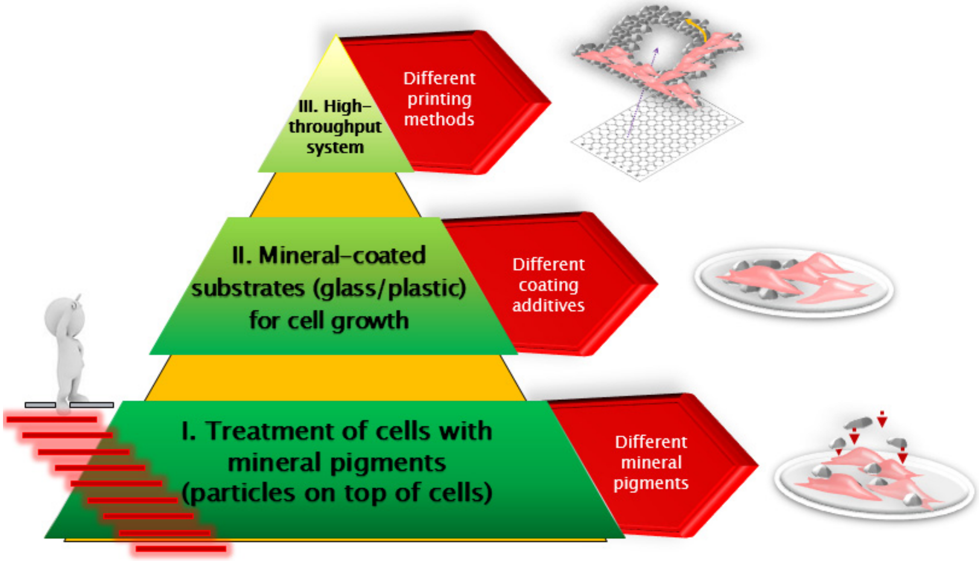

Figure 1. Project outline.

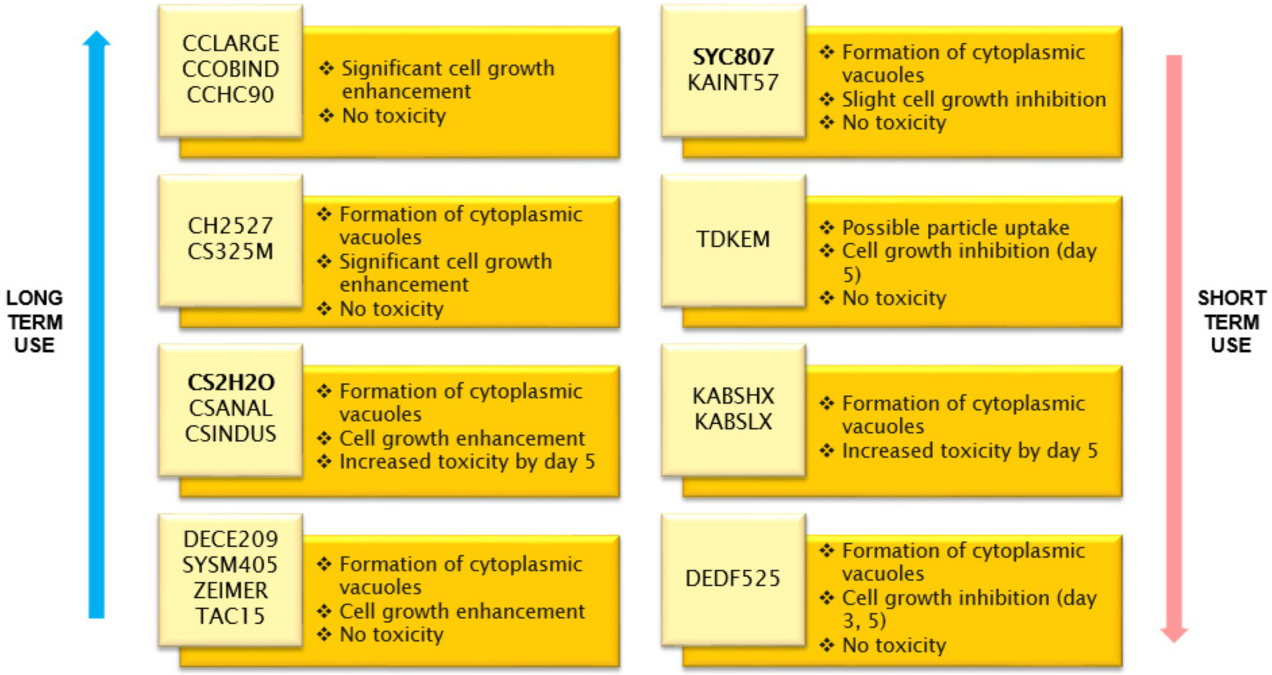

Figure 2. Mineral arrangement according to the biological interaction with human dermal fibroblasts including changes in cell growth, cell morphology and cellular toxicity.

2 MATERIALS AND METHODS

Minerals of different chemical structures, shapes and sizes were selected for this study, including calcium carbonates (CCLARGE, CCOBIND, CCHC90, CH2527), calcium sulphates (CS2H2O, CS325M, CSANAL, CSINDUS), silica (SYC807, DECE205, DEDF525), silicates (SYSM405, TAC15, KAINT57, KABSHX, KABSLX, ZEIMER), and titanium dioxide (TDKEM).

As for the experimental design, human dermal fibroblasts (HDFs) were seeded into multiwell plates and left to attach overnight. Then, minerals were suspended in serum free cell culture media to facilitate dispersion, added as treatment to the previously attached cells, and left to interact up to five days.

The particle characterisation consisted of scanning electron microscopy (SEM), transmission electron microscopy (TEM), Fourier transform infrared spectroscopy (FTIR), and zeta potential measurements. The interaction between the HDFs and the mineral particles was characterised through methods such as MTT colorimetric assay, LDH colorimetric assay, calcium colorimetric assay, live cell imaging, immunofluorescence microscopy, and complementary studies through collaborations with the laboratories of calcium signalling and stress signalling at Abo Akademi University.

3 RESULTS

The initial screening of materials showed that different minerals are able to trigger various modifications in cell behaviour including increased cell proliferation and various morphological changes. It was observed that minerals have an initial effect on cell growth (slight decrease) after one day of interaction with cells, without any significant toxicity. This period of adaptation is then followed either by recovery of the cells with time which leads to cell growth enhancement, or to the rejection of the minerals showed by cell growth inhibition or increased toxicity. Minerals can be arranged according to the results obtained from the biological assessment (Figure 2), and further grouped into minerals that can be used for longer periods of times, and minerals suitable for short term interaction with HDFs.

Calcium carbonates are largely known and used in biomedicine due to their biocompatibility. In this research, the calcium carbonate minerals were the ones with most cell growth enhancement without exerting toxicity or significant changes to the cell morphology. In general, there were mainly two types of morphological changes observed within the studied minerals. First, a decreased size or elongation of the cells that resulted in increased proliferation since a higher amount of cells were able to fit in the same available area for growth; and secondly, cytoplasmic vacuolation (Figure 3) which often included modifications to nuclear shape and did not induce cell death. Most significant cytoplasmic vacuolation occurred when cells interacted with the calcium sulphates. Thus, calcium ion release from the minerals and intracellular calcium signalling were further studied varying the initial concentration of calcium in the cell culture media, and the concentration of the minerals. Results show that the calcium sulphate samples were able to greatly increase the amount of calcium in the cell culture media. In addition, the amount of serum (and calcium) present in the cell culture mediawas proportional to the amount of vacuoles in the cells. However, the calcium sulphates did not have an effect on intracellular calcium signalling despite the morphological effects and the significant calcium ion release, indicating that there may be other mechanisms involved in the process.

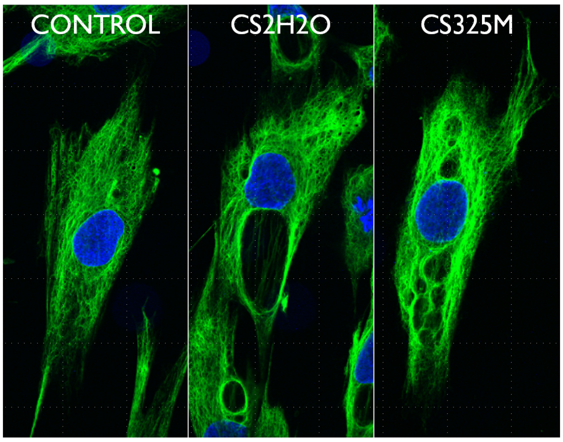

Figure 3. Spinning disk microscopy images of human dermal fibroblasts without treatment (regular morphology), and treated with the calcium sulphates CS2H2O and CS325M (cytoplasmic vacuolation). Blue represents the cell nuclei, and green represents the vimentin filaments inside the cells.

4 REFERENCES

[1] B. Alberts, A. Johnson, J. Lewis, M. Raff, K. Roberts and P. Walter. Molecular Biology of the Cell, Garland Science, edition 5, (2008).

[2] K. Ng, B. Gao, K. W. Yong, Y. Li, M. Shi, X. Zhao, Z. Li, X. Zhang. B. Pingguan-Murphy, H. Yang and F. Xu. Paper-based cell culture platform and its emerging biomedical applications. *Mater. Today* **20**(1):32-44 (2017).

[3] Y.-H. Chen, Z.-K. Kuo and C.-M. Cheng. Paper – a potential platform in pharmaceutical development. *Trends Biotechnol.* **33**(1):4-9 (2015).

Studying the reactivity of cellulose by oxidation with 4-acetamido-2,2,6,6-tetramethylpiperidine-1-oxo-piperidinium cation

PEGAH KHANJANI, VILLE LOVIKKA,
SAIJA VÄISÄNEN, THAD MALONEY,
and TAPANI VUORINEN

Aalto University, School of Chemical
Engineering, Finland
pegah.khanjani@aalto.fi

1 Abstract

Accessibility and reactivity of cellulose to solvents and reagents are key parameters on the production of cellulose derivatives. Different factors such as, crystallinity, microfibril aggregation, size of pores, and solubility of cellulose influence on their reactivity. Several indirect methods, such as fiber saturation point (FSP), water retention value (WRV) and surface area have been developed to characterize the reactivity of cellulosic samples. Here we report on using oxidation with 4-acetamido-2,2,6,6-tetramethylpiperidine-1-oxo-piperidinium (4-AcNH-TEMPO$^+$) cation as a probe reaction to quantify the accessible methylhydroxyl group of cellulose. In fact, 4-AcNH-TEMPO$^+$ easily oxidized hydroxymethyl groups of cellulose into carboxylate groups. An iodometric titration method was introduced to calculate the concentration of the oxoammonium component during oxidation reaction. Finally the 4-AcNH-TEMPO$^+$ reactivity was correlated with several pulp characteristics, including WRV, FSP, surface area, chemical composition, crystallinity.

2 Materials and Methods

Bleached never-dried and dried softwood kraft pulps were obtained from Finnish pulp mills. Suspensions of the pulps in water/buffer solution were prepared with 10 min ultrasonic treatment. Potassium iodide (KI) and 4-acetamido-2,2,6,6-tetramethylpiperidine-1-oxo-piperidinium (4-AcNH-TEMPO$^+$) tetrafluoroborate were purchased from Sigma-Aldrich. A pH 9 buffer solution was prepared by dissolving 185 mg boric acid (VWR) and 80 mg of NaOH (VWR) in 500 ml of distilled water. The pH 2 citrate buffer solution (AVS TITRINORM) was purchased from VWR. Research quality dextran (T2000, 2,000 kDa) and acetone (99.8%) were provided by Pharmacosmos A/S and WVR International, respectively. CO_2 (99.8%) was delivered by Oy Aga AB. UV/Vis absorption spectra were measured with a Shimadzu UV/2550 spectrophotometer.

3 Results

Recently, we showed that TEMPO$^+$, the active reagent in TEMPO-mediated oxidation of cellulose, can be quantified in the catalytic system by iodometric titration. It was found that TEMPO$^+$ consumed an equivalent amount of I^- and produced TEMPO and I_2 in a 2:1 ratio [1]. The same stoichiometric ratio was now found for the reaction between 4-AcNH-TEMPO$^+$ and I^-. In order to increase the accuracy of the quantification of 4-AcNH-TEMPO$^+$, the I_2 formed was determined by spectrophotometry utilizing the absorption of I_3^- at 288 nm.

The xylopyranose units of xylan lack the hydroxymethyl group, which decreases the reactivity of pulps with high xylan content. To make the readings comparable, the degree of oxidation of cellulose and glucomannan was calculated from their content in the samples and the amount of easily reactive hydroxymethyl groups (Table 1).

Drying in the laboratory significantly decreased the initial reaction rate of all the pulps (Table 1). In general, drying also reduced the extent of oxidation of the pulps. These were expected results as drying at elevated temperature is known to hornify pulp fibers and decrease their accessibility

[2]. Besides drying, any acidic, neutral or alkaline hydrothermal treatment at high temperature may lead to hornification of the cell wall [3].

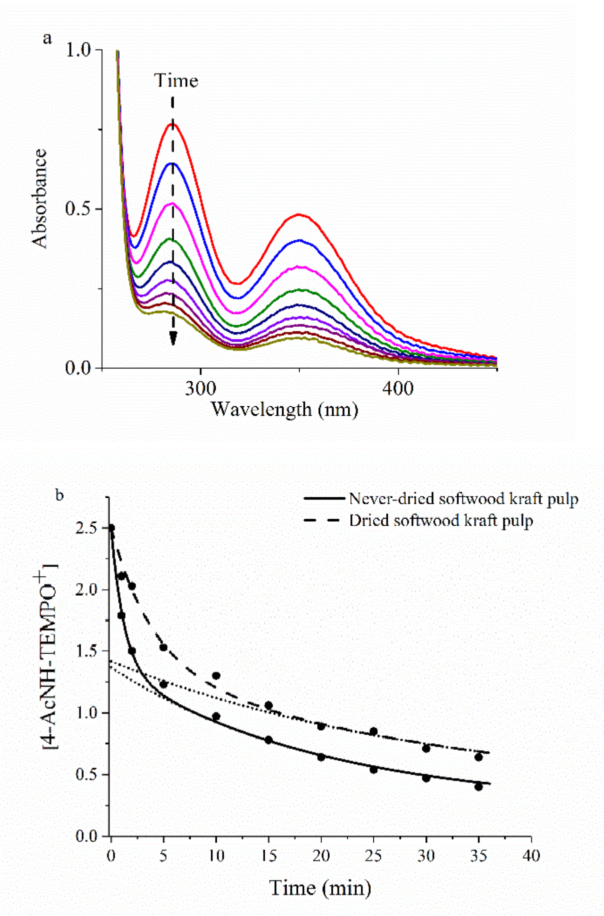

Figure 1. UV-Vis spectra for iodometric analysis of 4-AcNH-TEMPO$^+$ from its reaction mixture with never-dried softwood kraft pulp (a) and consumption of 4-AcNH-TEMPO$^+$ during oxidation of never-dried and dried softwood kraft pulp at pH 9 at room temperature (b).

REFERENCES

[1] T. Pääkkönen, C. Bertinetto, R. Pönni, G. K. Tummala, M. Nuopponen, and T. Vuorinen, 'Rate-limiting steps in bromide-free TEMPO-mediated oxidation of cellulose—Quantification of the N-Oxoammonium cation by iodometric titration and UV–vis spectroscopy', *Applied Catalysis A: General*, **505**, 532–538, (2015).

[2] M. A. Hubbe, R. A. Venditti, and O. J. Rojas, 'What happens to cellulosic fibers during papermaking and recycling? a review', *BioResources*, **2**, 739–788, (2007).

Sample	Pulp	
Raw material	Softwood	
Process	Kraft	
Cellulose (%)	81	
Xylan (%)	10	
Glucomannan (%)	9	
Drying	ND	D
WRV (ml/g)	1.53	1.09
FSP (ml/g)	1.20	0.78
SSA (m^2/g)	282	148
Reactivity (mmol/g)	0.59	0.57
Initial reaction rate (min^{-1})	0.80	0.26
Degree of oxidation	0.12	0.11

Table 1. Characteristics of the chemical pulps and their indirect and direct measures of reactivity.

This method complements the more traditional, indirect methods, such as WRV, FSP and SSA, in characterizing various pulps. Although the direct reactivity measure often correlates with WRV, FSP and SSA of cellulosic samples, that is not always the case.

[3] R. Pönni, E. Kontturi, and T. Vuorinen, 'Accessibility of cellulose: Structural changes and their reversibility in aqueous media', *Carbohydrate Polymers*, **93**, (2) 424–429, (2013).

[4] R. Pönni, T. Vuorinen, and E. Kontturi, 'Proposed nano-scale coalescence of cellulose in chemical pulp fibers during technical treatments', *BioResources*, **7** (4), 6077–6108, (2012).

Characterization of hot water extracted wood hemicelluloses by Matrix-Assisted Laser Desorption/Ionisation – Time of Flight analysis

VALENTIN GUIGON, CHRISTINE CHIRAT, DOMINIQUE LACHENAL

Univ. Grenoble-Alpes, CNRS, Grenoble INP, LGP2, F-38000 Grenoble, France
Valentin.Guigon@lgp2.grenoble-inp.fr

1 INTRODUCTION

Hemicelluloses which make up 30% of wood composition are of great interest because they are made of polysaccharides that are real platform chemicals. Those saccharides can be derived in numerous different biobased value-added products fulfilling numerous functions, some of them being equivalent to those of petrol-based products such as chemicals, biofuels and biomaterials.

Hemicelluloses as such cannot be exploited. They first need to be extracted from wood chips generally by hot water extraction. In the case where monomeric sugars are looked for, a depolymerization treatment has to be applied to convert them from polysaccharides or oligosaccharides to monosaccharides.

This paper, following a previous one [1], focuses on the degree of polymerization (DP) of polysaccharides after different steps and treatments to assess their efficiency in term of reducing the size of polysaccharides. To do so, a Matrix-Assisted Laser Desorption/Ionisation – Time of Flight (MALDI-ToF) analysis was performed.

2 MATERIALS AND METHODS

2.1 Treatments conditions

Two hot water extractions were conducted separately on two samples from the same hardwood chips mixture using multi-reactor ERTAM. Temperature, temperature rise time, temperature plateau time, temperature decrease time were programmed thanks to a software at respectively 170°C, 30’, 65’ and 30’for the first hot water extraction (HWE1) and 170°C, 30’, 120’, 30’ for HWE2. Liquor/wood ratios were respectively 6.7 and 3.

A depolymerization treatment was also carried following HWE2 on the obtained hydrolysate. Its conditions are not discussed in this paper.

2.2 MALDI-ToF and Electrospray principles

The mass spectroscopy MALDI-ToF consists of several steps.

First, the sample is mixed with a matrix consisting of an organic solvent which is added in large amounts then crystalize, entrapping the sample. Then, the mix is ionized thanks to a laser beam. Ions that are thus released are accelerated by an electrostatic field toward the time of flight analyzer. The analyzer converts the time of flight to a mass/charge (m/z) ratio, the lighter ions having the shortest time of flight. The molecular weight can finally be calculated.

For hardwood hemicelluloses, the molecular weight is shared between several components: pentoses that are xylose or arabinose units [2, 3, 4, 5], acetyl units, 4-O-methylglucuronic acid units and hexoses (glucomannans).

3 RESULTS AND DISCUSSION

3.1 First Hot Water Extraction (170°C, 65 min)

Oligosaccharides extracted during HWE1 have low DP: 10 for xylans 11 for hexans (m/z=1677 for xylans and 1823 for hexans, Figure 1.). Those xylans contain one or two 4-O-metylglucuronic acid units and are strongly acetylated as shown by their degrees of acetylation (DA) which are contained between 0.2 and 0.7 (up to seven acetyl units for ten xylose units). Those

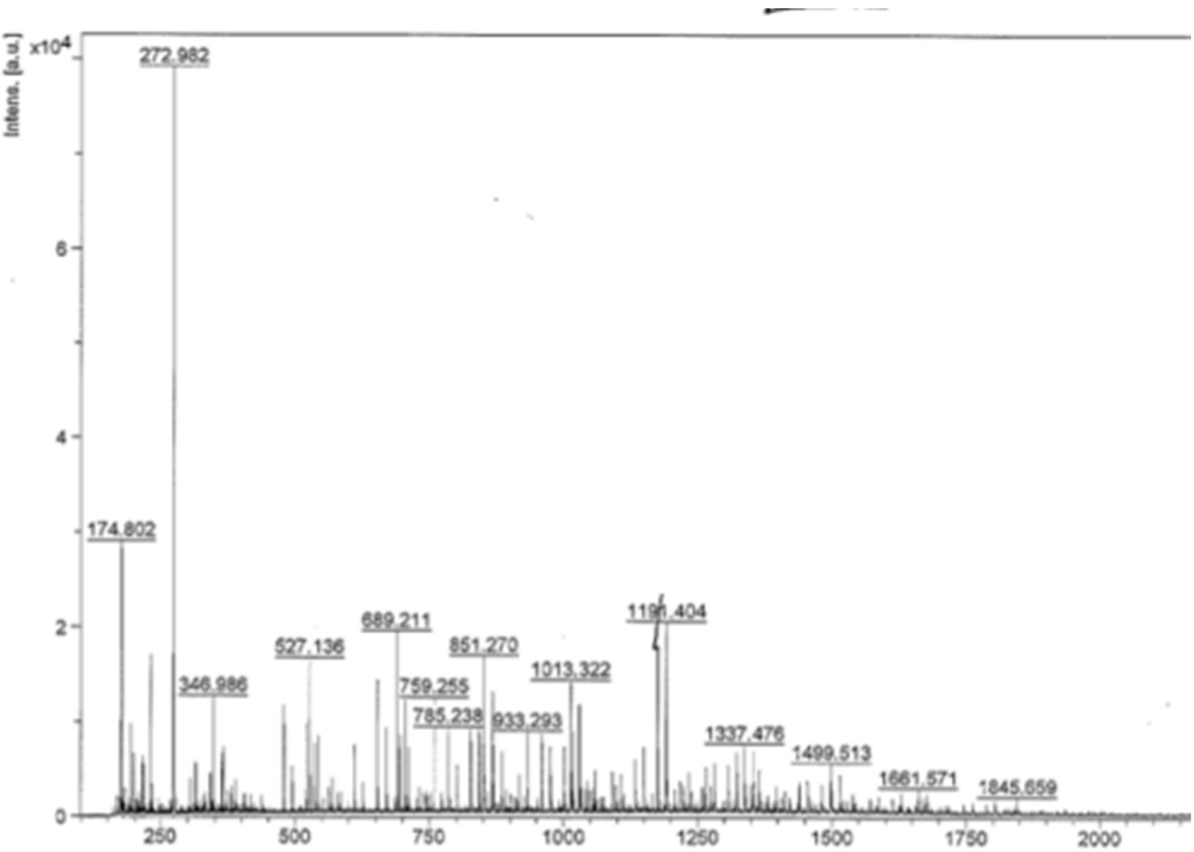

Figure 1. MALDI-ToF spectrum for HWE1

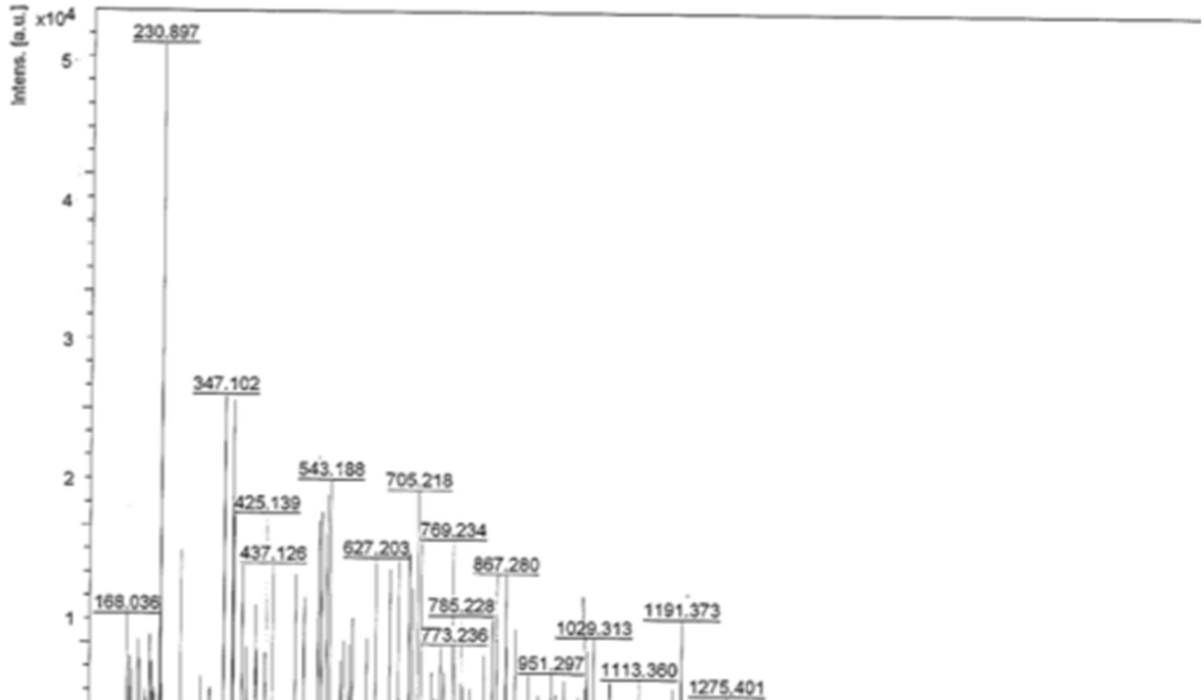

Figure 2. MALDI-ToF specter for HWE2

values are true to literature [4, 6, 7, 8, 9, 10]. Hexans can also be acetylated: most of them have a three or less acetyl units, corresponding to the values found in the literature [11, 12, 13].

3.2 Second Hot Water Extraction (170°C, 2 hours) followed by depolymerization treatment

The second HWE is harsher than HWE1 so oligosaccharides extracted during HWE2 should have a lower DP. This can be seen on Figure 2 where peaks are more predominant in the low m/z domain. Xylans and hexans have a DP of 8 at most whereas it was respectively 10 and 11 after HWE1. The number of acetyl units decreased as well with at most respectively 5 and 2 acetyl units for xylans and hexans compared to 7 and 3 after HWE1. The number of 4-O-methylglucuronic acid units on xylans remained equal. Thus, it can be assumed that HWE2 which is harsher than HWE1 released more acetyl units in the form of acetic acid in the sample.

A depolymerization treatment was applied after HWE2. As it can be seen on Figure 3, peaks in the highest DP domain disappeared and the intensity of peaks generally decreased as well (ca. $1.6.10^4$ a.u.
for the highest peak VS ca $2.0.10^4$ for the majority of HWE2 peaks). The m/z values of the peaks reveal that pure xylans have now a maximum DP equal to 4 VS 7 prior to the depolymerization treatment. Branched xylans have a DP up to eight with one or two 4-O-methylglucuronic acid units as it was before the treatment but they have now at most four acetyl units compared to five previously. Hexans have a maximal DP of 6 as well with the same number of acetyl units (two).

Thus, it can be assumed that both HWE2 and the depolymerization treatment contributed to globally lower the DP of solubilized hemicelluloses.

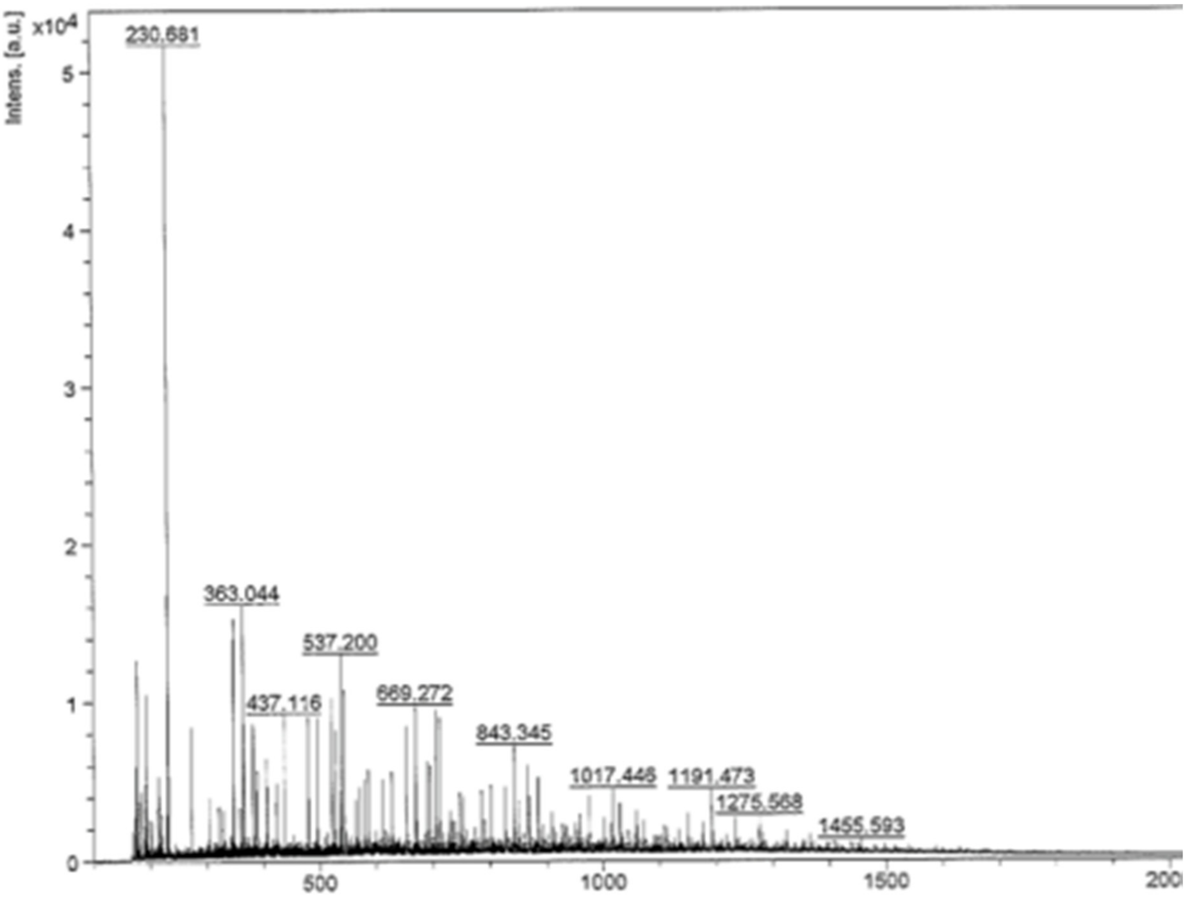

Figure 3. MALDI-ToF specter for HWE2 followed by a depolymerization treatment

4 CONCLUSIONS

Hydrolysates obtained after three treatments (Hot Water Extraction 170°C-1h, HWE 170°C-2h, depolymerization treatments) were analyzed by mass spectroscopy MADLI-ToF. On the whole oligosaccharides solubilized during HWE2 have a lower degree of polymerization than those solubilized during HWE1, which is normal given the fact that conditions were more severe in HWE2. Furthermore, a new depolymerization process was proved to be successful: oligosaccharides were smaller after this treatment. Further analyses such as molar mass distribution need to be carried in order to gain knowledge of remaining oligosaccharides.

REFERENCES

[1] V. Guigon. Depolymerization of oligomers from wood hemicelluloses. European Doctoral Students Summer Conference 2016, Stockholm, 61-64, (2016)

[2] A. Jacobs, P.T. Larson., O. Dahlman. Distribution of uronic acids in xylans from various species of soft- and hardwood as determined by MALDI mass spectrometry. *Biomacromolecules* **2**(3):979-990 (2001).

[3] M. Kabel, H. Schols, G.J. Voragen. Complex xylo-oligosaccharides identified from hydrothermally tearted eucalyptus wood and brewery's spent grain. *Carbohydrate Polymers* **50**(2):191-200 (2002).

[4] A. Teleman, M. Tenkanen, A. Jacobs, O. Dahlman. Characterization of o-acetyl-(4-o-methylglucurono)xylan isolated from birch and beech. *Carbohydrate Research* 336:373-377 (2002).

[5] A. Jacobs, O. Dahlman. Characterization of the Molar Masses of Hemicelluloses from Wood and Pulps Employing Size Exclusion Chromatography and Matrix-Assisted Laser Desorption Ionization Time-of-Flight Mass Spectrometry. *Biomacromolecules* **2**(2): 894-905 (2001).

[6] M. Sanglard. Production simultanée de fibres cellulosiques blanchies et polyxylosides d'alkyle dans le cadre d'une bioraffinerie papetière (In French). PhD thesis, Grenoble University (2013).

[7] A. Jacobs, J. Lundqvist et al. Characterization of water-soluble hemicelluloses from spruce and aspen employing sec/maldi mass spectroscopy. *Carbohydrate Research* **337**(8):711-717 (2002).

[8] A. Reis, P. Pinto, D. V. Evtugin et al. Electrospray tandem mass spectrometry of underivatised acetylated xylo-oligosaccharides. *Rapid Communications in Mass Spectroscopy* **19**(23):3589-3599 (2005).

[9] B. Quéméner, J. J. Ordan Ortiz, L. Saulnier. Structural characterization of underivatized arabino-xylo-oligosaccharides by negative-ion electrospray mass spectrometry Quéméner. *Carbohydrate Research* **341**(11):1834-1847 (2006).

[10] A. Reis, M. A. Coimbra. Fragmentation pattern of underivatised xylo-oligosaccharides and their alditol derivatives by electrospray tandem mass spectrometry

[11] A. Teleman, M. Nordström, M. Tenkanen, A. Jacobs, O Dahlman. Isolation and characterization of O-acetylated glucomannans from aspen and birch wood. *Carbohydrate Research* **338**(6):525-534 (2003).

[12] X. Xing, S. W. Cui, S. Nie et al. Study on Dendrobium officinale O-acetyl-glucomannan (Dendronan®): Part II. Fine structures of O-acetylated residues. *Carbohydrate Polymers* **117**:422-433 (2015)

[13] O. Dahlman, A. Jacbos, M. Nordström. Characterization of Hemicelluloses from Wood Employing Matrix-Assisted Laser Desorption/Ionization Time-of-Flight Mass Spectrometry. *Hemicelluloses: Science and Technology* **6**:80-93

ACKNOWLEDGEMENTS

The authors would like to thank the FUI BIO3 project for the funding of this PhD thesis work.

Comparative study of CO_2 and CH_4 pressure dependence in the HPP NDIR platform.

B.GAYNULLIN, C.HUMMELGÅRD, C.MATTSSON, H.RÖDJEGÅRD and G.THUNGSTRÖM

bakhram.gaynullin@senseair.com
christine.hummelgard@senseair.com
claes.mattsson@miun.se
henrik.rodjegard@senseair.com
goran.thungstrom@miun.se

1 INTRODUCTION

HPP (High Performance Platform) is the latest family of high sensitive gas concentration sensors from SenseAir AB - **Figure 1**. It is a non-dispersive infra-red (NDIR) sensor with optical path length of 96 cm [1]. The optical path consists of 16 passes in a 6 cm long White cell [2]. Hence, high resolution is obtained in a small and compact cuvette with a total internal volume of 35 cm^3. The optics, including the reflective lenses, is fabricated using plastic moulding with integrated thermal stabilization for low production cost and high performance.

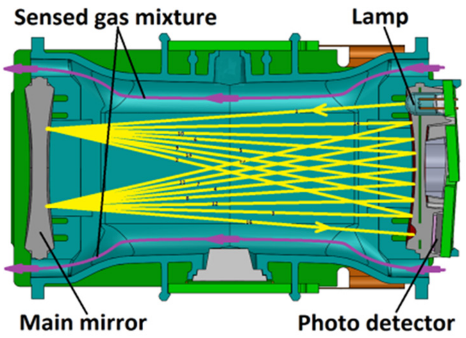

Figure 1. HPP optical design

The current research was performed on HPP sensors equipped with optical filters for measuring concentration of methane (CH_4, 3.5 µm wavelength) and carbon dioxide (CO_2, 4.3 µm wavelength). There is significant demand in high accurate measurements of these gases in environmental research, detailed air quality monitoring, vertical atmosphere concentration profiling, leakage detection, and etc.

Detailed studies of pressure dependence of measured concentration values allow for development of compensation methods improving accuracy of obtained results to ppm and sub-ppm level.

2 MATERIALS AND METHODS

The non-dispersive infra-red (NDIR) gas sensors employ Lambert-Beer's law transforming transmittance τ into mixing ratio q_{true} [3]. Transmittance τ is the ratio of received to incident light intensity, which decreases exponentially with distance travelled through a uniform absorber:

$$\tau = \frac{I}{I_0} = e^{-k_\vartheta x} \qquad (1)$$

Here k_ϑ is the absorption coefficient and x is the path length. For an ideal gas at pressure P, temperature T and volume mixing ratio q_{true}, the absorption coefficient can be written as:

$$k_\vartheta = \frac{q_{true} P}{kT} \cdot \sigma_\vartheta \qquad (2)$$

where k is the Boltzmann constant. All spectral dependence is contained in the absorption cross section, σ_ϑ (area per molecule). Mixing ratio q_{true} corresponds to volumetric, or fractional, concentration expressed in ppm (part per million):

$$q_{true} = \frac{kT}{P} \times \frac{1}{x\sigma_\vartheta} \times \ln\left(\frac{I_0}{I}\right) \qquad (3)$$

Equation (3) clearly presents dependence between mixing ratio q_{true}, gas pressure and transmittance.

Technically, the measurement algorithm implemented in NDIR sensors operates only with transmittance without any reference to gas pressure.

Any NDIR sensor can be presented by its transformation function F_{sensor} of transmittance into measured concentration:

$$M_{Conc} = F_{sensor}\left(\frac{I_0}{I}\right) \quad (4)$$

M_{Conc} is measured concentration value.

Unfortunately the visible dependence in equation (3) cannot be used as a theoretical model for accurate pressure compensation of measured concentration value because there are more factors introducing unpredictable non-linear dependence [4].

For simple compensation calculation some brief information can be found in manuals and application notes from NDIR sensor manufactures in [5, 6]. Unfortunately the proposed approaches do not provide highly accurate compensation in a wide range of measured concentrations as well as for a wide range of pressure conditions. More detailed investigations done by Tomomi Yasuda, Seiichiro Yonemura and Akira Tani [7] was performed only on concentration common for HVAC system (1100 ppm) in very narrow barometric pressure range – around 1 Bar. There only test results of sensor performance are presented without any recommendations about compensation approach.

2.1 Initial data collection

Data collection is performed using a pressure characterization lab test system [4].

Concentration data was collected using reference gases with concentrations 100, 800 ppm CO_2 and 50, 250 ppm CH_4 in a pressure range between 0.5 and 1.2 Bar in steps of 0.1 Bar.

Respective dependencies of measured concentration **M_{Conc}** vs relative pressure deviation from standard value are presented in **Figures 2-5:**

2.2 Data processing

According to the ideal gas law [8] pressure dependence could be described as:

$$M_{Conc} = T_{Conc}\left(1 + \frac{P - P_0}{P_0}\right) \quad (5)$$

T_{Conc} is the true concentration measured under normal pressure conditions, 1.013 Bar. **M_{Conc}** is the concertation measured under variable pressure. Equation (5) implies a linear relation between measured concentration and relative pressure deviation. Data presented in Figures 2-5 show a non-linearity in the obtained results.

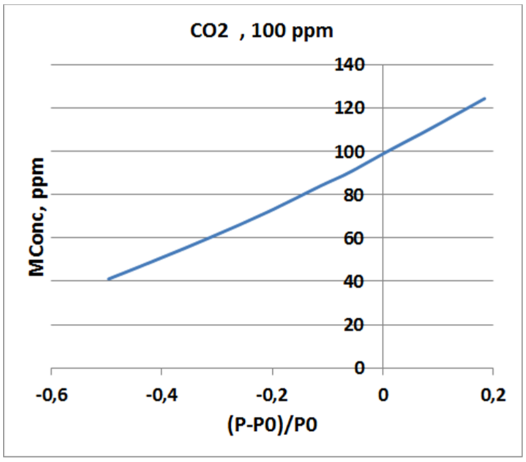

Figure 2. CO_2 reference concentration 100

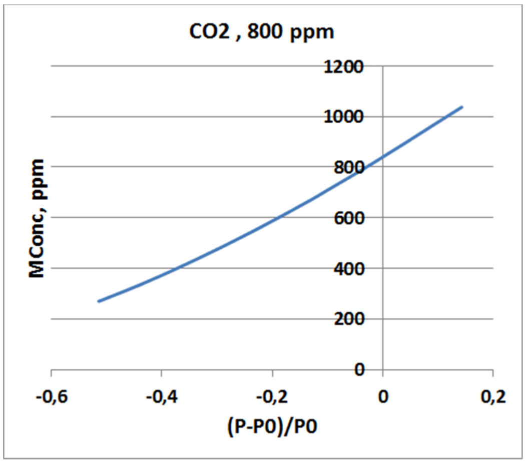

Figure 3. CO_2 reference concentration 800

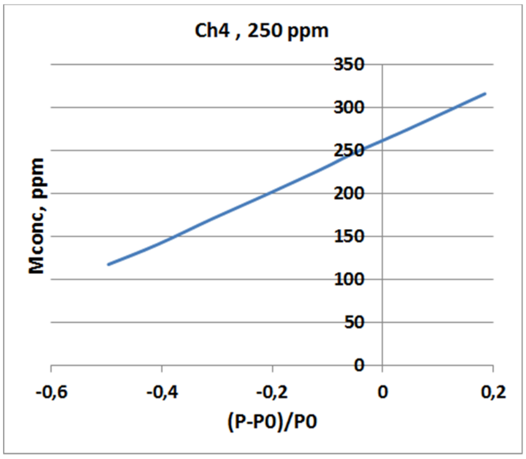

Figure 4. CH_4 reference concentration 250

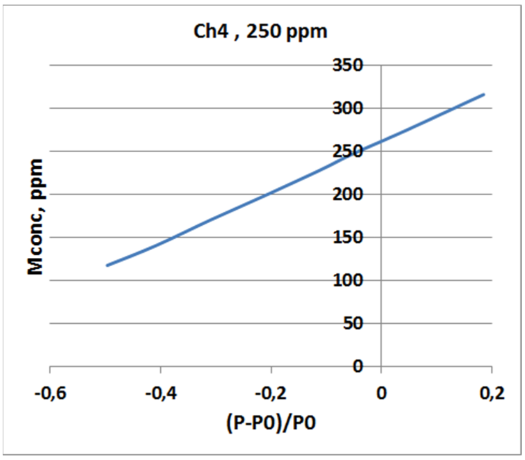

Figure 5. CH_4 reference concentration 250

For a detailed investigation the data is transformed into the following form:

$$\frac{M_{Conc}}{T_{Conc}} = A + B\left(\frac{P-P_0}{P_0}\right) + C\left(\frac{P-P_0}{P_0}\right)^2 + D\left(\frac{P-P_0}{P_0}\right)^3 \quad (6)$$

A, B, C, D are polynomial coefficients derived from test data.

3 DISCUSSION

Investigation results presented in **Figures 6-7** demonstrate a significant deviation from theoretical dependence introduced by the ideal gas law.

The deviation from the theoretical model could be explained by several reasons:

- The interference filter for the specific optical spectrum selection. Significant variations of the filter performance introduce difficulties when modelling its transmission characteristic.
- A multi-reflection optical path, presented in modern compact sensors, where mirrors forward the light beam to the filter surface within a wide range of angles that make the spectral characteristic more unpredictable.
- Complex absorption spectrum matching numerous molecular vibration modes. This is especially true for CO_2 with different saturation rate of each spectral line and nonlinear dependence of pressure, temperature and concentration. This makes the entire system difficult to model in a practical scenario.

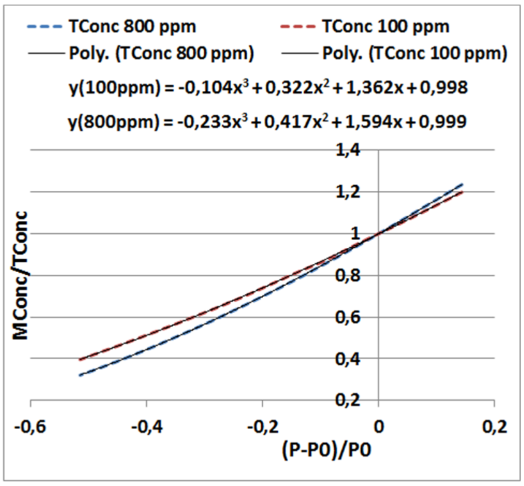

Figure 6. Normalized pressure dependence for CO_2

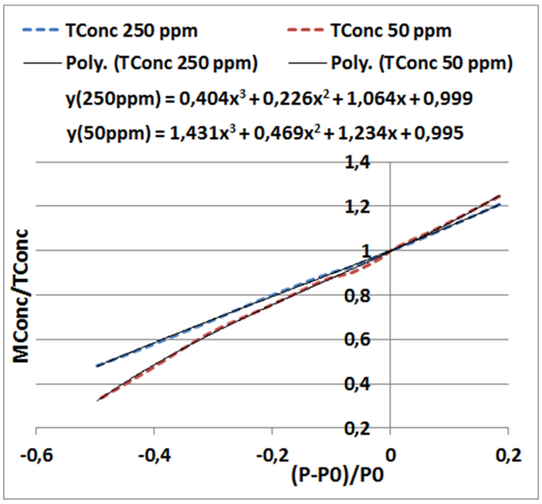

Figure 7. Normalized pressure dependence for CH_4

•Other, - design and sensor part features introducing additional unknown disturbance factors that needs to be taken in account.

4 RESULTS AND CONCLUSION

Study of the pressure dependence for the measured concentrations of CO_2 and CH_4 has shown that a direct implementation of a compensation model based on the ideal gas law cannot be used for an accurate measurement system such as the HPP platform. One effective solution could be an empirical approach based on preliminary collected data from the sensors in a well-controlled environment with variable pressure, reference gases and stable temperature. In this case using equation (5) transformed for derivation of compensation factor:

$$K = \frac{M_{Conc}}{T_{Conc}} = A + B\left(\frac{P - P_0}{P_0}\right) + C\left(\frac{P - P_0}{P_0}\right)^2 + D\left(\frac{P - P_0}{P_0}\right)^3 \quad (6)$$

Polynomial coefficients **A** (commonly equal to 1), **B, C, D** derived based on preliminary collected and processed data are stored in the sensor memory. The HPP sensor's firmware calculate compensation factor using the polynomial coefficients and current pressure value from an on-board pressure sensor.

The obtained normalized concentration is equal to true value with some tolerance:

$$N_{Conc} = \frac{M_{Conc}}{K} \approx T_{Conc} \quad (6)$$

Derivation of the polynomial coefficients could be performed during pressure calibration.

Depending on specific design and accuracy requirements calibration could be design linked (performed once for specific sensor type), batch linked (performed for batch of sensors) or for special high accurate applications could be performed individually for each specific sensor.

5 REFERENCES

[1] C. Hummelgård et al. Low-Cost NDIR based Sensor Platform for sub-ppm Gas Detection Urban Climate 14 (2015) 342-350

[2] 4. White, J., 1942. Long optical paths of large aperture. J. Opt. Soc. Amer. 32, 285–288

[3] http://www.spectralcalc.com/info/CalculatingSpectra.pdf

[4] Bakhram Gaynullin, Christine Hummelgård, Henrik Rödjegård, Maksym Bryzgalov. "A practical solution for accurate studies of NDIR gas sensor pressure dependence.", submitted to IEEE SENSORS 2016, Orlando, Florida USA

[5] http://www.senseair.com/wp-content/uploads/2012/06/PSP107.pdf

[6] http://www.vaisala.com/Vaisala%20Documents/Application%20notes/CEN-TIA-Parameter-How-to-measure-CO2-Application-note-B211228EN-A.pdf

[7] Tomomi Yasuda, Seiichiro Yonemura and Akira Tani "Comparison of the Characteristics of Small Commercial NDIR CO2 Sensor Models and Development of a Portable CO2 Measurement Device", Sensors 2012, 12, 3641- 3655;

[8] Michael J. Moran, Howard N Shapiro. Fundamentals of engineering thermodynamics. Chichester : Wiley, edition 3 (1998)

Quantitative analysis of wavy flatness deviations using an optical surface measuring device

GERRIT ROOSEN[A], TIEMO ARNDT[A]
and FRANK MILETZKY[A, B]

A) Papiertechnische Stiftung,
Pirnaerstr. 37, 01809 Heidenau, Germany
gerrit.roosen@ptspaper.de
B) Technische Universität Dresden,
Marschnerstraße 39, 01307 Dresden-Johannstadt, Germany

1 INTRODUCTION

Flatness defects are a phenomenon every papermaker is dealing with. These undesired effects occur when the surface of a paper web deviates from a mathematically flat area; their appearance can vary greatly. [1] The most frequently mentioned flatness defects are curl, cockling and wavy structures (e.g., fluting). Because all of them can lead to broke and problems during further processing by the customer it is necessary to provide a method to quantify their dimensions and appearance. This will provide new starting points for identifying the origins of these out-of-plane deformations. In the present paper we will discuss different approaches to quantify and classify wavy flatness deviations.

The defect is described as the occurrence of several waves with wavelengths in the range between 10–30 mm. [2,3] The waves (compare Figure 1) are aligned in machine direction (MD), without running obliquely, rather stationary and can be interrupted provided that they converge again in a straight line later on. The wavelength is nearly constant, whereas the peak to valley values may vary. [4] Compared to fluting, which can occur in heatset web offset printing, this specific defect can be found directly at the pope reel winder. [5]

The possible causes of these wavy structures have been discussed in very few papers. One of them is the so-called "fibre orientation streaks" (FOS). [6] The streaks show areas where fibres have a higher degree of orientation in MD compared to the adjacent areas. Wavy structures can be formed during drying since the shrinkage behaviour of fibres is different in longitudinal- and cross directions. [7,8]

(a) Under oblique illumination

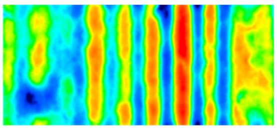

(b) Corresponding topographical image

Figure 1. Visual appearance of wavy structures. Size of images a) and b): 200 mm x 100 mm [4]

These fibre orientation streaks can result from coherent structures forming under turbulent flow conditions in the headbox. [9] Depending on the former type of the wet end, the streaks can appear only on the wire side in case of hybrid formers or on both sides if gap formers are used. [6] Another work suggests that the fibre orientation defect correlates with the wavy structure phenomenon. Along the wave, a streak with higher fibre orientation and two-sidedness was noticed, resulting in a higher restraint potential. [10] Besides FOS, there can also be basis weight- and moisture streaks. [2,3,6]

Moreover, descriptions of load- and moisture induced waviness can be found in literature. The theory behind tension-induced waviness is based on the Poisson effect. The effect describes the phenomenon that a material which is stretched in one principal direction shrinks in the direction perpendicular to the principal direction. If shrinkage is restricted, as in case of a paper web constrained by rollers, the material buckles out of plane. Waves can appear on the paper web, and the wavelength of the surface structure decreases with increasing web tension, whereas the tension has no significant effect on the height of the waves. [11,12]

In order to investigate the appearance of such out-of-plane deformations, it is necessary to quantify them. The resulting data can be used for correlation analyses of e.g. grammage, thickness, fibre orientation or QCS data collected in the manufacturing process.

2 EXPERIMENTAL PROCEDURE

2.1 Topographical Device

A suitable topographical method was needed to evaluate the dimensions of wavy structures. Devices used to investigate the topography of an object can be classified into three groups based on signal generation (compare Figure 2). To ensure that the results are not distorted by mechanical compression, an optical method must be chosen here.

A comparison of three different optical measurement systems has been made in a previous publication. Regarding the maximum sampling size, the spatial resolution, measuring time and mobility, the Macroscope VR-3200 (Keyence GmbH, Neu-Isenburg, Germany) was found to be the most suitable device for analysing the wavy structures described above. [4]

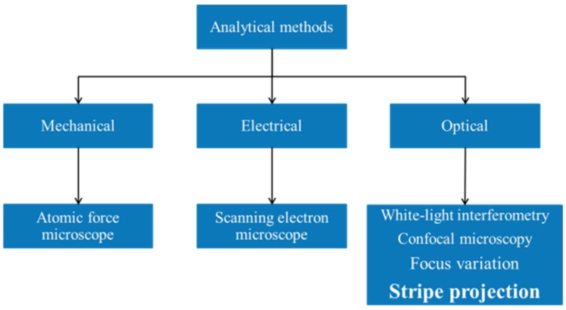

Figure 2. Overview of different topographical measurement systems

Figure 3 illustrates the function of the VR-3200 equipment. Bands of light are projected onto the surface of the object being measured. When the reflected light is observed from another angle at the receiver lens, height differences on the object make the bands of light appear distorted. An image of these distortions is taken using a CMOS sensor, and triangulation calculations are performed to determine the height and position at each point. [13] Due to an implemented stitching function, a maximum sampling size of 200 mm x 100 mm can be analysed, which makes the VR-3200 a suitable device.

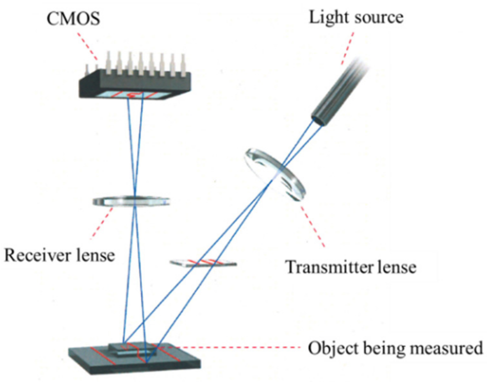

Figure 3. VR-3200 measurement principle [13]

2.2 Paper Samples

Several different grades of conventionally manufactured base and finished papers were used as test samples. The grammage was in a range of 30 g/m^2 to 300 g/m^2. All trials were executed under standard atmosphere. In order to reduce undesired large scale effects like curl, the topography images were bandpass filtered (compare Figure 4).

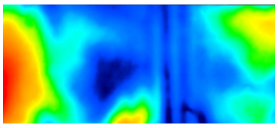

(a) Unfiltered

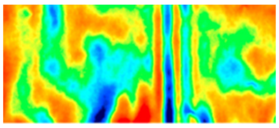

(b) Filtered

Figure 4. Topographical image of a paper sample. Size of images a) and b): 200 mm x 100 mm

3 RESULTS AND DISCUSSION

Generally speaking, there are several different ways to characterise a surface profile, where R_a (arithmetic mean deviation) and R_q (root mean square deviation) are the most common parameters. (ISO 4287-1997) The amplitude, wavelength, number and orientation of waves are the most critical ones for describing wavy flatness deviations. In this chapter we will discuss a method to automatically differentiate between defective and faultless samples (compare Figure 5, (a) and (d)) in order to analyse the dimensions of waves and simultaneously classify them in a non-subjective way.

3.1 Wavelength Quantification

There are several possibilities for quantifying the wavelength of paper samples. One is to use the software provided for the Macroscope. It makes it possible to analyse profiles on a single line or averaged over the entire measuring area. A huge disadvantage of the technique is its subjective component caused by the fact that the user can choose the points for profile analysis.

In order to quantify the wavelength of the samples in an objective, fast and automatic way, the mean value of each raw data column is calculated. The resulting mean profile is subjected to a fast Fourier transform (FFT), a well-known detection method for periodical phenomena. The results can be seen in Figure 5 (b) and (e). The graph of the defective sample has a characteristic peak, which provides information about the most prominent wavelength. This wavelength can be accurately calculated by means of the width of one single pixel, which correlates very well with the manually measured values. The problem of using FFT for this specific case lies in the fact that even visually faultless paper samples have a characteristic wavelength. In case of sample (a) it is 25.75 mm, which is in the typical wavelength range of defective samples (between 10 mm and 30 mm). For classifying this defect, an FFT analysis alone is thus not sufficient. A combination of several approaches is needed.

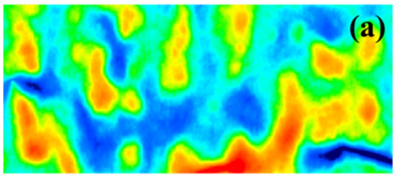

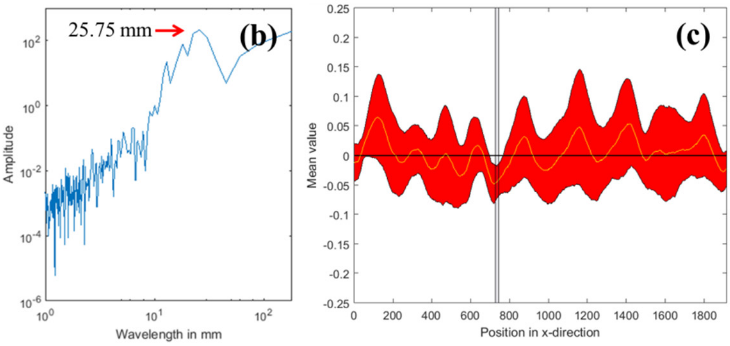

(a) Faultless sample (filtered)
(b) Result of FFT analysis
(c) Result of equation (1), n = 1.8

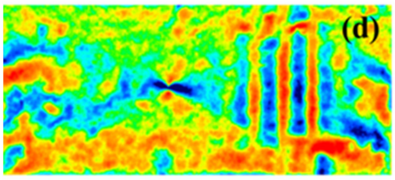

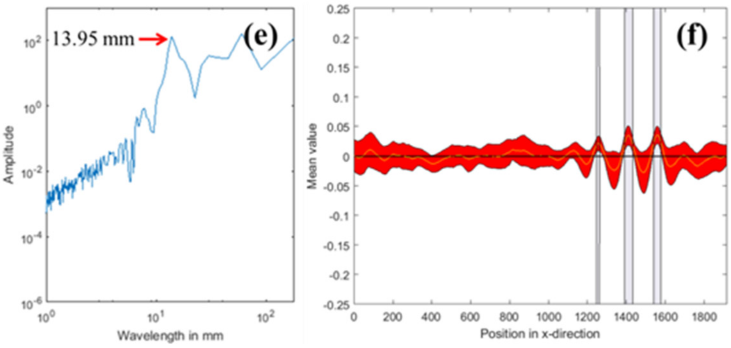

(d) Defective sample (filtered)
(e) Result of FFT analysis
(f) Result of equation (1), n = 1.8

Figure 5. Analytical results of defective and faultless samples in comparison. Size of images a) and d): 200 mm x 100 mm

3.2 Number of Waves

As mentioned before the number of waves present in a sample is another important characteristic of the defect. One possibility for visualizing the areas of interest uses the mean profile and standard deviation. The results can be seen in Figure 5 (c) and (f), where the yellow line represents the mean profile and red the mean profile plus and minus the standard deviation. It can be stated that the mean profile and standard deviation of areas with explicit wavy structures that are stationary in cross direction vary significantly from the base line (black vertical line). These areas of distinct wavy structures can be visualised by means of the equation

$$|\, xmean_i \,| > n * \sigma_{xmean_i} \qquad (1)$$

in which

$xmean_i$ - mean of each column
n - variable factor
σ_{xmean_i} - standard deviation of each column.

It is now possible to automatically count the number of bars representing the waves, ignoring all standalone bars (compare Figure 5 (c)).

3.3 Template Matching Algorithm

The aforementioned analytical methods fail to provide objective results as to whether a paper sample is defective or not. Therefore a novel evaluation algorithm was programmed. The basic idea was applying a 2-dimensional cross-correlation to the topographical images. Pre-selected

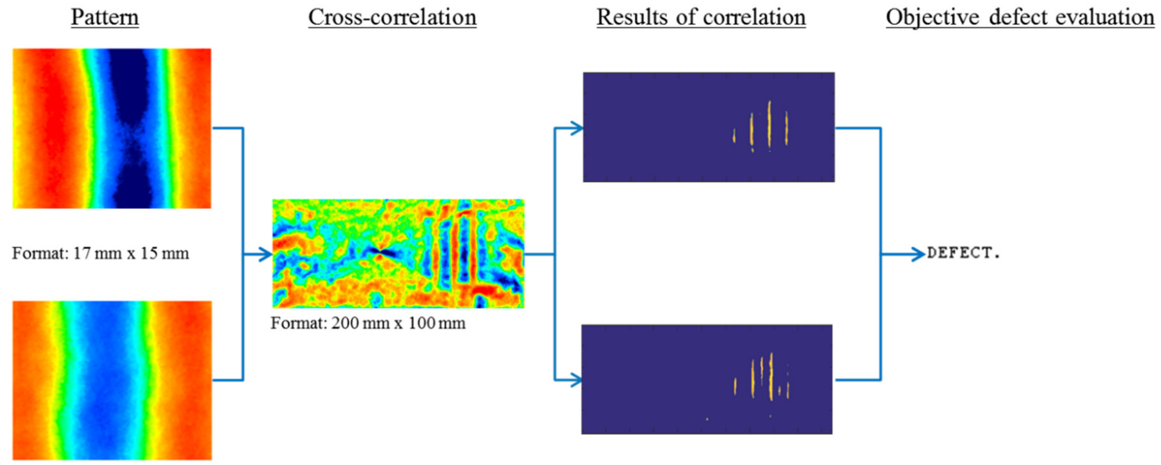

(a) Defective sample

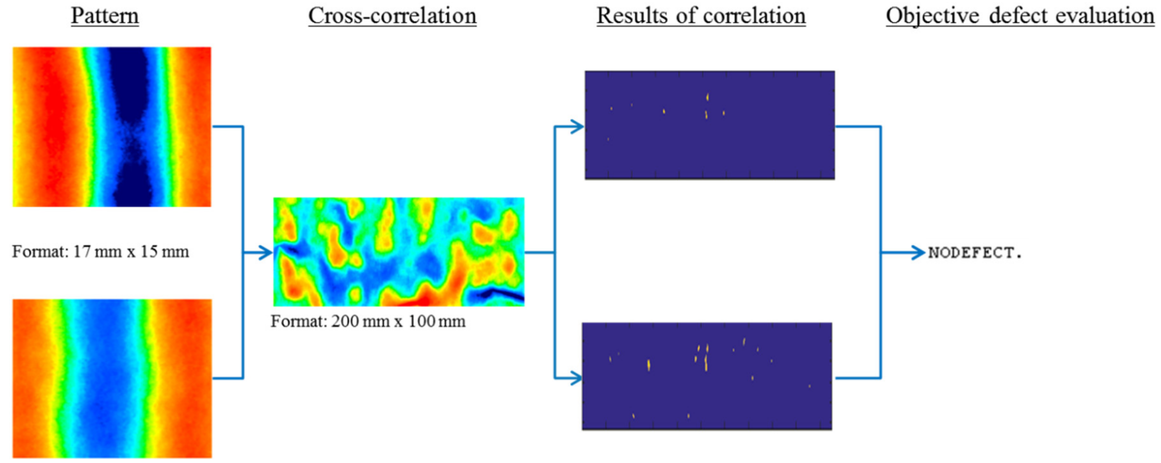

(b) Faultless sample

Figure 6. Results of the template matching algorithm

patterns (compare Figure 6) with characteristic structures of wavy flatness deviations were compared with the original sample whose pattern size is significantly smaller. The number of patterns used can vary, which has a direct effect on the evaluation time.

The programmed algorithm works as follows:

1. Loading the topographical image of the analysed sample, trim it to a certain size by cutting off the edges and convert it into an 8-bit grayscale.
2. For cross-correlation, the predefined patterns are used to compare how their signals resemble the ones of the original image.
3. The pattern image is moved by one pixel.
4. Steps 2 and 3 are repeated until the whole image has been scanned.
5. The areas where each pattern fits most are visualized and transferred to a single parameter.
6. The calculated value will then be transferred and shown as output: Defect or no defect.

The algorithm makes it possible to gather information about the presence of wavy flatness deviations in the sample in a non-subjective way.

4 CONCLUSIONS AND OUTLOOK

A new method was developed to quantify and classify all kinds of out-of-plane deformations. The focus of this paper was on wavy flatness deviations. The template matching algorithm allows the user to differentiate between faultless and defective paper samples in an objective way. FFT analysis and equation (1) can be used to gather information about the dimension of waves. This leads to new starting points for clarifying the root causes of the problem. Since the exact wave positions and dimensions are known, each pixel can be assigned to the results of different analytical methods. Highly resolved measurements like fibre orientation, thickness and grammage analyses can be used to perform correlation analyses. In addition, profiles can be obtained over the entire width of a paper machine and compared with different types of process data.

Further investigations will focus on the question how to differentiate this defect from similarly looking ones, since wavy structures can come in a huge variety of forms. It is planned to use machine learning as a method of data analysis. One of the questions yet to be addressed is how to extract so-called features for areas of interest in an image. These features can then be used to train a machine learning algorithm for the evaluation of classifier models.

5 ACKNOWLEDGEMENT

We gratefully acknowledge the financial support of the German Federal Ministry of Economics and Technology BMWi for research project MF 160068. We would also like to thank the involved companies for supporting the project.

REFERENCES

[1] H. Geenen. Über die Behebung von Planlagestörungen bei ungestrichenen Papieren. *Wochenblatt für Papierfabrikation* **114**(3): 69–70 (1986).

[2] M. A. Mac Gregor. Some impacts of paper making on paper structure. *Paper Technology* **42**:33–44 (2001).

[3] T. Waech and D. Sze. Paper waviness and fiber alignment streaks in paper forming. CPPA Annual Technical Meeting, Montreal, (1997).

[4] G. Roosen. Investigations of the influence of the head box on wavy structures. Diploma thesis, Technical University of Dresden (2015).

[5] A. Kulachenko. Mechanics of Paper Webs in Printing Press Applications. PhD thesis, Royal Institute of Technology, Stockholm (2006).

[6] A. Kiviranta and P. Pakarinen. A new insight into fiber orientation streaks.

Tappi Papermakers Conference, Atlanta, Tappi Press (2001).

[7] D. Page and P. Tydeman. A new theory of the shrinkage, structure and properties of paper. Technical Section of the British Paper and Board Makers' Association, London, 397–413, (1962).

[8] T. Uesaka. General formula for hygroexpansion of paper. *Journal of Materials Science* **29**(9):2373–2377 (1994).

[9] M. Wilczek. Kohärente Strukturen in turbulenten Strömungen. Diploma thesis, Westfälische Wilhelms-Universität Münster (2007).

[10] U. Hirn, W. Bauer and M. Wiltsche. Lokale Faserorientierung und ihr Einfluss auf kleinflächige Planlagestörungen. 16. PTS-Symposium Chemische Technologie der Papierherstellung, Munich, 37.1–37.14, (2004).

[11] C. Land. Effect of web tension on load- and moisture-induced waviness. *Nordic Pulp and Paper Research Journal* **20**(2):237–241 (2005).

[12] C. Land. Laboratory method for studies of moisture-induces waviness. Licentiate thesis, Karlstad University (2004).

[13] Keyence GmbH. Instant 3D Measurement. VR-3200 Brochure (2004).

Water purification using nonleaching and bacteria adsorbing cellulosic fibers

ANNA OTTENHALL, JOSEFIN
ILLERGÅRD and MONICA EK

Department of Fibre and Polymer
Technology, School of Chemical Science
and Engineering, KTH Royal Institute of
Technology, Teknikringen 56, SE-100 44
aott@kth.se

1 INTRODUCTION

Drinking water contaminated by fecal bacteria can cause lethal diseases and it is known to globally be the second most common cause of death among children under five years of age. [1] Portable purification systems, often referred to as poin-of-use (POU) techniques, are easy ways to obtain clean drinking water when there is no large-scale water treatment available.

In this study [2], the potential to purify water using bacteria adsorbing cellulosic fibers and papers, functionalized with polyelectrolytes, according to the Layer-by-Layer method, is investigated. The adsorbed polyelectrolytes create a positive charge on the fiber surface that physically attracts and bonds with bacteria. [3]

Different types of cellulosic materials have been modified and tested for the bacterial removal capacity in water. The modified materials have been evaluated both by adsorption of bacteria in water as well as through cross flow filtration.

Freely dispersed bacteria adsorbing cellulosic fibers can remove greater than 99.9 % of *Escherichia coli* from non-turbid water, with the most notable reduction occurring within the first hour. A filtering approach using modified cellulosic fibers is desirable for purification of natural water samples. An initial filtration test showed that polyelectrolyte multilayer modified cellulosic fibers can remove greater than 99 % of bacteria from natural water. The bacteria adsorbing cellulosic fibers do not leach any biocides, and it is an environmentally sustainable and cheap option for disposable water purification devices.

2. EXPERIMENTAL

2.1 Bacterial reduction

The bacterial removal capacities of the modified materials were tested with *E. coli* as a model organism. Filter paper from Safe Water Book (SWB), containing silver as antibacterial agent, was used as a commercial reference. [4] The bacterial reduction capacity was evaluated by incubating 0.1 g of material with 10 ml of bacterial suspension, 10^6 CFU/mL, during 4 hours. The amount of bacteria remaining in the water was evaluated by cultivation on Petrifilm.

2.2 Time dependence

The time dependence was evaluated by cultivating samples of bacterial suspension incubated with material after different periods of time, from 1 to 4 hours. The amount of remaining bacteria in the water was determined through cultivation.

2.3 Filtration with natural water sample

Water from Nybroviken, Stockholm, was used as a natural water sample during a cross flow filtration evaluation. The water sample had an initial bacterial concentration of approx. 130 CFU/mL.

3. RESULT & DISCUSSION

3.1 Bacterial reduction

All materials were compared with non-modified reference material, which showed no bacterial reduction. The bacterial reduction test showed that more than 99.9 % of the initial bacteria are removed after 4 hours of incubation with the polyelectrolyte modified materials (Figure 1).

The highest bacterial removal capacity, which was 99.98 % of the initial bacteria after 4 hours, was noted for the cellulose fibers in dH_2O and TEMPO cellulose in ¼-Ringer’s solution. The commercial reference reduced the viable bacteria with 100 % in dH_2O and 99.996 % in ¼-Ringer’s solution.

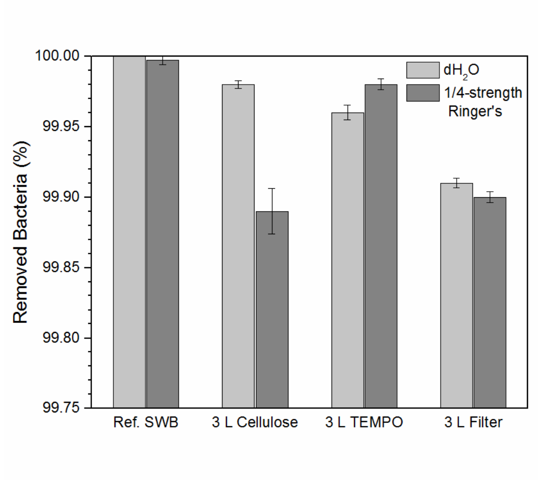

Figure 1. The percentage of removed bacteria from suspension after 4 hours of incubation with modified materials.

3.2 Time dependence

The time it takes to remove bacteria from water is an important parameter when treating drinking water. The number of remaining bacteria in suspension after 1, 2, 3, and 4 hours of contact-time were therefore evaluated. The test shows that all modified materials greatly decreased the bacterial concentration after only one hour of contact-time (Figure 2). The results from the time dependence test are promising, as many techniques used to purify water require several hours to obtain safe drinking water.

3.3 Filtration with natural water sample

The three layer modified filter removed >99 % of the bacteria compared to the unmodified filter that removed 43 % of bacteria from the water sample (Figure 3). The commercial reference removed >99 % of the bacteria in the natural water sample.

4. CONCLUSION

The bacterial reduction capacity of the functionalized cellulosic fibers is good and the material could with an optimized product design, preferably cross-flow filtration, be a promising alternative for a disposable POU water purification device.

Cellulose is a natural biomaterial that is relatively cheap and safe to handle, and combined with the nonleaching bacteria adsorbing modification, it presents an environmentally friendly option for current POU treatment techniques based on releasing toxic compounds. Cellulosic fibers are great for making paper sheets and

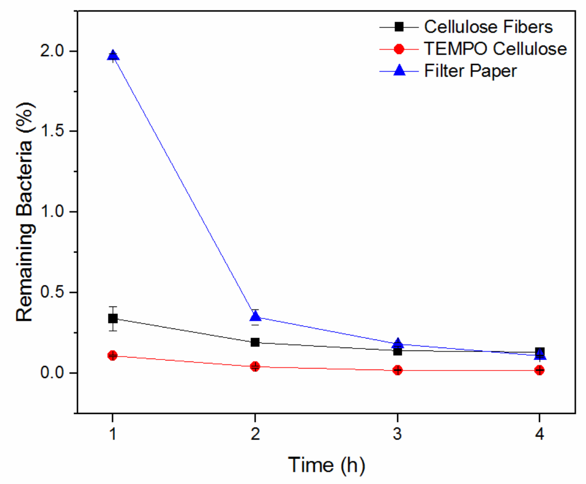

Figure 2. The results from the time dependence test showing the percentage of bacteria remaining in suspension in hourly increments after incubation with modified materials.

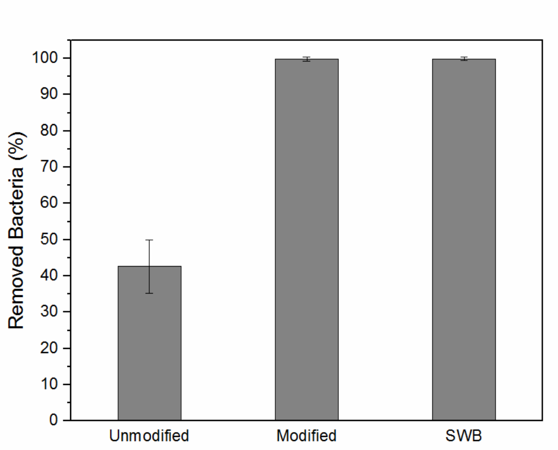

Figure 3. Result from the filtration test using natural water from Nybroviken.

are currently used in a variety of filters ranging from simple coffee filters to advanced fuel and air filters in cars. The functionalized cellulosic fibers can be processed into paper sheets, which could be used for water filtration. The water filter would then rely on physical removal of bacteria through electrostatic interactions and should be able to allow a higher flux compared to filters relying on size exclusion of bacteria. However, the pore size of the filters must still be small enough to obtain sufficient contact between the functionalized fibers and all bacteria in the water, as it is critical for an efficient contact-active POU technique.

REFERENCES

[1] R. Bain, R. Cronk, R. Hossain, S. Bonjour, K. Onda, J. Wright, H. Yang, T. Slaymaker, P. Hunter, A. Prüss-Ustün, J. Bartram. Global assessment of exposure to faecal contamination through drinking water based on a systematic review. *Trop. Med. Int. Health* 2014, **19** (8), 917−927.

[2] A. Ottenhall, J. Illergård and M. Ek. Water purification using functionalized cellulosic fibers with nonleaching bacteria adsorbing properties. *Environ. Sci. Technol.* **DOI:** 10.1021/acs.est.7b01153 (2017).

[3] J. Illergård. The creation of antibacterial fibers through physical adsorption of polyelectrolytes. PhD thesis, KTH Royal Institute of Technology (2012).

[4] *Folia Water*, website, http://www.foliawater.com/safe-water-book-1 , (accessed February 9, 2017)

A quick and simple method to prepare functionalized cellulose nanocrystals with high yield

DONGFANG LI, JONATAN
HENSCHEN, MONICA EK

Department of Fiber and Polymer
Technology, KTH Royal Institute of
Technology, Teknikringen 56-58, SE-100
44 Stockholm, Sweden
hens@kth.se

1 INTRODUCTION

Cellulose nanocrystals (CNCs) have driven increased attention over the last decade, due to the possibilities to use these nano-particles to prepare renewable materials with many interesting properties for several applications [1, 2]. A classical process to prepare CNCs uses a considerable amount of water in acid hydrolysis and washing. In the end, around 44 wt% of the raw material (normally bleached sulfite pulp) is converted to CNCs [3]. The low yield and extensive washing procedures make the production of CNCs in larger scale a costly process.

Here, we report a quick and simple method to prepare functionalized cellulose nanocrystals (CNCs) with high yield. A solvent-free modification of cellulose was carried out to prepare cellulose derivatives with anionic charges that were determined by conductometric titration. CNCs were made from the aqueous suspensions of the cellulose derivatives through sonication. The gravimetric yields of CNCs were calculated based on the dry weights of raw materials. Transmittance Electron Microscopy (TEM) was used to determine the width and length of nanoparticles. Dynamic Light Scattering was used to determine the z-average sizes of the nanoparticles in the aqueous suspensions. X-ray diffraction was used to measure the crystallinity indexes of the CNCs.

2 EXPERIMENTAL

2.1 Pulps

Commercially available softwood and hardwood dissolving pulps (cellulose content 96-97%), bleached softwood kraft pulp (cellulose content>80%), and microcrystalline cellulose (Avicel PH-101) were used as cellulose raw material. Each dried pulp was manually torn into smaller pieces (approximately 2×2 cm^2).

2.2 Modification of cellulose and preparation of CNC suspension

Modification of cellulose was carried out through constant heating and agitation without using water or any organic solvents. Cellulose derivatives were obtained as fine and white powders (Figure 1) after sufficient washing to remove the excess chemical and by-products. Aqueous suspensions of cellulose derivatives with the consistencies of 3-5% were prepared. Each suspension was then sonicated with 40% amplitude and centrifuged at 4500 rpm for 30 min. The supernatant was collected to obtain a suspension of CNC. The gravimetric yields of the cellulose derivatives and CNCs were calculated based on the dry weights of raw materials.

2.3 Characterization

Charge density of each cellulose derivative was determined by conductometric titration as described elsewhere[4]. Transmittance Electron Microscopy (TEM) images were recorded on an HT7700 transmission electron microscope (Hitachi, Japan) with a voltage of 80 kV. Dynamic light scattering (DLS) was performed on a Zetasizer ZEN3600 instrument (Malvern Instruments Ltd., UK) to determine the z-average sizes of the nanoparticles in the water suspensions. X-ray diffraction was used to measure the crystallinity indexes of the CNCs.

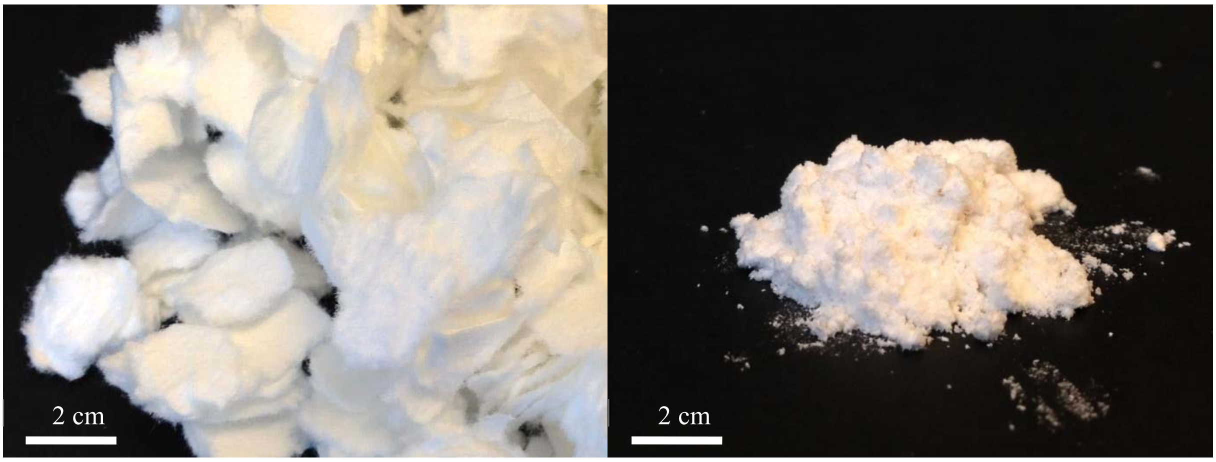

Figure 1. Comparison between a raw material (left) and a cellulose derivative prepared after the modification (right).

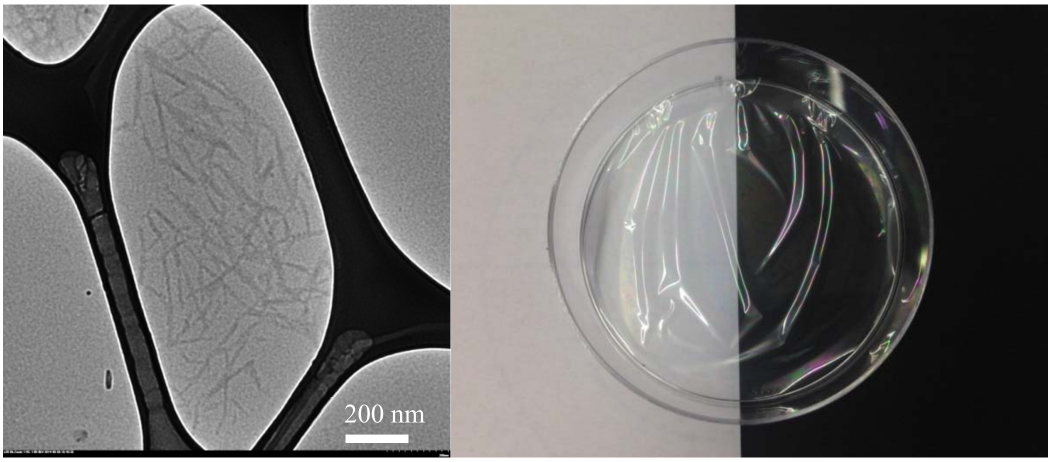

Figure 2. TEM image of the nanocellulose in diluted aqueous suspension and an image of a film prepared by solvent-casting of the aqueous suspension of the nanocellulose.

Figure 3. Concentrated aqueous suspension of the nanocellulose observed between the crossed polarizers.

3 RESULTS AND DISCUSSION

Cellulose derivatives with charge densities of 0.1-1.3 mmol/g were prepared through a solvent-free modification. Depending on the reaction conditions and raw materials, the cellulose derivatives could be obtained with gravimetric yields of 82-99%.

It was possible to obtain nanocelluloses after the sonication of the aqueous suspensions of the cellulose derivatives, and the gravimetric yields of dried nanocelluloses were as high as 42-81%. By Dynamic Light Scattering, the z-average sizes of the nanoparticles were 169-535 nm with narrow distributions. An example of TEM images shows that the shape of the nanocellulose was more like a rod rather than a fibril, with an average length of 150-220 nm, and an average width of 16-20 nm (Figure 2). When the concentrated suspension was observed between the crossed polarizers, a birefringence pattern was shown (Figure 3). In addition, iridescent films could be prepared by solvent-casting of the aqueous suspensions of the nanocelluloses (Figure 2). By X-ray diffraction, the crystallinity indexes of the nanocelluloses were 68%-80%, which confirmed that the nanocelluloses were mostly crystalline. Considering the dimensions and crystallinity indexes of the nanocelluloses, they can be categorized as CNCs.

4 CONCLUSIONS

Cellulose derivatives with high charge densities were prepared through a quick, simple, and solvent-free modification of cellulose, and were obtained as dry and very fine powders. This enabled us to prepare functionalized nanocellulose in the form of crystals. Compared to the conventional ways for the preparation of nanocellulose, the method reported in this study is simpler with much shorter procedures and is more economic in terms of no use of solvents and high yields.

REFERENCES

[1] Beck-Candanedo S., Roman M. and Gray D.G. Effect of reaction conditions on the properties and behaviour of wood cellulose nanocrystal suspensions. *Biomacromolecules*, **6**(2):1048-1054 (2005).

[2] Habibi, Y., Lucia, L.A. and Rojas, O.J. Cellulose nanocrystals: chemistry, self-assembly, and applications. *Chem. Rev*., **110**(6):3479-3500 (2010).

[3] Dong, S., Bortner, M.J. and Roman, M. Analysis of the sulfuric acid hydrolysis of wood pulp for cellulose nanocrystal production: a central composite design study. *Ind Crops Prod*., **93**:76-87 (2016).

[4] Habibi Y., Chanzy H. and Vignon M.R. TEMPO-mediated surface oxidation of cellulose whiskers. *Cellulose*, **13**(6):679-687 (2006).

Test rig for the production of highly oriented papers in the context of building with paper

R. GÖTZINGER, S. SCHABEL

TU Darmstadt, Paper Technology and
Mechanical Process Engineering (PMV)
goetzinger@papier.tu-darmstadt.de

1 BUILDING WITH PAPER AT THE TU DARMSTADT

In January 2017 the project “BAMP – Bauen mit Papier” (building with paper) started at the TU Darmstadt. The aim of this project is to make paper accessible as building material. Therefore an interdisciplinary team consisting of ten doctoral students from architecture, mechanical and process engineering, civil engineering, paper engineering and chemical engineering work together. They investigate the fundamentals of paper and building physics, new test methods, new design methods, material combinations and forming techniques. The project is publicly founded by LOEWE (Germany - federal state Hessen) with approx. 4.6 million € and the project duration is four years.

1.1 Focus and procedure

The Team focuses on residential buildings which have a short expected useful life of about one year. Three topics are taken into account: Static behavior, fire and moisture resistance. In several iteration steps different demonstrators are developed. Market available material is used to build large demonstrators, so to speak small houses. The construction and the design are developed and the material is tested. In parallel smaller demonstrators are built to test new developed materials.

1.2 Fiber orientation

The strength of paper is influenced by the fiber orientation. For example the tensile strength can be higher by factor two or more in direction of orientation.
In order to improve the static behavior of tubes and boards in areas with high loads, the influence of highly oriented paper is investigated. To create paper with high orientation of the fibers a test rig is developed at the PMV. The produced paper is used to build and test mock-ups. With the gained data the influence of fiber orientation on mechanical properties is descried in a model and existing models of paper are improved.

2 TEST RIG FOR THE PRODUCTION OF HIGHLY ORIENTED PAPER

The test rig was inspired by an experimental setup designed by Dolatshahi and Kortschot [1]. The principle is to let a capillary traverse above a wire, a highly dilute suspension being applied to the wire by the capillary.

Dolatshahi and Kortschot achieved high orientation with an average fiber orientation angle of 7 °. The size of the produced paper was 140 mm x 20 mm with a weight of about 20 g/m²

2.1 Development at the PMV

For the experiments planned in the context of building with paper, larger dimensions are necessary. Based on the above-mentioned principle a test rig was developed in several student works [2, 3, 4, 5]. Instead of using a suction roll as Dolatshahi and Kortschot did, a rotating wire is used. Like in a paper machine the water is removed by a suction zone behind the wire (Figure 1). In order to avoid a rotation of the fibers in the suspension due to the gravity or the impingement on the wire, the wire was arranged vertically. A small angle between capillary and wire should guarantee a smooth transition by as far as possible tangential deposition of the fibers.

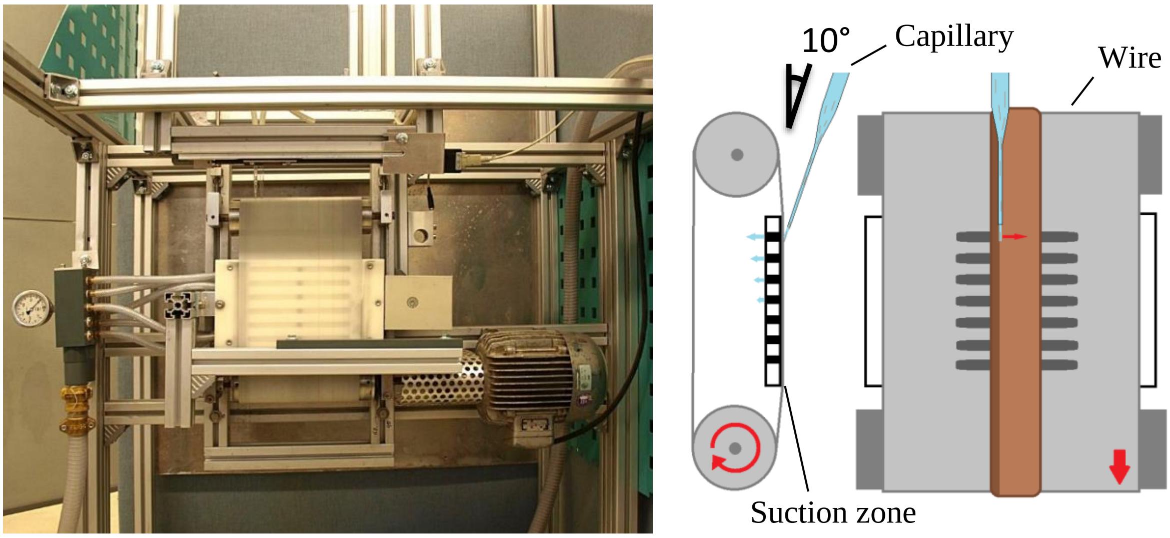

Figure 1. Left: Test rig developed in student works. Right: Schematic diagram [3].

First results showed that the principal works but several problems have been reported which need to be solved to meet the requirements for the produced paper.

2.2 Alternatives

Examples for other laboratory machines available on the market where a fiber orientation can be reached are the M/K sheet former or the Dynamic sheet former. From the results of Dolatshahi and Kortschot and first results of the new test rig it can be expected that a higher degree of orientation and so a higher increase in paper strength in machine direction can be reached than with the conventional laboratory machines.

2.3 Outlook

The focus of further development is on an improvement of the approach flow, adjustment of the capillary, improvement of the suction zone and automation of the control.

Later it should be possible to place a certain fiber at a specific position on the wire. Thereby it should be possible to adjust the paper properties locally.

Other areas of application are the control of liquid transport in paper, paper with defined pores and fiber composite materials.

REFERENCES

[1] S. Dolatshahi and M. T. Kortschot. The effect of fiber orientation on the zero-span testing of paper. 14th Fundamental Research Symposium, Oxford, 931-946, (2009).

[2] C. Klein, O. Kourkis, C. Vogt, X. Wu. Konstruktion einer innovativen Laborapparatur zur Herstellung von Vliesstrukturen mit definierter Faserorientierung. Advanced Design Project, Technische Universität Darmstadt (2013).

[3] O. P. Bardsley. A Machine for the Manufacture of Paper with Highly-Aligned Fibres: Operation, Analysis and Results. Project report, Technische Universität Darmstadt (2014).

[4] C. Schaumburg. Design und Inbetriebnahme einer Maschine zur Herstellung hochorientierter Fasermatten (In German). Bachelor-Thesis, Technische Universität Darmstadt (2014).

[5] T. Ulyanova. Konstruktive Weiterentwicklung eines Laborgerätes zur Herstellung von Faservliesen mit unidirektionaler Faserorientierung (In German). Master-Thesis, Technische Universität Darmstadt (2015).

γ-valerolactone-based biorefinery: a shortcut from wood to textile fibers

HUY QUANG LÊ [1], JUHA-PEKKA POKKI [2], YIBO MA [1], MARC BORREGA [3], VILLE ALOPAEUS [2], HERBERT SIXTA [1].

[1] Department of Bioproducts and Biosystems, Aalto University, Finland.
[2] Department of Chemical and Metallurgical Engineering, Aalto University, Finland.
[3] VTT Technical Research Center Finland.
huy.le@aalto.fi

1 INTRODUCTION

This work describes a novel biorefinery concept based on the fractionation of woody biomass in a γ-valerolactone (GVL)/H_2O binary mixture. *Eucalyptus Globulus* wood can be effectively fractionated in a single step into its principal components without the addition of any catalyst or additives [1]. The pulp fraction, characterized by high yield, high cellulose purity and high bleachability, can be directly spun to produce regenerated cellulose fibers. The spent liquor (SL), rich in lignin, carbohydrates, furans and organic acids, is a potential source for chemical and energy production. The recovery of GVL from the SL was investigated by multi-stage vacuum distillation and near-critical CO_2 extraction.

2 EXPERIMENTAL

Eucalyptus globulus wood (46.4% cellulose, 22.1% hemicellulose and 29.3% lignin) was fractionated in an aqueous GVL solution. No catalyst or additives were added. Small scale trials with sawdust (particle size < 125µm) were conducted in 30mL vials heated in a microwave reactor (Anton Paar Monowave 300). Reaction temperature, time and liquor-to-wood (L:W) ratio were 180°C, 120 minutes and 10 L/kg, respectively. The GVL content in the fractionation liquor ranged from 0 – 98 wt%. The fractionation of wood chips was done in 225 mL bombs heated in a silicon oil-bath reactor (Haato-tuote 43427). The reaction temperature and L:W ratio were 180°C and 10 L/kg, respectively, the GVL content in the liquor was 50 and 60 wt%, and the fractionation time (retention time at 180°C) ranged from 60 to 180 minutes. For wood chips, an impregnation time of 60 minutes at 120°C was employed. For each fractionation trial, the pulp was separated from the SL by filtration, followed by washing. The pulp fraction was analyzed for yield, molar mass distribution, intrinsic viscosity, carbohydrate and lignin content, molar mass distribution. The SL was analyzed for carbohydrate, furanics and soluble lignin content.

A selected pulp sample was bleached by an Elemental-Chlorine-Free (ECF) sequence of D_0-Ep-P. Selected unbleached and bleached pulps produced from wood chips were spun to regenerated cellulose fibers by the IONCELL-F spinning process [2].

The first suggested GVL recovery scheme is multi-stage vacuum distillation. Lignin was precipitated from SL by water addition and collected by centrifugation. GVL was distilled from the lignin-lean SL at reduced pressure. The concentrated SL underwent another precipitation-distillation cycle.

We also tested the extraction of GVL from its aqueous solution by near-critical CO_2 in an equilibrium cell design for phase equilibria study [3].

3 RESULTS AND DISCUSSION

3.1 Eucalyptus wood fractionation

The fractionation of sawdust in small scale identified the optimum GVL concentration for delignification. The extraction of the wood main components, namely cellulose, hemicelluloses and lignin, during GVL/H_2O fractionation is showed in Figure 1. The results indicate that the cellulose fraction was recovered almost quantitatively at any GVL concentration, while the delignification was optimal at about 50 – 60 wt% GVL. Hemicellulose removal increased with increasing the water content due to enhanced hydrolytic degradation.

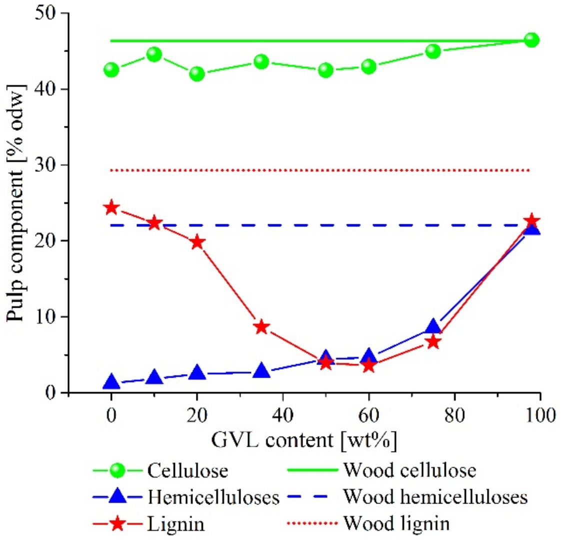

Figure 1. Effect of GVL concentration of the fractionation liquor on the separation of eucalyptus sawdust main components. (odw: oven-dried wood).

The high cellulose content in the pulps produced in 50% and 60% GVL liquors, coupled with the relatively low hemicellulose and lignin content suggests the potential to convert GVL/water pulp to dissolving pulp of viscose grade after bleaching. This was further investigated by the fractionation of wood chips in 50 and 60 wt% GVL solutions. In comparison to fractionation with 60 wt% GVL, employing 50 wt% GVL liquor gave a slight advantage on delignification and hemicellulose removal at the expense of pulp viscosity.

The removal of wood components and the viscosity of the pulps along the course of fractionation in 50 wt% GVL are shown in Figure 2a. The defibrillation of wood occurred in the early stages of fractionation, with almost no rejects detected after 60 minutes of reaction. Extending the reaction time beyond 60 min slightly increased the removal of wood components, but the intrinsic viscosity decreased considerably. In all cases, wood chips were effectively converted into pulps with high cellulose yield and purity. As illustrated in Figure 2b, the reduction of L:W did not impair the extent of hemicellulose removal and delignification but the degree of polymerization of cellulose was significantly affected.

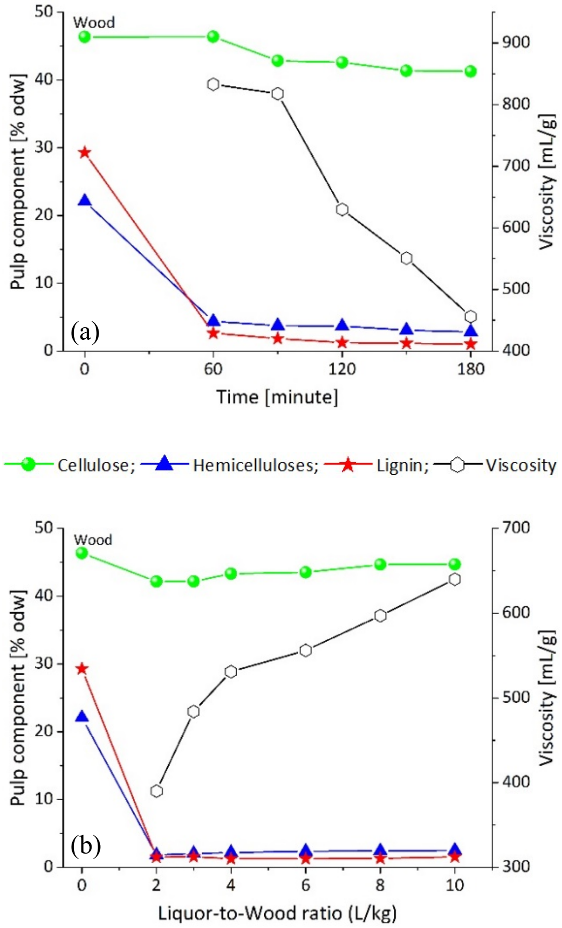

Figure 2. (a) Effect of time in oil-bath digester and (b) effect of L:W in air-bath digester on wood components removal during the fractionation of eucalyptus wood chips with 50 wt% GVL liquor. (odw: oven-dried wood).

3.2 Textile fibers production

The pulps produced in 50 wt% GVL at L:W=10 L/kg were selected for their conversion into regenerated cellulose fibers. The pulp obtained after 180 minutes of fractionation was spun directly without bleaching.

The pulp produced after 150 min fractionation time was bleached with a short ECF sequence prior to spinning. A commercial bleached hardwood acid sulfite pulp with similar chemical composition and molecular mass distribution as the GVL pulps (Table 1 and Figure 3), was selected as the reference pulp and spun to regenerated cellulose fibers with the same IONCELL-F procedure.

Table 1. Properties of selected pulp samples employed in the spinning trials.

Properties	U-GVL	B-GVL	Reference
Cellulose [%odp]	92.7	93.6	94.9
Hemicellulose [%odp]	5.2	5.8	4.2
Lignin [%odp]	2.1	0.6	0.9
ISO-brightness [%]	-	86	89
Viscosity [mL/g]	456	470	524

odp: oven-dried pulp
U-GVL: unbleached GVL/water pulp
B-GVL: bleached GVL/water pulp

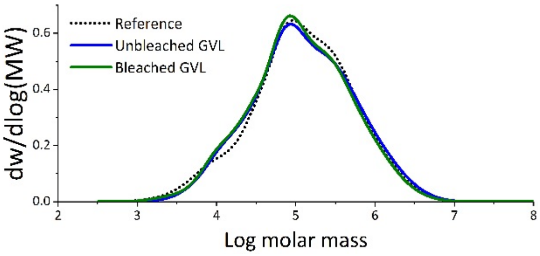

Figure 3. Molecular mass distribution of unbleached and bleached GVL/water pulps, compared to a commercial bleached acid sulfite hardwood dissolving pulp used as reference. (dw/dlog(MW): differential mass fraction)

The mechanical properties of the regenerated fibers produced from both unbleached and bleached GVL/H_2O pulp were comparable to those of the reference fiber. They also exhibited better tensile properties than other manmade cellulosic fibers available in the market such as the TENCEL® and viscose fibers (Figure 4).

3.3 By-products and chemical recovery

During the course of fractionation, under mild acidic condition, the hemicelluloses and a small fraction of the cellulose were hydrolyzed and extracted into the SL as oligomeric and monomeric carbohydrates.

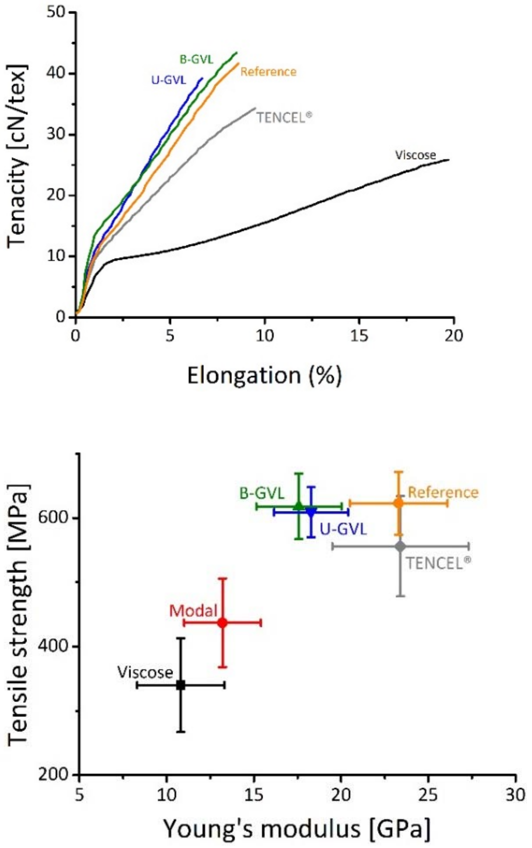

Figure 4. (a) Stress-strain curves and (b) Young's modulus (right) of GVL fibers in comparison to different commercial textile fibers [4].

With increasing fractionation time, the monomeric sugars in the SL was subjected to dehydration reactions to furanic compounds, which further reacted to degradation products like organic acids, and eventually humins. More than 90% of the lignin in the wood chips was dissolved into the SL. Table 2 demonstrate a typical composition of the SL.

Table 2. Content of a the SL obtained from the fractionation of eucalyptus wood chips in 50 wt% GVL, with L:W=10 L/kg, at 180°C for 180 minutes.

Components	Amount [%odw]
Cellulose	0.5
Hemicellulose	4.3
Lignin	28.1
Furanics	4.9
Organic acids	9.9

odw: oven-dried wood

Lignin was precipitated from the SL by water addition. GVL lignin is a typical organosolv lignin characterized by being sulfur-free, rich in functionalities (especially phenolic), having high purity, low molar mass and low polydispersity. The diluted liquid was subjected to distillation at reduced pressure to obtain an aqueous distillate containing the more volatile compounds (such as furfural, formic acid and acetic acid) and an organic one rich in GVL. The residual liquid, rich in GVL and extracted components, was subjected to another dilution-lignin precipitation-distillation cycle. This method recovered ca. 91% GVL and 90% of the lignin in wood. Higher recovery could be achieved by increasing the precipitation-distillation cycle or by recirculation of the post-distillation residual liquid back to the feed.

Besides, inspired by a pioneering research [5], we tested and confirmed that near-critical CO_2 extraction enables an efficient separation of GVL from its aqueous solution. Base on this positive result, we are constructing an extraction unit using near-critical CO_2 to recover GVL from the SL.

4 CONCLUSION

GVL/H2O mixtures enable a quantitative and selective fractionation of all lignocellulosic components in just one single step, with a solid cellulose fraction that can be directly used as dissolving-grade pulp, and a liquid fraction that contains the extracted sugars and lignin which can be further processed to valuable chemical and energy. Furthermore, the process is sulfur-free and the high pulp bleachability offers the possibility for a Total-Chlorine-Free bleaching, thus making the process environmentally friendly. Altogether, our process fulfills the requirements of a modern biorefinery.

REFERENCES

[1] H. Q. Lê *et al.* Wood biorefinery based on γ-valerolactone/ water fractionation. *Green Chem.* **18** (20): 5466–5476 (2016).

[2] H. Sixta *et al.*Ioncell-F: A High-strength regenerated cellulose fibre. *Nord. Pulp Pap. Res. J.* **30**(1): 43–57 (2015).

[3] P. Uusi-Kyyny *et al.*Design of equilibrium cells for phase equilibria and PVT measurements in large ranges of temperatures and pressures. I. Vapor-Liquid-Liquid Equilibria. *J. Chem. Eng. Data* **61**: 2700–2711 (2016).

[4] R. Adusumali *et al.* Mechanical properties of regenerated cellulose fibers for composites. *Macromol. Symp.* **244**: 119–125 (2006).

[5] J. S. Luterbacher, *et al.* Nonenzymatic sugar production from biomass using biomass-derived γ-valerolactone. *Science* **343**: 277–280 (2014).

Coating of cellulose fibres with inorganic nanoparticles in the course of the Cellulose xanthate (CX) process

MICHAEL WEIßL[1], MARA JULIN[1] and STEFAN SPIRK[2]

1) Institute for Chemistry and Technology of Materials, Graz University of Technology, 8010 Graz, Austria

2) Institute for Paper, Pulp and Fibre Technology, Graz University of Technology, 8010 Graz, Austria
michael.weissl@student.tugraz.at

1 Introduction

The industrial production of wood based cellulose fibres in the late 19th century partly replaced natural fibres made from cotton, jute and flax. One of the oldest, but still most successful processes for the production and in situ modification of man-made cellulose fibres is the so called viscose process developed by Cross, Bewan and Beadle. The different fiber modification techniques such as coating or incorporation of inorganic particles into the fiber matrix have attended great interest due to the large variety of material properties (anti-bacterial, flame resistant, conductive) which can be realized through this type of modification. [1,2,3]

1.1 Laboratory scale fibre spinning

For a successful operation of the fiber spinning unit two major requirements have to be met. First, the viscose solution (Fig.1) has to be injected, which requires control over the viscosity. Second, the generated fibers have to be collected without destroying the fiber structure. After adjusting the ideal operation conditions (injection speed, viscose age, collector speed), the lab scale fiber production accurately worked

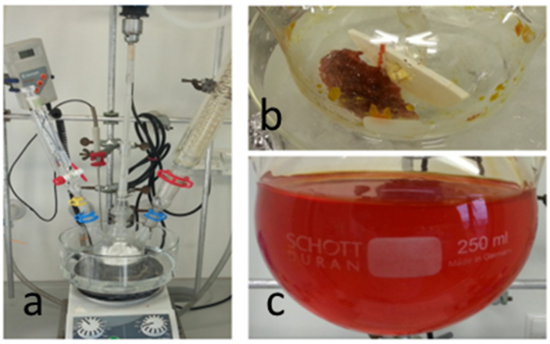

Figure 1. Different steps of laboratory scale viscose production. A: addition of CS_2 to the alkali cellulose ,b: cellulose xanthate , c: spinning solution obtained by dilution of b with NaOH.

2 Indirect process: Ion exchange in alkali cellulose fibers

For the ion exchange, alkali cellulose fibres were added to aqueous solutions of metal salts ($CuCl_2$, $FeCl_3$, $SnCl_2$, $AgNO_3$) at different concentrations. The aim was to exchange the sodium ions against other metal ions. After stirring over a period of 30 minutes differently coloured fibres were obtained (Fig. 2a-d).

The silver exchanged fibers exhibited a similar width as the alkali cellulose fibers. Images of the fibres after ion exchange indicate that metal ion could be fixed on the fibre surface. Further analysis by scanning electron microscopy (SEM) clearly proved the presence of such particles on the fibre surface. (Fig.2)

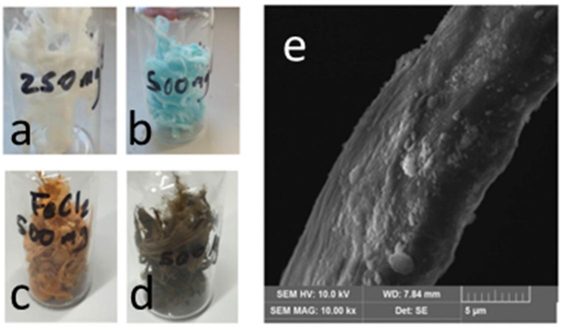

Figure 2. Comparison of alkali cellulose fibres after ion exchange with Sn (a), Cu (b), Fe (c) and Ag (d) and a SEM image of fibers equipped with copper. (e).

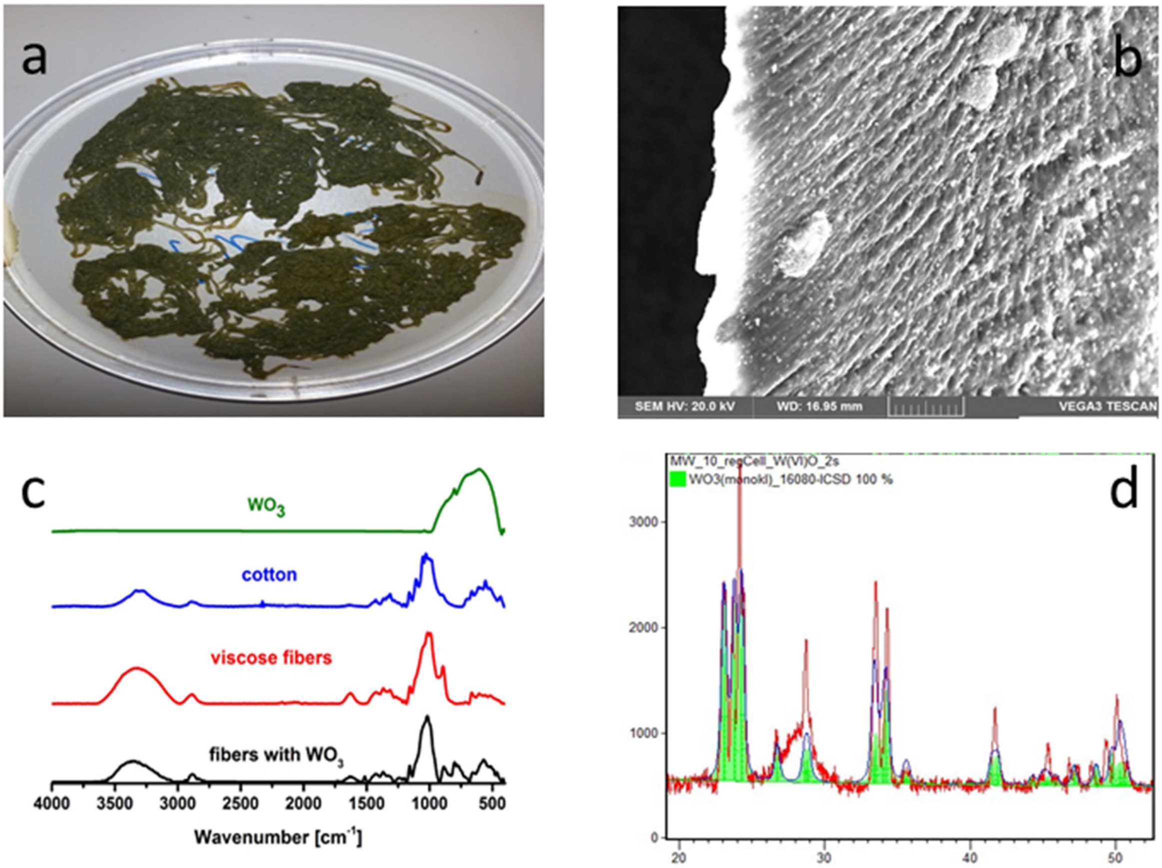

Figure 3. Viscose fibers containing WO_3 after spinning (a), a corresponding SEM image (b), ATR-IR spectra of a standard viscose fibre and a tungsten modified fibre (c) and a XRD pattern of the tungsten containing viscose fibres (d)

3 Direct process: Incorporation of WO_3 into viscose

Tungsten oxides are interesting materials for polymer and fiber reinforcement. For the incorporation of WO_3 into the fibers, commercially available particles were suspended in viscose solution and subjected to fiber spinning. After regeneration of the fibers x-ray diffraction analysis (XRD), attenuated total reflection infrared spectroscopy (ATR-IR) and SEM were utilized to characterize the produced fiber materials (Fig 3). SEM imaging proved that inorganic particles are regularly distributed in the fiber matrix and an agglomeration of the particles to larger clusters could be avoided. XRD was employed to control the chemical structure and the influence of cellulose xanthate onto the WO_3 particles and ATR-IR spectroscopy verified that the regeneration from CX to cellulose II is not affected by the presence of tungsten nanoparticles during the spinning process.

REFERENCES

[1] Klare, H.; (1985) 100 Jahre Celluloseregeneratfaserstoffe – Geschichte und Perspektiven. Acta Pol.; Bd. 36; S. 347-352

[2] Cross, C. F.; Bevane, J.; Beadle., C.; (1892). Brit. Pat. 8700

[3] Hämmerle, F. M.; (2011). The cellulose gap. Lenzinger Berichte, 89, 12-21.

Magnetic materials from fines in paper making pulps

MATHIAS HOBISCH,[a*] WOLFGANG FISCHER, RENE ECKHART,[a] ARMIN ZANKEL,[b] WOLFGANG BAUER,[a] and STEFAN SPIRK[a]

[a]Institute of Paper, Pulp and Fibre Technology, [b]Institute of Electron Microscopy and Nanoanalysis,
Graz University of Technology, 8010 Graz, Austria, mathias.hobisch@tugraz.at

1 INTRODUCTION

In the past years, there has been a growing interest in the investigation of different streams in the course of paper production. In this context, paper fines are a versatile source for new materials with advanced applications. Fines are small cellulosic fibers, which are capable to pass a mesh with holes 76 microns in diameter. (Fig. 1a) The role of the fines in papermaking production is still not completely clear which originates to some extent to challenges in the localization of the fines in the final paper furnishes. However, for the fibrillary fractions (secondary fines) it is well supported by experimental evidence that they improve some paper properties like paper strength. [1]

1.1 Utilization of magnetic fines

In this contribution, we explore how to equip such fines with functional magnetic nanoparticles (NPs). This is interesting from two perspectives: On one hand isolated paper fines could be easily localized in paper sheets, on the other hand side, the magnetic moment of the particles can be directly exploited to create new materials with applications ranging from memory storage to switchable devices based on cellulose. [2] As magnetic NPs we chose cobalt ferrite ($Fe_{3-x}Co_xO_4$). These NPs are easily applicable by either in-situ synthesis filling the lumen in case of fibers, or an in-situ co-precipitation method. [2]

Here, we focused our efforts on the distribution of fines in paper and their detection via mapping techniques and X-ray microtomography. Paper fines were separated from bleached sulfite pulp. (Mixture of spruce and beech) After loading various amounts of nanoparticles onto the fines, (Fig. 1b) they were reblended with the pulp. A constant fines concentration in handsheets was achieved by white water recirculation during sheet formation. [3] Since the NP loaded fines may influence sheet formation and bonding ability, fundamental paper properties have been tested and compared either for different synthesis methods as well as for different fines concentrations.

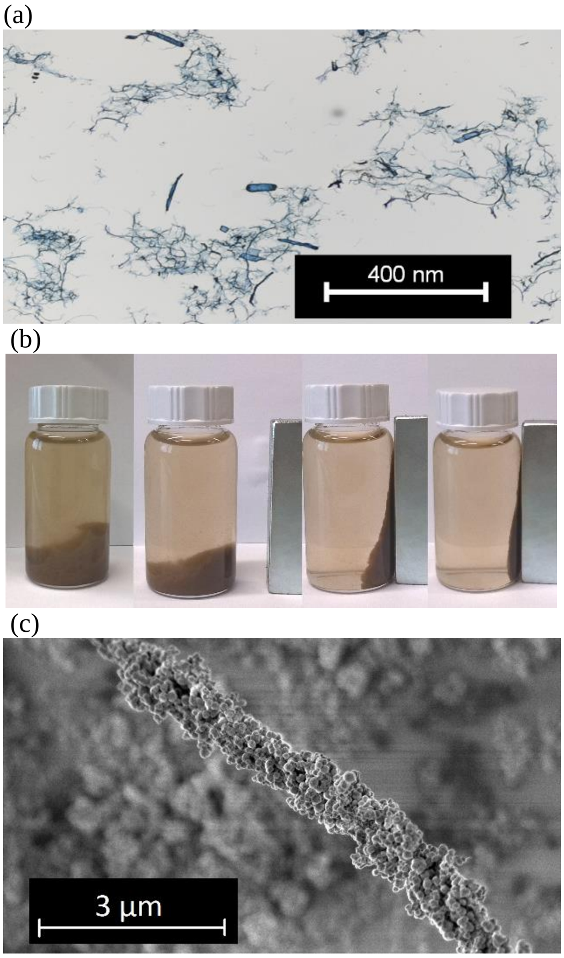

Figure 1. Visualisation of the process steps localizing paper fines in the hand sheet. The paper fines visualized by microscope. (a) Magnetism proved the synthesis (b) and nanoparticle (50 - 150 nm) visualized by LVSEM (c)

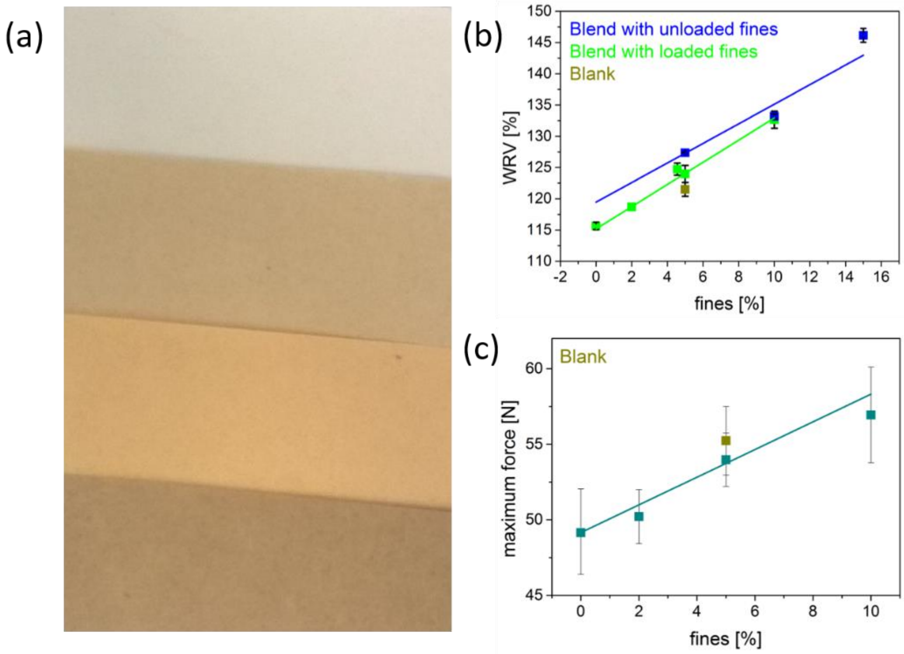

Figure 2. Formed paper sheets varying the amount of fines in the paper (0, 2, 5, 10 wt% fines from top to bottom) (a) WRV (b) and Mechanical properties (c) illustrating the impact of fines in paper sheets.

2 RESULTS

Two different synthesis pathways for in-situ synthesis of cobalt ferrite NP have been tested. All the methods yield rather spherical NPs with sizes in the range of 50 to 150 nm. (Fig. 1c) Importantly, the in-situ synthesis works best reducing the fixation time in 0.33 M NaOH and does not affect the morphology and structure of the fines as proven by Scanning Electron Microscopy (SEM). The excess of NPs, loosely adhering on the surface were rinsed away to prevent agglomeration. Via thermogravimetric analysis, loading was quantitatively determined to be between 56 and 70 wt%. Energy-Dispersive X-Ray (EDX) proved the fair distribution of cobalt and ferrite on the fines. Paper properties were determined (WRV, thickness, density and mechanical properties) which proved that the NP had no significant effect on the technological properties of fines in the sheet formation process. Preliminary results are shown based on the water retention value (WRV) (Fig. 2b) and the maximum force. (Fig. 2c) A linear dependence was noticed by increasing the amount of fines as published in literature, [1,4] for loading and unloaded fines alike.

REFERENCES

[1] B. Krogerus, L. Eriksson, A. Sundberg, J. Mosbye, A. Ahlroth, I. Östlund, and L. Sjöström. Fines in closed circuits - Final report. *KCL*, (2002)

[2] S. Liu, X. Luo, and J. Zhou. Magnetic Responsive Cellulose Nanocomposites and Their Applications. InTech, edition 1, (2013)

[3] R. Giner, W. J. Fischer, Rene Eckhart, and W. Bauer. White water recirculation as a means to evaluate fines properties. *BioResources*. 10(4): 7242-7251 (2015)

[4] M. Mayr, R. Eckhardt, H. Winter, and W. Bauer. A novel approach to determining the contribution of the fiber and fines fraction to the water retention value (WRV) of chemical and mechanical pulps. *Cellulose*. 24(7):3029-3036 (2017)

Kraft lignin precipitation with flue gas

THOMAS PICHLER, MARLENE
KIENBERGER, SILVIA MAITZ,
ANDREAS PIRSCHNER
and MATTHÄUS SIEBENHOFER

Institute of Chemical Engineering and
Environmental Technology
thomas.pichler@tugraz.at

1. INTRODUCTION

Due to the use of wood as raw material and high volume production the pulp and paper industry serves as backbone in the biorefinery. The high volume of biomass throughput makes pulping a great source for isolation of valuable byproducts from process streams. The most prominent substance is lignin, which is dissolved in high concentration in the black liquor (BL) from kraft pulping.

On the one hand the isolated lignin can serve as raw material or bulk chemical in different applications. On the other hand, the removal of lignin can be advantageous for the mill because the heating value of BL is lowered. BL is burned for chemical recovery and energy production, so lignin removal allows an increase of pulp production without an increase of the heat load. Especially for mills with recovery boilers operating at or even beyond maximum capacity, the recovery of lignin is a feasible way to raise production without expensive boiler upgrade. [1,2]

1.1 Basics

Black liquor lignin precipitates by simple acidification. Lignin is then isolated by filtration and purification of the slurry. Acidification is mainly applied with CO_2, sulphuric acid or combination of both.

The filtration is a critical step of the separation process, as precipitation pH and temperature influence the particle growth and the formation of lignin agglomerates and hence influence the resistance of the filter cake. High filtration resistance renders an economic processing impossible.

Besides precipitation pH and temperature, the CO_2 concentration influences the process performance, like precipitation time and foam formation. [2-4]

The present work aims at the development of a process and device, which makes use of flue gas from the mill as CO_2 source for acidification of the BL.

2. EXPERIMENTAL

2.2 Black liquor characterization

For characterisation, BL from the first evaporation step of a local pulp mill was investigated. Density, viscosity, lignin concentration and dry matter content were analysed.

Density and viscosity of the black liquor were measured with a SVM 3000 viscosimeter from Anton Paar GmbH. The lignin concentration was measured using a Shimadzu UV-1800 spectrophotometer at 280 nm and an absorption coefficient of 23.7 L/g·cm. The dry matter content was determined by drying at 105°C. The buffer capacity of black liquor was obtained from 1 M HCl consumption.

Titration was carried out at 70°C. The pH value was measured using a WTW SenTix 42 electrode.

2.3 Precipitation experiments

In accordance to literature the precipitation temperature was set to 70°C. [2]

Gas flow rate was adjusted to 0.3 Nm^3/h to acidify a batch of 3.4 kg BL. Experiments were carried out with pure CO_2 and with a gas mixture of 16 vol% CO_2 and N_2.

Latter mixture corresponds with off gas quality of the paper mill. pH set point for precipitation at 70°C was 9.1 to avoid H_2S liberation.

The CO_2 concentration of the precipitator purge gas was monitored with a smartMODUL PREMIUM^{EVO} NDIR gas sensor from smartGAS.

2.4 Lignin separation and filtration experiments

After the target pH of 9.1 was reached, the reactor was emptied and the lignin slurry was cooled down to 40°C. The slurry was filtered using a suction filter with Macherey-Nagel MN615 filter paper at a constant vacuum of 900 mbar generated by an ILMVAC V01 vacuum pump.

To evaluate the specific filter cake resistance α according to the Darcy equation for constant pressure difference, the filtration rate was recorded over time.

Viscosity measurement of the filtrate at filtration temperature was performed with a SVM 3000 viscosimeter from Anton Paar GmbH. The lignin content of the filtrate was measured spectrophotometrically (see 3.1).

3. RESULTS

3.1 Characterisation

Table 1 summarizes the results for the BL characterization.

Table 1: Properties of black liquor

Parameter	Value	Unit
Density	1180	g/l
pH	12.9	-
Lignin content	143	g/l
Dry Matter	32	%

Figure 1 shows the titration curve of the BL. The titration curve is well in accordance with data from literature, where neutralisation of the hydroxide ions is followed by the actual precipitation of lignin and sulphide neutralisation. [4]

3.2 Precipitation

As expected, the time required to reach the target pH of 9.1 was significantly longer when dilute CO_2 was used compared to pure CO_2. Usage of dilute CO_2 leads to foam formation at the beginning of neutralisation, but throughout the experiment the foam layer does collapse. Figure 3 summarizes the pH gradient and the CO_2 concentration in the feed gas and purge gas for the precipitation experiments.

Analysis of the filtrate showed, that with dilute CO_2 26.3% and with pure CO_2 48.5% of the available lignin were precipitated.

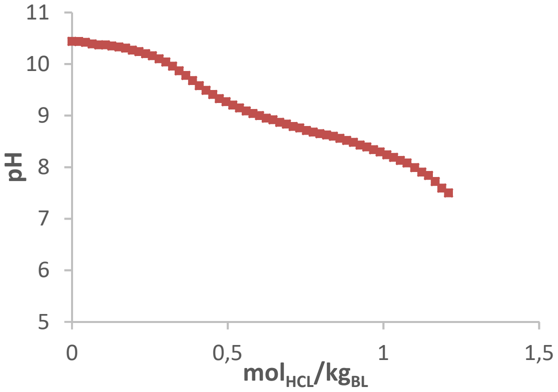

Figure 1: Titration profile of black liquor at 70°C

3.3 Filtration

The specific filter cake resistance for precipitates formed with pure as well as dilute CO_2 is $2.4 \cdot 10^{12}$ 1/m².

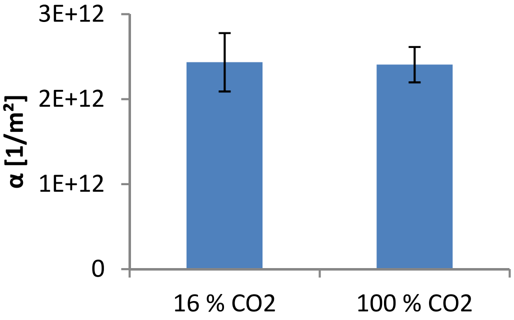

Figure 2: Specific filter cake resistance of the precipitated lignin

4. DISCUSSION

Results show that lignin precipitation performed with dilute CO_2 is possible. Foaming is observed at the beginning of the precipitation but stops at conditions for continuous processing. Lignin precipitation with dilute CO_2 takes longer compared to pure CO_2, but the target pH of 9.1 was reached within an hour. After cooling to 25°C, the pH differs slightly. The

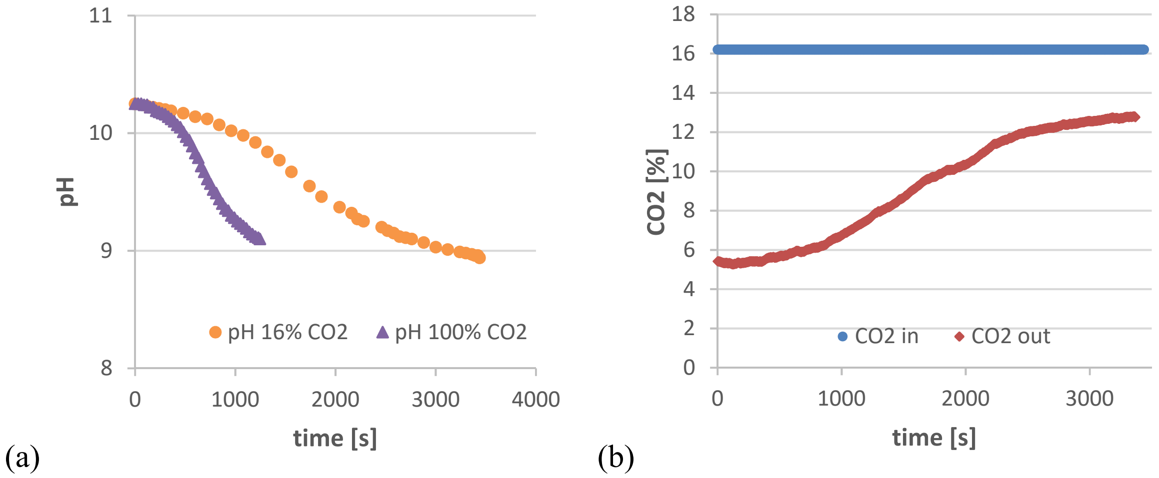

(a) (b)

Figure 3: (a) pH versus time, T = 70°C, orange dots = 16% CO_2, purple triangles = 100% CO_2; (b) CO_2 concentration versus time, blue line = $c_{CO2,\ in}$ red line = $c_{CO2,\ out}$, T = 70°C.

experiment with 100% CO_2 led to a pH after cooling of 10.62 and the experiment using 16 vol% CO_2 led to a pH of 10.78. The pH difference results in the different yields.The CO_2 concentration and the increased residence time in the precipitation reactor do not affect the filtration properties of the lignin. Results imply that the precipitation with flue gas is possible and they are the basis for further investigations to develop a continuous lignin precipitation/isolation process.

5. ACKNOWLEDGEMENTS

The K-Project Flippr² (861476) is funded as part of COMET - Competence Centers for Excellent Technologies promoted by BMVIT, BMWFJ, Styria and Carinthia. The COMET program is managed by FFG.

6. REFERENCES

[1] P. Tomani, “The Lignoboost Process,” *Cellul. Chem. Technol.*, vol. 44, no. October 2005, pp. 53–58, 2010. Journal Reference

[2] L. Kouisni, P. Holt-Hindle, K. Maki, and M. Paleologou, “The LignoForce System: A new process for the production of high-quality lignin from black liquor,” *Pulp Pap. Canada*, vol. 115, no. 1, pp. 18–22, 2014. Journal Reference

[3] H. Wallmo, T. Richards, and H. Theliander, “An investigation of process parameters during lignin precipitation from kraft black liquors : A step towards an optimised precipitation operation,” *Nord. Pulp Pap. Res. J.*, vol. 24, pp. 158–164, 2007. Journal Reference

[4] H. Wallmo, T. Richards, and H. Theliander, “Lignin precipitation from kraft black liquors: kinetics and carbon dioxide absorption,” *Pap. ja Puu*, vol. 89, no. 7–8, pp. 436–442, 2007. Journal Reference

Measuring ink spreading and penetration for high speed inkjet printing

SARAH KRAINER[1,2] and
ULRICH HIRN[1,2]

[1]Institute of Paper, Pulp and Fiber Technology, TU Graz, Austria
[2]CD Laboratory for Fiber Swelling and Paper Performance, Graz, Austria

1 INTRODUCTION

In this study High Speed Inkjet (HSI) ink penetration is investigated. In HSI printing the penetration speed and wetting of the ink is important, especially at short timescales. Therefore, the use of measurement techniques which can capture these parameters at short timescales is advisable. Four measurement techniques are evaluated: Penetration Dynamics Analyzer (PDA), Fibro – Contact angle measurement, IGT – Penetration Test and Automatic Scanning Absorptometer (ASA). These test the liquid / paper behaviour using different principles of measurement. We want to compare the techniques and evaluate the plausibility of the results from these different instruments.

HSI inks are complex mixtures containing different components influencing the properties of the ink. Water serves as carrier, additionally colourant, binder, solvents and surfactants are the most common ingredients [1]. Each component affects the behaviour of the ink on the paper and complicates the understanding of ink absorption into paper [2],[3]. For better understanding of the effect of HSI printing ink composition on penetration and spreading, we have studied four model liquids.

2. MATERIALS AND METHODS

Four water based model liquids have been selected with respect to their viscosity and surface tension. The goal is to achieve model liquids which behave as much as possible like inks on the paper. The tested model liquids are pure water, 80% water/20% glycerol, 80% water/20% glycol and 50% water/40% glycerol/10% hexanediol. These are compared to three different types of HSI ink. The first type is a dye ink, the second one a pigment ink and the third one is an ink containing latex particles. Every measurement has been made with two colours of each ink-type: yellow and magenta.

Same as for inks, the paper grade significantly influences the penetration process. Therefore we have tested the performance of the model liquids on three different woodfree, uncoated, fine papers from an industrial supplier. These papers are an unsized HSI paper grade, an HSI unsized pigmented paper and an AKD sized paper.

The PDA measures the speed of liquid penetration into the paper. An ultrasonic emitter and ultrasonic receiver are placed to the opposite of each other, shown in Figure **1**. When the sample is released into the testing cell, filled with liquid, the transmitter instantly starts to transmit signals through the sample. These are reflected, scattered or absorbed during the process of liquid penetration, represented through the red lines in Figure **1**. As penetration proceeds, the receiver records the changes in the signal [4]. The results for the AKD sized paper are shown in Figure ***4***.

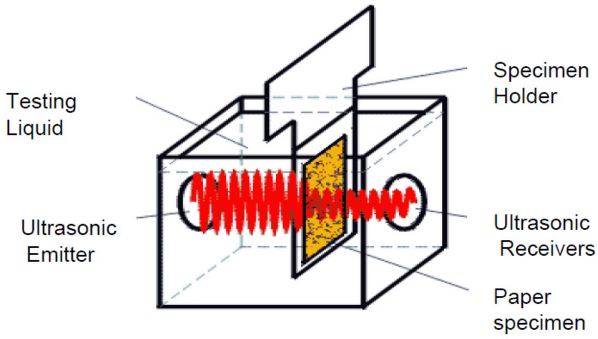

Figure 1: Drawing of the PDA testing cell, paper specimen and sample holder

The curves are the average of 10 measurements for each liquid The faster the liquid penetrates into the paper, the higher is the change in intensity and the steeper is the slope of the curve. The second parameter measured by the PDA is the time at the highest intensity (wetting time in Figure 4), which represents the wetting. The longer it takes to reach 100% intensity, the slower is the wetting. The contact angle measurements were performed according to TAPPI standard T558 using a FIBRO DAT 1100 instrument [5], [6]. The Fibro contact angle instrument creates drops with a volume of 4 µl. Once the drop is released onto the substrate's surface, it starts taking pictures of the drop, shown in Figure *2*. The software of this measurement instrument fits a tangent at the droplet's surface at the contact point of paper and liquid and calculates the contact angle. This is done for every picture the camera has taken. The results are plotted in a curve, which shows the calculated contact angle over time (Figure 5). These curves are the average of results from about 80-100 drops per liquid.

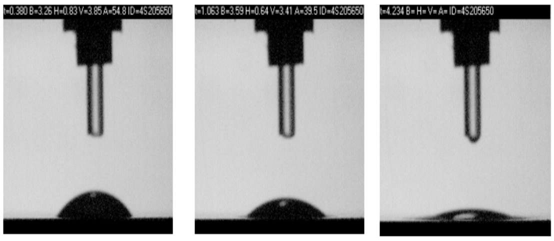

Figure 2: Drop pictures of the contact angle measurement

The change of contact angle occurs due to penetration and spreading of the droplet. The higher the change of the contact angle is, the faster is the spreading and the steeper is the slope of the curve displayed in Figure **5**.

The IGT Printing Ink Penetration Test measures the speed of liquid uptake dynamically. We have carried out the work according to standard NEN 1836-1:2006 [7]. 16 paper strips have been measured per liquid. A drop of a defined volume of the printing ink or the model liquid is placed on a roll, sketched in Figure 3a. The roll and the paper are moving forward with increasing speed. The drop is pushed forward in the nip between roll and paper and simultaneously absorbed in the paper. As a result the ink or model liquid forms a blob on the paper strip. The faster the ink penetrates, the shorter is the blob. Another parameter is the aspect ratio i.e. ratio between blob width and blob length. The higher the wetting, the higher is the aspect ratio. Three representative blobs for the model liquids water/glycerol, water/glycerine/hexandiol and for one ink are shown in Figure 3b. The yellow blob of the ink has the highest penetration speed, represented by the shortest length.

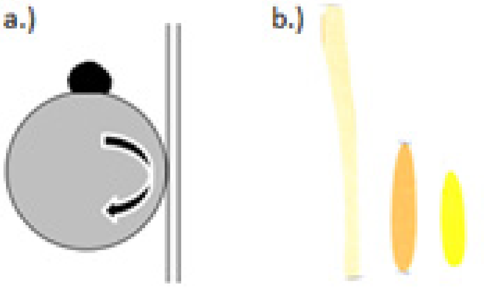

Figure 3: a.) IGT instrument: roll with liquid drop and paperstrip b.) blobs of water/glycerin, water/glycerin/hexandiol and ink

The ASA (Automatic Scanning Absorptometer) setup provides quantitative information about the liquid absorption as a function of time on time scales of 10 ms up to 10 s. During an ASA measurement, liquid is supplied from a scanning head which moves along a spiral path, shown in Figure **7**. In Figure **8** one can see the head on the paper samples surface, supplied with the liquid via a tube. The speed is kept constant over a certain part of the track, after it will accelerate to the next constant speed [8],[9]. In this way the system measures the liquid penetration at different times of contact between the nozzle and the paper. Two parameters are defined: the penetration speed (slope of the curve) and the absorbed amount of liquid, which is measured.

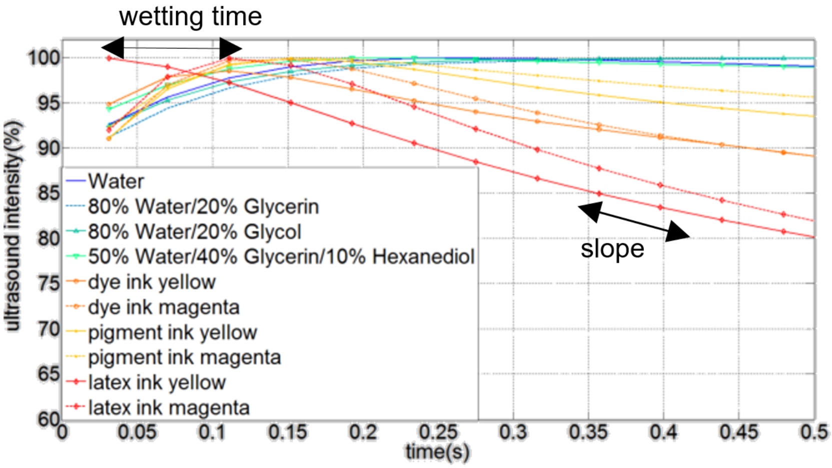

Figure 4: The PDA results show the change of ultrasound intensity over time. We define the time to the highest signal intensity as the wetting time of the liquid and the slope of the curve as the penetration speed of the liquid into the paper.

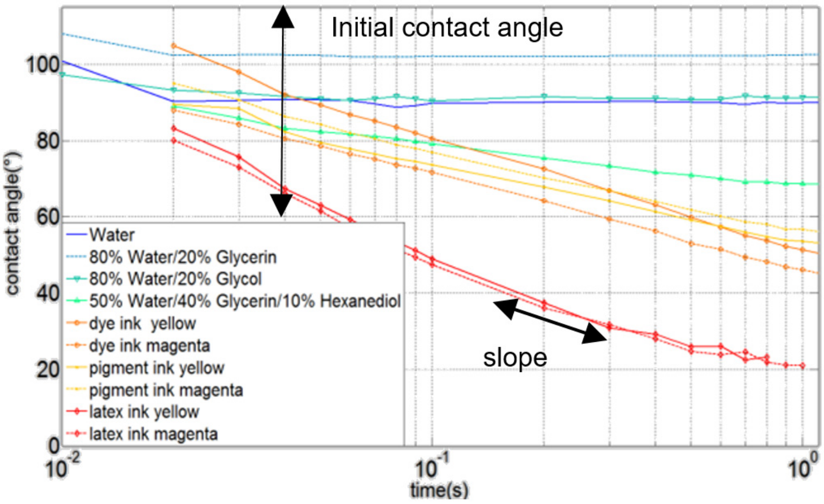

Figure 5: The contact angle as a function time. The initial contact angle is defined as the value at 0.05s. The slope of the curve between 0.02s and 0.09s represents the wetting of the liquid on the paper surface.

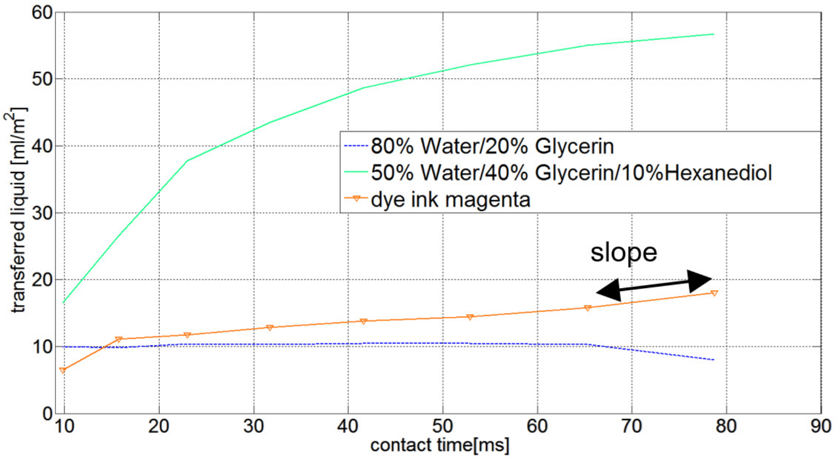

Figure 6: ASA - Measurement results show the absorbed amount of liquid over time. The slope of the curve represents the penetration speed.

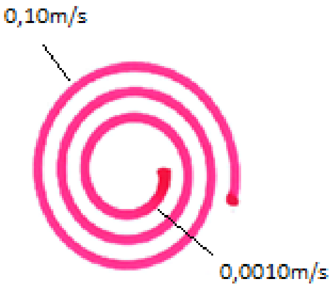

Figure 7: spiral path of the ink on the paper. Highest speed is at the outer side of the spiral and the lowest speed at the inner side.

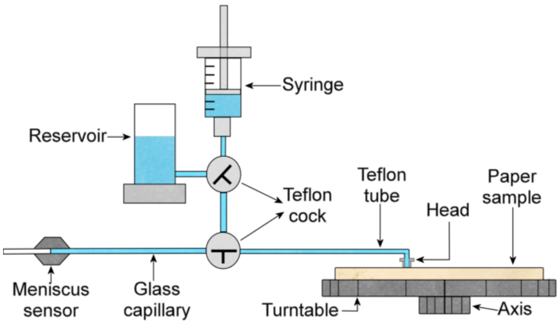

Figure 8: Drawing of the Automatic Scanning Absorptometer set up. The head on the paper sample is supplied with the liquid via a tube. The meniscus sensor measures the amount of liquid, which is absorbed in the paper.

3. RESULTS

Figure 4 shows the results of the PDA Measurement. The slope of each curve is an indicator for the penetration speed of the liquid. The wetting is represented through the time to the highest signal intensity. The inks of one type behave similar, their curves nearly overlap which indicates good repeatability for this measurement technique. The four model liquids have the lowest penetration speed represented by the flat slope of these curves. Comparing these to the ASA results one can see that the model liquids also have the lowest penetration speed for this measurement. The model liquids have the highest wetting time, in contrast to that the latex inks have the lowest value for this parameter. These observations correspond to the contact angle measurement (shown below). The model liquid with hexandiol fits fairly well to the dye ink, the slope of this model liquid and of the dye inks are close to each other. Also the wetting time is similar.

In Figure 5 the contact angle measurement results are displayed. The initial contact angle is defined as the value measured after 0.05 seconds and the wetting of the liquids is indicated by the slope of the curves. The inks of one type show similar results, i.e. equivalent curves which again indicates good repeatability of the measurement. The wetting represented by the slope of each curve is for all model liquids lower than for the inks. The latex inks have the fastest wetting, i.e. the steepest slope. This results correspond to observations from the PDA. Furthermore, one can see that the model liquids without hexanediol have an almost constant contact angle, which indicates very slow wetting. The model liquid with hexanediol again shows similar behaviour like the HSI inks.

The IGT results do not correspond to the PDA and contact angle measurement results. The aspect ratio does not show the same tendency for the wetting of the papers as the other techniques. Also the blob length, which represents the penetration speed does not confirm the results from the PDA and the ASA. The blob length is the shortest for the AKD sized paper. This shows the strongest penetration. The aspect ratio is the highest for this paper, which would suggest the highest spreading. The AKD sized paper should have the slowest wetting and the lowest penetration speed, as detected by the other measurements. Therefore we conclude that the IGT measurement does not deliver useful results.

The ASA measurement results are shown in Figure *6*. The absorbed volume of liquid is directly measured by the system. The slope of the curve represents the penetration speed. The ASA results show the highest penetration speed for the printing ink and the lowest one for the glycerine/water mixture. The horizontal, at times even negative slope of the water/glycerine liquid is curious. It is not plausible that the penetration speed is zero or even negative. We believe that that this effect is due to the effect of surface roughness, which drags fluid away under the measurement nozzle and thus adds to the measured liquid consumption without actual penetration into the paper.

Due to lack of space it is not possible to show the results of the four instruments for the unsized and the pigmented paper. The outcomes of these measurements however essentially gave the same results as described for the AKD sized paper.

4. CONCLUSIONS

From the measurements of the four instruments, we have defined parameters describing the wetting of the liquid (responsible for ink spreading) and for penetration speed of the liquid. For the PDA we use the slope of the curve as indicator for the penetration speed and the time at the highest intensity as an indicator for the wetting. For the contact angle measurement the slope of the curve represents the wetting of the liquid and the initial contact angle was determined after 0.05 seconds. The ASA measures the transferred liquid volume and the slope of the result curve represents the penetration speed.

For the sample size and the number of samples investigated in this study all four instruments show good repeatability.

For the model liquids the results show that the mixtures glycerol-water and glycol-water behave quite similar to water. The mixture water/glycerine/hexandiol behaves very similar like the HSI dye inks. This liquid is more similar to the pigment and latex inks than the other model liquids, but still not as suitable as for the dye inks. Summarized the model liquid with hexanediol fits well with the dye inks and is an appropriate model liquid for mimicking the penetration and wetting of these inks.PDA and ASA measurement deliver similar results for the penetration speed. The model liquids have slower penetration speed than the HSI inks. For wetting (ink spreading) PDA and contact angle showed similar results, the printing inks had strongest wetting. The IGT measurements gave implausible results, indicating that this technique is not suitable for measuring penetration speed or wetting of HSI inks.

5. BIBLIOGRAPHY

[1] C. Schmid, “Formulation and Properties of Waterborne Inkjet Inks,” in The Chemestry of Inkjet Inks, S. Magdassi, Ed. World Scientific Publishing Co. Pte. Ltd., 2010, pp. 123–140.

[2] J. Blechschmidt, Taschenbuch der Papiertechnik. Carl Hanser Verlag München, 2013.

[3] U. Lindqvist, L. Hakola, J. Heilmann, B. Zhmud, and E. Wallström, “Interaction Characteristics in Different Applications of Ink- Jet Printing,” TAGA J., vol. 2, p. 99 ff, 2006.

[4] Y. J. Lee, J. J. Pawlak, O. Rojas, and J. Skowronski, “Paper and paper machine variables affecting the attenuation of ultrasonic signals during wetting,” in Int. Paper Physics Conference, 2007, pp. 143–148.

[5] The TMI Group of Companies, “DAT Dynamic Absorption Tester Model 68-96 DAT Dynamic Absorption Tester Model 68-96,” 2015.

[6] A. Hladnik, “Dynamic wetting and liquid sorption in paper - FIBRO 1100 DAT measuring,” Papier, vol. 25, no. (3-4), pp. 44–48, 1997.

[7] NN, “IGT Information Leaflet W24 ‘Print Penetration’. IGT Testing Systems,” IGT Testing Systems, 2006. [Online]. Available: http://www.igt.nl/EN_bestanden/W_information_leaflets/W24.pdf,

retrieved Oct 7th 2016.

[8] T. Enomae, H. Kataoka, F. Onabe, D. Papier, and J. Robertson, “In-Plane Distribution of Paper Absorbency Measured by Liquid Absorption Profilometer.,” Sen’i Gakkaishi, vol. 55, no. 2, pp. 265–291, 2004.

[9] T. A. P. Van Stiphout, “Liquid Absorption in porous Media studied by Automatic Scanning Absorptometer,” Eindhoven University of Technology, 2016.

3D-Cellulose Mouldings: Dewatering Behaviour and Process Optimisation

R. KLEINERT, T. GAILAT and
H. GROSSMANN

TU Dresden
Institute of Natural Materials Technology,
Professorship of Wood Technology and
Fibre Materials Technology
rene.kleinert@tu-dresden.de

1 INTRODUCTION

Against the background to generate higher added values out of cellulose fibres the Professorship of Wood Technology and Fibre Materials Technology, TU Dresden initiated different projects* aiming at exploiting new potential applications predominantly in lightweight construction, automotive industry and possibly in medical technology.

In several publications [1, 2, 3] it was demonstrated that a highly fibrillated cellulose pulp called FibCell – developed in collaboration with a mill for speciality papers – was processed by shaping technologies like Pressure-Filtration or Thermo-Pressing in order to produce test specimens for strength analyses. The resulting specimens (tubes and bars, see Fig. 1) consisting of 100 % natural fibres, achieved Young's moduli up to 11.4 GPa and tensile stresses up to 89.0 MPa which is superior to all polymers and most bio-derived composites. Additionally the dense structure of this material (density = approx. 1.5 g/cm³) results in excellent barrier properties against oxygen and grease as well as good electrical insulation resistance. These properties can only be brought to bear after dewatering and drying highly diluted FibCell suspensions which is not only energy and time consuming but inevitably accompanied by cumbersome and hard-to-control shrinking phenomena with the existing laboratory process technology.

Figure 1. Test specimens from highly fibrillated wood cellulose fibres (FibCell)

2 OBJECTIVES

While the aim of the first research projects was to produce specimens and to characterise the FibCell material the investigations described in this paper focussed on improving the manufacturing process in terms of productivity, energy efficiency and quality consistency. Analyses of the two main process steps – simultaneous dewatering/shaping and subsequent thermal drying – show that the latter process step is the most time and energy consuming part.

As the energy demand for thermal drying is strongly affected by the initial dry content, the main objective was not only to accelerate the mechanical dewatering process but as well to increase the resulting dry content. The focus, therefore, was to determine the impacts of the relevant process parameters and to develop a model of the dewatering step. Optimisation measures derived from the model should provide the base for an advanced technical design of a new and innovative laboratory device for processing FibCell suspensions into mouldings.

3 MATERIAL

With an annual production of approx. $1.5 \cdot 10^{12}$ tons cellulose is the most abundant polymer on earth [4, 5]. Cellulose is renewable, biodegradable and can be physically and chemically modified in many different ways. This makes it an

---

* ZIM KF 2418621 / ZIM ZF 4100904

alternative generally suitable to substitute a broad variety of far less environmentally compatible materials, like e. g. synthetic polymers, in different applications supporting the envisaged development towards a bio-economy.

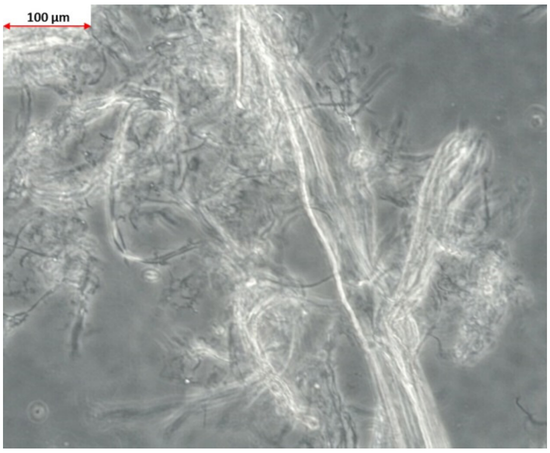

Figure 2. Microscopy picture of FibCell pulp used within this project for the production of cellulose mouldings [3]

Characterised by a low density of 1.54 g/cm³ in combination with a very high theoretical Young's modulus from 124 GPa up to 155 GPa (calculated for crystalline cellulose), cellulose definitely meets the requirements of lightweight construction materials [6, 7].

In order to develop high-strength, pure cellulose mouldings it seemed reasonable to utilise a cellulose fibre pulp with a high content of fibrils providing a high specific surface for the creation of hydrogen bonds in the dried product. The fibre pulp which was – after many trials – used for the investigations was a specially treated NBSK (Nordic Bleached Softwood Kraft) pulp normally used for the production of special packaging papers. It was prepared in conical refiners to a Schopper Riegler Value (beating degree) of over 85 SR which is equivalent to a Canadian Standard Freeness (CSF) level lower than 100 ml. Fig. 2 shows a microscopic image of this pulp called FibCell depicting its high amount of fibrils and fines as well as the existence of longer fibres and fibre fragments.

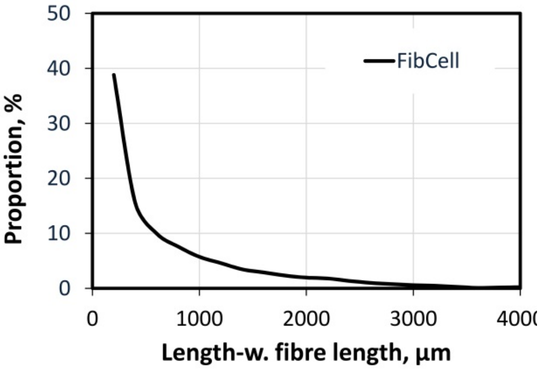

Figure 3. Length-w. fibre length distribution of FibCell pulp [8]

The length-weighted fibre length distribution of FibCell pulp is illustrated in Fig. 3 and confirms the presence of longer fibres as a not negligible part of an otherwise highly fibrillated pulp. The mean length-w. fibre length is 921 µm. The initial dry content of the FibCell suspension was 3 % for all trials.

4 METHODS

To evaluate the relevant parameters and to exemplary describe their specific impact on the dewatering process of FibCell, trials were performed with the *Voith FiberXPress* (see Fig. 4).

By means of the Design of Experiments (DoE) method the variables pressure, temperature and grammage were analysed in the following limits:

- temperature: 20...55...90 °C
- pressure: 0.1...0.55...1.0 MPa
- grammage: 1.0...1.5...2.0 kg/m²

Figure 4. Voith FiberXPress

The target variable was the required dewatering time to reach a dry content of 5, 10 and 20 % respectively. At a dry content of 20 % the shaped mould is already dimensionally stable and can be dried in a more efficient way due to the lower amount of energy for heating up the water. In additional trials best conditions were chosen to identify the maximum dry content which is achievable by mechanical means in the *FiberXPress*.

For modelling the dewatering process according to DoE a fractionated factor plan (see Tab. 1) was used to minimise the number of trials.

Run	3**(3-1) fractionated factor plan			
	x_1 temp.	x_2 pressure	x_3 gsm.	y dry content
1	-1	-1	-1	y_1
2	-1	0	1	y_2
3	-1	1	0	y_3
4	0	-1	1	y_4
5	0	0	0	y_5
7	0	1	-1	y_6
7	1	-1	0	y_7
8	1	0	-1	y_8
9	1	1	1	y_9

Table 1. Fractionated factor plan to investigate the impact of variables temperature, pressure and grammage on the required time for dewatering

5 RESULTS AND DISCUSSION

The impact of the most relevant variables, i.e. temperature, pressure and grammage, on the mechanical dewatering of FibCell suspensions was analysed by the DoE method. With the data obtained from the trials the process model was developed using *Statistica13* software. Fig. 5 shows the correlation between values predicted on the basis of the calculated model and those values recorded during the trials. It was found that the model correlated very well within its defined limits. This indicates that the results are reliable.

The model allowed to determine the main effects of the variables on the dewatering process. They are highlighted in Fig. 6.

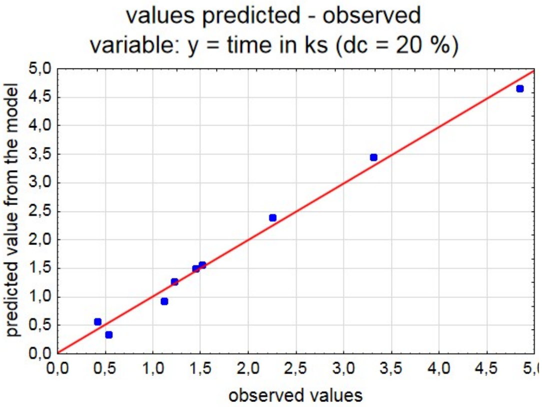

Figure 5. Correlation between predicted values of the model and observed values from trials

The Pareto diagram indicates that the grammage of the resulting moulding – which strongly correlates with its thickness and porosity – has the highest impact on the dewatering time. With a linear effect higher than 2 and a quadratic effect of 0.7 an increase in grammage will lead to a significantly longer dewatering time to reach a certain dry content. Also the temperature showed a strong impact on the dewatering, which is predominantly a consequence of the pronouncedly temperature-dependant viscosity of water. By reducing the viscosity of the water at elevated temperatures the flow-off from the fibre lumen and dwelled fibre wall could be enhanced.

During dewatering/shaping the linear effect of temperature is twice as high as that of pressure. This confirms the results of *WAHLSTROM* [9, 10] that a strong increase

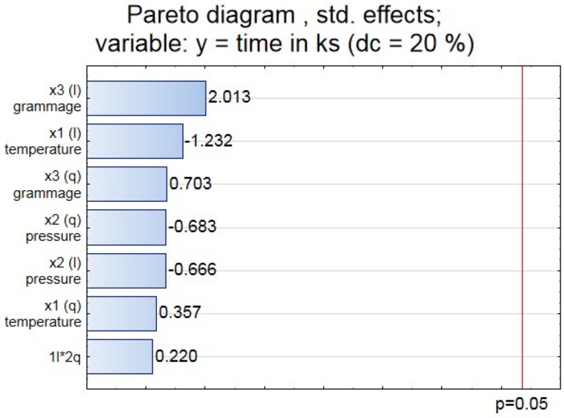

Figure 6. Pareto diagram with standardised effects of the investigated variables on the required time for dewatering until a dry content of 20 % (y)

in pressure will not lead to an equally strong increase of dewatering. The dry content will rather tend to approach a certain limit asymptotically. Fig. 7 shows the required time for mechanical dewatering of FibCell up to 20 % dry content as a function of temperature, pressure and grammage. In each case one variable is constant. At a constant grammage of 1.5 kg/m² (see Fig. 7a) it is evident that an increase in temperature accelerates dewatering. The same applies to an increase in pressure but here this effect is even stronger at elevated temperatures. For the production process of FibCell mouldings, therefore, a high temperature (close to 100 °C) is indispensable to reduce the production time to the largest extent. At a constant pressure of 1 MPa (see Fig. 7b) the remarkable impact of temperature and especially grammage is obvious. It can be seen, that the dewatering time strongly increases with increasing grammage as a result of the higher filtration resistance. Aiming at reducing the filtration resistance during moulding production the constructive process design needs to enable a mechanical dewatering in all directions.

Fig. 7c illustrates the time for dewatering as a function of pressure and grammage at a constant temperature of 70 °C.

It shows that the impact of grammage greatly exceeds the impact of pressure. The fastest dewatering in the shaping step up to 20 % dry content could be achieved with a combination of low grammage (1.0 kg) and high pressure (1.0 MPa).

Based on the findings of these trials further investigations were made to identify the highest possible dry content of FibCell by mechanical means. A FibCell fibre mat with a grammage of 1 kg/m² was pre-pressed at 90 °C and at a pressure of 1 MPa until a dry content of 20 % was reached. The time for pre-pressing was between 300 s and 400 s. In the following main pressing step the pressure was stepwise increased from 1 to 9 MPa, the latter being the maximum pressure which can be exerted by the *FiberXPress* device. Under these conditions a dry content of almost 68 % was achieved within 20 min. But already at a pressure of 5 MPa the final dry content was 63 %. This is by far more efficient than what can be achieved with standard lab equipment and offers a wide range for process optimisation including:

- high process temperature
  (decrease in water viscosity)
- dewatering in all directions during the shaping step
- controlled pressures up to min. 5 MPa.

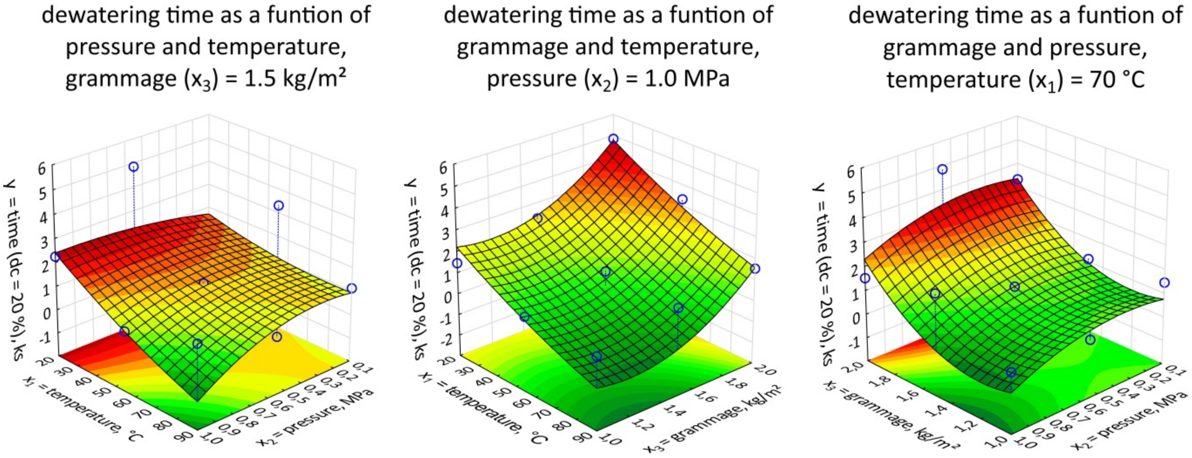

Figure 7. Required time for the mechanical dewatering depending on temperature, pressure and grammage, (a) at constant grammage = 1.5 kg/m², (b) at constant pressure = 1.0 MPa and (c) at constant temperature = 70 °C

6 CONCLUSIONS

With a density slightly higher than half of that of aluminium and 80 % lower than that of steel it appears surprising that pure cellulose has not yet really fallen in the crosshairs of materials scientists. The main drawback is that – according to the state-of-the-art technology – the superior strength properties of cellulose will only be brought to bear after dewatering and drying highly diluted suspensions of strongly fibrillated cellulose fibres.

Until now the production of 3D cellulose mouldings is not only energy and time consuming but inevitably accompanied by cumbersome and hard-to-control shrinking phenomena. The results of this work show that there is a considerable potential for process optimisation which would allow to process cellulose suspensions in a far more reasonable way. According to these findings it is crucial to allow dewatering in all directions through the entire inner surface of the mould cavity. It is equally important to maintain the highest possible temperature (lowest viscosity of the water) throughout the whole pressing process in order to achieve the maximum dry content in a reasonable time and to reduce shrinking phenomena as well as energy consumption of the final drying stage. Further work will focus on process design, material formulation and a sustainable extension of the material properties.

ACKNOWLEDGEMENT

This work was performed on the basis of research projects financially supported by the Federal Ministry for Economic Affairs and Energy. We thank the German Bundestag, the AiF Project GmbH and our collaborating partners.

Supported by:

Federal Ministry
for Economic Affairs
and Energy

on the basis of a decision
by the German Bundestag

REFERENCES

[1] R. Kleinert, H. Grossmann, T. Gailat, P.-G. Weber and I. Greiffenberg. Alternative Applications for biogenic Cellulose Fibres. *ipw*. **10**: 30–34 (2015).

[2] R. Kleinert, H. Grossmann, T. Gailat, P.-G. Weber and I. Greiffenberg. New Application Areas for Cellulose Fibres. *Papir*. **15**: 43-46 (2016).

[3] R. Kleinert, H. Großmann, T. Gailat. New Applications - 3D Mouldings from Cellulose Fibres. Tappi 2016 PEERS Conference, Jacksonville, Tappi Press, (2016).

[4] A. Steinbüchel, E. Vandamme and S. De Baets (Eds.) Biopolymers Vol. 6: 290–292, Wiley-VCH, (2002).

[5] D. L. Kaplan (Ed.) Biopolymers from Renewable Resources. Springer-Verlag, Edition 1, (1998).

[6] F. A. M. Rizk and G. N. Trinh. High Voltage Engineering. CRC Press, edition 1, (2014).

[7] F. Tanaka and T. Iwata. Estimation of the elastic modulus of cellulose crystal by molecular mechanics simulation. *Cellulose* **13** (5): 509-517 (2006).

[8] R. Kleinert and S. Heinemann. Properties of high-fibrillated cellulose fibres for 3D-Moulding affecting the drying process. Presentation at *Paper&Biorefinery Conference,* Graz, (2017)

[9] B. Wahlstrom. Opportunities in pressing Part I. *Tappi J.* **64** (1): 75–78 (1981).

[10]B. Wahstrom. Opportunities in pressing Part II. *Tappi J.* **64** (2): 57–60 (1981).

Hydrophobic paper as functional construction material

FELIX SCHÄFER and
MARKUS BIESALSKI

Technische Universität Darmstadt,
Macromolecular Chemistry
and Paper-Chemistry
Alarich-Weiss-Straße 8, 64287 Darmstadt,
+49-6151-16-23733,
schaefer@cellulose.tu-darmstadt.de

1 INTRODUCTION

Over the last years sustainable and environmental friendly materials have increasingly moved into the focus of scientific research. In line with this trend, the project “BAMP! – building with paper” was recently established at TU Darmstadt. The goal of this interdisciplinary collaborative research project is to use paper as a light-weight construction material for building temporary housings. Versatile properties of paper, such as very high specific tensile strength, low density and recyclability are beneficial for the development of such bio-based construction materials. However, paper also has some limitations, such as hydrophilicity and flammability, which need to be overcome for any successful approach in using paper as such [1]. The main focus of this sub-project within BAMP! is centred around possible solutions for these limitations, without losing the above mentioned mechanical properties. In the literature, already some solutions of paper hydrophobication exist, such as the lamination of the paper with hydrophobic polymers [2] or the application of halosilane coatings [3]. However, all existing methods show certain restrictions such as delamination, poor biodegradability or high toxicity.

To obtain a first understanding how a polymer interacts with the cellulose fibres, a polyurethane (PU) polymer is coated onto the paper surface. Polyurethane polymers are formed via a polyaddition of a di- or poly-isocyanate with a polyol. The advantage of using a polyurethane as the coating polymer is, that during the polyaddition reaction the isocyanate group can also react with the hydroxyl groups of cellulose [4]. Through this, a covalent bond between polyurethane and the fibres is accomplished, which would negate the process of delamination. This introduced polymermatrix now needs to be examined on how it influences the properties of the cellulose fibres like tensile strength, bending stiffness and hydrophobicity. In addition, analysis ought to be made, to verify if the polymer is bond to the fibre and to what extent.

Although the analysis of the macroscopic properties of the modified cellulose is relatively easy from an experimental point of view, the verification of the covalent bond is highly complex. Since the structure of the carbamate link between the isocyanate and the polyol and the link of isocyanate and the hydroxyl group of cellulose is broadly similar, it can’t be distinguished by trivial means. Thus, different approaches need to be developed to determine the bond between cellulose and polymer.

2 MATERIAL

For the research of the behaviour of polyurethane on the cellulose fibres two different kinds of fibres were used: Long cellulose fibres from pine wood pulp and short fibres from a eucalyptus tree. The formulation used for the coating of the papers was provided by *MC Bauchemie*. The coating is a two component system of which both compounds were dissolved in toluene and applied via spray coating. Thereby the ratio of polyol to diisocyanate was differed to observe an influence of isocyanate excess. The applied coating was analysed via scanning electron microscopy (SEM). To determine the covalent bond between cellulose fibre and polymer the fibres were modified with hexamethylene diisocyanate (HDI). The unbound isocyanate on the paper fibres were first extracted and the attached isocyanates hydrolysed to a secondary amine. To these both a 5-carboxy-X-rhodamine-N-succinimidylester or fluorescein isothiocyanate (FITC) were attached and the unreacted molecules were extracted. Through this modification, the remaining amount of diisocyanate could be determined via fluorescent confocal microscopy.

3 RESULTS

3.1 Determination of covalent bonds

For verification of the covalent bond between cellulose fibres and polyurethane a model system needed to be found, in order to distinguish the urethane linkage of fibre and isocyanate from polyol and isocyanate, respectively. Therefore, the attached isocyanate was first functionalised with a fluorescent molecule before linkage to paper fibres. This was carried out, because the functionalisation of the fibres with diisocyanates and the amination couldn’t be analysed via infrared microscopy, due to the strong IR-signals of the cellulose substrate itself. These signals overlapped with the ones of isocyanate/amine compound and the functionalization couldn’t be verified.

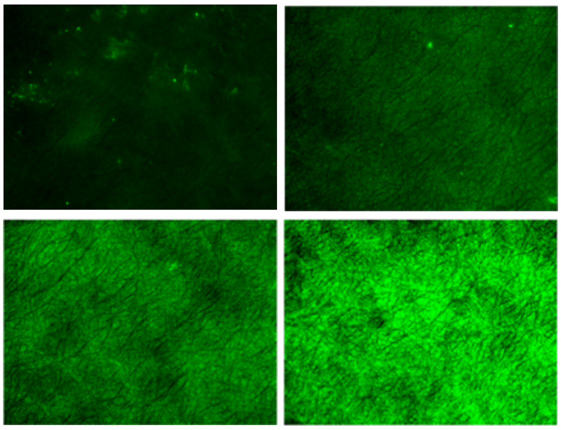

Figure 1. With fluorescein isothiocyanate (FITC) functionalised papers analysed with confocal microscopy. Reference paper (top left), 1 wt-% (top right), 2 wt-% (bottom left) and 5 wt-% diisocyanate in correlation to paper mass (bottom right).

To bypass this problem, measurements with confocal microscopy were conducted. As displayed in the following Figure 1 the fluorescence of the functionalised paper increases with higher amounts of isocyanate.

Thereby, the intensities of the fluorescence were processed and set into correlation with the other modified papers. These results show, that the fluorescent molecule was successfully covalently attached, because of the increase of fluorescence with increasing diisocyanate content on the papers (Figure 1). The small amounts of fluorescence in the reference paper results from the autofluorescence of the fibres. This is caused by natural molecules that remained on the cellulose fibres (e.g. lignin) and have no impact on the other results.

3.2 Visualisation of PU-coating

To determine further on how the polyurethane coating interacts with the cellulose fibres, paper substrate surfaces were analysed by scanning electron microscopy.

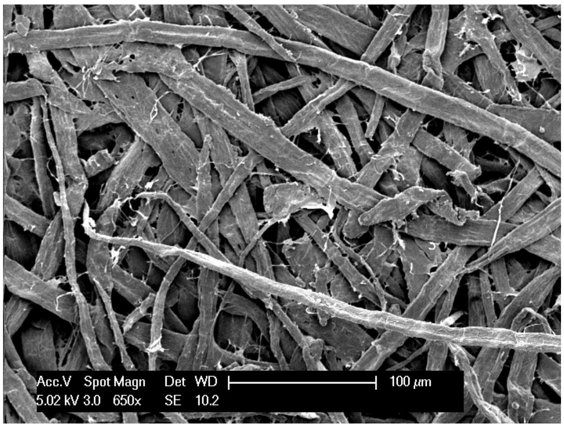

Figure 2a. SEM image of uncoated eucalyptus paper

By comparing the images of both, modified and non-modified paper substrates, it is noticeable that, by applying the coating onto the paper no continuous film was created. Rather each fibre was coated individually. The coating of each fibre results in a minimisation of the hydrophilicity of the paper. The verification of the increase in hydrophobicity is reviewed in the following section.

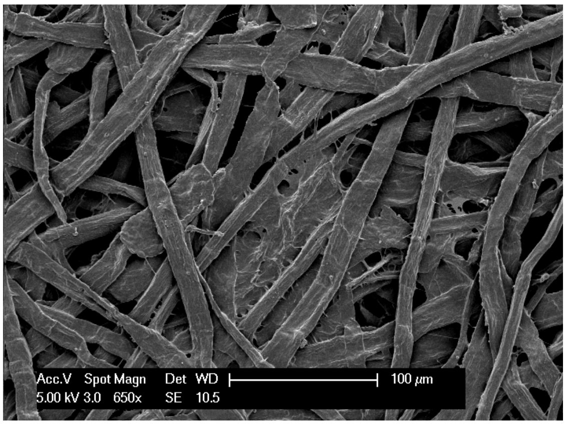

Figure 2b. SEM image of PU-coated eucalyptus paper

3.3 Change of paper properties

To observe the influence of the polyurethane coating on the two different cellulose fibres, tensile strength in wet and dry state, bending stiffness and the contact angles were measured. With the support of the *TexTest* Company it was also possible to measure the water tightness of some samples.

By comparing the measurements for the polyurethane coated eucalyptus and pinewood papers, it is noteworthy, that the tensile strength of both coated papers rises with increasing amount of coated polymer. The influence on the tensile strength of the variation of diisocyanate ratios cannot be determined, hence different results could not be shown for both cellulose fibres. In addition, it is to say that mechanical stability in wet state on both papers increased significantly (see Figure 3a/b).

For further characterization, the bending stiffness was measured. Thereby the bending stiffness also increased with rising amount of coated polymer.

By comparing the images of both, modified and non-modified paper substrates, it is noticeable that, by applying the coating onto the paper no continuous film was created. Rather each fibre was coated individually. The coating of each fibre results in a minimisation of the hydrophilicity of the paper. The verification of the increase in hydrophobicity is reviewed in the following section.

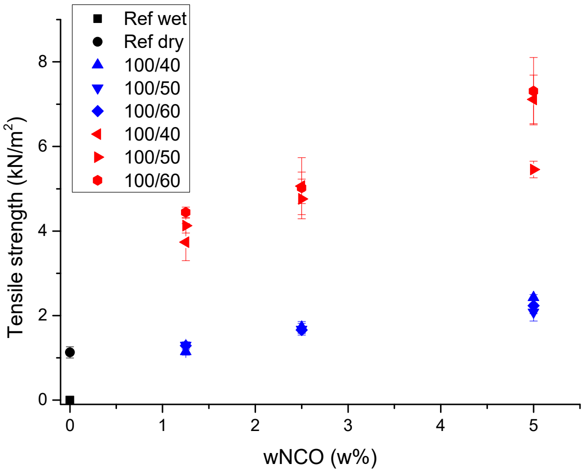

Figure 3a. Tensile strength measurements of polyurethane coated eucalyptus paper in dry (red) and wet (blue) state. Applied coatings formulations varied from 100/40 polyol-diisocyanate ratio to 100/60.

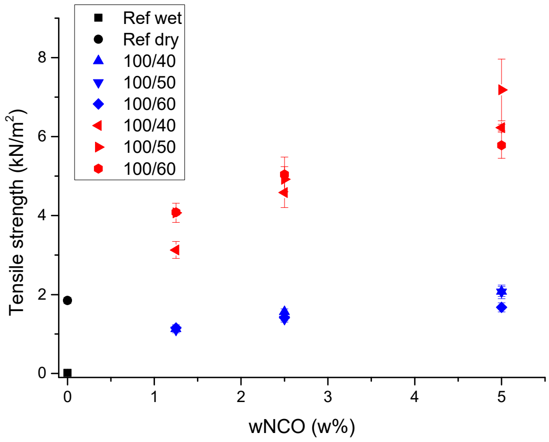

Figure 3b. Tensile strength measurements of polyurethane coated pinewood paper in dry (red) and wet (blue) state. Applied coatings formulations varied from 100/40 polyol-diisocyanate ratio to 100/60.

With these measurements, it was possible to determine that a very hydrophobic surface was obtained with the polyurethane coating. The static contact angle for eucalyptus papers reached a value of 123,5° (Figure 5) and 120° for pinewood papers, respectively. Uncoated papers, in comparison, could not be analysed, since the papers immediately absorbed the water droplet placed on top of the substrate. Neither the increase of coated polymer nor the variation of polyol-diisocyanate ratio had a significant influence on the contact

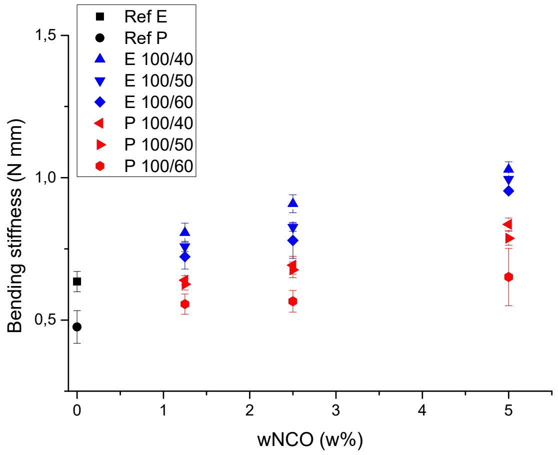

Figure 4. Bending stiffness of polyurethane coated pinewood (P red) and eucalyptus (E blue) papers. Applied coatings formulations varied from 100/40 polyol-diisocyanate ratio to 100/60.

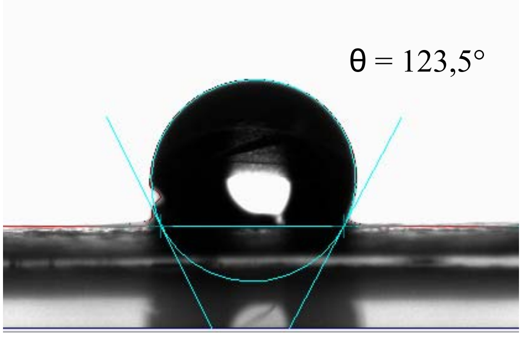

Figure 5. Contact angle measurement of polyurethane coated pinewood paper.

angle. Water tightness tests displayed a tightness of 75 mbar, which equals to a water column of 75 cm. Again, uncoated paper could not be measured with this method hence to its water absorption.

4 CONCLUSION

Within this research we could show, that it was possible to verify the formation of a covalent bond between diisocyanate and cellulose fibre. The correlation between increasing fluorescence with rising diisocyanate amount on the papers confirms the generation of the urethane linkage. Going further on the PU coated paper showed hydrophobic and reasonable water tightness properties. In addition, the mechanical properties of the papers have been enhanced.

5 OUTLOOK

For further research a method needs to be established, so that the used solvent toluene can be replaced with a more environmental friendly solvent like water. Also the analytic of the coated papers is going to be conducted further on with for example cross section SEM. Besides that the compatibility of the coating with the fire retardant or antimicrobial properties that are also going to be inserted into the papermatrix, in course of the BAMP!-project, needs to be tested.

REFERENCES

[1] D. Klemm, et al., Cellulose, chemistry and application. *Angew Chem Int Ed* 44 (2005): 3358-3393.

[2] J. Aenzer and K. Efimenko. Creating long-lived superhydrophobic polymer surfaces through mechanically assembled monolayers. *Science* 290.5499 (2000): 2130-2133.

[3] K.D. Lewis, J. Habermehl and W.J. Schulz. Biodegradable Hydrophobic Cellulosic Substrates and methods for their production using halosilanes. (2013).

[4] G. Odian, Principles of Polymerization, *Wiley* (2004): 130-134

Conference Program

Monday Oct 23rd, 2017

14:30	**Welcome**	W. Bauer / U. Hirn
	Session 1 Papermaking Fibers	
14:40	Exploiting Fibre Network Formation for Efficient Length-Based Separation of Cellulose Pulp	J. Redlinger-Pohn
15:00	Bleached pulp production from old corrugated carboards- kraft cooking of fiber mixtures modeling carboards	L. Dollié
15:20	Mineralisation of cellulosic structures	B. Lutsch
15:40	Removal of mineral oils from newspapers and folding boxboard using supercritical CO_2	S. Runte
16:00	**Coffee**	
	Session 2 Paper	
16:30	Evaluating the feel of cartons	D. Eriksson
16:50	Influence of mass distribution on electric breakdown strength of insulating pressboard	M. Vogel
17:10	Sequential water absorption into linerboard	R. Koppolu
17:30	**Poster Session**	
19:00	**Dinner**	

Tuesday Oct 24th, 2017

	Session 3 Lignin Valorisation	
08:30	Novel functional lignins as building blocks in preparation of polyurethane	M. Zieglowski
08:50	The Impact of the Fractionation Method on the Chemical Structure and Reactivity of Industrial Kraft Lignins	A. Tagami
09:10	Effect of Autohydrolysis on lignin structure	H. Curmi
09:30	^{19}F NMR and ^{13}C NMR Studies on Lignin Model Compounds: Insight to Lignin New Derivatization Technique	S. Esakkimuthu
09:50	**Coffee**	
	Session 4 New Fiber- and Cellulose based products I	
10:10	Fabrication of capicitive sliders	T. Plesa
10:30	Stimulus-responsive surface coatings and films from hydroxypropyl cellulose	M.Nau
10:50	Efficacy of natural plant extracts in antimicrobial packaging systems	K. J. Brobbey
11:10	Antibacterial Properties of CNF/PVAm modified fiber and studied by cellulose model surface	C. Chen
11:30	**Coffee**	
	Session 5 New Fiber- and Cellulose based products II	
11:50	Conversion of lignin-cellulose prefibres to carbon fibres	A. Bengtsson
12:10	A study of sealability properties of extrusion-coated fiber-based materials	M. Kraft
12:30	Cellulose-fiber-based insulation materials with improved reaction-to-fire properties	C. Zheng
12:50	**Lunch**	
	Student Workshop	
14:00	Workshop: The Mondi Speed Data Hackaton (Part 1)	
16:00	**Coffee**	
16:30	Workshop: The Mondi Speed Data Hackaton (Part 2)	
18:30	**Excursion to the vineyards of southern Styria**	
23:00	**Return**	

Wednesday Oct 25th, 2017

	Session 6 CNF and MFC	
08:30	Co-exfoliation and fabrication of graphene/microfibrillated cellulose composites and influence on functional properties	J. Phiri
08:50	Unique functionalization technique for tailor-made nanocelluloses	K. Sahlin
09:10	Swelling and Young’s modulus of nanocellulose films in liquids	R. Kummala
09:30	Analysis of drying deformation of 3D printed nanocellulose structures	V. Klar
09:50	Xyloglucan adsorption for measuring specific surface area of cellulose nanofibers	C. Moser
10:10	**Coffee**	
	Session 7 Cellulosic Materials and Water	
10:40	Cellulose as a dispersion stabilizer	C. Costa
11:00	Interaction of cellulose fibres with aqueous foam	A. Ketola
11:20	Assessing the accessibility of cellulose by dynamic vapour sorption coupled with deuterium exchange	S. Väisänen
11:40	Hydrophobic Coating on Cellulosic Textile Material by Betulin and a Betulin Based Polymer	T. Huang
12:00	**Lunch**	
13:40	**Return to Graz**	

Poster Session Monday Oct 23rd, 2017, Time 17h30

Posters	
Influence of mineral pigments on cell behaviour	D. Soto Véliz
Studying the reactivity of cellulose by oxidation with 4-acetamido-2,2,6,6-tetramethylpiperidine-1-oxo-piperidinium cation	P. Khanjani
Characterization of hot water extracted wood hemicelluloses by Matrix-Assisted Laser Desorption/Ionisation - Time of Flight analysis	V. Guigon
Comparative study of CO_2 and CH_4 pressure dependence in the HPP NDIR platform	B. Gaynullin
Quantitative analysis of wavy flatness deviations using an optical surface measuring device	G. Roosen
Water purification using nonleaching and bacteria adsorbing cellulosic fibers	A. Ottenhall
A quick and simple method to prepare functionalized cellulose nanocrystals with high yield	J. Henschen
Test rig for the production of highly oriented papers in the context of building with paper	R. Götzinger
γ-valerolactone-based biorefinery: a shortcut from wood to textile fibers	H. Q. Lê
Coating of cellulose fibres with inorganic nanoparticles in the course of the Cellulose xanthate (CX) process	M. Weißl
Magnetic materials from fines in paper making pulps	M. Hobisch
Kraft lignin precipitation with flue gas	T. Pichler
Measuring ink spreading and penetration for high speed inkjet printing	S. Krainer
3D-Cellulose Mouldings: Dewatering Behaviour and Process Optimization	R. Kleinert
Hydrophobic functionalization of paper for building with paper	F .Schäfer

ISSN 1799-4896 (print)
ISSN 1799-490X (electronic)